Role of Polymeric Immunoglobulin Receptor in pancreatic ductal adenocarcinoma

Prabhu Arumugam

This thesis is submitted for the degree of Doctor of Philosophy

University of London

2016

Queen Mary University of London

Barts Cancer Institute, Centre for Tumour Biology

Barts and the London School of Medicine and Dentistry

Charterhouse Square, London EC1M 6BQ

DECLARATION OF AUTHORSHIP

I declare that the work presented in this thesis is my own, with contributions from others properly cited and acknowledged. The work was performed between August 2012 and July 2016, with an interruption for illness from January 2015 to April 2015, in the Centre for Tumour Biology, Barts Cancer Institute, Barts and the London school of Medicine and Dentistry.

Prabhu Arumugam

August 2016

ACKNOWLEDGEMENTS

Completing a PhD is an extraordinarily long period of time, especially to maintain focus and drive to finish an independent project. Having come from a medical background, the chance to be an independent thinker and manage how my work would progress has been a new experience and one that I have enjoyed. It has also pushed me as an individual and challenged me to achieve, but to also think outside the box.

It has been at times incredibly difficult, with innumerable long days and multiple repeats of experiments that do not seem to work and with what seems like no end in sight. As much as a PhD is an independent project, it is during these, at times desperate moments that you realise how the people around you help.

A good supervisor is in my eyes an essential component of a PhD, both to provide a guiding direction and as a mentor. Prof Kocher has been more than that to me. I have had numerous personal and health issues during my PhD and Hemant has been a constant source of support. He has given me time to adjust and develop, but has also been the person to ensure that my standards do not slip. I have had a lot of messages from Hemant very early in the morning to ensure that I am still working! Hemant, for all of your help, support and advice, I will always be grateful!

My second supervisor, Melania has always been on hand to help me with the complexities of science and thank you for all your help. Good luck in the new job! To the other PI's, Richard, John and Kebs, thank you also for all your help and support! Debbie, our lab manager has dealt for many years with my lack of adherence to health and safety regulations! Mainly my part-time use of a lab coat! But her perseverance finally won me over! Thank you for all your help Debbie, truly our lab would not function without you!

My funding allowed me to continue with clinical work at the Royal London Hospital and Mr Bhattacharya was someone who I have the upmost respect for as a clinician. His talks about the history of medicine were always entertaining! To

everyone else at the Royal London, thank you for looking after me.

In the time of my PhD, I have managed to get married and got a dog! My wife, Jo, has had to deal with life as a PhD widow at times, and I have driven her to her final tether trying to finish my thesis. However, she has always been by my side and has pushed me to finish. She has also made me realise that there is much more to life than work. She has introduced me to good wine and cheese and her homemade cakes! I am a very lucky man to call her my wife and for her love and support, I could not have asked for any more. Thank you!

My parents didn't comprehend why I had undertaken a PhD initially. The idea of working longer hours for a lower wage to them seemed illogical! But irrelevant of my decisions have always supported me and I could not have asked for better parents. They have given me everything and I thank them for all they have given to me.

For anyone else undertaking a PhD, you realise how important others in the lab are. When I joined, I was a novice. But others in my group taught me everything and without their help, I don't think I would have lasted! Leonardo, Jen, Stacey, Abbie and Myrto were the first people I met in the lab and more than supporting me, provided me a constant source of humour. Having them around meant the lab was good fun, no matter how late we were in the lab. The friendship still continues and I hope it continues. To all of you, thank you for the innumerable memories.

The social aspect of our lab revolves around Ami! The girl is a social icon and having someone like that helps to detach from the rigours of meeting deadlines and failed experiments. To the Beta 6 crew of Zareen, Claire, Caroline, Banu, Ketan thank you for your help and support.

To the newer members of our group: Tom, Archana, Vickna, Ahmet, Francesca, Abi and Cindy. I hope you enjoy yourselves and that I have taught you guys something! Good luck to you all, I'm sure you will be successful where ever you go.

The pancreatic think-tank of Bakhouche and Sara, God bless your happy souls! Two incredibly good-hearted and kind people, but also incredible scientists. I am very honoured to have shared a lab with you both and best of luck to you both.

Mike and Ed are the people I ask for any science related problems. Thank you both for your advice. Mike, I also spend most Monday afternoons winding up about how bad Chelsea played on the weekend. Fevzi, good luck my brother, I hope we meet again in the future! Rachel and Alistair, thank you for the random chats, mainly about the location of Sarantos! To the Friday afternoon football squad, thanks for the laughs! Lastly, my fulltime dog-walking, cake-eating buddy Yasmine! She asked for a special mention in my thesis and so she will have her wish. Good luck chumpy!

To everyone else in the lab, thank you for all your help and support and good luck in the future. I should also thank my friends and family outside of the BCI. Thank you for all your friendship! Keep in touch!

Prabs

SCIENTIFIC ACKNOWLEDGEMENTS

Having come from a medical background, I have had to learn and acquire new skills related to laboratory and technical procedures for the entirety of the PhD. There has been no formal taught component and knowledge basis has come from reading around the topics and learning techniques from senior PhD students, post-doctoral researchers and other principal investigators.

Fundamental laboratory and tissue culture health and safety knowledge was taught to me by our laboratory manager (Deborah Buckle) and a mandatory Control of Substances to Health (COSHH) course.

Fundamental aspects of basic tissue culture, handling cells and preliminary functional assays were taught to me by Dr Stacey Coleman (PhD student, Kocher lab) and Dr Athina-Myrto Chioni (Post-doctoral, Grose lab). Complexities and problem solving of cell lines and further options were learned from reading and contacting manufacturers and discussions with Dr Michael Allen (Post-doctoral, Jones lab) and Dr Edward Carter (Post-doctoral, Grose lab).

Techniques of western blotting and polymerase chain reaction (PCR) were learnt from Dr Abbie Fearon (PhD student, Grose lab) and Dr Jennifer Watt (PhD student, Kocher lab).

The procedure of manipulation of cell lines with siRNA, shRNA and over expression was taught by Dr Melania Capasso (second supervisor, PI), Dr Richard Grose (PI) and Dr Athina-Myrto Chioni (Post-doctoral, Grose lab). I also sought advice from Dr Michael Allen (Post-doctoral, Jones lab) and Dr Edward Carter (Post-doctoral, Grose lab).

Organotypic cultures had an established protocol within the Kocher group, but the process was taught to me by Dr Elisabete Carapuça ((PhD student, Kocher lab) and Dr Mo Ghallab (PhD student, Kocher lab). Dr Ghallab, along with Dr Cristina Ghirelli (Post-doctoral, Capasso lab) taught me the procedure of isolating primary stellate cells from pancreatic specimens.

As a medical student in 2008, I undertook a summer project with Prof Kocher and

part of the project was to create Tissue Microarrays (TMA). I was taught to manually create TMA blocks from multiple patient samples, cut sections and stain for immunohistochemistry. These were taught to me by Prof Kocher, Dr Fieke Froeling (PhD Student, Kocher lab) and George Elia (Senior Biomedical Scientist).

Immunohistochemistry and immunofluorescence techniques were taught to me by Dr Fieke Froeling (PhD Student, Kocher lab), Dr Elisabete Carapuça (PhD student, Kocher lab), Dr Jennifer Watt (PhD student, Kocher lab) and Ami Desai (Lab technician, Marshall Lab). This was alongside reading articles and forums for improving techniques. Histopathology training was given to me by Dr Joanne ChinAleong, Consultant Histopathologist.

ARIOL scanning was initially taught to me by Dr Abasi Ene-Obong (PhD student, Kocher lab). Further settings and complexities were taught to me by Dr Linda Hammond (Post-doctoral and Microscope manager) and Andrew Clear (Laboratory technician, Haemato-oncology), both of whom taught Dr Ene-Obong.

Use of the microscopes and panoramic scanner were taught by Dr Linda Hammond (Post-doctoral and Microscope manager) and Prof Kocher.

Although the above individuals were instrumental in my technical development, I also spent time reading about topics through journals, contacting manufacturers and online forum discussions to overcome technical issues. Improvements were also made whilst discussing the topic in weekly one-to-one, group and laboratory meetings.

ABSTRACT

Introduction: Polymeric immunoglobulin receptor (pIgR) traffics Immunoglobulins (IgA and IgM) through epithelial cells in normal mucosae but neither are expressed in the normal pancreas. Recent work has demonstrated pIgR to be upregulated in hepatocellular carcinoma, even though it is not expressed in normal liver cells. High pIgR levels are associated with poor survival and distant metastases for a number of cancers such as nasopharyngeal cancers, lung and oesophageal cancers.

Recent work from our laboratory suggested pIgR may be upregulated in pancreatic ductal adenocarcinoma (PDAC). My aim was to assess pIgR's role in PDAC by interrogating human PDAC tissue samples as well using cell biology experimental tools.

Methods: pIgR expression was manipulated (siRNA and shRNA) in cell lines to evaluate its subsequent effect on cell behaviour in 2D assays as well as 3D organotypics models. Tissue Microarrays of patients with PDAC were analysed after pIgR, αSMA, E-Cadherin and Picrosirius Red staining to assess their role as a combined bio-marker panel.

Results: Cytokines such as interleukin 4 (IL4) and Tumour Necrosis Factor (TNFα) could not modulate pIgR expression in PDAC cell lines despite this effect being seen in other studies using colorectal and nasopharyngeal cancer cell lines. Down-regulation in pIgR expression in Capan1 cell line resulted in reduction of cellular proliferation ($n= 3$, $P<0.05$, Friedman test), adhesion ($n= 3$, $P<0.05$, Kruskal-Wallis) and migration ($n= 3$, $P<0.05$, Kruskal-Wallis). In 3D organotypic models, pIgR downregulation resulted in reduced cancer cell invasion ($n= 9$, $P<0.05$, Kruskal-Wallis) and diminished contraction of gels ($n= 9$, $P<0.05$, Kruskal-Wallis).

In human PDAC, decreased E-cadherin expression correlates with increased pIgR expression through pancreatic intra-epithelial neoplasia (PanIN) progression. There was no IgA expression in PDAC. pIgR expression had no clinical correlation with routine prognostic measures such as differentiation, lymph node metastasis (n= 88, P=0.5012, Kruskal-Wallis). Even in combination with stromal indices (α-smooth muscle action (SMA) and Picrosirius red), low pIgR scores had no statistically significant impact on prognosis but had a trend towards better survival (n= 88, P=0.2791, Mann-Whitney U test).

Conclusion: pIgR may be involved in progression from pre-neoplastic lesions such as PanIN to PDAC. pIgR may have a biological impact on cellular motility and invasion due to yet to be deciphered signalling cascades with marked effect on cellular phenotype. Careful analysis is required to study the impact of pIgR on prognostic impact bearing in mind the histological sub-types of pancreatic cancer.

LIST OF PUBLICATIONS

Arumugam P, Partelli S, Coleman SJ, Cataldo I, Beghelli S, Bassi C, Wijesuriya N, Aleong JA, Froeling FE, Scarpa A, Kocher HM. Ezrin expression is an independent prognostic factor in gastro-intestinal cancers. J Gastrointest Surg. 2013 Dec;17(12):2082-91

Haider S, Wang J, Nagano A, Desai A, **Arumugam P**, Dumartin L, Fitzgibbon J, Hagemann T, Marshall JF, Kocher HM, Crnogorac-Jurcevic T, Scarpa A, Lemoine NR, Chelala C. A multi-gene signature predicts outcome in patients with pancreatic ductal adenocarcinoma. Genome medicine. 2014;6(12):105

Coleman SJ, Watt J, **Arumugam P**, Solaini L, Carapuca E, Ghallab M, Grose RP, Kocher HM. Pancreatic cancer organotypics: High throughput, preclinical models for pharmacological agent evaluation. World J Gastroenterol. 2014 Jul;20(26):8471-81

Solaini L, Atmaja BT, Watt J, **Arumugam P**, Hutchins RR, Abraham AT, Bhattacharya S, Kocher HM. Limited utility of inflammatory markers in the early detection of postoperative inflammatory complications after pancreatic resection: Cohort study and meta-analyses. Int J Surg. 2015 May;17:41-7

Carapuça EF, Gemenetzidis E, Feig C, Bapiro TE, Williams MD, Wilson AS, Delvecchio FR, **Arumugam P**, Grose RP, Lemoine NR, Richards FM, Kocher HM. Anti-stromal treatment together with chemotherapy targets multiple signalling pathways in pancreatic adenocarcinoma. J Pathol. 2016 Jul; 239(3):286-96.

Di Maggio F, **Arumugam P**, Delvecchio FR, Batista S, Lechertier T, Hodivala-Dilke K, Kocher HM. Pancreatic stellate cells regulate blood vessel density in the stroma of pancreatic ductal adenocarcinoma. Pancreatology. 2016 Nov - Dec; 16(6):995-1004.

Arumugam P, Fletcher N, Kyriakides C, Mears L, Kocher HM. Lymphoepithelial cyst of the Pancreas. Case Rep Gastroenterol 2016; 10:181-192.

Arumugam P, Balarajah V, Watt J, Abraham AT, Bhattacharya S, Kocher HM. The role of laparoscopy in hepatobiliary malignancies: A review. Indian J Med Res 2016 Apr; 143(4): 414-9.

Solaini L, Atmaja BT, **Arumugam P**, Hutchins RR, Abraham AT, Bhattacharya S, Kocher HM. The role of perioperative inflammatory-based prognostic systems in patients with colorectal liver metastases undergoing surgery. A cohort study. Int J Surg. 2016 Dec; 36(Pt. A):8-12.

Arumugam P, Bhattacharya S, Chin-Aleong J, Capasso M, Kocher HM. Expression of polymeric immunoglobulin receptor and stromal activity in pancreatic ductal adenocarcinoma. Pancreatology. 2017 Mar - Apr; 17(2):295-302.

King H, Thillai K, Whale A, **Arumugam P**, Eldaly H, Kocher HM, Wells CM. PAK4 interacts with p85 alpha: implications for pancreatic cancer cell migration. Sci Rep. 2017 Feb 16; 7:42575.

LIST OF ABBREVIATIONS

ATRA	All-trans retinoic acid
CAF	Cancer-associated fibroblast
CDNK2A	Cyclin-dependent kinase inhibitor 2A
CEA	Carcinoembryonic antigen (CEA)
Col	Collagen
CRP	C-reactive protein
DPC4	Deleted in pancreatic cancer
ECM	Extra-cellular matrix
EMT	Epithelial mesenchymal transition
GFAP	Glial fibrillary acidic protein
Hb	Haemoglobin
IgA	Immunoglobulin A
IL	Interleukin
IPMN	Intraductal papillary mucinous neoplasm
MCN	Mucinous cystic neoplasm
OT	Organotypic culture
PanIN	Pancreatic intra-epithelial neoplasm
PCC	Pancreatic cancer cells
PDAC	Pancreatic ductal adenocarcinoma
pIgR	Polymeric immunoglobulin receptor
Shh	Sonic hedgehog signalling
SMAD4	Mothers against decapentaplegic homolog 4
αSMA	alpha smooth muscle actin
TGFβ	Transforming growth factor beta
TNFα	Tumour necrosis factor alpha
WCC	White cell count

TABLE OF CONTENTS

DECLARATION OF AUTHORSHIP **2**

ACKNOWLEDGEMENTS **3**

SCIENTIFIC ACKNOWLEDGEMENTS **6**

ABSTRACT **8**

LIST OF PUBLICATIONS **10**

LIST OF ABBREVIATIONS **12**

TABLE OF CONTENTS **13**

LIST OF FIGURES **18**

LIST OF TABLES **22**

CHAPTER I: INTRODUCTION **23**

1.1 Pancreatic Cancer **24**

1.1.1 Classification of pancreatic neoplasms 24

1.1.2 Epidemiology 26

1.1.3 Diagnosis 26

1.1.4 Treatment 29

1.1.4.1 Surgery 29

1.1.4.2 Chemotherapy 30

1.2 Pathophysiology of pancreatic cancer **31**

1.2.1 Germline Genetic alterations found in PDAC 31

1.2.2 Precursor lesions and PanIN 32

1.3 Stroma of PDAC **34**

1.3.1 Pancreatic Stellate Cells 36

1.4 Cancer-Stroma interactions **38**

1.5 Role of pIgA/ pIgR **39**

1.5.1 The pIgR gene 41

1.5.2 Structure of pIgR 41

1.5.3 Regulation of pIgR expression 44

1.5.4 Transcytosis of pIgR 45
1.51.6 Immunoglobulins 51
1.5.7 J-Chain 53
1.6 The role of pIgR in cancer 54
1.7 The role of pIgR in Hepatocellular Carcinoma 57
1.8 The role of pIgR in pancreatic adenocarcinoma 58
1.9 Aims 62
1.10 Objectives 62

CHAPTER II: MATERIALS AND METHODS 63
2.1 Tissue microarray 64
2.2 Cell Culture 68
2.2.1 Cell Lines, media and culture reagents 68
2.2.1.1 Pancreatic Cancer Cells 68
2.2.1.2 Stromal Cells 69
2.2.1.3 Pancreatic ductal epithelial cells 69
2.2.1.3 MOCRI cells 69
2.2.1.4 Culture conditions and routine cell culture 69
2.3 Immunostaining 71
2.3.1 Cells cultured on coverslips 71
2.3.2 Paraffin embedded gels and patient tissues 71
2.3.3 Immunofluorescence 72
2.3.4 TMA core Analysis 73
2.3.4.1 ARIOL imaging 74
2.3.4.2 Methods of Immuno-scoring 75
2.3.4.3 Limitations of Ariol 76
2.3.4.4 Application 76
2.3.5 Identification of PanIN for assessment 77
2.3.6 Survival and Statistical analysis 77

2.3.7 Picrosirius Red staining 78
2.4 Western Blotting....79
2.4.1 Isolation of protein 79
2.4.2 Western blot analysis....79
2.4.3 Stripping membranes....80
2.4.4 Densitometry and analysis....80
2.5 Quantitative real-time PCR 80
2.6 Antibodies 82
2.7 Modulation of pIgR in cell lines....83
2.7.1 Small interfering RNA (siRNA) oligos....83
2.7.2 Collection of supernatant 83
2.7.3 Introduction of siRNA into Capan1 cells 83
2.7.4 Introduction of shRNA into pancreatic cancer cells 84
2.7.5 Incubation of pancreatic cancer cell lines with cytokines....85
2.7.6 Introduction of plasmid DNA into pancreatic cancer cells....85
2.7.6.1 pIgR cDNA from Addgene 85
2.7.6.2 Other methods of pIgR over-expression....88
2.8 Functional Assays....89
2.8.1 Cell Counts....89
2.8.2 Cell Proliferation Assay....89
2.8.3 Scratch Assay....90
2.8.4 Adhesion Assay....90
2.8.5 Transwell Migration Assay....90
2.9 Organotypic culture 91
2.10 Statistics....94

CHAPTER III: RESULTS PART I....96
3.1 Immunofluorescence staining of human paraffin sections....97
3.2 Normal human expression of pIgR and immunoglobulins....97

3.2.1 Confirmation of expression of pIgR in PDAC 100
3.2.2 Validation of staining intensity 101
3.3 pIgR expression across peri-ampullary lesions 104
3.4 pIgR expression and PanIN lesions 108
3.5 pIgR and patient survival 115
3.6 pIgR and systemic factors 118
3.7 pIgR and tissue factors 124
3.7.1 αSMA Immunofluorescence staining of paraffin sections 124
3.7.2 Comparing survival with αSMA staining 126
3.7.3 Association of pIgR and αSMA staining 132
3.7.4 Picrosirius Red staining of paraffin sections 133
3.7.4 Association of pIgR and Picrosirius Red staining 136
3.7.5 Comparing survival of combined pIgR, αSMA and Picrosirius Red 138
3.8 Discussion 142
3.8.1 Role of pIgR in gastrointestinal cancers 142
3.8.2 Association of pIgR in the pre-malignant phases of PDAC 144
3.8.3 Effect of pIgR on stromal content 145
3.8.4 Role of pIgR as a biomarker in PDAC 146

CHAPTER IV: RESULTS PART II 148
4.1 Introduction 149
4.2 pIgR expression in pancreatic cancer cells 150
4.3 Upstream precursors to pIgR in pancreatic cancer cells 152
4.4 Effect of pIgR siRNA on Capan1 pancreatic cancer cells 157
4.5 Effect on pIgR expression in cancer cells after RNAi and co-culture with PSC in 3D 160
4.6 Optimisation of pIgR shRNA 164
4.7 Effect of pIgR shRNA on Capan1 pancreatic cancer cells 165

4.8 Effect of pIgR shRNA on cancer cell phenotype using organotypic model 172

4.9 Changes in epithelial and stromal activity upon pIgR knockdown.....178

4.10 Optimisation of pIgR over-expression 190

4.10.1 Optimisation of Digestion.....190

4.10.2 Optimisation of Cloning.....190

4.10.3 Optimisation of Transformation.....191

4.10.4 Other methods of pIgR expression 191

4.11 Discussion 196

4.11.2 Downstream effect of pIgR 198

4.11.3 Modulation of pIgR in PDAC cancer cells 199

4.11.4 Modulation of pIgR and its association with EMT.....200

4.11.5 Modulation of pIgR and its association with stellate cells 201

CONCLUSIONS 202

FURTHER WORK 204

REFERENCES: 205

APPENDIX: TMA Maps.....221

LIST OF FIGURES

Figure 1.1: Normal pancreatic pathology demonstrated on H&E 25

Figure 1.2: PanIN progression 33

Figure 1.3: Gene expression changes 39

Figure 1.4: pIgR structure 43

Figure 1.5: Molecular regulation of pIgR expression 44

Figure 1.6: pIgR through an epithelial cell 48

Figure 1.7: Immunoglobulins 51

Figure 2.1: PanIN progression 77

Figure 2.2: Quantification of Picrosirius Red stain 78

Figure 2.3: Picrosirius Red staining in human PDAC sections 79

Figure 2.4: Representative image of pcDNA 4/T0 vector 87

Figure 2.5: Diagrammatic representation of organotypic models 92

Figure 2.6: Quantification of Organotypic cultures 92

Figure 2.7: Quantification of Organotypic culture cell area 93

Figure 2.8: Quantification of Organotypic culture gel thickness 93

Figure 2.9: Quantification of Organotypic culture cell layer thickness 94

Figure 3.1: IgA is not expressed in human pancreas. 98

Figure 3.2: pIgR is not expressed in normal human pancreas. 99

Figure 3.3: pIgR and E-Cadherin expression in human PDAC. 100

Figure 3.4: Distribution of pIgR expression scores 102

Figure 3.5: Inter-observer variability of scoring methods. 103

Figure 3.6: Cancers of the peri-ampullary region 105

Figure 3.7: Representative images from TMA of human sections. 106

Figure 3.8: pIgR expression across peri-ampullary lesions 107

Figure 3.9 A: Inverse relationship of pIgR and E-Cadherin. 110

Figure 3.9 B: Nuclear features of PanIN. 112

Figure 3.9 C: PanIN and PDAC variability 112
Figure 3.10: Inverse relationship of pIgR and E-Cadherin expression. 114
Figure 3.11: Patient characteristics. 115
Figure 3.12: Correlation between pIgR and survival. 117
Figure 3.13: Association of pIgR expression and patient cohort. 119
Figure 3.14: Association of pIgR expression and systemic factors. 120
Figure 3.15: Correlation of pIgR expression with length of In-patient stay. 121
Figure 3.16: Correlation of pIgR staining intensity and pre-operative Ca19-9 result. 121
Figure 3.17: Association of pIgR staining intensity and inflammatory markers. 122
Figure 3.18: Representative images of sections from human PDAC. 125
Figure 3.19: Correlation between αSMA and survival. 128
Figure 3.20: Association of αSMA and gender. 129
Figure 3.21: Association of αSMA and White cell count (WCC). 130
Figure 3.22: Association of αSMA and tumour differentiation. 131
Figure 3.23: Correlation of pIgR and αSMA staining 132
Figure 3.24: Picrosirius Red stain in tissue sections of human PDAC. 134
Figure 3.25: Association of Picrosirius red and survival. 135
Figure 3.26: Correlation of Picrosirius Red and αSMA staining. 136
Figure 3.27: Correlation of pIgR and Picrosirius red. 137
Figure 3.28: Panel 1 biomarker for PDAC. 139
Figure 3.29: Panel 2 biomarker for PDAC 140

Figure 4.1: Protein expression of pIgR in PDAC cell lines. 150
Figure 4.2: Protein expression of pIgR in primary pancreatic stellate cells. 151
Figure 4.3: mRNA expression of pIgR in pancreatic cancer cells and PS1 cells. 151
Figure 4.4: Effect of introduction of cytokines and ATRA to PDAC cells. 155
Figure 4.5: Other attempts at over-expression of pIgR. 155
Figure 4.6: Effect of pIgR siRNA on Capan 1 pancreatic cancer cells. 158
Figure 4.7: Secreted pIgR after siRNA with or without Tunicamycin treatment. 158

Figure 4.8: Cell proliferation after pIgR siRNA.....159
Figure 4.9: Effect of pIgR expression in cancer cells alone after RNAi.....161
Figure 4.10: Effect of pIgR expression in cancer cell co-cultures after RNAi.....162
Figure 4.11: Effect of pIgR knockdown in Organotypics. 163
Figure 4.12: Confirmation of pIgR knockdown.....165
Figure 4.13: qRT-PCR of wild type and transfect shRNA. 165
Figure 4.14: Phase contrast microscopy of pIgR shRNA cells.....166
Figure 4.15: Cell counts after 7 days of shRNA transfection.....167
Figure 4.16: Association of pIgR knockdown and EMT.....168
Figure 4.17: Functional effects of pIgR shRNA on Capan1 cells. 170
Figure 4.18: Effect of pIgR knockdown on scratch assay. 171
Figure 4.19: Haematoxylin and Eosin stained sections from organotypic cultures...173
Figure 4.20:Close up cross sectional H&E stained sections from Organotypics. 174
Figure 4.21: Effect of pIgR knockout in cancer cell lumen formation. 175
Figure 4.22: Effect of pIgR knockout in Organotypic gel structure. 176
Figure 4.23: Effect of pIgR knockdown in cancer cell layer.....178
Figure 4.24: pIgR and E-cadherin interaction in pIgR knockdown 3D models. 180
Figure 4.25: pIgR and E-cadherin interaction in pIgR knockdown 3D models. 181
Figure 4.26: pIgR expression in organotypic models.....182
Figure 4.27: E-cadherin expression in organotypic models. 182
Figure 4.28: Cytokeratin interaction in pIgR knockdown 3D models.....183
Figure 4.29: Cytokeratin and αSMA interaction in pIgR knockdown 3D models. 184
Figure 4.30: Cytokeratin expression in organotypic models. 185
Figure 4.31: αSMA expression in organotypic models.....185
Figure 4.32: Zeb1 interaction in pIgR knockout 3D models. 186
Figure 4.33: Zeb1 interaction in pIgR knockout 3D models. 187
Figure 4.34: Zeb1 expression in organotypic models. 187
Figure 4.35: Picrosirius Red expression in pIgR knockout 3D models.....188
Figure 4.36: Picrosirius red expression in organotypic models.....188

Figure 4.37: Ezrin expression in pIgR knockout 3D models. 189
Figure 4.38: Ezrin expression in organotypic models. 189
Figure 4.39: Confirmatory images of digestion of pIgR cDNA. 192
Figure 4.40: Modification of PCDNA4/T0 193
Figure 4.41: Sequencing result of pIgR OSLO clone confirming a 97% alignment. .194
Figure 4.42: Introduction of pIgR into Hela cells.....195

LIST OF TABLES

Table 1: Staging and TNM classification.....29

Table 2: Summary of germline mutations.....32

Table 3: Summary of cellular and non-cellular components.....36

Table 4: Table summarising characteristics of PaSC's.....37

Table 5: Table summarising role of pIgR in other cancers.....56

Table 6: Pancreatico-biliary disease: patient numbers.....65

Table 7: Pancreatic Cancer Cell lines.....68

Table 8: Staining scoring Criteria.....74

Table 9: Primers used for quantitative reverse transcription PCR.....81

Table 10: Antibodies used for experiment.....82

Table 11: Association of pIgR expression in PDAC.....116

CHAPTER I

INTRODUCTION

1.1 Pancreatic Cancer

Encompassing two distinct functional units of cells, the pancreas can give rise to several different tumour types. These tumour types show distinct clinical behaviours and genetic profiles. Pancreatic ductal adenocarcinoma (PDAC), a tumour type with characteristic histology, is the most common type of cancer of the pancreas, accounting for greater than 85% of pancreatic neoplasms (1).

1.1.1 Classification of pancreatic neoplasms

Composed of exocrine and endocrine compartments, the pancreas regulates digestion and glucose metabolism (2). The pancreas consists of numerous small glands called acini, which constitutes the exocrine function of the pancreas. These smaller acini drain into small, intercalated ducts, which join to form the intra-lobular and then inter-lobular ducts, which eventually anastomose to the main pancreatic duct and onwards to the duodenum (**Figure 1.1**). Acini function to produce inactive enzymes such as trypsin, elastase, lipase and amylase, which are activated in the acidic environment of the duodenum. Interspersed within the exocrine tissue, are islets of endocrine cells (3).

The classification of neoplasms is based on the presumed cellular origin of the cancer cells (ductal, endocrine and acinar cells) as well as the gross configuration of the tumour (solid, cystic or intraductal) (3). Since pancreatic ductal adenocarcinoma (PDAC) is the commonest tumour of the pancreas, the terms PDAC and pancreatic cancer are used synonymously, although this is incorrect.

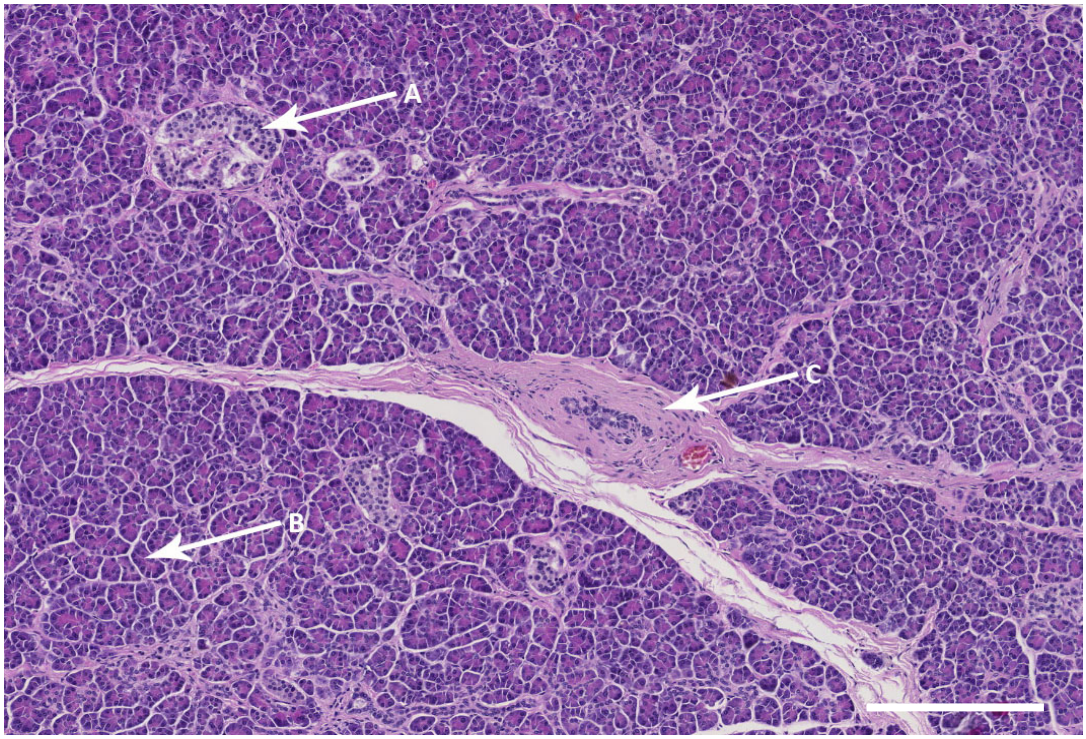

Figure 1.1: Normal pancreatic pathology demonstrated on Haematoxylin and Eosin (H&E).

(A) Representation of Islet of Langerhans and the endocrine portion of the pancreas. (B) Representation of pancreatic acini and the exocrine portion of the pancreas. (C) The interlobular duct. Scale bar 100µm. Picture taken by Dr Prabhu Arumugam with Dr Joanne ChinAleong, Consultant Pathologist

1.1.2 Epidemiology

PDAC has a dire prognosis and outcomes have not significantly improved in the last 40 years. It was the 10th most common cancer in 2011 (UK: 9.7 per 100000), but its incidence is increasing In 2008, there were 8085 new cases in the UK and by 2011, there were 8773 reported cases (4328 male and 4445 female) (4).

Peak incidence for the disease is between the seventh and eight decade of life, approximately 80% of cases are seen in the over 60s (5) and there is no difference between sexes (6). The mortality rates of PDAC vary among countries; the five-year survival in the UK is 3%, which is a marginal increase in the last 40 years. However, patients with localised, resectable disease have a 5-year survival of 15-18% (7). At present, only pancreatic resection can improve survival significantly. However, due to late presentation and aggressive tumour behaviour, a minority of patients (5-10%) can undergo potentially curative surgery (8).

Although the causes of PDAC remain incompletely understood, development of late onset diabetes in patients over the age of 65 is associated with an eight-fold increase of developing PDAC within three years, compared to the normal population (9). Smoking is the only proven risk factor, with the risk of PDAC, in those who smoke 25 cigarettes or more per day, 3.1 times the risk of non-smokers (10).

1.1.3 Diagnosis

Signs and symptoms of PDAC are, at best, vague and non-specific. They include malaise, abdominal pain, and nausea or weight loss in early stages of disease. Tumours of the head of the pancreas often obstruct the common bile duct, resulting in obstructive jaundice, whilst tumours of the tail and body present later, usually with pain. Obstruction of the major pancreatic ducts can also cause malabsorption, steatorrhoea and/or pancreatitis. Tumour-secreted soluble factors affecting β-cell function results in new-onset diabetes in small tumours in approximately 40% of patients (11, 12).

Blood tests are non-specific. Serum liver function and full blood counts may

demonstrate obstructive jaundice and normochromic anaemia. Biomarkers have been stipulated, but the only one with clinical usefulness is carbohydrate antigen 19-9 (CA 19-9), with a sensitivity of 70-90% and specificity of 90%. CA 19-9 lacks the desired sensitivity and specificity for early detection (13). The accepted use for CA 19-9 remains in monitoring response to treatment and in identifying recurrence in treated patients with known PDAC (14).

Evaluation of a patient with suspected PDAC is focused on confirming diagnosis and staging of disease. Although a useful investigation, ultrasound does not exclude PDAC, thus the modality of choice in patients with suspected pancreatic cancer is pancreatic protocol computed tomography (CT), which is a tri-phasic cross-sectional imaging, with thin slices and specific aspect of venous phase of intravenous contrast. Sensitivity for detecting lesions more than 2cm is 90% with accuracy of determining resectability for 80-90% of patients (13, 15).

Consensus on further staging and investigations has no uniformity. Endoscopic ultrasound (EUS) can accurately demonstrate small tumours (as small as 3mm) (16). In conjunction with fine needle aspiration (17), EUS provides a relatively safe method of tissue analysis, and has progressively replaced ERCP with brush cytology (18). EUS alone does not achieve the accuracy required sensitivity to distinguish between chronic pancreatitis and malignancy (75%) but with FNA, it rises to >90% (19). EUS has drawbacks such as user-dependency and being invasive; thus, it is associated with complications.

Endoscopic retrograde cholangiopancreatography (ERCP) has classically been used for biliary obstruction and was the first choice imaging modality until EUS-FNA produced better and safer results. It is still used as an alternative for FNA aspiration tissue sampling and has the benefit of being able to pace a stent to palliate biliary obstruction when surgery is not elected or must be delayed

Magnetic resonance imaging (MRI) scanning can be used to identify lesions less than 2cm. Magnetic resonance cholangiopancreatography (MRCP) with gadolinium enhancement allows tumour detection at an earlier stage, potentially

useful for screening individuals at high risk of PDAC (20).

Positron emission tomography (PET) scanning uses fluorine 18-fluorodeoxyglucose (FDG), which is the most widely used radioisotope to identify active tumour cells, especially in patients with metastases and post-chemotherapy progress imaging. FDG-PET sensitivity and specificity is variable: 46-71% and 63-90% respectively, thus PET-CT is much more effective (92% sensitivity). PET-CT is most effective in diagnosing metastasis and post-treatment imaging (21); however, it is not in routine clinical use.

Preoperative staging laparoscopy is the exploration of certain areas of the abdomen to check the extent of disease infiltration: mainly peritoneal seeding, small surface liver metastases and involvement of the coeliac/mesenteric vessels that are below the detection threshold of currently available imaging techniques, and can prevent unnecessary laparotomy (22). Depending on a center's expertise, laparoscopic staging maybe appropriate in some patients, especially in those with lesions in the body or tail, or in patients with higher risk of Pancreatic cancer is staged according to the American Joint Committee on Cancer (AJCC) tumour-node-metastasis (TNM) classification, however there are no universally accepted criteria for resection. Thus, decisions for further management of patients are based on outcomes by a multidisciplinary team. CT classification broadly categorises patients with PDAC as either resectable, borderline resectable, locally advanced or metastatic disease. Pancreatic staging guides potential treatment options, as shown in Table 1. Patients with locally advanced disease (Stage III) are ineligible for surgery due to involvement of local vascular structures.

Stage	TNM Classification	Tumour characteristics	Clinical classification	Incidence at diagnosis (%)	5 year survival rate (%)
0	Tis, N0, M0		Resectable and borderline resectable	7.5	15.2
IA	T1, N0, M0	<2cm size, confined to pancreas			
IB	T2, N0, M0	>2cm size, confined to pancreas			
IIa	T3, N0, M0	Growth into adjacent organs			
IIB	T1-3, N1, M0	Lymph node involvement			
III	T4, any N, M0	Invasion into Coeliac artery and SMA	Locally advanced	29.3	6.3
IV	Any T, any N, M1	Metastatic disease	Metastatic	47.2	1.6

Table 1: Staging and TNM classification related to incidence, treatment and prognosis (23)

1.1.4 Treatment

The majority of patients present with distant metastasis, commonly to the liver and peritoneal cavity (13).

Treatment is based on the extent of the disease, with the only potential curative treatment being surgical resection. Palliative surgery can be used to relieve symptoms of gastric outlet and/ or biliary obstruction, whilst endoscopic or percutaneous biliary stenting are preferred options. Chemotherapy and radiation therapy may be used as palliative treatment or in the adjuvant setting with surgery (16).

1.1.4.1 Surgery

About 10% of all patients with PDAC are fit patients with resectable disease. They should be referred to a high volume specialist centre for surgical resection, as there is considerable evidence that operative mortality can be kept to low single figures when undertaken in specialist centres (24).

1.1.4.2 Chemotherapy

The objectives of chemotherapy and radiotherapy in PDAC may be considered in three sections; neoadjuvant or adjuvant therapy (given during or after surgery to improve survival), management of locally advanced disease not amenable to surgical therapy and metastatic disease, where the primary objective is palliation and prolongation of a symptom free life.

In the past three decades, the standard chemotherapies for management of palliative stages of PDAC consisted of fluoropyrimidines like F-fluorouracil (5-FU) and the antimetabolite drug gemcitabine, which were mostly equivalent in randomised clinical trials, contributing 0-10% to tumour response and with an overall survival (OS) of 4 to 6 months (25). Several combinations with other chemotherapies and/ or biological agents were studies, mostly with inconclusive or negative results. Gemcitabine alone, Gemcitabine-Capecitabine combination (26), Gemcitabine-nab Paclitaxel (27) and FOLFIRINOX (28)re all considered first-line therapy, whilst FOLFIRINOX provides better survival, it is only suitable for good performance status patients (28). As a second line treatment, 5FU-folinic acid and nanoliposomal Irinotecan combination provides the best results (29).

Neoadjuvant therapy, with the aim to reduce size or extent of tumour prior to surgery to enhance successful surgical removal remains under investigation in the context of clinical trials (30).

Adjuvant regimens had traditionally consisted of gemcitabine and fluorouracil-based chemotherapy. These have been shown to increase the median and 5-year survival compared to surgery alone (31) (32). Understanding the biology of pancreatic cancer with particular reference to genetic alterations and tumour-stroma interactions could potentially alter the therapeutic landscape and improve the survival of these patients.

1.2 Pathophysiology of pancreatic cancer

Pancreatic ductal adenocarcinoma is speculated to originate in the ductal epithelium, presumably from small intra-lobular ducts, evolving from the pre-malignant pancreatic intraepithelial neoplasia (PanIN) (33) to fully invasive cancer. The progression from minimally dysplastic epithelium (PanIN 1) and finally to invasive carcinoma is paralleled by the successive accumulation of mutations that include activation of the *KRAS2* oncogene, inactivation of tumour suppressor gene *CDKN2A* and TP53 (34). Genetically engineered mouse models have demonstrated that targeted activation of *KRAS2* with concomitant inactivation of Trp53 or *CDKN2A* results in development of PDAC (35) (36).

Almost all patients with fully established PDAC carry one or more of the four common genetic alterations (37). Ninety per cent of tumours have activating point mutations in the *KRAS2* oncogene. Transcription of the mutant *KRAS* gene produced an abnormal Ras protein that is “locked” in its activated form, resulting in aberrant activation of proliferative and surviving signalling pathways. Similarly, 95% of tumours have inactivation of the *CDKN2A* gene due to either loss of heterozygosity or point mutations, resulting in loss of the p16 protein (regulator of the G1-S transition of the cell cycle) and a corresponding increase in cell proliferation (16). *TP53* is either mutated or there is loss of heterozygosity in 50 to 75% of tumours, permitting cells to bypass DNA damage control checkpoints and apoptosis signals and contributing to genetic instability (38). *DPC4* is lost in approximately 50% of cancers, resulting in aberrant signalling by the transforming growth factor β (TGF- β) cell-surface receptor (39).

Recent work has demonstrated that PDAC contains an average of 63 genetic mutations, the majority of which are point mutations (40). These alterations defined a core set of 12 cellular signalling pathways and processes that were each genetically altered in approximately 67 to 100% of tumours (41).

1.2.1 Germline Genetic alterations found in PDAC

A number of germline mutations have been associated with an increased

risk of pancreatic cancer; in the majority of families the genetic basis of familial occurrence is incompletely understood. History of BRAC1, BRAC2, familial adenomatous polyposis, Peutz-Jeghers syndrome and Lynch syndrome within families are also associated with higher prevalence of pancreatic cancer (42). Mutations in BRCA2 can be found in 6-12% of families with two or more cases of pancreatic cancer (42). Other inherited cancer syndromes are listed in Table 2.

Gene with germline mutation	**Familial disorder**	**Effect**
PRSS1	Recurrent acute pancreatitis (43) (autosomal dominant)	Chronic pancreatitis and thus increased risk of PDAC (44)
SPINK1	Hereditary pancreatitis (autosomal recessive)	Chronic pancreatitis and thus increased risk of PDAC (45)
CDKN2A	FAMMM syndrome (autosomal dominant)	20% increased risk of PDAC by age of 75 (46)
STK11	Peutz-Jeghers (autosomal dominant)	26% increased risk of PDAC (47)
BRCA2	80% risk of breast cancer	3.5-fold increased risk of PDAC (48)
APC	Familial Adenomatous Polyposis	Fourfold increased risk of PDAC (49)
Mismatch repair genes	Hereditary non-polyposis colorectal cancer	3.7% risk of PDAC (49)

Table 2: Summary of germline mutations leading to familial pancreatic cancer (50)

1.2.2 Precursor lesions and PanIN

There are three types of precursor lesions in PDAC that follow a multistep progression from neoplasia showing mild dysplasia to invasive cancer. They are pancreatic intraepithelial neoplasia (PanIN); intraductal papillary mucinous neoplasm (IPMN); and mucinous cystic neoplasm (MCN). Some of these lesions may be detected on imaging, often incidentally and subsequently kept under observation or resected, to prevent development of invasive carcinoma.

PanIN are microscopic proliferative epithelial lesions in the small calibre pancreatic ducts (51). The most common precursor lesion in pancreatic cancer, a four-tier classification system was established in 2001 (52). Histopathologically, the grading ranges from PanIN-1 to PanIN-3 with increasing dysplasia to invasive carcinoma (**Figure 1.2**). Telomere shortening (53) and mutations in *KRAS*, *p16/CDKN2A*, p53, *SMAD4* and *BRCA2* genes have all been identified in PanIN lesions (54). PanIN lesions are not radiologically detectable and early detection and prevention remains a theoretical possibility.

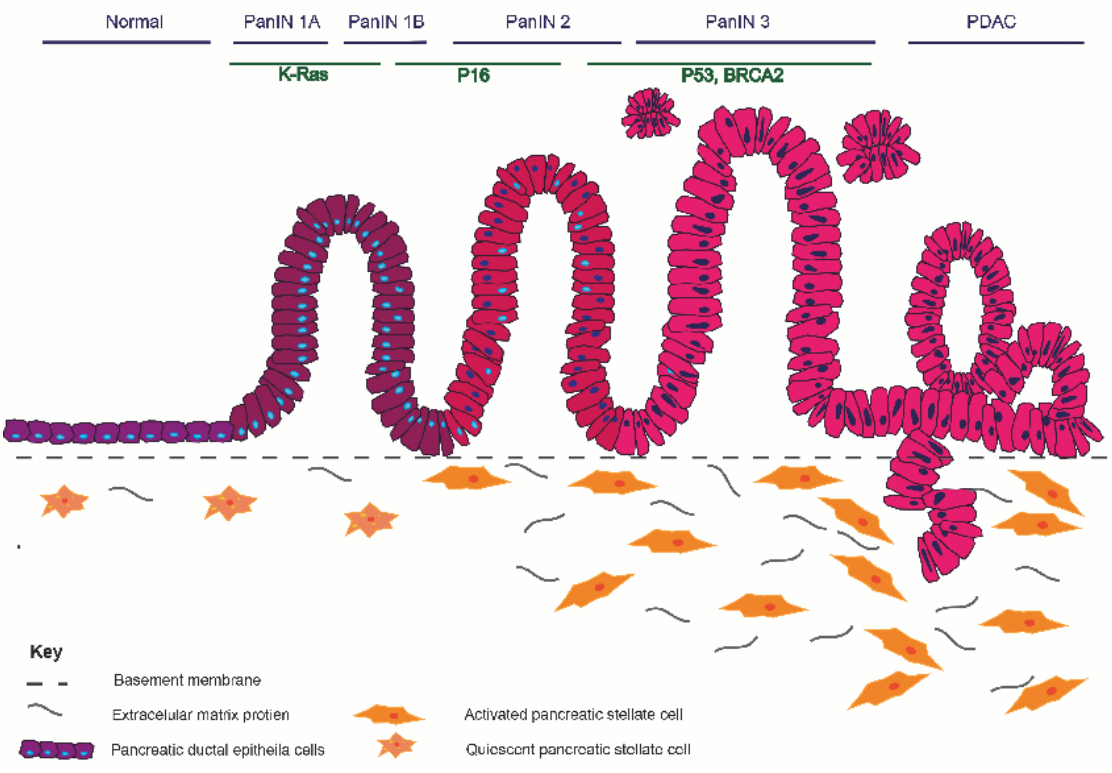

Figure 1.2: PanIN progression demonstrating increasing genetic mutations with increasing dysplasia

IPMNs are cystic lesions arising in the main duct or branch duct epithelium of the pancreas, characterised by papillary proliferation and mucin production. They are classified according to their malignant transformation from those with low-grade dysplasia to those with invasive carcinoma or according to their location (main duct; branch duct or mixed type with involvement of both main and branch ducts). IPMN lesions can be detected radiologically. Analysis of the cyst fluid via endoscopic

ultrasound to quantify amylase, Carcinoembryonic antigen (CEA) as well as cytology can differentiate between cystic lesions (55).

MCNs are mucin-producing cystic lesions of the pancreas characterised by the presence of ovarian type stroma, usually solitary, incidental finding in younger female patients, located in the body or tail of the pancreas. Like IPMNs, MCN can be identified on cross-sectional imaging and with high CEA fluid levels and EUS aspirate. They are distinguished from IPMNs based on a lack of communication with the main pancreatic duct (56). 3.9-30% of MCNs will progress to invasive cancer, usually PDAC (57); thus surgical resection is recommended.

1.3 Stroma of PDAC

The formation of a dense stroma, termed a desmoplastic reaction is peculiar to PDAC (41) (58). Myofibroblasts (known to be derived from pancreatic stellate cells) play a critical role in the formation and turnover of the stroma. Alongside providing a mechanical barrier, the stroma also constitutes a dynamic barrier that is critically involved in the process of tumour formation as well as progression (59).

Factors such as TGFβ1, platelet-derived growth factor (PDGF) and fibroblast growth factors can activate these cells to secrete collagen and other components of the extracellular matrix. Stellate cells regulate the reabsorption and turnover of the stroma via its production of matrix metalloproteinases (60) and are also implicated for the poor vascularity: a characteristic of PDAC (61).

Stromal cells express multiple proteins such as cyclooxygenase-2, PDGF receptor, vascular endothelium growth factor, stromal cell-derived factor, chemokines, integrins, secreted protein, acidic, cysteine-rich (SPARC) and hedgehog pathway elements among others that have been associated with poor prognosis and resistance to treatment.

Consequently, in experimental models, stromal disruption was studied by with Hedgehog inhibitor. This disrupted the stromal architecture, increasing tumour vascularity and facilitating efficient delivery of Gemcitabine. As a result, metastasis

decreased and the overall survival of mice treated with the combination of inhibitor and Gemcitabine was significantly increased compared to control (62), suggesting targeting the stromal component of PDAC may improve delivery and efficacy of chemotherapy. However, this approach failed in human clinical trials (63).

Conversely, Ozdemir et al (64) used transgenic mice with deleted αSMA+ myofibroblasts in pancreatic cancer to investigate the potential role of tumours lacking stromal content and its potential effects on drug delivery. They identified mice that were depleted had diminished survival and did not respond to gemcitabine, underscoring the need for caution in targeting carcinoma-associated fibroblasts in PDAC. Rhim et al (65) also investigated the role of sonic hedgehog (66), a soluble ligand overexpressed by neoplastic cells in PDAC. It is established that Shh drives formation of desmoplastic stroma. Rhim investigated Shh deletion in mice and identified tumours with reduced stromal content were more aggressive and suggested stroma may, infact, act in restrain tumour growth. It is therefore proposed that homeostatic restoration of desmoplastic stroma rather than its ablation slows pancreatic cancer progression (67).

Cellular components		Non-cellular components	
Fibroblasts and Pancreatic stellate cells	Most prominent role in desmoplastic reaction (59)	**Fibrous proteins**	Including collagen, elastin, fibronectin, desmin and laminin (68)
Endothelial cells	Hypoxia, secondary to fibrosis and anti-angiogenic components, results in increased tumour growth and metastasis (69)	**Proteoglycans**	Hydrating and buffering in interstitial space (70)
Inflammatory cells	Tumour associated macrophages, neutrophils and T cells localise to stroma, secreting growth factors and cytokines with stimulate the desmoplastic reaction (71)		
Nerve cells	Abundant nerve supply in the pancreas, making pain associated with disease a major challenge (72)		

Table 3: Summary of cellular and non-cellular components of the desmoplastic reaction within the stromal component

1.3.1 Pancreatic Stellate Cells

Stellate cells have been found in a variety of organs, including the liver and intestine, but pancreatic stellate cells (PSCs) were first identified in 1998 by Apte (73) and Bachem (74). Since then, they have been shown to have a key role in maintaining tissue architecture through the regulation of ECM protein synthesis and degradation.

In normal tissue, PSCs exist in a quiescent state, compromising 4-7% of pancreatic parenchyma, with an abundance of vitamin A droplets in their cytoplasm. In the normal pancreas, PSCs become activated in response to any form of insult, triggering fibrosis through various stromal interactions accommodating the wound healing process. On resolution, the PSCs return to their quiescent state until they are called upon in the damage limitation role (59).

Characterisation feature	Activated PSC	Quiescent PSC
Appearance	Star shaped	Spindle shaped and smaller
αSMA expression	Positive (in >90%)	Negative
Desmin expression	Positive in 20-40%	Negative
Vimentin expression	Positive	Positive
GFAP expression	Positive	Negative
Adherence in tissue culture	+++	+
ECM protein secretion	+++	+
Receptor expression	+++	+
Density	+++	+

Table 4: Table summarising differing characteristics of activated and quiescent PaSC's (75)

Quiescent PSCs have a positive effect on epithelial integrity through integrin β1-dependent maintenance of the basement membrane, demonstrating a role in acinar functionality (76). An additional role in exocrine function has been demonstrated, whereby the gastrointestinal hormone cholecystokinin (CCK) induces acetylcholine secretion by PSCs, which in turn stimulates amylase secretion by acinar cells (77). Furthermore CCK has been shown to have direct activating effect on PSCs, and induces collagen synthesis (78). The exact source of activated PSCs (myofibroblasts phenotype) is still a matter of much debate; however a consensus exists that in the context of benign inflammation or malignancy, the surrounding cancer, immune or endothelial cells release various growth factors and inflammatory cytokines, that, in turn, activate PSCs through paracrine signaling networks (79).

There are numerous potential pathways that exist to communicate between PSCs and cancer cells, emphasising the complex bi-directional relationship, which is not completely understood. An exciting prospect exists whereby if the PSCs can be targeted, one can exert an influential effect on the key and complex interplay between the cancer cells, ECM and tumour vasculature (80).

1.4 Cancer-Stroma interactions

Kadaba et al (70) investigated the role of desmoplastic stroma and the suggestion that dynamic stromal cell participation in cancer progression impacts on patient prognosis. By reconstructing tumour micro-environments in physio-mimetic organotypic cultures, the role of specific desmoplastic stromal cells, such as pancreatic stellate cells (PSC), in PDAC was studied.

Progressive accumulation of desmoplastic stromal cells, believed to be triggered by cancer-induced activation of fibroblasts/ stellate cells to myofibroblasts has a pro-survival and pro-invasive effect on tumour cells, in addition to stiffening of the ECM gels.

Laser-capture micro-dissection and gene-expression micro-array analysis as well as quantitative real-time RT-PCR validation in independent experiments (**Figure 1.3**), confirmed several of the most up-regulated and down-regulated genes across two PDAC cell lines (Capan1 and AsPC1) and clustered them into four groups affecting one or more key cellular functions. Polymeric Immunoglobulin Receptor (pIgR) was identified as a gene significantly upregulated in cancer cells upon exposure to PSCs. pIgR, involved in the transcytosis of molecules in epithelial cells, was hypothesised to provide the missing link between inflammation, EMT and metastasis (81). Kadaba et al noted pIgR expression was increasingly observed in cancer cells when PSCs were most predominant and was inversely correlated with E-cadherin expression, which was confirmed in human PDAC samples. I sought to take this work further by trying to understand the biological role for pIgR in pancreatic cancer and its potential prognostic impact, in a hypothesis driven manner. I would next introduce pIgR to the reader of this Thesis.

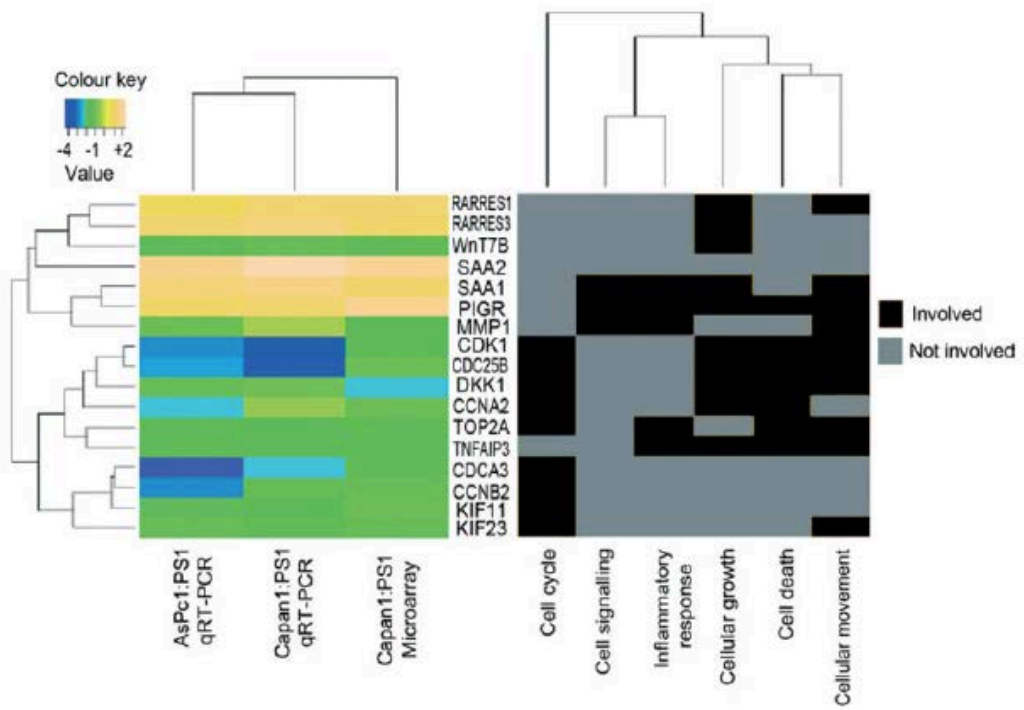

Figure 1.3: Gene expression changes as identified by gene-expression micro-array and verified by qRT-PCR.

Kadaba et al (70) identified pIgR as a gene involved in cellular functions such as cell signalling, inflammatory response, cell growth, death and movement. Figure produced from Kadaba et al (84).

1.5 Role of pIgA/ pIgR

Plasma cells are terminally differentiated B lymphocytes, play an integral role in the humoral immune response due to their ability to produce large volumes of antibodies which are antigen-specific. (82). Plasma IgA cell, are found throughout the lamina propria within organised mucosal-associated lymphoid tissues (83), underlying mucosal surfaces of the intestinal epithelium (84). 80% of the human body's plasma cells are located in the gastrointestinal system, thus, emphasising their importance in gastro-intestinal immune barrier (85).

Immunoglobulin A destined for the mucosal secretions is secretory IgA (SIgA) (86), which is produced by selective transport of polymeric IgA (pIgA) across epithelial cells lining mucosal surfaces (87). The transport of polymeric immunoglobulins (IgA, and to a lesser extent IgM) across mucosal epithelial cells is

mediated by virtue of its interaction with the polymeric immunoglobulin receptor (pIgR) (88), a trait only found in vertebrates (89).

SIgA (90) contains dimer of IgA subunits with a J-chain, covalently bound to a glycoprotein of about 80kDa (known as secretory component, which is synthesized by the epithelial cells lining mucous membranes and exocrine glands) (91). Further experimentation has identified the secretory component is a fragment of an integral membrane protein, called polymeric immunoglobulin receptor (pIgR)(88). Brandtzaeg and Prydz subsequently provided direct evidence for an integrated function of the J-chain and pIgR in the epithelial transport of immunoglobulins, by demonstrating that only polymeric IgA and IgM containing the J-chain (92) could bind to the surface of human intestinal epithelial cells expressing pIgR (91). Although IgA and IgM can be transported by pIgR at similar rates, the larger size of IgM restricts its diffusion to the receptor through the extracellular matrix and basement membrane, so the smaller polymeric IgA molecule is transferred more efficiently (93).

pIgR is synthesized as an integral membrane protein in the rough endoplasmic reticulum and then travels to the Golgi apparatus. In the last station of the Golgi, known as the trans-Golgi network (TGN), pIgR is sorted into vesicles that deliver it to the basolateral surface of the epithelial cells (91), where pIgR can bind to pIgA (produced by plasma cells, most commonly found in the lamina propria underlying the epithelium (94)) (Figure 1.6). With or without bound pIgA, pIgR is endocytosed and delivered to basolateral early endosomes (BEEs) (95). The receptor and ligand then move through a common endosomal compartment (CE) and are sorted into apical recycling endosomes (AREs) for delivery to the apical membrane. At this point, the extracellular portion of the pIgR, comprising five Ig-like domains, is proteolytically cleaved, losing its C-terminal domain to form the secretory component (SC). This secretory component is then covalently linked to the (IgA)2-J-chain complex by a disulphide bond, thereby protecting the SIgA from denaturation and proteolysis in external fluids (96). The carbohydrate residues on

SC help to anchor SIgA to the mucous lining of the epithelium, thereby ensuring effective immune protection (97). By attaching to the dimeric backbone of the secretory IgA, the SC-SIgA complex molecule confers resistance to digestion by trypsin and pepsin (98).

At this surface, cleavage of the extracellular ligand-binding portion of pIgR results in release of secretory component in free form or as part of the SIgA complex. A fraction of the pIgR at the apical surface may be re-internalised into the apical early endosomes (AEEs) and then delivered back to the apical surface through ARE. Mice with two disrupted alleles at the *pIgR* locus have markedly reduced IgA in external secretions (99), accompanied by elevated serum IgA, demonstrating pIgR is necessary for transcytosis of pIgA across epithelial *in vivo* (100).

1.5.1 The pIgR gene

The human pIgR gene, encoded by a single copy gene (101), is localised in the q31-q41 region of chromosome 1(102). Containing 11 exons, the gene spans 18kb (102). Situated between exon 1 and 2, the first intron is the longest (Figure 1.4). The initiation codon and the leader peptide are encoded by exon 2. Analysis has identified single-nucleotide polymorphisms in the human pIgR gene, some of which have been associated with increased risk of IgA nephropathy and nasopharyngeal cancer (103).

1.5.2 Structure of pIgR

The pIgR protein consists of three major functional regions: an extracellular ligand-binding region, a short hydrophobic membrane spanning domain and a relatively long cytoplasmic tail (Figure 1.5). The extracellular ligand-binding portion is comprised of five domains with homology to immunoglobulin variable domains, which is loosely connected by a structured linker peptide, sometimes called domain 6, to the transmembrane domain. The cytoplasmic tail of pIgR contains elements that interact with intracellular signalling proteins to regulate cellular trafficking.

Within the five extracellular Ig-like domains, the Cys residues that form disulphide bonds stabilise the characteristic “immunoglobulin fold” which are invariant across species. Interspecies homology is greatest in domain 1, especially within segments that have been shown to be critical for binding of IgA and IgM.

Domains 2 and 3 of pIgR are encoded by a single large exon in pIgR from mammalian species, which is sometimes spliced out in rabbit mRNA (104), but is invariably included in pIgR transcripts from other mammalian species.

The sixth extracellular domain of pIgR has a more random structure than the five immunoglobulin homology domain and is poorly conserved across species. Proteolytic cleavage of pIgR within this domain leads to the release of secretory component from the apical surface of epithelial cells, either free or bound to SIgA or SIgM. Given the random structure and poor conservation of domain 6, it is likely that multiple proteases can cleave pIgR to secretory component.

Membrane-bound pIgR and soluble secretory component have been shown to interact with a variety of physiological and pathophysiological ligands, through both peptide and carbohydrate-based motifs. The association of pIgR with polymeric IgA and IgM involves multiple structural elements that participate in both non-covalent and covalent bonds. Biochemical and mutagenesis studies have demonstrated that any domain of pIgR is both necessary and sufficient for binding of polymeric IgA and IgM (87).

The binding studies with isolated domain 1 suggest that structural determinants within this domain contribute to the specificity of pIgR for native pIgA, but the precise topology of the pIgR-pIgA interface and the role of the J-chain remain a mystery. The two N-glycan chains linked to domain 1 of pIgR do not appear to contribute to the interaction of pIgR with pIgA (105).

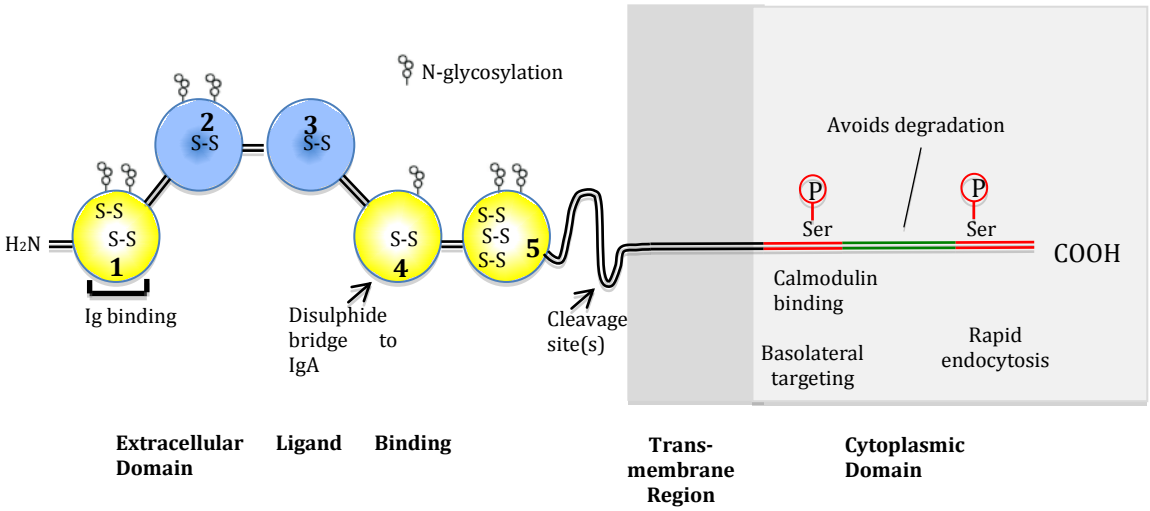

Figure 1.4: pIgR structure.

The pIgR is a transmembrane protein, which contains an extracellular ligand binding comprising five domains with homology to immunoglobulin variable regions and a long cytoplasmic tail. The tail also contains signals for intracellular sorting and endocytosis. The immunoglobulins 1, 4 and 5 (yellow) contain signals for non-covalent and disulphide bonding to polymeric IgA. The immunoglobulins 2 and 3 (blue) are less important, and are even absent in rabbit pIgR. During transcytosis, a disulphide bridge is formed between domain 5 of pIgR and the Fcα region of dimeric IgA. A peptide of unknown structure links domain 5 to the membrane-spanning region and contains sites for proteolytic cleavage of pIgR to secretory component (SC) (106). Seven N-glycan residues on domains 1, 2, 4 and 5 contribute to innate immune function of SC and may facilitate transcytosis of pIgR. The cytoplasmic domain or tail or pIgR contains highly conserved signals for intracellular sorting, endocytosis and transcytosis (107). Figure adapted from information in Kaetzel(108).

1.5.3 Regulation of pIgR expression

pIgR expression is restricted to mucosal and glandular epithelial cells. Since pIgR makes only one trip across these cells before being cleaved and released at the apical surface and because of the 1:1 stoichiometry between secretory component and dimeric IgA in SIgA, one molecule of pIgR must be produced for every molecule of dimeric IgA that is transported across an epithelial cell. Thus, upregulation of pIgR expression would increase the capacity for epithelial transcytosis of IgA. Regulation of pIgR expression involves complex interactions among host-, microbial- and environmental-derived factors, involving transcriptional and post-transcriptional mechanisms (94). A variety of cytokines, hormonal and microbial influences have been investigated, and a summary is provided in Figure 1.5.

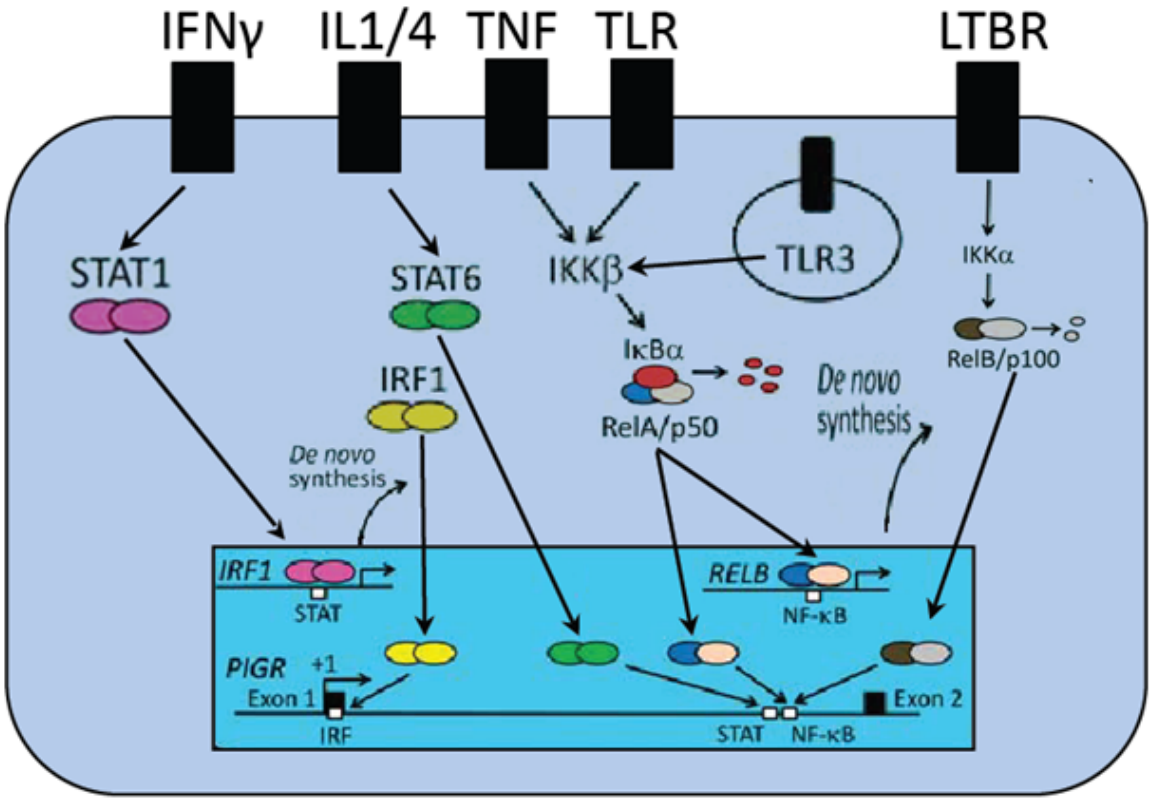

Figure 1.5: Molecular regulation of pIgR expression.

pIgR expression can be up- or down-regulated. Pro-inflammatory cytokines, interferon-γ (INF-γ), tumour necrosis factor (TNF) and interleukin-1 (IL-1) play a role in upregulation of pIgR expression (109). The roles of Toll-like receptors (TLR) and Lymphotoxin beta receptor (LBTR) are incompletely understood.

Adapted from (110). Figure adapted from information in Haelens et al

1.5.4 Transcytosis of pIgR

Although epithelia act as a physical barrier, they possess the ability to transport specific molecules via several routes (111). As polarised cells, they have distinct plasma membrane domains, which are the result of polarised trafficking of proteins and lipids. Thus epithelial plasma membranes are divided into two components, an apical surface facing the lumen and a basolateral surface contacting adjacent cells and underlying connective tissue, with distinct protein and lipid composition. Apical and basolateral surfaces are separated by cellular junctions, thereby preventing mixing of proteins and outer-leaflet lipids between two surfaces (95).

The polarised distribution of apical and basolateral components is the result of three processes. Newly synthesised proteins of the plasma are synthesised in the rough endoplasmic reticulum and transported through the Golgi to the trans-Golgi network (TGN), where they are sorted into vesicles that deliver them to apical or basolateral surfaces (112, 113). Some proteins are transported from the TGN to endosomes, and only then to the cell surface (114). Secondly, some proteins are selectively retained at the cell surface, often through an interaction of their carboxyl termini with PDZ-domain-containing proteins (115). The third step is that components not retained at the surface are rapidly endocytosed and delivered to early endosomes, from where they can be recycled back to the cell surface, transferred to late endosomes or transported across the cell and delivered to the opposite surface, in a process known as transcytosis (116). This provides the body a method of selectively uptaking and secreting molecules (95). All epithelial cells use biosynthetic sorting from the TGN and selective recycling or transcytosis to transport proteins to the correct surface, but relative importance varies with cell type.

Although IgA is being discussed primarily, it is important to note that IgM can also bind to pIgR. Both IgA and IgM have the ability to form polymeric structures, thus are the only two immunoglobulins that can bind to pIgR. Their ability to bind with pIgR allows them to pass through the epithelial layer and subsequent reach the external secretions (117). Under normal conditions in vertebrates, IgA, IgM and IgA immune complexes have been shown to bind to pIgR (118).

The process of pIgR mediated transport of pIgA begins in the rough endoplasmic reticulum of intestinal epithelial cells, where pIgR is synthesised as an integral membrane protein, and subsequently travels to the Golgi apparatus, which processes proteins produced by the endoplasmic reticulum. The Golgi apparatus, a wafer shaped stack in appearance, has two sides, one side facing the endoplasmic reticulum, *cis*, and the other facing the plasma membrane of the cell, *trans* (119). Proteins enter the *cis* side, and progress through a series of cisternae, which vary in number, shape and organisation in different cells types. Historically, the cisternae have been classified as three major groups, cis, medial and trans cisternae, but there are also two further groups called the *cis* and *trans* Golgi Networks, that have more variable structures. Having entered at the *cis* side and travelled one of the Golgi cisternae networks, the proteins gradually become modified and packaged. The final, packaged proteins exit at the *trans* side, ready for transport to various destinations by placement into one of three vesicles, dependent upon the molecular marker they carry (120).

These vesicles are exocytic, secretory or lysosomal, and will deliver pIgR to the basolateral surface of the epithelial cell (121). Exocytic and secretory vesicles contain proteins destined for extracellular release, while lysosomal vesicles deliver digestive proteases destined for the lysosome.

It was originally assumed that sorting of transmembrane proteins to the basolateral surface was the default pathway, and did not require a specific sorting signal. Further work has demonstrated that basolateral sorting requires a specific signal in the cytoplasmic domain, these being the 17 amino acids that lie closest to

the membrane (122). The 17 amino acid chain identified by Casanova et al was deemed necessary and sufficient for targeting of pIgR from the TGN to the basolateral surface, and is conserved across species.

It is also now apparent that there are multiple biosynthetic pathways for trafficking and recycling in polarised epithelial cells. There are two basic routes by which proteins and lipids reach their correct destination surface, they being either a direct or indirect route. In the direct route, proteins are sorted in the trans-Golgi network (TGN) into carriers that take them directly to the apical or basolateral surface (114). In the indirect route, proteins are sent first to one surface, usually basolateral. From there, the proteins are endocytosed and delivered to early endosomes. Endocytosed proteins can either recycle to the surface of origin, be degraded in late endosomes and lysosomes or be transcytosed to the opposite surface (116).

It is now agreed that material endocytosed from the basolateral surface enters basolateral early endosomes (BEE). These are largely vesicular structures that contain both membrane and fluid-phase markers fluorescein isothiocyanate (FITC) and horseradish peroxidase (HRP) (123), whilst also including material destined for degradation.

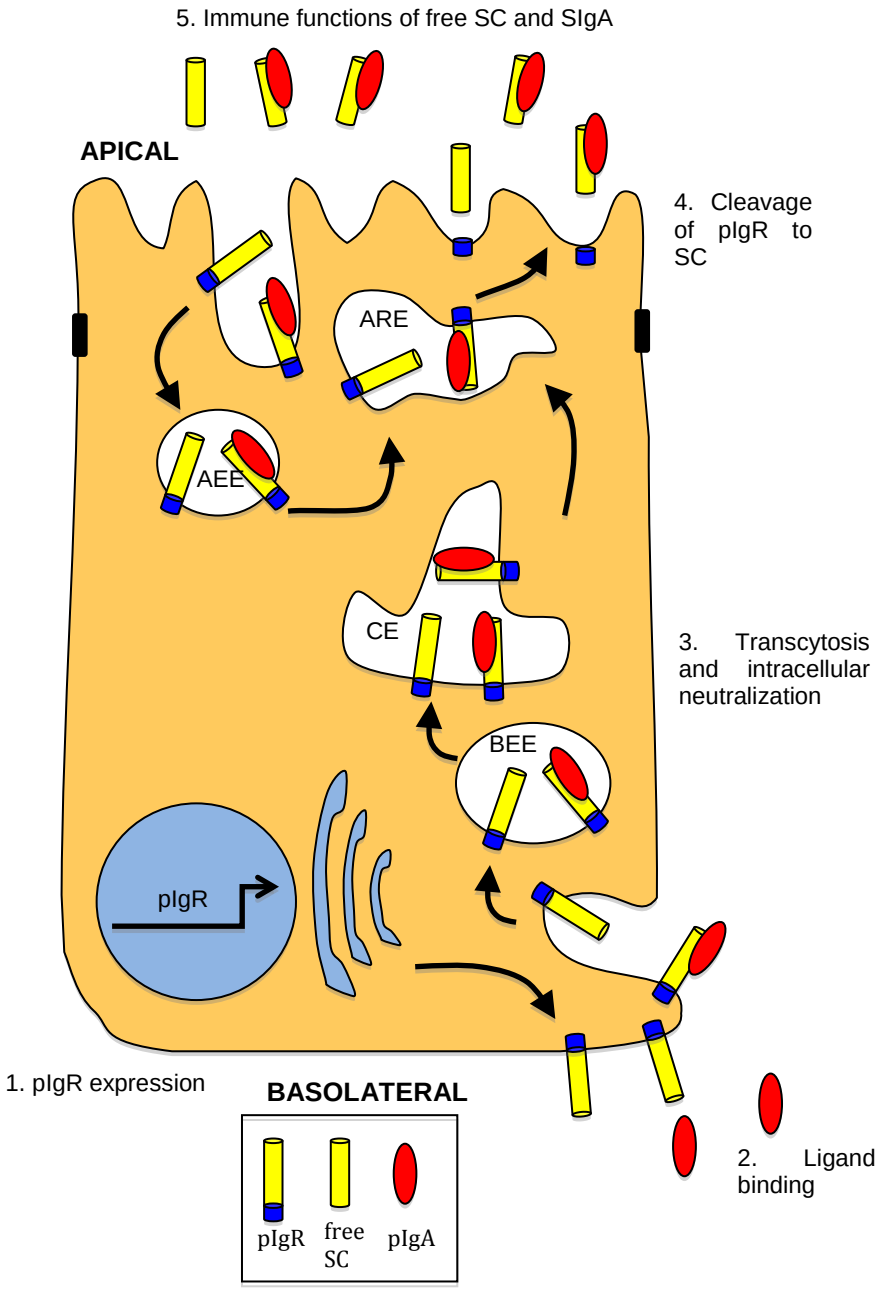

Figure 1.6: pIgR through an epithelial cell.

In the simplified epithelial cell illustrated, the apical surface is at the top and the basolateral surface at the bottom. Ligand binding occurs on newly synthesised pIgR that is targeted to the basolateral surface. Following receptor-mediated endocytosis, ligand-bound or unoccupied pIgR is transported through a series of intracellular vesicles, where neutralisation of pathogens and antigens can take place. At the apical surface, pIgR is proteolytically cleaved to secretory component (SC). At the mucosal surface and in external secretions, free SC and secretory IgA (SIgA) contribute to innate and adaptive immune defence. pIgA, polymeric IgA; BEE, basolateral early endosome; CE, common endosome; ARE, apical recycling endosome; AEE, apical early endosome Figure adapted from information in Kaetzel et al (107).

The next compartment in this intra-cellular transportation pathway is the common endosome (CE), identified by Rab10 (124), consists of tubules orientated along the apical-basolateral axis. These contain both transcytosing proteins (e.g. pIgR) as well as recycling proteins, in concentrations that are equivalent to the BEE, thus suggesting that sorting of recycling and transcytosing molecules has not occurred in either of the BEE or CE. IgA and pIgR moves from the CE to the apical recycling endosome (ARE), identified by Rab11 marker (125), next, which contains tubulovesicular and C-shaped elements that are largely clustered around the centriole, located beneath the center of the apical surface. This is the last known stage in the transcytotic pathway. For molecules endocytosed from the apical surface, it is likely that they first enter an apical early endosome (126, 127) (**Figure 1.6**).

Transcytosis of pIgR is regulated at multiple levels (121). Song et al demonstrated binding of pIgA can augment the rate of transcytosis in rabbit pIgR (128), whilst Singer et al indirectly demonstrated binding of Polymeric IgA (pIgA) to pIgR causes dimerisation of pIgR (129).

Within ten seconds of pIgA binding, several cytoplasmic proteins become tyrosine phosphorylated (130). Although the pIgR isn't itself a tyrosine kinase or phosphorylated on tyrosine, but it acts to recruit p62*yes*, a non-receptor tyrosine kinase, to the plasma membrane. The exact role of p62*yes* remains inconclusively proven, but mice with deletions in both alleles for p62*yes* exhibit minor defects in basal transport of pIgA from blood to bile, and exhibit a marked defect when challenged with a large bolus of intravenous pIgA (131).

Rab proteins are small GTPases that have been shown to regulate the formation of vesicles at the plasma membrane and the delivery of endocytosed proteins to multiple cellular locations (132). It also transpired that bound Rab3b (Rab in its GTP-bound state) appeared to block the transcytosis of pIgR, which then recycles to the basolateral surface.

Subsequent to cleavage, the pIgA-pIgR complex releases SIgA into the lumen (133, 134). SIgA, the secretory form, binds to antigens within the lumen, thus protecting intestinal mucosal surfaces against colonisation and invasion by pathogens (135).

The process of transcytosis of pIgA by pIgR promotes intracellular neutralisation and transcellular excretion of antigens and pathogens and ensures continuous delivery of SIgA to the epithelial surface and external secretions. Epithelial cells effectively sacrifice the extracellular domain of pIgR as cleaved SC, during each round of pIgA transport, as either free or complexed to pIgA. Although there is effective wastage and a metabolic cost of producing a new molecule of pIgR for each round of pIgA transport, this is effectively compensated for by the immune functions contributed by SC.

The role of pIgR in transportation of complexes of pIgA and protein antigens from lamina propria to luminal surface of mucosal epithelial cells was originally identified by Mazanec et al (118). Locally produced pIgA antibodies within the mucosa might serve to trap antigens derived from the environment, diet or luminal microbiota in the mucosal tissue during infections and to target these antigens for excretion. Antigens remain bound to the pIgA antibody throughout transcytosis, escaping lysosomal delivery and degradation and are released along with SIgA at the apical surface (136).

Despite considerable investigation and speculation during the past three decades, the exact mechanism by which pIgR is cleaved to SC remains a mystery. The previously described domain 6, that links the immunoglobulin-like domain 5 to the transmembrane region of pIgR, has demonstrated cleavage. Further investigation by purifying SC from human colostrum pooled from multiple women demonstrated a ragged C-terminus, with Ser552 as the dominant C-terminal residue (137). The main issue remains the length of the linker peptide is poorly conserved across species, and that the C-terminal protein sequence is only a trait found in humans.

Further difficulties remain with identification of the proteases that cleaves pIgR to SC. Ogura show that cleavage of pIgR was inhibited by leupeptin, but enhanced by PMA stimulation (138). Leupeptin has also been identified as an inhibitor of cleavage of pIgR to SC in rat liver and MDCK cells, thereby suggesting a requirement for a cysteine protease (139), but a SC protease remains elusive. This suggests that the protease (or indeed proteases) are not cell-specific and possibly that multiple proteases might participate in SC cleavage.

1.51.6 Immunoglobulins

Immunoglobulins are produced by plasma cells and belong to the immunoglobulin superfamily. Their structure is two large heavy chains and two small light chains (140), with various combinations of chains producing different types of immunoglobulin. IgA, which exists as two types, is predominately found in mucosal areas, such as the gut, respiratory tract and urogenital tract, and prevents colonisation by pathogens. To a lesser extent, it is also found in saliva, tears and breast milk (141). IgM is expressed on the surface of B cells, as a monomer, but is secreted in a pentameric form with very high avidity. It eliminated pathogens in the early stages of humoral immunity before there is sufficient IgG.

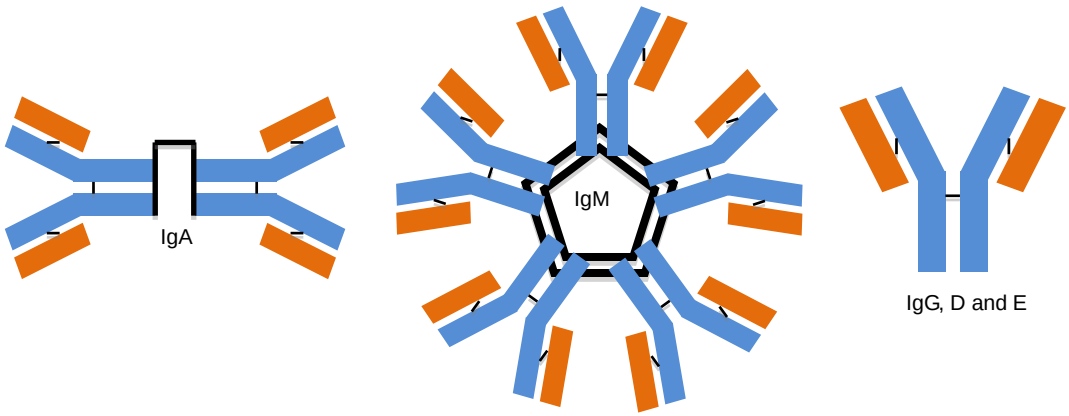

Figure 1.7: Immunoglobulins

Formed from two heavy chains (blue) and two light chains (orange), whilst the black lines are O-linked sugars. The IgG, D and E all have similar configurations, only slightly different bonds between the chains. IgA forms dimers or polymers, whilst IgM forms a pentameric structure.

Immunoglobulin A (IgA), an antibody that plays a crucial role in mucosal adaptive immunity (141) (142), has two isotypic forms (IgA1 and IgA2) (143). Unlike other immunoglobulins, it can exist in a variety of molecular forms, each with a characteristic distribution in various body fluids (144), the predominant form being the dimeric version.

IgA1 predominates in serum (~80%), and most lymphoid tissues have a predominance of IgA-producing cells. IgA2 have their heavy and light chains linked with non-covalent bonds instead of disulphide bonds, and percentages are higher in secretions in serum (~35%) (145). In secretory lymphoid tissues, e.g. gut-associated lymphoid tissue, the share of IgA2 production is larger than in non-secretory lymphoid organs, e.g. spleen and peripheral lymph nodes (146).

The first line of specific defence against environmental antigens is secretory immunoglobulin A (sIgA) (86), and is the main immunoglobulin found in mucous secretions. sIgA is transported in massive quantities, up to three grams per day in the average adult (147), and equates to 75% of the total immunoglobulin produced in the body (148).

It is also possible to distinguish the forms of IgA based on their location, thus serum IgA or secretory IgA. Serum IgA, which is synthesised mainly in the bone marrow, is predominantly a monomer of IgA1. This IgA is composed of two $\alpha 1$ chains, each of 60kDa and containing one variable domain, a hinge region, and three constant domains (CH1, CH2 and CH3). The $\alpha 1$ chains are linked by disulphide bonds to each other and the two light chains (λ or κ chains) that are identical to those found in other immunoglobulins (149). Approximately 10% of the IgA compromises dimeric and higher polymeric forms, and the proportion of these forms increases in a number of disease states (150).

Secretory IgA (SIgA) is the form of IgA synthesised at mucosal surfaces and found in secretions, e.g. within the gut and respiratory tract, and is found as a

polymer of two to four IgA monomers. Dimeric and polymeric forms of IgA contain an additional protein known as the J-chain (91), which links the IgA monomers via the tailpiece (an 18 amino-acid extension of the α chain). In addition to the J-chain, dimeric and polymeric forms of IgA are complexed with a heavily glycosylated protein called the secretory component (SC). The secretory component is part of the cell surface receptor that mediates the transport of polymeric IgA across the epithelial barrier, and is thought to provide stability to the structure of SIgA to increase its resistance to proteolytic degradation (92). Secretory immunoglobulin A (SIgA), consisting of ten protein chains linked by disulphide bonds, forming the IgA-J-IgA-SC complex.

SIgA differs from IgG in two ways: it is polymeric in nature and it contains covalently bound secretory component, the cleaved extracellular portion of transmembrane secretory component which constitutes polymeric immunoglobulin receptor (151). SIgA is generated via the active transport of pIgA to the intestinal lumen by SC/ pIgR-expressing epithelial cells (152).

1.5.7 J-Chain

The J-chain, rich in acidic amino acids, comprises a single polypeptide chain containing eight Cys residues, six of which form intra-chain disulphide bridges (153). Its presence has been demonstrated in a wide range of vertebrate species, from mammals to fish and amphibians (154) and it is a highly conserved structure across different species.

The J-chain is expressed by antibody-producing cells and is incorporated into polymeric IgA or IgM shortly before or at the time of secretion (155), and its presence promotes formation of pIgA and pentameric IgM (156). The J-chain is the key protein in the generation of SIgA because it promotes polymerisation of IgA and because its presence in these polymers is believed to be required for their binding to SC/pIgR (157, 158).

Since the immune system has a large role in elimination of pre-cancerous lesions and cancer mitigates the risk by escaping immune-surveillance, immune-oncology is a burgeoning field of investigation (159-161). Currently, adaptive immunity is being studied with great zeal, with significant therapeutic benefit for patients with melanoma, and haematological malignancies (162, 163).

For epithelial tumours, study of innate immunity the first line of defence seems to be the most logical addition (164). In this context, studying immunoglobulins and its cognate receptor seems to be a valid avenue of investigation (165).

1.6 The role of pIgR in cancer

Initial work regarding the role of pIgR focused around Streptococcal pneumonia, which traverses the respiratory epithelial barrier to invade, allowing it to cause disease locally or disseminate via blood circulation throughout the body. *S. pneumoniae* choline-binding protein A, a pneumococcal surface protein, interacts specifically with the human polymeric immunoglobulin receptor, which is expressed by cells in the respiratory epithelium. Choline-binding protein A is required for efficient colonization of the nasopharynx *in vivo*. Additionally, a strain of *S. pneumoniae* invades a human pharyngeal cell line in a human polymeric immunoglobulin receptor-dependent manner. These findings raised the possibility that the interaction between choline-binding protein A and human polymeric immunoglobulin receptor may be a key determinant of *S. pneumoniae* pathogenesis (166).

This triggered an interest in nasopharyngeal cancers (167). More recently, the role of pIgR has gained more importance in its role in gastrointestinal cancers (**Table 5**).

Agesen et al (168) investigated Affymetrix gene expression in 315 patients with colorectal cancer, stratifying patients based on stage of disease. They identified pIgR to be one of 13 genes for prognosis prediction specific to patients with stage II

colorectal cancer. Of the 13 genes, 5 demonstrated low expression, whilst 8 had high expression in stage II colorectal cancer disease. Poor prognosis and higher relapse rates were noted with low pIgR expression.

Traicoff et al (169) investigated in vitro models of colon adenoma to carcinoma progression, alongside differential display RT-PCR. They identified pIgR was highly expressed in normal colon epithelium, but was decreased in 6 of 8 colon tumours, and negligible in 8 of 10 colon cell lines. Thus hypothesising low pIgR expression to correlate with progression from colon adenoma to carcinoma.

Gologan et al (170) investigated pIgR expression in the upper gastrointestinal tract, investigating pIgR expression in 42 cases of adenocarcinoma of the distal oesophagus and gastro-oesophageal junction. They noted pIgR negative adenocarcinomas to be associated with lymph node metastasis and a trend towards reduced survival.

Fristedt et al (171) further explored pIgR expression in adenocarcinoma of the upper gastrointestinal tract, investigating 173 patient samples, and separating them according to intestinal metaplasia and adenocarcinoma. pIgR expression was significantly higher in intestinal metaplasia compared to normal tissues, whilst reduced pIgR expression in primary tumours was significantly associated with more advanced tumour stage.

Furthermore, loss of PIGR expression has been linked to tumour progression in non-small cell lung cancer (172), while overexpression of PIGR has been associated with the less aggressive type 1 endometrial cancer (173) as well as correlating with a better prognosis in bladder cancer (174) and epithelial ovarian cancer (175).

PIGR has been described as a putative cancer biomarker in a few studies on different cancer forms, the majority of which indicate an association between low PIGR expression and more aggressive disease (Table 5).

	Year	Organ	Findings
GASTROINTESTNAL CANCERS			
Fristedt et al (176)	2014	Pancreatic and periampullary	High pIgR expression signifies more favourable tumour phenotype and low expression independently predicts a shorter survival in patients with pancreatic and peri-ampullary cancer.
Liu et al (177)	2014	Hepatic colorectal metastasis	Positive pIgR expression associated with poor prognosis of patients with colon carcinoma hepatic metastasis. There is scope for pIgR to be a predictor for poor prognosis of patients after resection
Fristedt et al(171)	2014	Oesophageal and gastric	High pIgR expression predicts a decreased risk of recurrence and improved survival in patients with adenocarcinoma of the upper GI tract.
Kadaba et al (70)	2013	Pancreatic Stroma	Reciprocal relationship of E-cadherin and pIgR in cancer cells. Demonstrate context-specific cancer-stroma crosstalk required to be precisely defined for effective therapeutic targeting.
Alvi et al (178)	2013	Barrett's Oesophagus	One of four genes noted to be used to distinguish between Barrett's and dysplasia/ Oesophageal adenocarcinoma
Agesen et al (168)	2012	Colorectal Cancer	One of 13 genes noted to be present in patients with stage II colorectal Ca and the probability of relapse
Ai et al (179)	2011	Hepatocellular Cancer	pIgR plays a role in the induction of EMT. pIgR as a potential link between hepatitis B virus-derived hepatitis and HCC metastasis and provide evidence in support of pIgR as a prognostic biomarker for HCC and a potential therapeutic target.
RESPIRATORY CANCER			
Su et al (180)	2011	Nasopharyngeal Cancer	Missense mutation in human pIgR, A580V, is associated with IgA nephropathy and nasopharyngeal carcinoma
Ocak et al (181)	2012	Lung tumourgenesis	pIgR expression lost in pre-invasive and invasive respiratory lesions
Chang et al (182)	2005	Nasopharyngeal Cancer	Nasopharyngeal cancers show significant downregulation of pIgR
Fan et al (167)	2005	Nasopharyngeal Cancer	pIgR gene may be associated to risk of Nasopharyngeal cancer development
Khattar et al (172)	2005	Lung Cancer	PIGR expression varies in different types of lung carcinoma, and is down-regulated during tumour progression

Table 5: Table summarising role of pIgR in other cancers

1.7 The role of pIgR in Hepatocellular Carcinoma

I have focused on hepatocellular carcinoma (HCC) because of its relevance to pancreatic diseases as well as the most detailed study published on pIgR thus far. HCC is the fifth most common cancer worldwide and the third leading cause of cancer related death worldwide (183). HCC has been associated with chronic hepatitis (184), secondary to inflammation due to hepatitis B virus (HBV) or hepatitis C virus (HCV) and alcohol consumption (185). Indeed, over half the cases of HCC worldwide have been attributed to chronic hepatitis B (186).

Despite the strong association between chronic hepatitis and HCC being known for decades, the molecular mechanisms to the progression remain unclear. HCC progression develops against a backdrop of persistent inflammation, extensive tissue remodelling and excessive deposition of extracellular matrix components (187). Increasingly, links between inflammation and HCC tumourgenesis have begun to explain the development of metastasis. The epithelial-mesenchymal transition (EMT), in which epithelial cancer cells lose their apico-basal polarity and become motile mesenchymal cells (188), effectively endowing tumour cells with metastatic competence (189), has been implicated in cancer invasion and metastasis (190) and also resistance to therapy (191).

Ai et al (81) identified pIgR as a possible inflammatory stimulus marker even though pIgR aberrant expression has previously been associated with HCC (192). Ai et al demonstrated pIgR over-expression is implicated in EMT initiated cross-talk mediated by transforming growth factor beta (TGF-ß) and TNF-α, interferon-δ and interleukin-4. TGF-ß is critical in promoting immune evasion and angiogenesis (193). Ai et al also noted, *in vivo* pIgR-overexpressing cells yielded higher extent of lung metastases compared with control counterparts in murine experiments associated with decreased levels of epithelial markers (E-Cadherin, cytokeratins) and enhanced levels of mesenchymal markers, Vimentin and phospho-Smad2/3 in pIgR-over-expressing HCC human specimens (194), thus postulating a linkage

between pIgR over-expression and EMT and inflammation.

.

1.8 The role of pIgR in pancreatic adenocarcinoma

Peri-ampullary cancers include those of pancreas (PDAC), extrahepatic bile duct, ampullary and small intestinal (including duodenal) adenocarcinoma (195). Survival after resection of adenocarcinoma of peri-ampullary location (pancreatic head, distal bile duct, ampulla, duodenum) differs greatly, with duodenal and ampullary displaying a much better survival than pancreatic head PDAC or distal bile duct cholangiocarcinoma (196).

.

Furthermore, there is differences in survival for ampullary cancers: intestinal versus pancreatobiliary (PB) histopathologic phenotypes demonstrates the importance of sub-types of cancers(197). The intestinal type proved to be associated with considerably better prognosis than the PB subtype, which has been confirmed by several recent series (196, 198, 199).

To enhance this further, additional molecular-based biomarkers are needed, to better define clinically relevant sub-groups of these tumours, and, thus, pave the way for novel treatment strategies (176). One such example could be pIgR.

Comparatively few studies have investigated the expression and prognostic significance of pIgR in human cancer, but the majority indicate associations of a high pIgR expression with a more favourable phenotype and an improved survival (168, 170, 171, 175, 200). However, adverse prognostic implications of pIgR expression in human cancer have been observed in hepatitis B-derived hepatocellular carcinoma, where high pIgR expression was found to be associated with a greater metastatic potential and poor prognosis (179). One could speculate that if pIgR is naturally expressed in the particular tissue (epithelium), such as the gut or respiratory tract, then in the context of cancer, low expression confers poor prognosis. Should pIgR not

play a natural role in a particular tissue such as liver (or pancreas), then its expression in cancer may be associated with a poor prognosis (179).

Kadaba et al demonstrated pIgR to be unregulated in pancreatic cancer cells upon exposure to stromal cells *in vitro* in 3D organotypic models (70). Using quantitative real-time RT-PCR, they investigated several of the most up-regulated and down-regulated genes across two pancreatic cancer cell lines (Capan1 and AsPC1). Kadaba et al then clustered them into four groups affecting one or more key cellular functions and identified pIgR as being significantly up-regulated in cancer cells upon exposure to stellate cells.

Kadaba et al found that PIGR expression was predominantly observed in cancer cells when stellate cells were most predominant (stellate proportion of 0.66–0.83) and was inversely correlated with E-cadherin expression. Thus, they confirmed the reciprocal changes in E-cadherin and PIGR changes in human PDAC samples. This reciprocal relation of E-cadherin and PIGR expression correlated with the stromal predominance in human samples (70).

Fristedt et al (176) investigated pIgR expression in human pancreatic and peri-ampullary adenocarcinomas. They sampled 175 patients who underwent pancreatoduodenectomy resection and separated patients according to intestinal and pancreato-biliary type, based on morphological origin of tumour. They also investigated and sampled lymph node metastasis and correlated with clinic-pathological parameters.

The study is large and all the patients have, surprisingly, distant metastasis-free survival. Initial data in the manuscript focuses on pIgR expression in non-malignant, benign pancreas and lymph node metastases. This is irrelevant of histological tumour type and 98% of all primary tumours expressed pIgR of some intensity. 89.5% of lymph node metastases also expressed pIgR. There is extensive variability in the pattern of pIgR staining, and although it is noted, no explanation is

given as to why the variability exists.

The results and conclusion state that patients with low pIgR expression have adverse clinico-pathological characteristics, and a significantly shorter RFS and OS. pIgR expression was not predictive of response to any type of adjuvant chemotherapy, but the prognostic value of pIgR remained significant after adjustment for established clinico-pathological characteristics, including morphology, i.e. pancreato-biliary and intestinal type, and adjuvant treatment. Survival analyses, stratified by morphological type, demonstrated that the prognostic value of pIgR was significant in intestinal type tumours but not in pancreato-biliary type tumours.

However, a significant down-regulation of pIgR in lymph node metastases compared to primary tumours in the entire cohort, was more evident in pancreato-biliary type tumours than in intestinal type tumours, which supports a tumour suppressive role for pIgR in this type of tumours as well. The lowest expression of pIgR was seen in tumours of pancreatic origin, i.e. pancreato-biliary type and the highest in primary tumours of duodenal origin, i.e. intestinal type.

The results and their discussion suggest pIgR appears to be strongly expressed in normal mucosa of the gastrointestinal tract, including the duodenum, but also in normal pancreatic ductal but not acinar cells. There is no quantifiable statement regarding the intensity of staining in normal and pancreatic adenocarcinoma.

The finding that a high pIgR expression is associated with more favourable clinico-pathological characteristics and loss thereof with an adverse clinical outcome is in line with the vast majority of hitherto published studies in other cancer forms. However, the mechanistic basis underlying the potential tumour-suppressing role for pIgR in pancreatic and peri-ampullary adenocarcinoma, as well as in several other cancer forms, remains to be elucidated.

A theory remains that given the fact that an extensive desmoplastic stromal reaction is one of the hallmarks of pancreatic cancer (201), it may be hypothesized that elevated pIgR expression exerts tumour-promoting effects also in pancreatic and peri-ampullary adenocarcinoma. However, Kadaba et al (70) demonstrated a reciprocal relationship between expression of E-cadherin and pIgR in pancreatic cancer cells, and that this relationship, in turn, is dependent on the stromal content, in particular the proportion of activated stellate cells. The reciprocal relationship between pIgR and E-cadherin was also confirmed in an analysis of 51 human ductal pancreatic cancer samples (TMA), further indicating a link between pIgR and EMT also in pancreatic cancer.

Alongside, the work from Ai et al (179) which supports a tumour-promoting role for pIgR, where high pIgR expression was found to be associated with early recurrence and chronic hepatitis B-virus (HBV)-infection. Moreover, pIgR was found to induce epithelial-mesenchymal transition (EMT) *in vitro* and *in vivo* through activation of Smad signalling, suggesting a role for pIgR as a mediator of inflammation-induced EMT.

Thus, the work from Fristedt is contradicting to other stated work. However, their data remains the largest cohort of patients and further highlights the complexity and heterogeneous nature of tumours arising in the pancreas and peri-ampullary region. The raw data relating to individual histological diagnoses, especially primary pancreatic adenocarcinoma is not significant. Theoretically, the role of pIgR in carcinogenesis and tumour progression appears to differ by histological type and tumour origin.

With a strong association with inflammation and pancreatic cancer, the investigation that we aim to answer is the role of pIgR in pancreatic cancer and its expression with metastases. The aim of this study was therefore to examine the role and expression of pIgR in pancreatic cancer, and its prognostic impact.

1.9 Aims

To investigate the role of pIgR in pancreatic ductal adenocarcinoma.

1.10 Objectives

1. Investigate expression of pIgR in human peri-ampullary cancers including pancreatic cancer (PDAC) and its correlation with systemic and tissue factors (CHAPTER III).
2. Screen pancreatic cancer cells for pIgR expression and secretion (CHAPTER IV).
3. Investigate expression of pIgR in 3D model of pancreatic ductal adenocarcinoma and its correlation with EMT (CHAPTER IV).
4. Investigate changes after modulation of pIgR expression in PDAC (CHAPTER IV).

CHAPTER II

MATERIALS

AND METHODS

2.1 Tissue microarray

Tissue Microarrays contain numerous cores from various patients and allows rapid analysis of multiple patients.

Tissue microarrays were constructed from pancreatic tissues obtained, after establishing histological diagnosis, following surgical resection of the pancreas (in the form of pancreatoduodenectomy, distal pancreatectomy or total pancreatectomy).

Specimens were collected from patients undergoing pancreatic resections at the Royal London Hospital, Whitechapel, England. The enrolment criterion was suspected or proven pancreatico-biliary diseases (Ampullary carcinoma (AC), cholangiocarcinoma (CC), chronic pancreatitis (CP), mucinous cystic neoplasm (MCN), duodenal carcinoma and biopsies or resections for pancreatic ductal adenocarcinoma (PDAC), with ability of complete clinico-pathological and follow-up data. Overall survival was defined as the interval between surgery and either death. Data were censored to the last clinical observation made on 31st December 2015.

Patients gave written informed consented for the tissues obtained (City and East London Local Research Ethics Committee 07/H0705/87). 157 patients were sampled in total and two sets of microarrays were constructed. The first set (Batch A) had been constructed by Froeling and Mirza (59, 202), whilst the second set (Batch B) were constructed by Ene-Obong (203) and both had been used for previous published work. The number of patients with each disease on the two sets of TMA's is listed in (**Table 6**).

Pancreatico-biliary disease	Number of patients		
	Batch A	**Batch B**	**Total**
Ampullary Carcinoma	0	9	9
Cholangiocarcinoma	9	12	21
Chronic Pancreatitis	0	4	4
Mucinous cystic neoplasm	0	6	6
Duodenal carcinoma	0	5	5
Normal	0	14	14
PDAC (resected)	63	0	63
PDAC (biopsy)	0	35	35
Total	72	85	157

Table 6: Pancreatico-biliary disease: patient numbers incorporated within respective TMAs.

In order to construct each TMA, a representative slide of each patients donor block was cut and stained with haematoxylin and eosin (H&E). Prof Hemant Kocher and A. Ene-Obong identified multiple regions of tumour, stroma and normal pancreas on each slide and these were circled, using the Axiophot microscope (Carl Zeiss Micro Imaging LLC, New York, USA). The regions were colour coded, red represented stroma, blue represented normal and black represented tumour regions (203).

Once regions of slides had been identified, a map for each TMA slide was constructed on Excel (Microsoft, Seattle, USA), in order to aid TMA construction and for referencing during TMA analysis.

At least three cores from tumour and a further three from adjoining stroma, each being 1mm in diameter were obtained from the donor blocks and transferred to the recipient paraffin block at defined positions, according to the TMA map. Furthermore, three cores of adjacent normal tissues were sampled from patients with duodenal cancer and cholangiocarcinoma. One core of normal human spleen was

inserted in the recipient block in order to aid guiding and orientation of the TMA slide.

I ensured that always at least 3 cores were available for analysis per patient. On an average 6 cores were arranged on TMA per patient, but some cores were not analysed because of artefacts, loss of cores (dropouts), folded cores, missing cancerous tissues as the core goes deeper into the tissue.

TMA construction was performed using Tissue Arrayer Minicore® (Alphelys, Plaisir, France). Upon completion, recipient blocks were kept at 37°C overnight to ensure bonding of the cores with paraffin wax of the recipient block and sent to pathology for sectioning to multiple slides.

My involvement was to complete all clinic-pathological parameters. I reviewed all clinical data relating to all 157 patients. I started by reviewing clinic letters, assimilating histopathology reports, date of operations and survival, along with pre-operative blood test results. These results were added to the TMA map up until 31st December 2015. The clinico-pathological parameters acquired were as follows:

- Date of birth
- Date of operation
- Age at operation
- Date of death
- Survival (days)
- Histological diagnosis
- Histological differentiation
- TNM staging
- Resection status (R0/1/2)
- Nodal count and positivity
- Pre-operative total and differential While cell count (≤3 days from operation)
- Pre-operative CRP (≤3 days from operation)

- Pre-operative Ca19-9 (≤7 days from operation)

More than fifteen years after its introduction (204), the TMA technique can be considered a well-established platform for tissue biomarker studies, providing similar or even better prognostic information than full-face tissue section based analyses (205). However, issues related to suboptimal sampling remain. In our cores, we have observed loss of cores, folding of the tissue core and reduction of representative tumours in the tumour cores. Stroma was also sometimes noted in cores labelled at tumour.

There are a variety of possible explanations, such as technical errors made during sectioning and the three-dimensional nature of tumours. In order to minimise the errors, an abundance of tumour cores from each patient were taken to ensure confident analysis.

2.2 Cell Culture

2.2.1 Cell Lines, media and culture reagents

2.2.1.1 Pancreatic Cancer Cells

The following pancreatic cancer cell lines were used (**Table 10**)

Cell Line	Source	Differentiation	Mutation
Capan 1	Liver metastasis	Well	KRAS, TP53, INK4A, SMAD4, BRCA2 (206) (207)
Capan 2	From primary tumour	Well	KRAS, TP53, silent mutation of INK4A, SMAD4 (207)
CFPAC1	Liver metastasis in a patient with pancreatic cancer and cystic fibrosis	Well	KRAS, TP53, SMAD4 and methylated INK4A, CFTR (CFTRΔF508) (206) (208)
PaTu8988T	Liver metastasis	Well	KRAS, TP53 with methylation of the 5'CpG island of INK4A (209)
AsPC1	Ascites	Moderate	KRAS, TP53 and INK4A (210) (211)
HPAF	Ascites	Moderate	KRAS, TP53 and INK4A (211)
PaCa3	Primary tumour	Poor	Methylation of 5'CpG island of INK4A (212)
Panc1	Primary tumour	Poor	KRAS, TP53 and INK4A (211) (213)
PaTu8988S	Liver metastasis	Poor	KRAS, TP53 with methylation of the 5'CpG island of INK4A (214)

Table 7: Pancreatic Cancer Cell lines

2.2.1.2 Stromal Cells

Using the outgrowth method (74), pancreatic stellate cells were isolated from an unused, normal, adult male human pancreas (donation for transplantation) donated by the UK Human Tissue Bank (Ethics approval; Trent MREC (05/MRE04/82)). The resulting cell strain, designated FS1, was verified as being of stellate cell origin based on the expression of characteristic stellate cell markers, such as presence of lipid droplets in the cytoplasm and expression of cytoskeletal proteins GFAP, Desmin, Vimentin and αSMA (73). FS1 stellate cells were immortalised, using ectopic human telomerase reverse transcriptase (hTERT) expression by Dr Fiona Li and Ms Jennifer Sandle previously from our laboratory (215). Cells were labelled as PS1 after confirmation of immortalised cell telomerase activity and continuous passage without loss of phenotypic characteristics over the last nine years.

2.2.1.3 Pancreatic ductal epithelial cells

hTERT immortalised human ductal epithelium (DEChTERT) cell lines were used as control pancreatic ductal cell lines (216).

2.2.1.3 MOCRI cells

Using the Ethics approval in 2.2.1.2, pancreas from patients with PDAC were initially digested and centrifuged. The cells that were obtained were sorted by Flow Cytometry, by isolating EPCAM negative and CD45 negative cells; thus we theoretically excluded epithelial and lymphocytic cell lines. The resulting population of cells were tested for expression of cytoskeletal proteins, as described above. This was performed by Mo Ghallab and Christina Ghirelli (unpublished data) and therefore named MOCRI.

2.2.1.4 Culture conditions and routine cell culture

Pancreatic cells were cultured as adherent monolayers in sterile tissue culture

flasks in a humidified atmosphere at 37°C, 8% CO_2 in either RPMI (PAA Laboratories, E15-842; AsPC1, PaCa3, Capan1) or Dulbecco's Modified Eagle's Medium (DMEM, PAA Laboratories, E15-843; Capan 2, CFPAC1, Suit 2, HS766T, Panc1, Colo357, Mia, BxPc3, 818, PaTuT/ PaTuS) medium. This was supplemented with 10% foetal bovine serum (FBS, Biosera). PS1 stellate cells, after hTERT immortalisation were grown, at the same humidified culture conditions as PDAC cells, in DMEM: F12 (Invitrogen, 11320-074) medium, respectively, supplemented with 10% FBS and 1µg/ml Puromycin as a selection agent. Pancreatic ductal epithelial cells were grown in DMEM supplemented with 10% FBS (DEChTERT).

When cells reached 80% confluency, medium was aspirated off and Trypsin-EDTA (PAA Laboratories, L11-003) was added for 3-5 minutes at 37°C to detach cells from the surface. Once cell detachment was confirmed under a light microscope, the trypsin was deactivated with medium containing 10% FBS. The cell suspension was centrifuged for 3 minutes at 1200 revolutions per minute (rpm), followed by removal of supernatant and re-suspension of the cell pellet in standard medium. If counting cells was required, 20µl of cell suspension was pipetted into a haemocytometer prior to centrifugation and cells were counted manually under a light microscope. Cells were sub-cultured at various ratios (1:2 to 1:5) depending on their growth rate.

For storage of cells, cell pellets were re-suspended in a mixture of 90% FBS with 10% dimethyl sulphoxide (DMSO) which acts as a cryo-protectant. In one millilitre aliquots in a cryovial, cells were slowly frozen, first at -80°C to prevent ice crystal formation and then transferred to liquid nitrogen for long-term storage.

When recovering cells from liquid nitrogen stocks, cell suspensions were thawed as quickly as possible at 37°C in a water bath. Once thawed, cell suspensions were transferred to a 15ml falcon tube containing standard medium. To remove

DMSO, the cell suspension was centrifuged at 1200rpm for 3 minutes, the supernatant removed and re-suspended in standard medium and plated onto a tissue culture flask.

2.3 Immunostaining

2.3.1 Cells cultured on coverslips

Cells were seeded onto a 13mm diameter coverslips in a 6 well plate as a monoculture at a density of $2.5x10^5$ per well.

For immunofluorescence, cells were fixed with 4% formaldehyde, permeabilised with 0.1% saponin/ PBS, blocked with 6% BSA and incubated for 1 hour at room temperature with primary antibody (Table 8) followed by appropriated fluorescently labelled secondary antibody (Table 8). Nuclei were stained with 4',6-diamidino-2-phenylindole (217). Negative controls were incubated with isotype specific immunoglobulins at the same concentrations as the primary antibody used.

2.3.2 Paraffin embedded gels and patient tissues

For Immunofluorescent staining of paraffin embedded gels and patient tissue, 4µM sections were dewaxed in xylene (twice for 5 minutes) and rehydrated (in reducing concentrations of ethanol; 100%, 80%, 70%, 50% and distilled water). Antigens were retrieved by boiling sections in 10mM citrate buffer (pH 6.0) for 20 minutes. Sections were blocked with 6% BSA/PBS and incubated with primary antibody overnight at 4°C, followed by one hour incubation at room temperature with the appropriate secondary antibody and DAPI. Negative controls were incubated with isotype specific immunoglobulins at the same concentration as the primary antibody used. Positive controls for normal human pancreas whole sections, treated as described with pIgR primary antibody.

2.3.3 Immunofluorescence

For all experiments where pixel intensity was analysed, three separate experiments were carried out and at least three random fields were analysed. For every experiment, there were three biological and three experimental repeats.

To ensure that the replicate experiments for immune fluorescence staining had comparable images, a number of precautions were taken. All technical replicates had same antibody mastermixes and staining was carried out simultaneously. Image acquisition was done with same laser strength and offset/gain thresholds across experiments. The normalisation was set to respective negative control (IgG) and positive control (e.g., normal human duodenum) to ensure that the best signal to noise ratio was set. These setting were then kept constant for all image acquisition taken at same sitting on microscope. All post-image acquisition analysis was done in Image J or Photoshop with same settings across various replicates using standard operating procedure and pre-set formulae.

Total pIgR and E-Cadherin levels were quantified with Image J “Analyze” software function. Images were taken at x40 magnification; the area of green or red stain within the region of interest was determined. Colour images had colour channels split, using the ‘Split channel function’. The ‘Threshold’ function then provided initial thresholds that were set and kept constant for all images. The intensities in the green and red channel were normalised with IgG controls and background fluorescence and calculated in an unbiased, blinded manner The ‘Analyze’ function enabled small particles, less than 25µm to be omitted from calculation. Small sized particles maybe debris or dead cells, thus accounting for some background staining. Calculation of pixel intensity for each channel background was calculated using the “Process and subtract background” in Image J, to calculate background intensity staining and then subtract that from the final image staining pixel intensity. By utilising the subtract background macro, the mean of the region of interest (ROI) is subtracted from the

image, plus an additional value to equal the standard deviation of the ROI, multiplied by a scaling factor.

For organotypic staining, this method provides variable scales due to the relative intensity of staining and amount of cells staining positive.

2.3.4 TMA core Analysis

Expression of pIgR was analysed via Immunofluorescence using tissue microarrays. Immunofluorescence was performed as described in Section 2.3.3. The staining extent score was a scale of 0-4, corresponding to the percentage of immunoreactive tumour cells (0%-5%, 6%-25%, 26%-50%, 51%-75% and 76%-100% respectively. The staining intensity was scored as negative (score=0), background (score=1), mild (score=2), moderate (score=3) or intense (score=4). A score ranging from 0-8 was calculated by adding the staining extent score with the intensity score (**Table 7**).

There are numerous options relating to type of staining and method of immunoscoring. Whilst immunohistochemistry is a more established method for ascertaining staining patterns as this preserves architectural context, immunofluorescent staining gives added advantage of getting information from more than two channels (wavelengths) simultaneously in the same area or cell or even at sub-cellular level for example, membrane versus cytoplasm with little interference from other channels (wavelengths). Immunofluorescent is disadvantaged by transient signal as well as loss of architectural context which requires more training.

However, I chose immunofluorescence and the above system as it had been used and published in our group previously section (59, 218, 219).

Median			Percentage	
0	No Stain		0	0-5%
1	Background		1	6-25%
2	Mild		2	26-50%
3	Moderate		3	51-75%
4	Intense		4	>75%

Table 8: Staining scoring Criteria

A normal process for validation of scoring involves two clinicians scoring the data set. To confirm my ability to score the TMAs appropriately, a second consultant clinician (Prof Hemant Kocher) was recruited to score one TMA. The TMA slide contained 88 cores. Both my scores for pIgR expression and the second clinician's scores for the one TMA were validated against ARIOL. The scanner is an automated process that distinguishes intensities of cell staining and provides a numerical value, thereby providing a semi-quantitative result. Comparison is made between each core and sequential slides were used between each analysis process.

2.3.4.1 ARIOL imaging

ARIOL ® (Leica Microsystems, Milton Keynes, UK) is a high throughput automated scanning microscope and image analysis that is able to capture, store and analyse terabytes of imaging data (220). It has applications in clinical, genomic and research industries (203, 221) and has previously been used in our group for publication.

The ARIOL system consists of a computer connected to a server, in order to handle the large amounts of imaging data generated and is equipped with a barcode scanner, microscope, with automated mechanical stage embedded and a lighting system (Olympus BX, UCB). The system can be programmed to capture whole tissue sections and tissue microarrays.

The ARIOL system has been documented in primary colorectal adenocarcinoma (222), breast cancer (223), follicular lymphoma (224) and pancreatic adenocarcinoma (203) research. Automated systems can produce results in concordance with pathologists scoring, especially for markers with nuclear staining patterns and can provide standardised quantitative measurements of immunohistochemical staining (225).

2.3.4.2 Methods of Immuno-scoring

Biomarker quantification has relied exclusively on visual scoring performed by a pathologist or trained reviewer, which is semi-quantitative and can be limited by inter-observer agreement (226) . However, this system is still largely used in publications to date.

Additionally, visual analysis of tissue samples is time consuming and prone to human errors, which has led to a method for absolute quantification that is potentially consistent, replicable, time saving and have high throughput capabilities.

Theoretically, automated image analysis may offer solutions. The microscope component of the ARIOL ® is equipped with an automated mechanical stage, which can hold 8 slides sequentially; whilst the barcode scanner on the system ensures that every slide is unique, allowing for the programming of different assays per slide, all of which aid high throughput analysis.

The embedded software is equipped with applications to make it easy to parse scanned images into regions, allowing for calculations within regions. It also has controlled thresholds for scoring based on size, colour, intensity, pattern and shape with which the trained user can teach the Ariol to discriminate a false positive from an actual positive stain.

The high magnification of pixels also make it possible to differentiate shades of colours and cells juxtaposed to each other, thus cells maybe counted individually and enabling sufficient stringency to produce highly accurate, reproducible results.

The output is quantitative with values for useful parameters such as counts

(positive and negative), analysed area (μm^2), area of positive and negative staining (μm^2) and mean intensity of colours.

2.3.4.3 Limitations of Ariol

Despite the exceptional capabilities of Ariol, it is limited by its lack of user friendliness, inflexibility and ancient design, which consumes time and effort. Whilst a region can be selected and cells quantified, it is impossible to quantify the excluded region simultaneously, thus requiring the user to perform arithmetic to calculate the cell counts of the excluded regions by performing lengthy analysis and deducting the selected region from the whole region.

The system is also expensive; the system cost $300,000 in 2005. Most users have to spend hours on the system to gain expertise and to perform the many analyses that must be executed to overcome its inflexibilities. For accurate results, thresholds on what to quantify must be set, which is also time consuming. Scanning a series of TMA slides is also a very long process, taking up to six to seven hours. Based on the time to train and scan, the Ariol works out as being an expensive research tool.

2.3.4.4 Application

I used Ariol to perform quantitative analysis of pIgR expression in TMA's using the TMAsight assay on Ariol. I trained the software to distinguish and quantify positive and negative cells by their colour, size, shape and staining intensity. I was aiming to gain a representative intensity score for entire TMAs, thus I did not distinguish tumour from non-tumour within each core. The entire core area was marked with the marking tool on Ariol. Afterwards, the amount of positive cells in the core was quantified and divided by the amount of negative cells in the same core. This provides a ratio of density within each core.

2.3.5 Identification of PanIN for assessment

Pancreatic intraepithelial neoplasias (PanINs) are pre-invasive neoplasms that arise within the intralobular ducts of the exocrine pancreas. PanINs are small microscopic lesions that are less than 5mm. They are composed of a flat or papillary neoplastic epithelium. Depending on the extent of the cytological atypia, they are classified as PanIN 1 (low-grade dysplasia), PanIN 2 (moderate dysplasia) or PanIN 3 (high grade dysplasia) (227).

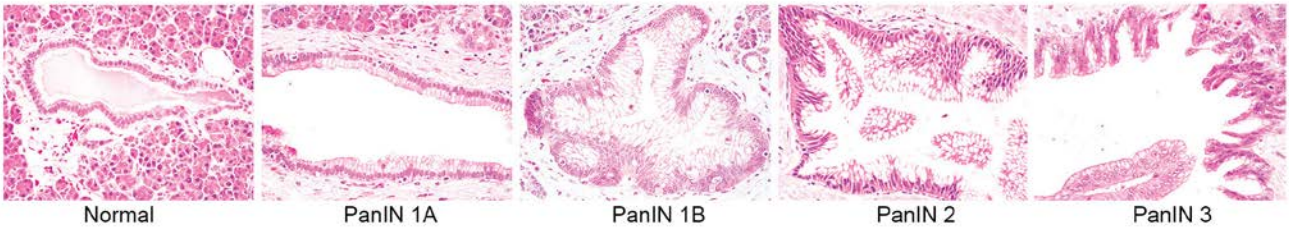

Figure 2.1: PanIN progression. Figure sampled from Brosens et al (228).

A simple cuboidal layer of cells characterises normal pancreatic ductal epithelium. PanIN 1 demonstrates columnar cell change and mucinous differentiation, but minimal nuclear atypia. PanIN 2 lesions lose the mucinous epithelium but demonstrate nuclear pleomorphism and crowding and some mitotic figures may be present. PanIN 3 relates to carcinoma *in situ*, with pseudopapillary formation, nuclear atypia, apoptotic debris and frequent mitotic figures (228).

2.3.6 Survival and Statistical analysis

Survival analysis to dichotomise groups according to high and low pIgR expression was performed using X-Tile (Rimm Lab, Yale University, http://medicine.yale.edu/lab/rimm/research/software.aspx).

Statistical analysis and graphical data representation were performed using the software PRISM V.6 (Graphpad, La Jolla, USA). Summary data are expressed as the median with interquartile range since the distribution was non-Gaussian. Comparisons were performed using Kruskal-Wallis test with Dunn's multiple comparison test. The level of significance was set at $P < 0.05$.

2.3.7 Picrosirius Red staining

Picrosirius Red staining was used to detect collagen fibres in tumours. Briefly, to obtain a 0.1% Picrosirius Red solution, 0.5 gram of Sirius Red (Sigma Aldrich Direct Red 80, 365548) was dissolved in 500 mL saturated aqueous solution of picric acid (1.3% in distilled water). Sections were de-waxed and hydrated as described previously, incubated with Picrosirius red solution for an hour at room temperature, after which, sections were washed twice in acidified water (0.5% acetic acid in distilled water), dehydrated through graded alcohols to xylene and mounted in DPX (Distrene, Plasticiser, Xylene; VWR 360294H).

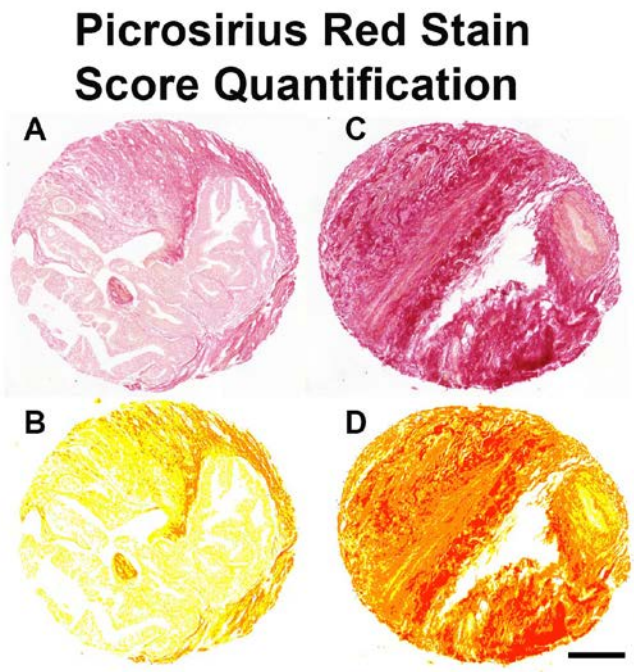

Figure 2.2: Quantification of Picrosirius Red stain

Unlike Masson's Trichrome, nuclei remain unstained, thus the stain is only a demonstration of collagen. Due to the variation, I used the panoramic scanner to scan the images and also provide a quantitative result for the intensity of the stain. By changing the core into an effective heat map, I could then map and mark the intensity of the red stain. This provides strongly positive areas. I excluded moderately and low expression of the red. The program counts the number of pixels within each core that are strongly expressing the red. Scale bar 200µm.

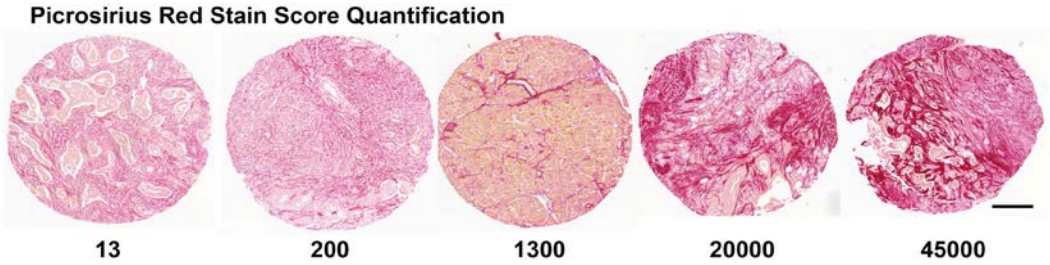

Figure 2.3: Picrosirius Red staining in human PDAC sections.

The intensity of the red colour varies hugely across various PDAC subtypes. As shown in the variety of images and the number below represent the numerical value of the intensity of stain. There is a large variability in the score, but as a general observation, values under 300 are largely negative, whilst values over 5000 are strongly positive for collagen. Scale bar 200µm.

2.4 Western Blotting

2.4.1 Isolation of protein

After relevant treatments, cells were washed with PBS and lysed at room temperature with lysis buffer. Scrapping with a rubber policeman collected cells. Cell debris was collected and added to an eppendorf tube and homogenised briefly using a sonicator. Protein concentration was determined with a Bio-Rad Dc protein assay (Bio Rad Laboratories) according to the manufacturer's instructions. Following protein concentration determination, sample buffer (4X) (Novex, NP0007) was added and samples stored at -80°C to avoid protein degradation.

2.4.2 Western blot analysis

Cell lysates in sample buffer were boiled at 100°C for 5 minutes to denature proteins before brief centrifugation to collect contents. Equal amounts of denatured protein (15-25µg) were loaded onto 10% Bis-Tris gels. After protein separation by electrophoresis, proteins were transferred to a nitrocellulose membrane (GE Healthcare Life Sciences, 10401196). Ponceau S (Sigma-Aldrich, P7170) was used to confirm adequate transfer. Non-specific binding was blocked by incubation with 5% milk, followed by incubation with primary antibody (Table 2) in 5% milk at 4°C overnight. Membranes were washed with 0.1% Tween20-TBS (TBST) (Applichem,

A13890500) and subsequently incubated with secondary HRP-conjugated antibody for one hour at room temperature. Specific protein bands were visualised using an Amersham ECL Western Blotting Detection Kit (GE Healthcare, RPN2106) and photographic film (Super RX, 4741019230).

2.4.3 Stripping membranes

Membranes were stripped using Reblot plus mild (Millipore, 2502) for 10 minutes, washed with PBS, blocked with 5% milk in PBS for 15 minutes and washed again in PBS. Membranes were then reprobed with primary antibody as above.

2.4.4 Densitometry and analysis

For Western blotting, densitometric analysis of specific bands was carried out using Image J software (Rasband, National Institute of Health, (https://imagej.nih.gov/ij/). To obtain a semi-quantitative measurement of the level of total protein, band densities were normalised to the loading control HSC70 housekeeping genes on the same membrane.

2.5 Quantitative real-time PCR

For reverse transcription PCR, cells were lysed with Quick-RNA Mini Prep (Cambridge Bioscience, #R1054A). Quantity and purity of RNA was measured with NanoDrop spectrophotometer (OD 260/280 ratio > 1.80).

cDNA was amplified in a reaction mix with the forward and reverse primer (Table 2.3) and quantified SensiFAST SYBR Hi-ROX One-Step Kit (Bioline, #BIO-73005). Briefly, kits formulated for first strand cDNA synthesis and subsequent real-time PCR in a single tube. The antibody-mediated hot-start DNA polymerase system reduces the chances of primer/ dimers formation.

Cycle numbers of denaturing at 95°C, annealing at 55°C and DNA extension at 72°C. For each gene, the first cycle when exponential amplification could be detected (C_T) was normalised to the endogenous expression of the housekeeping

gene GAPDH (glyceraldehyde 3-phosphate dehydrogenase).

Gene	Forward Primer	Reverse Primer	Tm	Size
pIgR (Kaetzel)	GGTCCCGAGGAGGTGAATAGTG	CTGACCTCCAGGCTGACATCAA	67	22
pIgR (Kadaba)	CTCTCTGGAGGACCACCGT	CTCTCTGGAGGACCACCGT	65	19
GAPDH	CCATGACCCCTTCATTGACC	TTGATTTTGGAGGGATCTCG	65	20

Table 9: Primers used for quantitative reverse transcription PCR (qRT-PCR). Two pIgR primers were used for sequencing, Kaetzel primers have been used elsewhere for pIgR sequencing (229), whilst the other pIgR primers were used previously in our group (70).

2.6 Antibodies

All antibodies are summarised in Table 10.

Antibody	Species raised in	Supplier (Cat No)	Dilution for IF/ IHC	Dilution for WB
Primary Antibodies				
αSMA	Mouse	Dako Clone 1A4 (M0851)	1:300	1:100
α Tubulin	Goat	Abcam (ab7291)		1:1000
Cytokeratin	Mouse	Dako (Z0662)	1:200	
E-Cadherin	Mouse	Abcam (ab1416)	1:100	1:500
Fibronectin	Mouse	Sigma (F0916)	1:300	
HSC70	Mouse	Santa Cruz (SC7298)		1:1000
IgA	Goat	Sigma Aldrich (I0884)	1:100	
Ki67	Rabbit	Abcam (ab15580)	1:100	
pIgR	Rabbit	Sigma Aldrich (HPA012012)	1:200	1:1000
pIgR	Rabbit	Santa Cruz (H-300) (SC20656)	1:200	1:1000
Twist1	Mouse	Abcam (ab50887)	1:500	
Vimentin	Mouse	Dako Clone V9 (M0725)	1:50	1:250
Zeb1	Rabbit	Santa Cruz (SC25388)	1:500	
Secondary Antibodies				
Anti-rabbit HRP	Mouse	Dako (P0448)		1:1000
Anti-mouse HRP	Goat	Dako (P0447)		1:1000
Anti-goat HRP	Rabbit	Dako (P0160)		1:1000
Fluorescein Goat Anti-rabbit (488)	Rabbit	Invitrogen (F2765)	1:400	
Fluorescein Goat Anti-mouse (546)	Mouse	Invitrogen (A-11030)	1:400	

Table 10: Antibodies used for experiment. HSC70 (Heat shock cognate 70kDa protein); αSMA (α-smooth muscle actin); pIgR (polymeric immunoglobulin receptor); HRP (horseradish peroxidise); IF (immunofluorescence); IHC (immunohistochemistry); WB (Western blot)

2.7 Modulation of pIgR in cell lines

2.7.1 Small interfering RNA (siRNA) oligos

Cells were transfected with a pool of siRNA oligos (ON-TARGET plus SMART pool human pIgR, Dharmacon, L0017729-00-0010). Non-targeting siRNA was used as a control (Dharmacon, D-001810-10-05).

2.7.2 Collection of supernatant

For conditioned medium to be used in the Western blot analysis cells were cultured in serum free medium for 12 hours, after which time the medium was collected, filtered and concentrated 20X using centrifugal pore size filter units (Millipore UFC 800324 NMWL 3000) according to manufacturer's instructions. The nature of the filter membranes means that solutes with molecular weights below 3000kDa were excluded from the membrane and collected in the centrifuge tube while the supernatant was collected from the filter device sample reservoir. Culture medium (serum free) was used as a negative control. Sample buffer (4X) (Novex, NP0007) was added to the concentrated condition medium and boiled at 100°C for western blotting.

2.7.3 Introduction of siRNA into Capan1 cells

PDAC cell line, Capan1, was plated into 6-well plates at a confluency of $5x10^4$ cells per well (50%) in standard medium containing FBS. The following day, the medium was removed from the cells and replaced by 1ml of fresh standard culture medium to achieve the correct final concentration of siRNAs. The Capan1 cancer cells were transfected with a pool of siRNAs targeting pIgR at a final concentration of 20nM, or with a pool of non-targeting siRNA at the same concentration, using INTERFERin™ (Polyplus, 409-10) as a transfection reagent. Transfection complexes were prepared in OptiMEM (Invitrogen, 51985-042), to which 4µl INTERFERin™ was added, vortexed for 10 seconds and incubated for 10 minutes at room temperature.

155µl of the mixture was added to the cell line in culture medium. Cells were incubated with the siRNA complex for 24, and cell lysed between 48 to 144 hours and subsequent confirmation of knockdown by Western blot.

2.7.4 Introduction of shRNA into pancreatic cancer cells

pIgR shRNA plasmids were kindly donated by Jing Ai, Shanghai Institute of Materia Medica (179). A total of three shRNA plasmids were donated; non-targeting shRNA (5'-UUCUCCGAACGUGUCACGUTT-3'), pIgR shRNA 1 (5'-GAACGUCGACCGAGUUUCA-3'), pIgR shRNA 2 (5'-CGUCGACCGAGUUUCAAUC-3'). Each plasmid was transformed using 50µl E. Coli bacteria (Thermo Fisher, C404010); heat shocked at 42°C for 45 seconds and streaked onto pre-warmed agar plates containing 100µg/ml Ampicillin. The plates were left to incubate overnight at 37°C and individual colonies were selected the following day and incubated in L-Broth with 100µg/ml Ampicillin overnight. The following day, the liquid broth was centrifuged for 10minutes at 5400rpm, half of the product being retained for glycerol stock (500µl glycerol and 500µl broth media) for long-term storage. The other half was subsequently processed using QIAprep Spin Miniprep Kit (QIAGEN, 27104) as per manufacturers' protocol, to generate enough DNA for subsequent introduction into cancer cell lines.

In order to transfect PDAC cells, AM12 Phoenix cells (ATCC, CRL-3214) were used as an amphotrophic vector to aid the transfection. AM12 cells are amphotrophic retroviruses and are cultured in DMEM supplemented with 10%FBS. AM12 cells were plated into 10cm petri dishes to a confluency of 60%, requiring one petri dish for each eventual shRNA construct. 24µg of each shRNA construct was added to 60µl of Lipofectamine® 2000 (Life Technologies, 11668027) and 10mls of OptiMEM (Invitrogen, 51985-042). The mixture of each shRNA and Lipofectamine® 2000 was added to each respective petri dish of AM12 cells. After 24 hours, the media was replaced with DMEM containing FBS. After a further 24 hours, the 5mls of

supernatant was collected, filtered with a 0.45µm filter and 6.25µl of Polybrene (Merck Millipore, TR-1003-G) added. 2mls of the mixture was added to Capan1 cells plated into 6 well plates at a confluency of $5x10^4$ cells per well (50%) in standard medium containing FBS. The 6-well plate was left at room temperature on a plate shaker at 1800rpm for 20 minutes before being left overnight at 37°C. The following day, media was changed to RMPI with 10%FBS and 1µg/ml Puromycin. Transfected cells were subsequently lysed and confirmation of knockdown by western blot.

2.7.5 Incubation of pancreatic cancer cell lines with cytokines

PDAC cell line, AsPC1, was plated into 6 well plates at a confluency of $5x10^4$ cells per well (50%) in standard medium containing FBS. AsPC1 cells were treated with 5µg, 10µg or 20µg of Interleukin 1β (Peprotech, 200-01B), Interleukin 4 (Peprotech, 200-04) or Tumour Necrosis Factor α (Peprotech, 300-01A). Cells were incubated with the relevant cytokine from 24 to 72 hours before cell lysis and confirmation of overexpression by Western blot.

2.7.6 Introduction of plasmid DNA into pancreatic cancer cells

2.7.6.1 pIgR cDNA from Addgene

In an attempt to elicit over expression of pIgR, pIgR cDNA was obtained (pBS-pIgR cDNA was a gift from Pamela Bjorkman (Addgene plasmid #12109)). Stab culture overnight elicited colonies, which were picked and processed using QIAprep Spin Miniprep Kit (QIAGEN, #27104) as per manufactures protocol, to generate enough DNA for subsequent introduction to mammalian cloning vectors.

Gel digestion using Xba1, HindIII and Bsa1 binding sites to ligate a 2900 base pair sequence of pIgR. Digestion products were purified from an agarose gel using QIAquick gel extraction kit (Qiagen, #27104). The desired band was excised from the ethidium bromide-stained agarose gel and three volumes of Buffer QG were added to 1 volume of the gel slice. The mixture was incubated at 50°C for 10 minutes followed

by adding 1 gel volume of isopropanol. The mixture was then applied onto a spin column and was centrifuged at 14,000 rpm for 1 minute (Eppendorf centrifuge, #5415C). This was followed by a wash with 0.75 mL buffer PE and centrifuged again as described above. Bound DNA was eluted from the spin column by adding 50 L buffer EB (10 mM Tris-Cl, pH 8.5). Eluted DNA was stored at 4°C until ready to use.

The cloned sequence was introduced into pCDNA4/TO (Invitrogen) in the presence of T4 DNA ligase (NEB) and transformed into TOP10 (DH5α) *Escherichia coli (E. Coli)* cells (Thermo Fisher, C404010). Transformed cells were selected on a LB plate containing 100 μg/mL ampicillin at 37°C for 16 hours. Positive transformants were inoculated into LB broth containing 100 μg/mL ampicillin for plasmid propagation. The following day, the liquid broth was centrifuged for 10minutes at 5400rpm, half of the product being retained for glycerol stock (500µl glycerol and 500µl broth media) for long-term storage. The other half was subsequently processed using QIAprep Spin Miniprep Kit (QIAGEN, 27104) as per manufactures protocol, to generate enough DNA for subsequent introduction into cancer cells.

In order to transfect PDAC cells, AM12 Phoenix cells (ATCC, CRL-3214) were used as a viral vector to aid the transfection. AM12 cells are amphotrophic retroviruses and are cultured in DMEM supplemented with 10%FBS. AM12 cells were plated into 10cm petri dishes to a confluency of 60%. 24µg of pIgR plasmid construct was added to 60µl of Lipofectamine® 2000 (Life Technologies, 11668027) and 10mls of OptiMEM (Invitrogen, 51985-042). The mixture of plasmid pIgR and Lipofectamine® 2000 was added to the petri dish of AM12 cells. After 24 hours, the media was replaced with DMEM containing FBS. After a further 24 hours, the 5mls of supernatant was collected, filtered with a 0.45µm filter and 6.25µl of Polybrene (Merck Millipore, TR-1003-G) added. 2mls of the mixture was added to PDAC cancer cell lines plated into 6 well plates at a confluency of $5x10^4$ cells per well (50%) in standard medium containing FBS. The 6-well plate was left at room temperature on a plate shaker at 1800rpm for 20 minutes before being left overnight at 37°C. The following

day, media was changed to DMEM with 10%FBS and 150 µg/ml Zeocin (Invitrogen).

Despite valiant attempts, introduction of pIgR into pancreatic cancer cells lines was unsuccessful. Trails initially with PCR based splicing failed to produce sufficient, high quality cDNA. Hence the attempt changed to gel based digestion. The sequence identified eventually and sequenced was a segment of pIgR, but again, we were unable to introduce it into non-pIgR expressing cell lines.

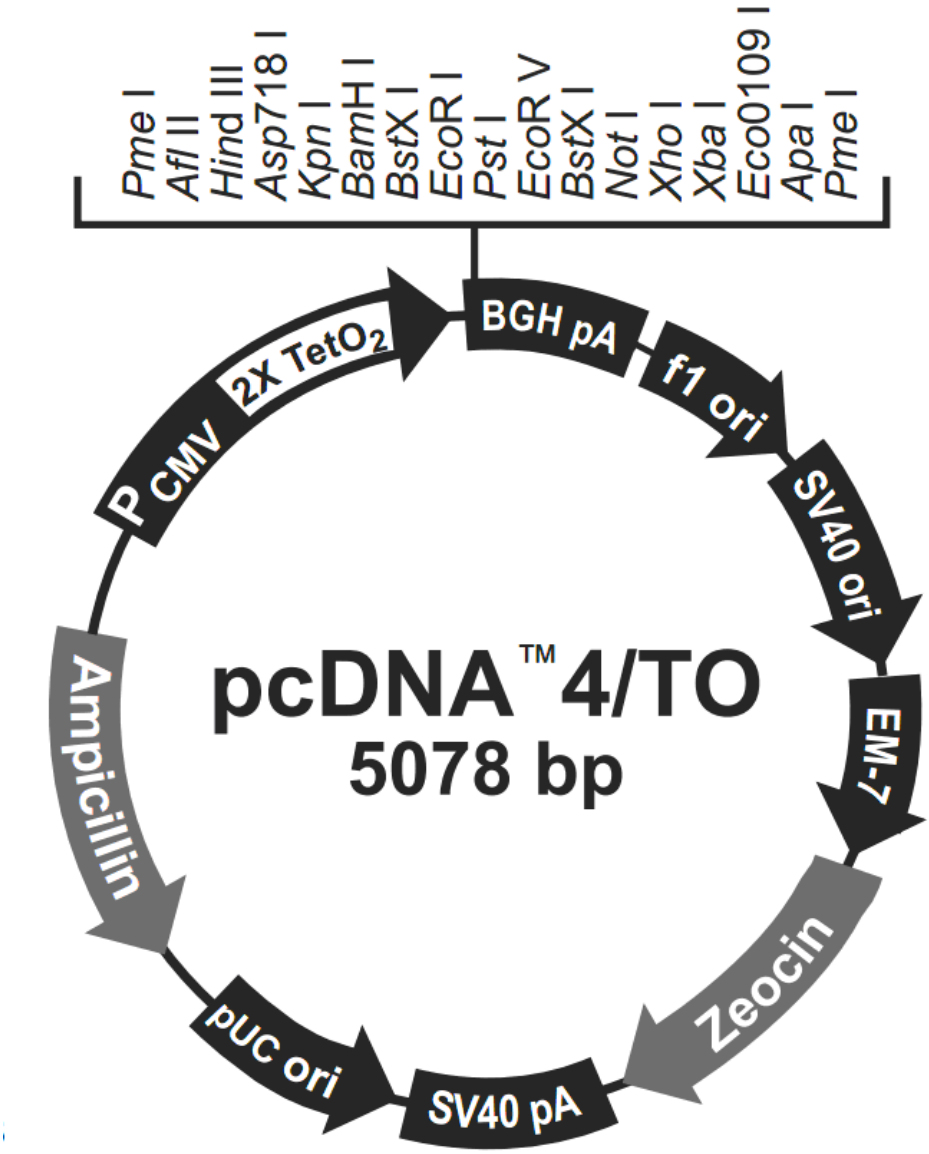

Figure 2.4: Representative image of pcDNA 4/T0 vector

2.7.6.2 Other methods of pIgR over-expression

In an attempt to confirm over-expression, three further vectors were used. Human pIgR cDNA-containing pcDNA3.1 (+) was a generous gift from Dr Finn-Eirik Johansen (Rikshospitalet University Hospital, Oslo, Norway) (179). For stable transfections, AM12 cells were grown to 60% confluency in 10cm petri dishes plates and transfected with 4 µg of full-length pcDNA3.1 (+) vector or pcDNA3.1 (+)-pIgR, using 10 µl of Lipofectamine 2000 (Invitrogen) following the manufacturer's instructions. As described in section 2,9,1, supernatant was collected and added to pancreatic cancer cells. A monoclonal population of stably transfected cells was selected using 500 µg/mL geneticin (G418) (Invitrogen).

TrueORF pIgR plasmid was purchased from OriGene Technologies (Rockville, MD, USA; Cat. no. RC212006). TrueORFs have a C-terminal fusion of MYC/DDK tag. The cloning expression vector is pCMV6-Entry. Transfection of cancer cells was performed using Lipofectamine 2000 (Life Technologies), according to the manufacturer's instructions. Briefly, DNA (0.2 µg/well) and Lipofectamine 2000 (1 µl/well) were separately diluted in 25 µl of Opti-MEM (Gibco). Next, DNA was added to the Lipofectamine 2000 reagent and the lipid/DNA mixtures were allowed to form complex for 5 min at room temperature. Cells were washed once with 100 µl of PBS and 100 µl of DMEM containing 15% FBS/well was added to each well. Next, lipid/ DNA mixture was added and cells were incubated at 37°C, 5% CO. After 24 h, transfection medium was removed and replaced with DMEM containing 10% FBS to start differentiation. To validate the expression of pIgR, anti-DDK mouse monoclonal antibody (1:1,000, OriGene, Cat#TA50011-100) was used. After 4 days of differentiation, differentiation was confirmed visually to observe the GFP under a fluorescent microscope.

The HaloTag® protein was purchased from Promega (Madison, WI, USA; Cat no. FHC20797). It is a genetically engineered derivative of a dehalogenase that forms

a covalent bond with various synthetic HaloTag® ligands. The 34 kDa monomeric protein can be fused at either the N-or C-terminus to proteins of interest and enables expression in both prokaryotic (E. coli) and various eukaryotic cells. Transfection of cancer cells was performed Lipofectamine 2000 (Life Technologies), according to the manufacturer's instructions. After 4 days of differentiation, differentiation was confirmed visually to observe the GFP under a fluorescent microscope.

2.8 Functional Assays

2.8.1 Cell Counts

Cancer cells were plated onto 6 well plates in triplicate at a density of $5x10^4$ and the next day treated with a pool of siRNAs targeting pIgR at a final concentration of 20nM, or with a pool of non-targeting siRNA at the same concentration, using INTERFERin™ (Polyplus, 409-10) as a transfection reagent (section 2.4). Untreated Capan1 cells were used as a control. For shRNA, cells were plated as above, but no additional treatment was provided. At 72, 96, 120 and 144 hours following treatment, cells were detached with Trypsin-EDTA, 500µl of cell suspension was added to 9.5ml of Isoton and counted with a Casy counter (Schärfe Systems, Germany). Based on a coulter counter principle, the Casy system detects electrical signals that are generated when cells pass through a measuring capillary.

2.8.2 Cell Proliferation Assay

Cancer cells (untransfected or transfected with relevant shRNA) were plated (5,000 cells per well) in a 96-well plate for 24 hours. Cell proliferation was analysed with Cell Proliferation Reagent WST-1 (Roche, #5015944), added 2 h before spectrophotometric reading, according to the manufacturer's instructions. This is also known as MTS assay.

2.8.3 Scratch Assay

Cancer cells (untransfected or transfected with relevant shRNA) were plated in triplicate onto a six-well plate at a density of 5×10^4 per well. 48 hours later (when cells had formed a confluent monolayer), a wound was administered across the cell monolayer using a pipette tip. Three areas were selected and marked for imaging, cells were washed twice with a medium so as to remove any cell debris, and images were taken from the marked area and repeated at 48 hours to assess wound closure by phase contrast microscopy. ImageJ was used to quantify the percentage of cells (pixel intensity) that had migrated across the wound over 48 hours; results are an average of three separate areas measured.

2.8.4 Adhesion Assay

Cancer cells (untransfected or transfected with relevant shRNA) were plated for half an hour on fibronectin (10 mg/ml)-coated 96-well plates. Non-adherent cells were washed off with PBS. Adherent cells were stained with Crystal Violet and dissolved in 1 % SDS, and adhesion was quantified using absorbance at 560 nm. This “adhesion index” was normalized to the adhesion of untransfected cells for each biological repeat (at least three) which contained at least three technical repeats.

2.8.5 Transwell Migration Assay

Cancer cells (untransfected or transfected with relevant shRNA) were cultured in triplicate in serum free medium on top of an 8μm Transwell® membrane (Corning #3428) coated with Fibronectin (Sigma Aldrich #F1141) at a density of $5x10^4$. After 24 hours, cells counts were calculated from cells that had invaded through the membrane for each biological repeat (at least three) which contained at least three technical repeats.

2.9 Organotypic culture

To investigate the invasion and proliferation of cancer cells in 3D, an air-liquid interface model was used (230) (231). The stromal, extracellular matrix (ECM) equivalent was composed of 75% collagen type 1 (BD Bioscience 354236) and 25% Matrigel (BD Bioscience 354234). Gels were composed of 10 parts; 5.25 parts collagen type 1, 1.75 parts Matrigel, 1 part 10X DMEM, 1 part DMEM and 1 part filtered FBS. The mixture was plated into 24 well plates coated with diluted collagen type 1 (1:100 in PBS). Gels were made in triplicate. Capan1 cancer cells were treated as previously described with either pooled non-targeting or on-targeting pIgR siRNA. Once the gels had polymerised, $1.7x10^5$ cancer cells mixed with $3.3x10^5$ stellate cells or $5x10^5$ cancer cells alone (control) were added to the gels in 1ml of medium and left to adhere overnight at 37°C. The next day, the gels were lifted onto a metal grid covered by a nylon membrane pre-coated with seven volumes of collagen type 1, one volume 10X DMEM, one volume DMEM and one volume FBS. 250µl of the mixture was pipetted onto the nylon membrane and allowed to polymerise for 15 minutes at 37°C, cross-linked with 1% glutaraldehyde/ PBS and left for one hour at 4°C. Glutaraldehyde was removed by washing the membrane 3 times with PBS and once with medium, then covering in medium and leaving overnight at 4°C. The following day, the submerged organotypic was raised to grids and fed from below with RPMI medium. Medium was changed every other day and gels were harvested at day 10 following treatment, fixed in 10% neutral buffered formalin, bisected and embedded in paraffin.

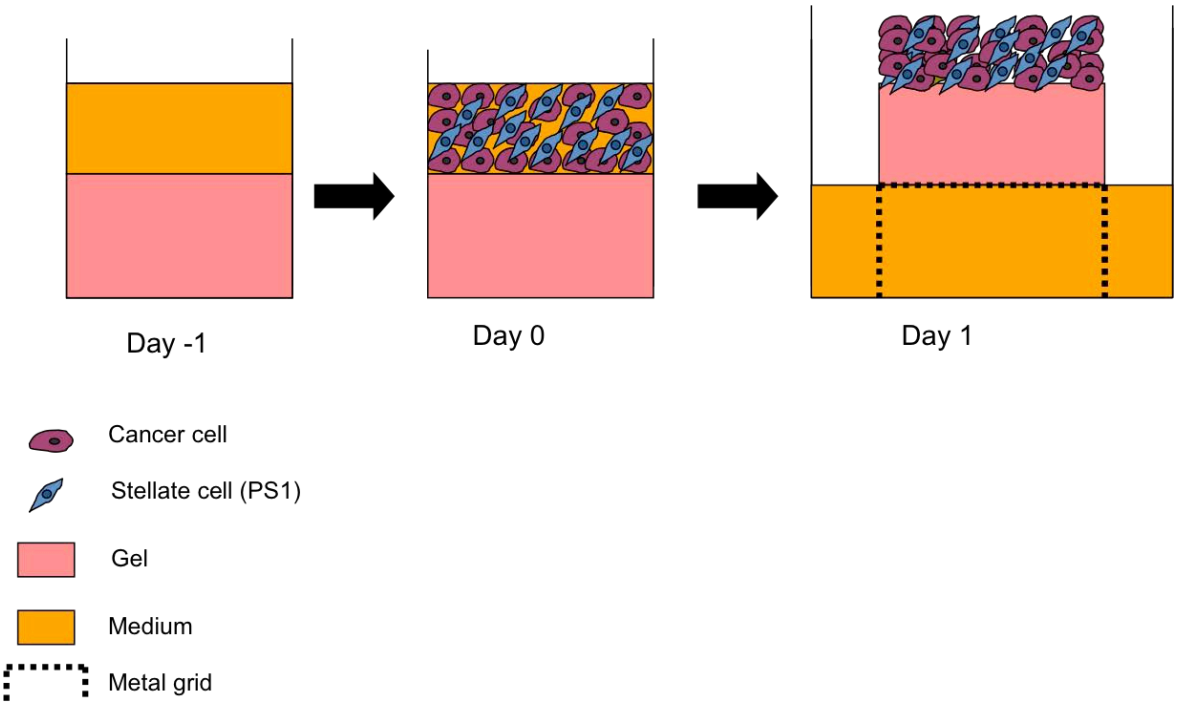

Figure 2.5: Diagrammatic representation of organotypic models

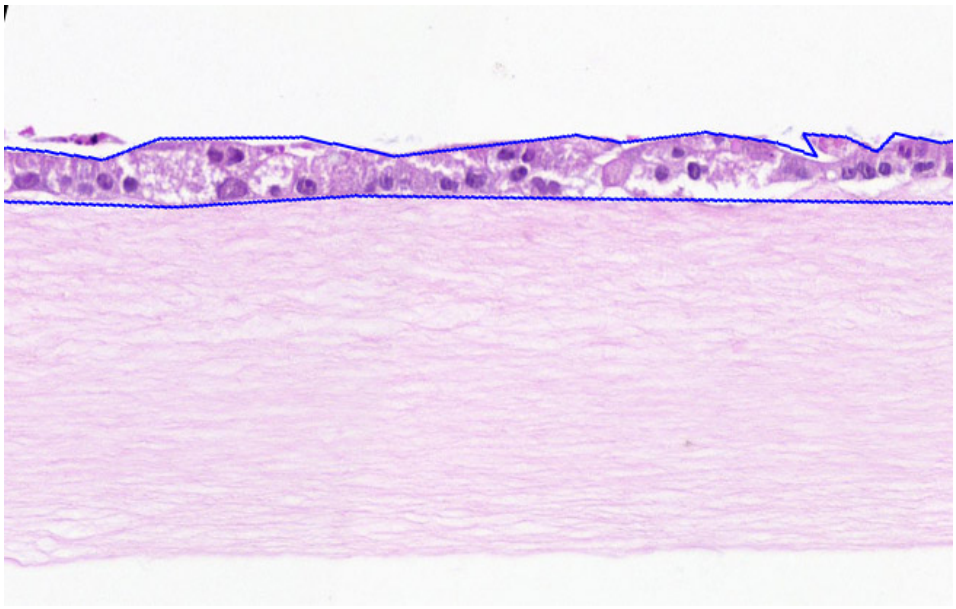

Figure 2.6: Quantification of Organotypic cultures.

H&E images were scanned using panoramic scanner. Areas of interest were marked manually, as shown. Panoramic scanner would then provide details such as area and number of nuclei within the marked line.

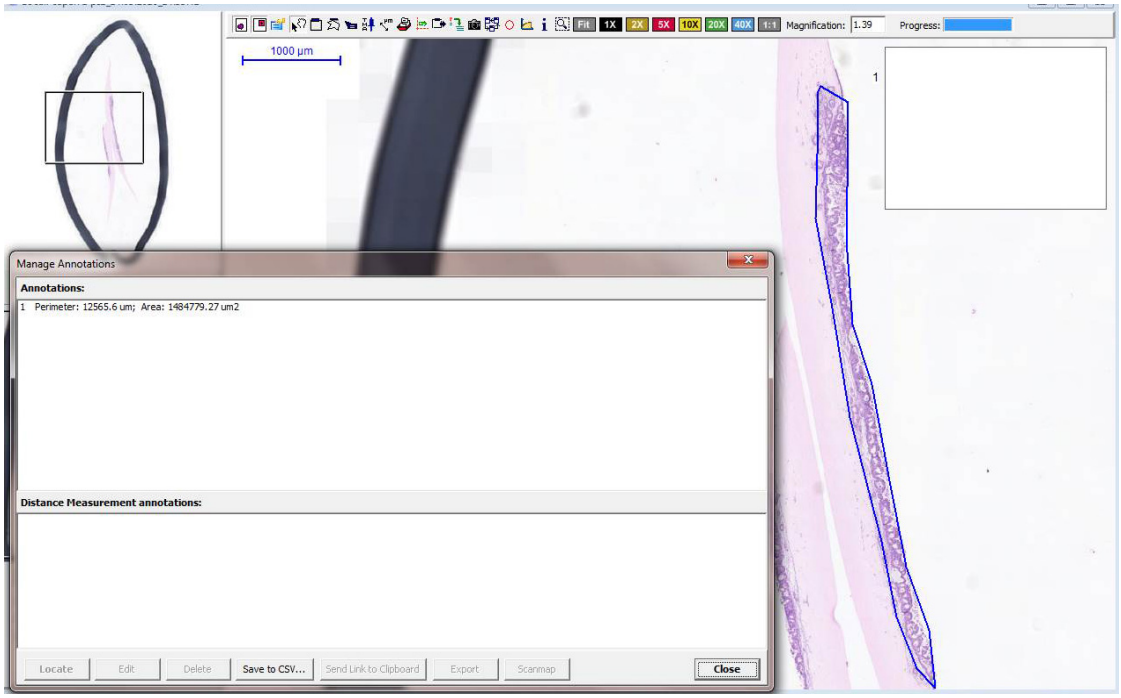

Figure 2.7: Quantification of Organotypic culture cell area.

Manual selection of areas of interest provided panoramic scanner program necessary information to calculate cell area, as shown.

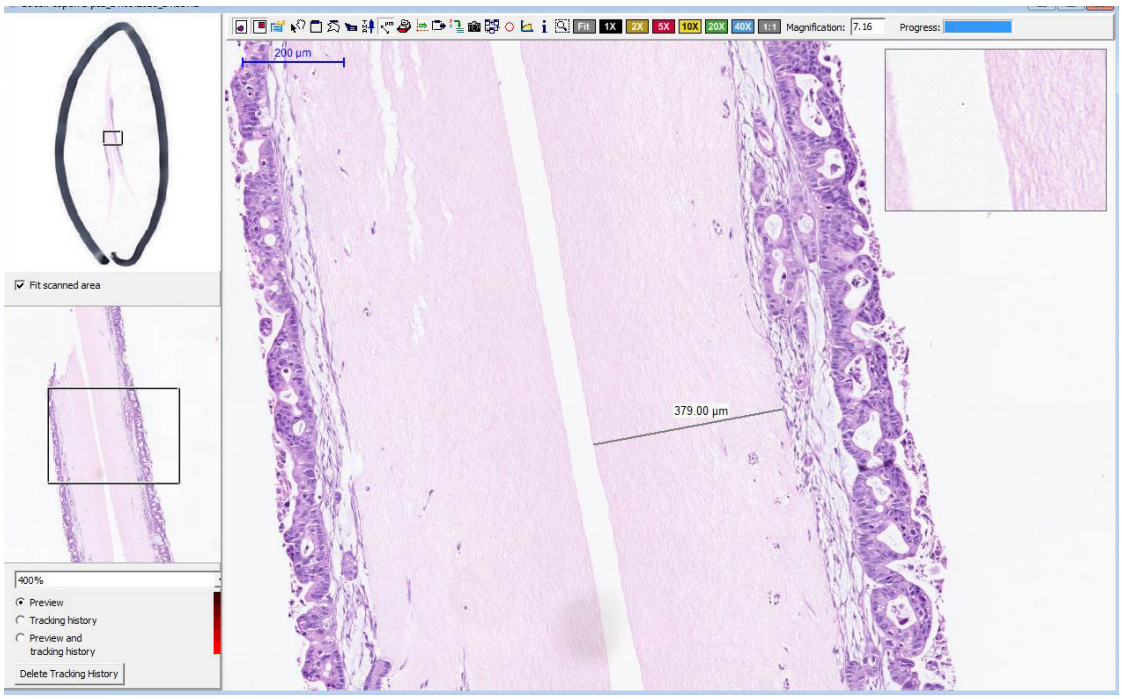

Figure 2.8: Quantification of Organotypic culture gel thickness.

Manual measurement of organotypic gel area thickness was performed using panoramic scanner.

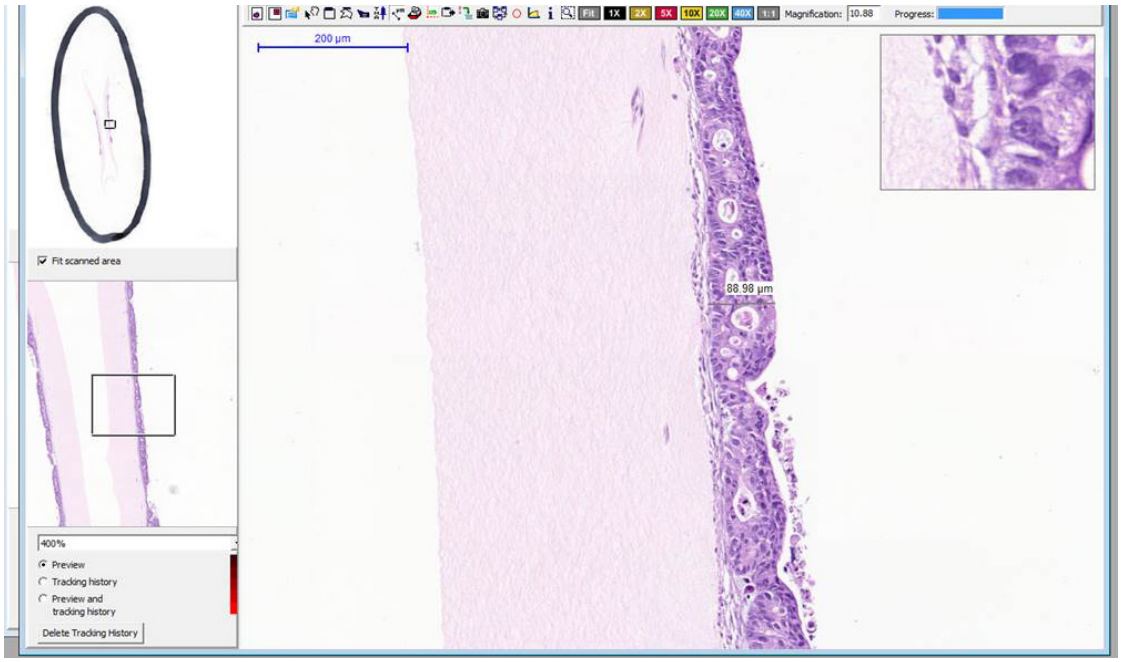

Figure 2.9: Quantification of Organotypic culture cell layer thickness.

Manual measurement of organotypic cell area thickness was performed using panoramic scanner.

2.10 Statistics

The quantification of all cell counts and intensity of staining in the organotypic sections was performed on six representative pictures per organotypic gel of which there were at least three technical replicates for each of the biological replicates (minimum three). For the human TMA, either individual cores or the whole section was scanned using either Axioplan microscope (Zeiss 40 V 4.8.10, Carl Zeiss MicroImaging LLC, New York, US), confocal laser scanning microscope LSM 710 (Carl Zeiss MicroImaging LLC, New York, US), Pannoramic 250 High Throughput Scanner (3DHISTECH Ltd., Budapest, Hungary) or ARIOL (Leica Biosystems, Wetzlar, Germany). The intensities of fluorescence in the green/red channels were normalized with IgG controls and positive controls (such as normal duodenum)and background fluorescence and calculated in an unbiased, blinded manner using either Adobe Photoshop CS6 (San Jose, CA USA) or Pannoramic Viewer Software (3DHISTECH Ltd., Budapest, Hungary) and Image J software (NIH, Maryland USA). Specifically regarding immunofluorescence quantification, the numbers of pixels for

green and red channels were counted using LSM710 software at a threshold above 100 intensity (100–255) per high-power field, with size (total pixels) and cellularity in the field kept constant across the various shRNA conditions. All analyses were performed either Prism 5 (Graph- Pad Inc., LaJolla, CA) and images organized in Adobe Photo- shop. Significance was defined as $P < 0.05$ using appropriate statistical tests (Mann–Whitney *U* test or Student *t* test).

Organotypic culture length and thickness was measured by summating the length of serial low-power fields across the gel from end to end, limiting to within the area of cellularity to avoid edge artifacts (70).

All statistical analysis was done using GraphPad Prism software. First data were ascertained to be normally distributed or not using Shapiro-Wilk test. Most data were not normally distributed or too low a sample size. Hence, non-parametric tests were used. All tests and post-hoc comparisons were applicable are described.

CHAPTER III

RESULTS:

PART I

3.1 Immunofluorescence staining of human paraffin sections

Previous work by Kadaba et al from my laboratory (70) noted pIgR expression in 3D organotypic models of PDAC. Furthermore recent publication by Fristedt suggested enhanced pIgR expression in pancreatico-biliary cancers (176). pIgR is involved in transport of IgA and IgM in epithelial tissues. It is assumed that there is no physiological role for IgA within normal pancreas or liver, and therefore pIgR is unlikely to be of importance in normal pancreas or liver, as they are not exposed to gut pathogens. However, recent work with hepatocellular cancer (179) has demonstrated that pIgR aberrant expression correlated with poor patient survival. I therefore studied expression of pIgR in a number of patient samples with pancreatico-biliary pathologies.

3.2 Normal human expression of pIgR and immunoglobulins

In order to confirm expression, normal pancreas and duodenum were identified in TMAs and historical tissue sections (n=15) were utilised as controls. Normal duodenum expresses pIgR and IgA naturally. Thus duodenum has been used as a positive control for staining.

Normal duodenum shows strong expression of IgA and pIgR, yet normal pancreas shows neither expression, whilst PDAC samples demonstrate expression of pIgR but not of IgA (**Figure 3.1**). This suggests a role of pIgR in PDAC apart from transport of immunoglobulins.

Epithelial cells express E-Cadherin in normal human pancreas and duodenum (**Figure 3.2**).

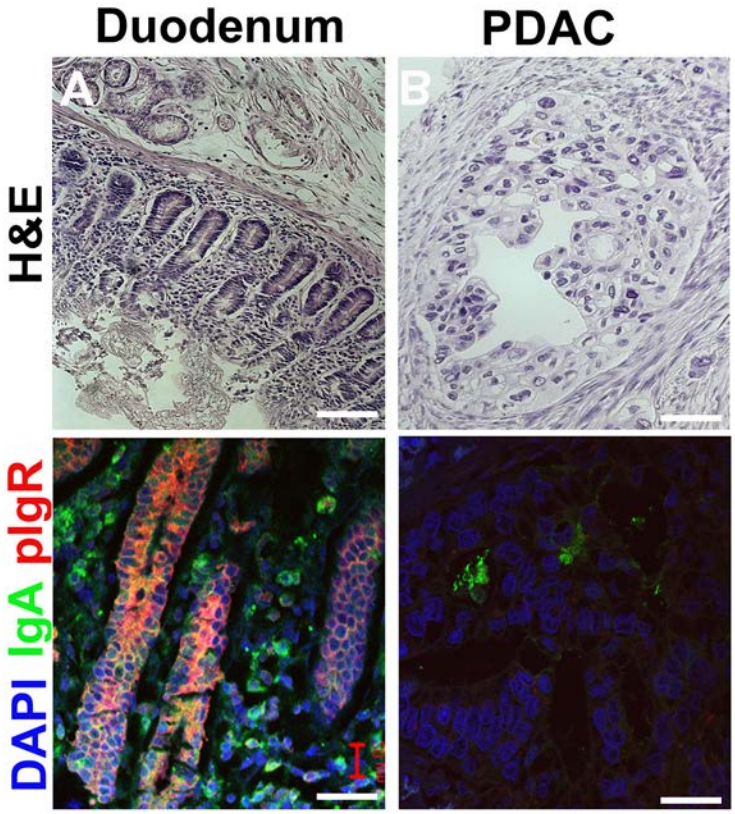

Figure 3.1: IgA is not expressed in human pancreas.

Representative images of H&E and immunofluorescence staining of normal human duodenum (A) and pancreatic cancer (B) sections. Sections were stained for IgA (green) and pIgR (red). Scale bar 20µm.

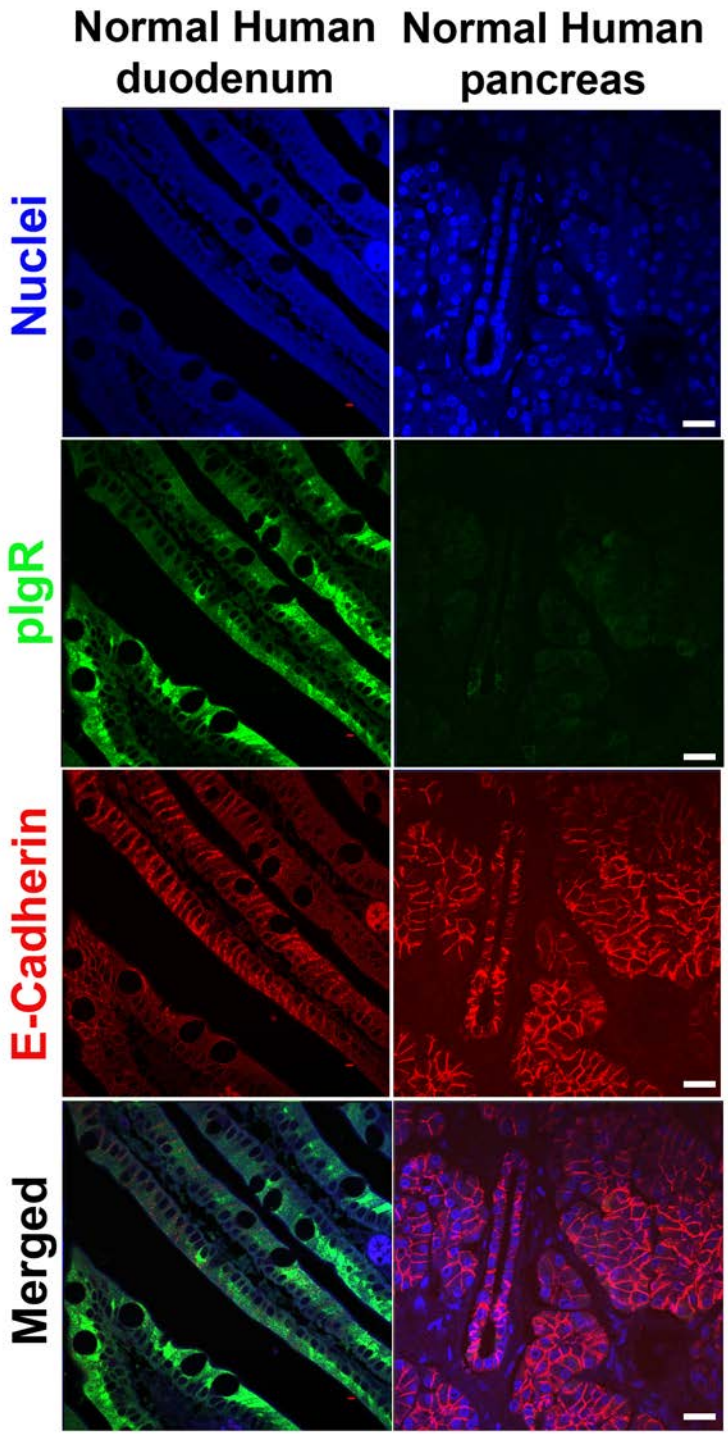

Figure 3.2: pIgR is not expressed in normal human pancreas.

Representative images of normal human duodenum and pancreas stained with pIgR (green) and E-Cadherin (red). Scale bar 20µm.

3.2.1 Confirmation of expression of pIgR in PDAC

pIgR and E-cadherin expression has been investigated by Kadaba et al in organotypics, who noted an inverse correlation. I sought to confirm this in human tissues (70). Having noted previously negative expression in normal pancreas, human TMA sections of PDAC were stained to confirm pIgR expression and E-Cadherin expression (**Figure 3.2 and 3.3**).

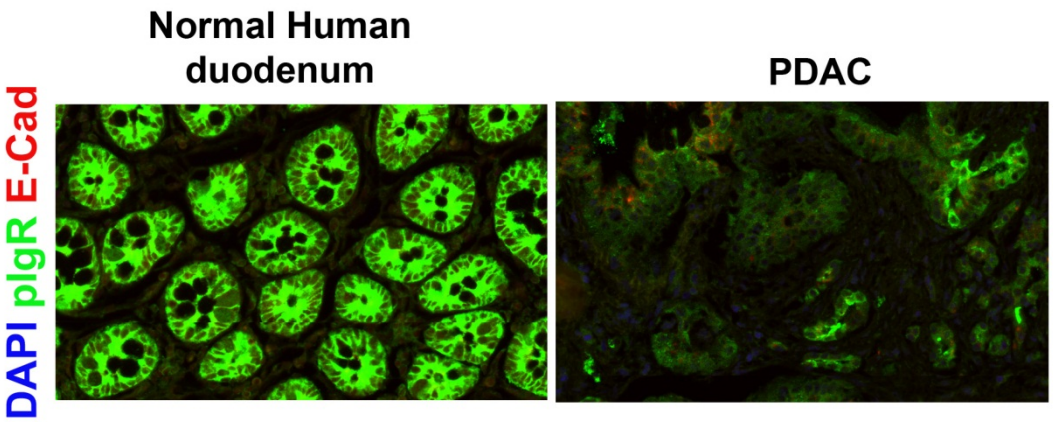

Figure 3.3: pIgR and E-Cadherin expression in human PDAC.

Representative images of TMA cores normal human duodenum and PDAC stained with pIgR (green). Scale bar 150µm.

3.2.2 Validation of staining intensity

Prior to investigating patient data, the intensity of staining quantification described in the Methods section was to be validated between manual scores and automated scores (ARIOL) systems. In order to test these methods, all independently scored one slide, containing 28 TMA cores. The distributions of the scores by each method are shown in Figure 3.4 and 3.5. A further correlation analysis was performed (without consensus meeting). Analysis of the scores given by clinicians shows a weighted Kappa of 0.675, which is a good (but not excellent) correlation of grading staining intensity, but there was no correlation between manual (clinicians) and ARIOL scoring (**Figure 3.5**).

Automated scoring seemed to give skewed scores because of background auto-fluorescence from Collagen which could not be corrected despite multiple attempts to compensate and train the ARIOL. Newer software, available since, may be able to compensate for this auto-fluorescence, but I did not have access to that technology (232). All scoring was therefore performed manually as described in Methods section.

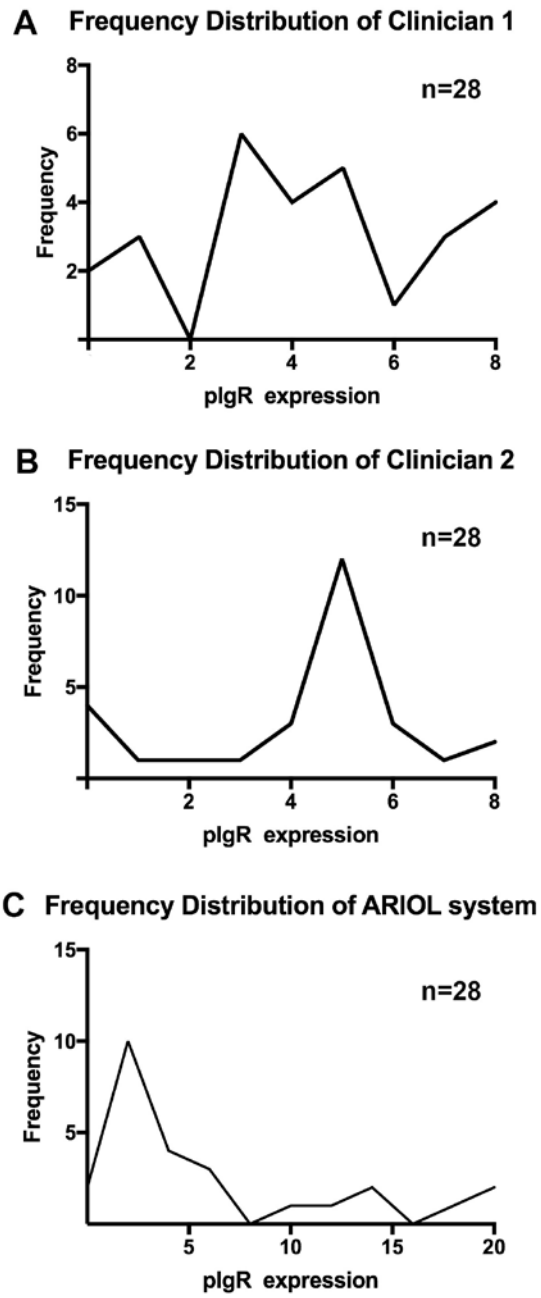

Figure 3.4: Distribution of pIgR expression scores across three independent scoring methods.

28 cores within a TMA with pancreatic cancer patient samples were stained and scored at the same time by different methods. Median score for Clinical 1 was 4 (Interquartile Range (IQR), 3-7), for clinician 2 was 5 (IQR, 3-5) and for ARIOL was 3 (IQR, 2-11). All scores for ARIOL more than 20 (n=2) were truncated to 20.

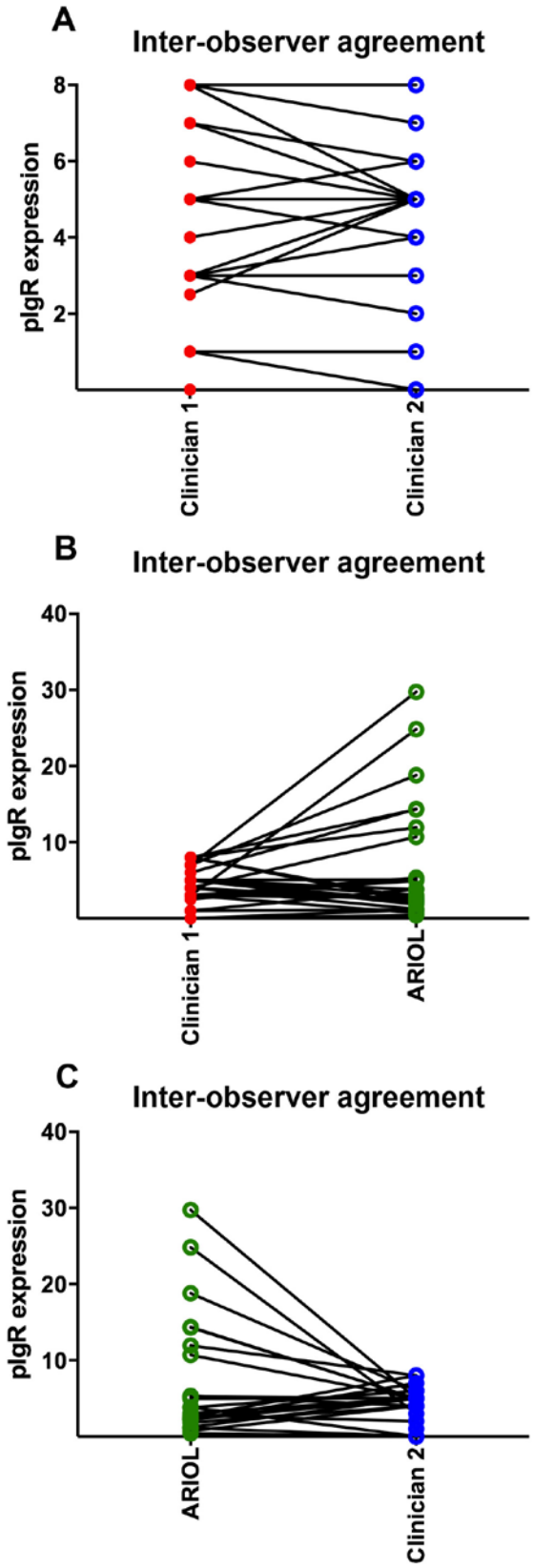

Figure 3.5: Inter-observer variability of scoring methods.

A-C Demonstrates inter-observer variability across the 3 methods of quantification. A) Clinician 1 vs. clinician 2 (Kappa 0.219, SE 0.096; weighted Kappa 0.675). B) Clinician 1 vs. ARIOL (Kappa 0.096, SE 0.077; weighted Kappa 0.265). C) Clinician 2 vs. ARIOL (Kappa 0.088, SE 0.064; weighted Kappa

0.175).

3.3 pIgR expression across peri-ampullary lesions

Having observed lack of pIgR expression in normal human pancreas and the subsequent expression in PDAC, I sought to explore pIgR expression in other human peri-ampullary pathologies because of the recent work by Fristedt et al (176).

pIgR is naturally expressed in intestinal or duodenal mucosa, thus loss in intestinal or duodenal sub-type of peri-ampullary cancer is expected.

Current classification of peri-ampullary tumours is complex due to a variety of reasons. This is mainly due to the common anatomical features and embryological origin of the periampullary region. Correct classification with respect to location of origin of cancer remains challenging to the pathologist, as there are no definitive markers to distinguish these different subtypes, if the tumour is not centred on one particular anatomical feature.

The differentiation of tumours is important because of the observed differences in survival. A major step was the recognition of the intestinal (INT) versus pancreatobiliary (PB) histopathologic phenotypes of ampullary carcinoma by Kimura et al (197). The INT type proved to be associated with considerably better prognosis than the PB subtype, which has been confirmed by several recent series (196, 198, 199) (**Figure 3.6**).

I could demonstrate pIgR expression in all cancers of the peri-ampullary origin (**Figure 3.7**). pIgR signal was dominant over the E-cadherin signal predominantly in the ampullary and duodenal cancers, where E-cadherin was markedly attenuated. Manual intensity and percentage of area scores were assimilated for pIgR staining to allow comparison between different pathologies. Not all patients had requisite minimum number of cores (n≥3) to derive a composite score. This was due to mal-folded TMA core or TMA drop-out or pre-dominantly stromal composition of core or absence of cancer in that particular section, all well appreciated drawbacks of TMA analysis. For the data available, staining intensity of pIgR did not differ amongst these

sub-types (**Figure 3.8**). PDAC (62%) and cholangiocarcinoma (13%) accounted for the majority of patients within the TMA. Unfortunately, there were insufficient patient numbers across all sub-types to provide comparative survival.

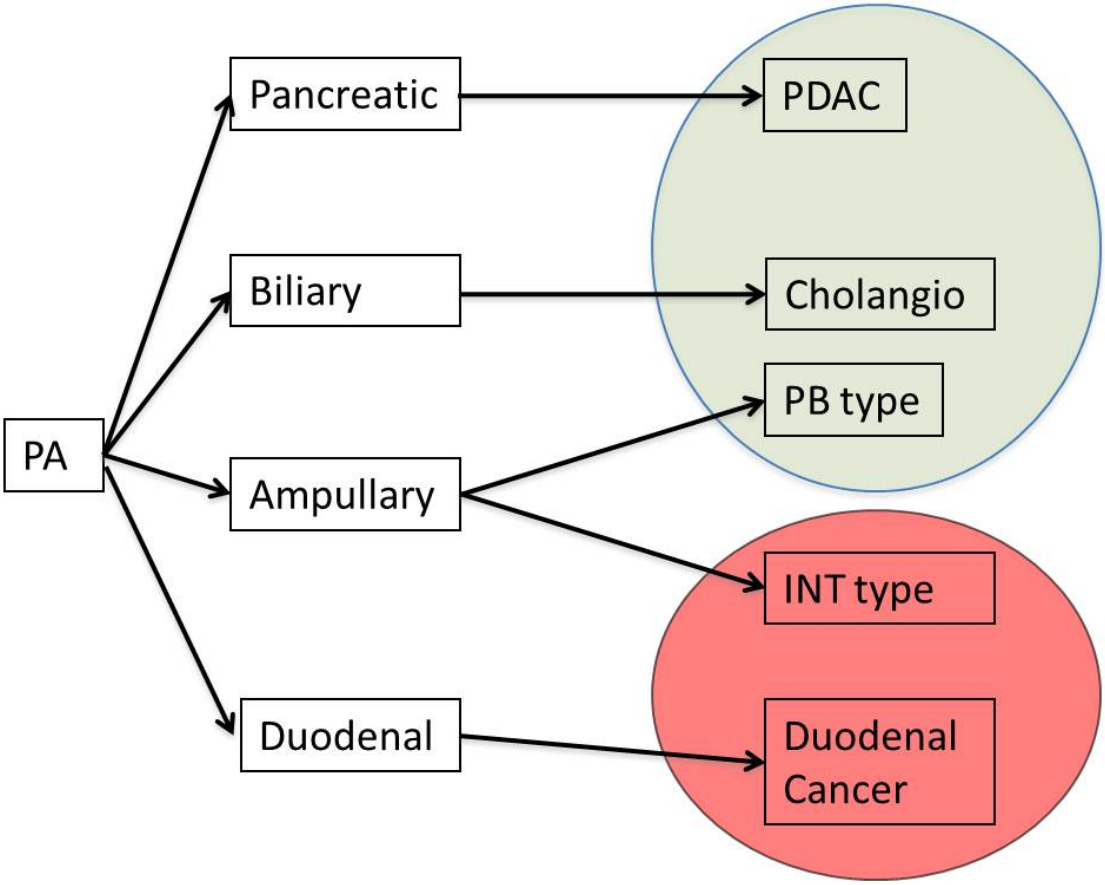

Figure 3.6: Cancers of the peri-ampullary region

Cancers of the peri-ampullary (PA) area can be divided into those arising from pancreatic, biliary, ampullary and duodenal tissues. Ampullary cancers are further subdivided into pancreaticobiliary (PB) and Intestinal subtypes (INT), based on pathological differentiation. In resected periampullary carcinoma, morphological type seems to provide more important prognostic information than the tumour origin, with pancreatobiliary versus intestinal differentiation being associated with significantly shorter survival rates (199, 233). Lesions of duodenum and Intestinal-type ampullary lesions generally have a better prognosis than the pancreaticobiliary type of cancers. Image assimilated based on Fristedt et al (176).

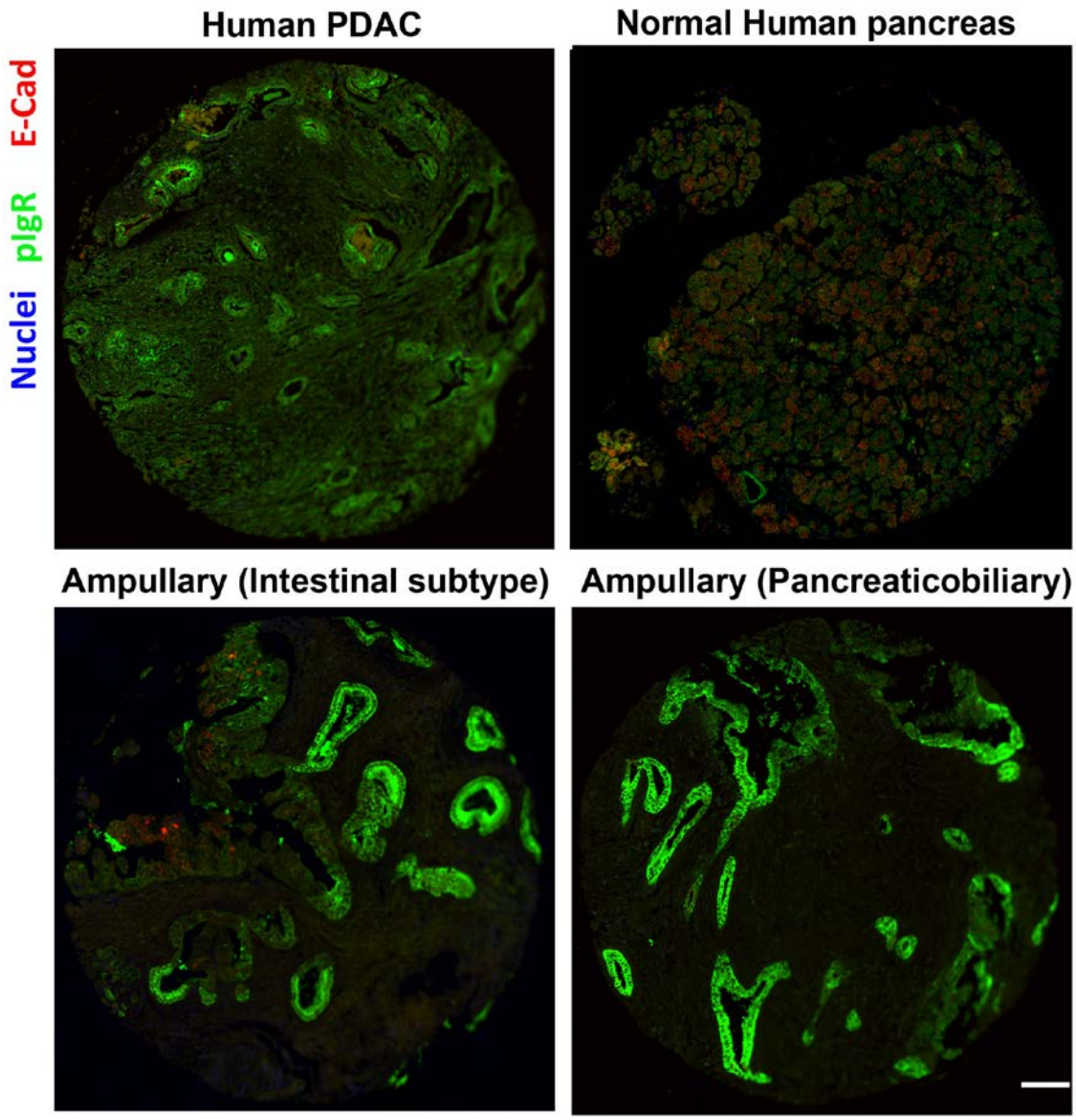

Figure 3.7: Representative images from TMA of human sections.

The cores are from the pancreas of patients with the relevant diagnosis. Sections stained with pIgR (green) and E-Cadherin (red). The strength of pIgR signal overwhelms the E-cadherin signal. Scale bar 150µm.

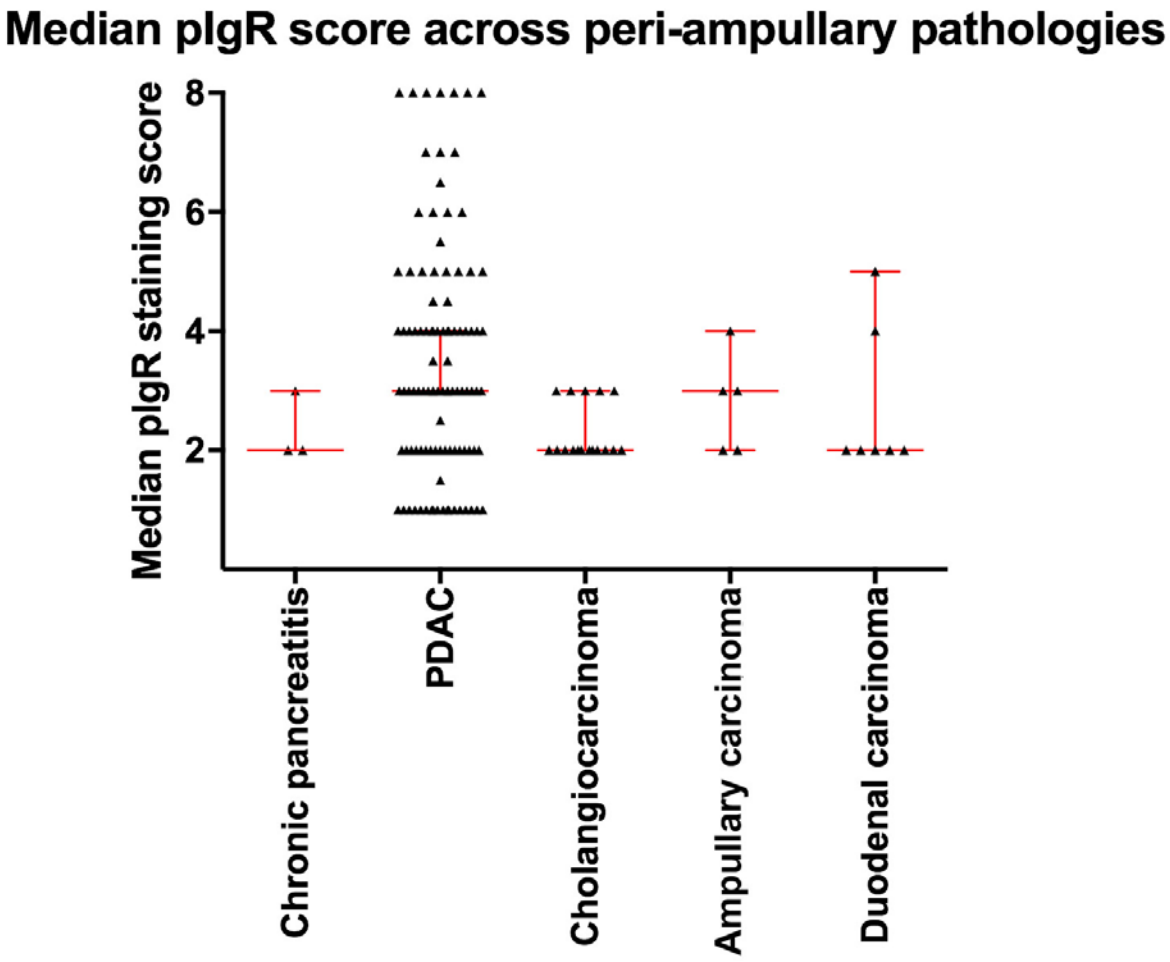

Figure 3.8: plgR expression across peri-ampullary lesions using manual scoring system.

Dot plot with median and interquartile range demonstrated no statistical significance in differences in median plgR staining score (Kruskal-Wallis, p=0.1318). Chronic Pancreatitis (n=3), PDAC (n=90), Cholangiocarcinoma (n=17), Ampullary (n=5), Duodenal (n=7).

3.4 pIgR expression and PanIN lesions

Previous work in PDAC *in vitro* models in our laboratory had suggested that E-cadherin (202) and pIgR (70) expression changes with increasing stromal activity.

Also, it is well established that as PDAC progresses through the PanIN stages, stromal activity increases (234). Hence I choose to study a relationship between pIgR and E-cadherin activity during PanIN evolution. To do this, I explored each TMA core and sought to investigate pIgR and E-cadherin expression within individual ducts, within cores containing PDAC. It is appreciated that in every instance of PDAC, there are ducts with PanIN morphology which can be assessed individually.

Assessing PanIN on immunofluorescent staining is challenging. I received training in assessing PanIN by Prof Kocher and Dr ChinAleong. JPEG images of corresponding H&E sections of TMA were also used to ascertain the presence of PanIN as well as the grade of PanIN. Normal ducts were scored from normal adjacent pancreas from pathologies other than PDAC. Examples are provided in Figure 3.9.

Each duct was graded based on pathological appearance as normal, PanIN 1, 2 or 3 and PDAC and each duct was then scored as previously (Section 2.3.4) for pIgR and E-cadherin expression (**Figure 3.9**). Each duct was then individually scored, thus giving rise to many more ducts than the cores or patients available.

Increasing expression of pIgR was noted in progressive PanIN progression stages. However expression of pIgR expression virtually disappeared in invasive PDAC (**Figure 3.10**). It must be mentioned here that the pIgR scores for PDAC analysis in Figure 3.8 are composite scores accounting for all PanIN within the cores and all cores for the same TMA. This would explain the apparent discrepancy in PDAC composite scores in Figures 3.8 and 3.10.

Furthermore, as expected a decreasing expression of E-cadherin was seen in PDAC evolution, which validated the methods I have used for identification of ducts as well as the scoring system I have used. (**Figure 3.10**) I demonstrate that pIgR expression is inversely related to E-Cadherin expression, thus validating findings of

Kadaba et al (235) from our laboratory in *in vitro* systems (**Figure 3.10**).

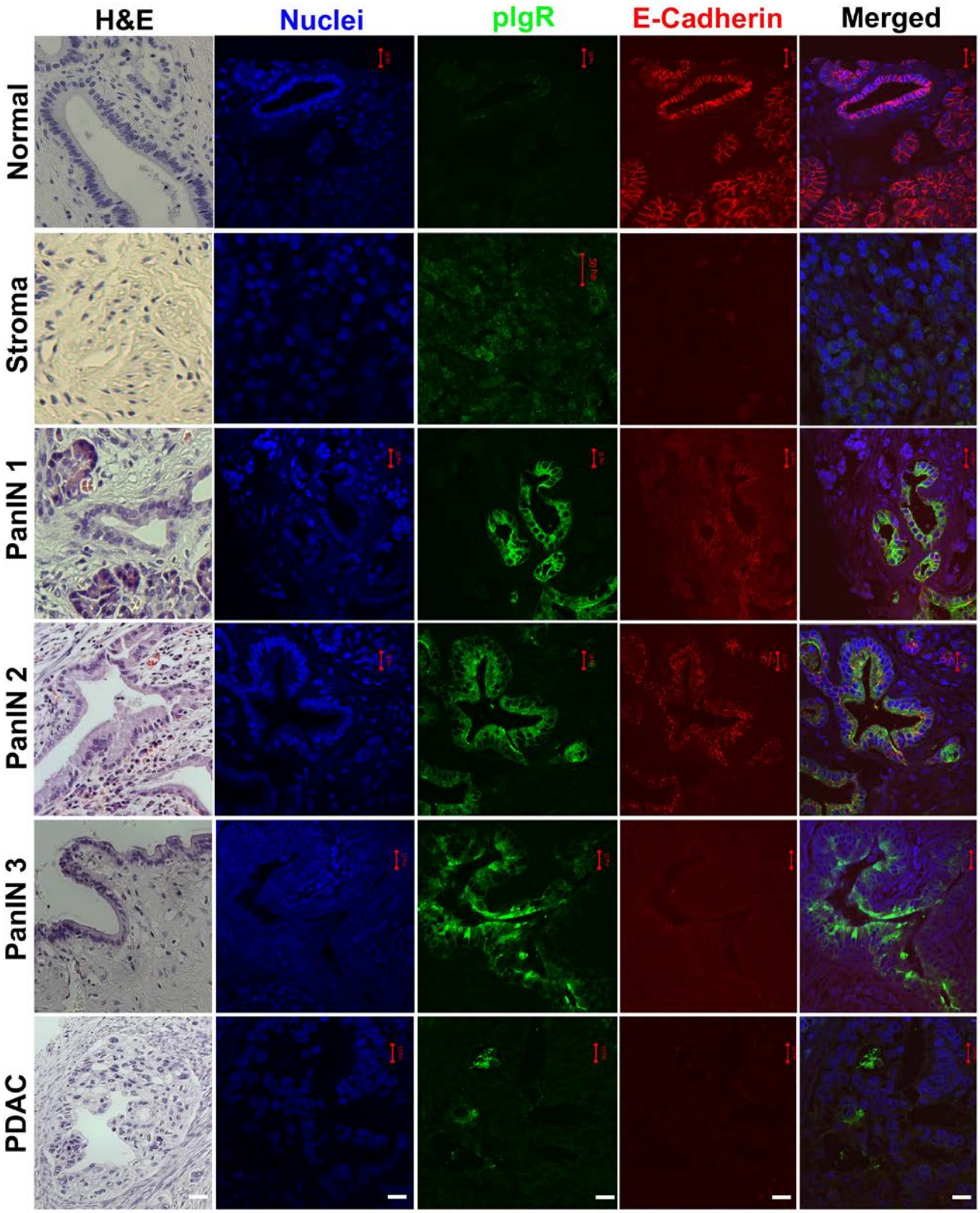

Figure 3.9A: Inverse relationship of pIgR and E-Cadherin.

Representative images of sections from human PDAC samples stained with pIgR (green) and E-Cadherin (red), comparing progression from normal pancreatic ducts to invasive PDAC via different PanIN stages. Scale bar 20µm.

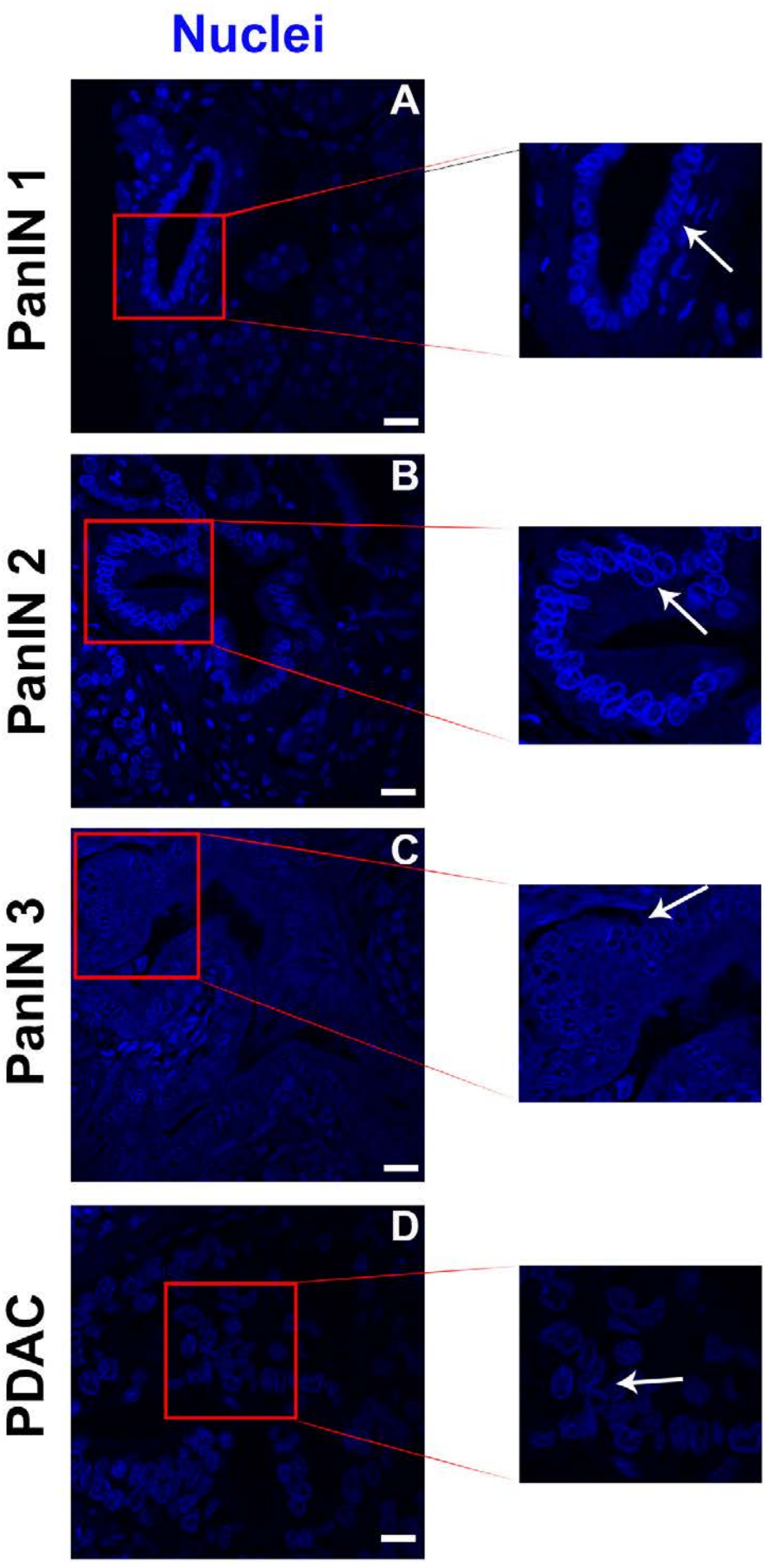
Nuclei
PanIN 1
PanIN 2
PanIN 3
PDAC
A
B
C
D

Figure 3.10B: Nuclear features of PanIN

A) PanIN 1 demonstrates columnar cell change and mucinous differentiation, without much nuclear atypia but some overlapping of nuclei (arrow). B) PanIN 2 lesions lose the mucinous epithelium but demonstrate nuclear pleomorphism and crowding (arrow) and some mitotic figures may be present. C) PanIN 3 relates to carcinoma *in situ*, with pseudopapillary formation, nuclear atypia (arrow), apoptotic debris and frequent mitotic figures. D) PDAC is invasive carcinoma and represents cancer breaching the basement membrane (arrow). Scale bar 20µm.

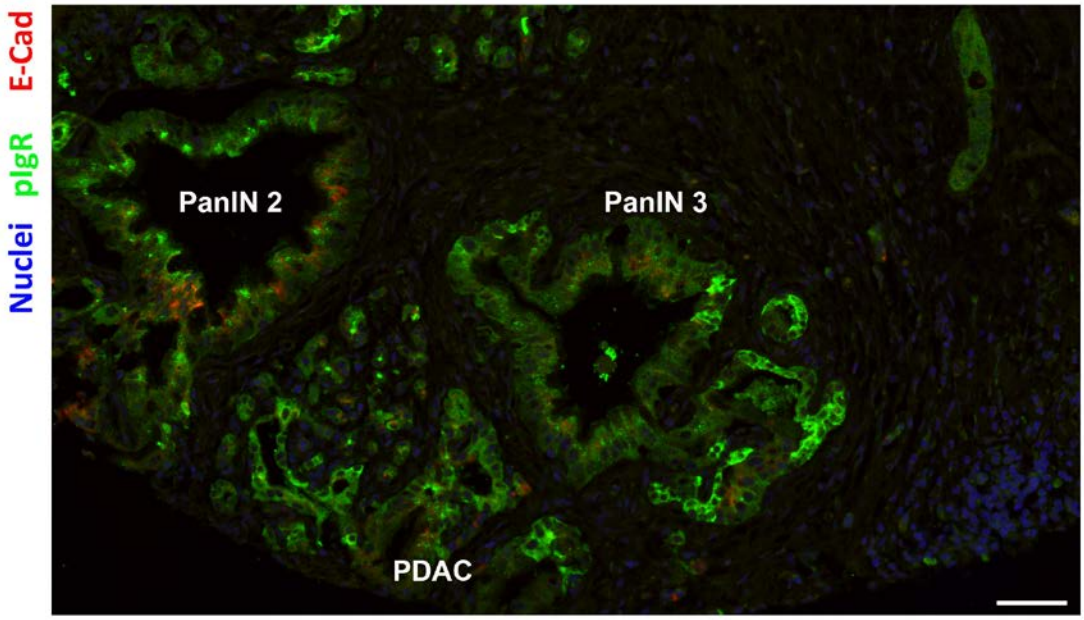

Figure 3.11C: PanIN and PDAC variability

Representative image of part of TMA cores from human PDAC, stained with pIgR (green) and E-cadherin (red) and demonstrating PanIN lesions admixed with PDAC. Scale bar 100µm.

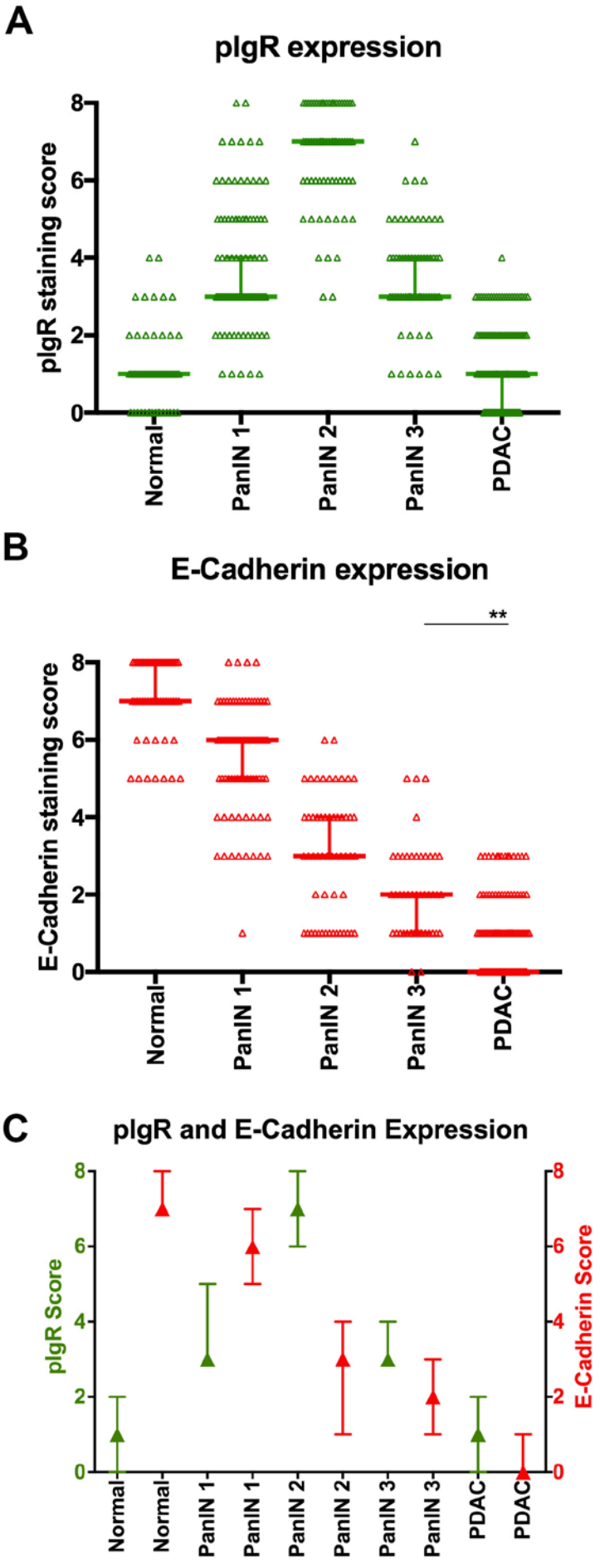
A
pIgR expression
pIgR staining score
8
6
4
2
0
Normal
PanIN 1
PanIN 2
PanIN 3
PDAC
B
E-Cadherin expression
**
E-Cadherin staining score
8
6
4
2
0
Normal
PanIN 1
PanIN 2
PanIN 3
PDAC
C
pIgR and E-Cadherin Expression
pIgR Score
E-Cadherin Score
8
6
4
2
0
Normal
Normal
PanIN 1
PanIN 1
PanIN 2
PanIN 2
PanIN 3
PanIN 3
PDAC
PDAC

Figure 3.12: Inverse relationship of pIgR and E-Cadherin expression.

Figures A&B demonstrate changes in expression of pIgR and E-Cadherin in precursor lesions and invasive PDAC. Data is represented as dot-plot with median and inter-quartile range. Highest mean pIgR score noted in PanIN 2 (6.690, 95% CI 6.387-6.994), whilst highest mean E-Cadherin score was noted in normal ducts (7.074, 95% CI 6.794-7.354).

A) pIgR expression in pancreatic ducts. Normal (n=55), PanIN 1 (n=93), PanIN 2 (n=71), PanIN 3 (n=63), PDAC (n=155). Kruskal-Wallis with Dunn's multiple comparison tests. All other comparisons show $p<0.0001$.

B) E-Cadherin in pancreatic ducts. Normal (n=54), PanIN 1 (n=81), PanIN 2 (n=55), PanIN 3 (n=46), PDAC (n=155). Kruskal-Wallis with Dunn's multiple comparison tests. PanIN 3 versus PDAC,** $p=0.0004$. All other comparisons show $p<0.0001$.

C) Summary median and inter-quartile scores of staining intensity of pIgR and E-cadherin in PDAC progression.

3.5 pIgR and patient survival

Median pIgR score was calculated for all ducts for each PDAC patient. Patients with incomplete follow up or unable to score at least three TMA cores accurately were removed from survival analysis. I therefore had 88 patients (of which 46 were male) to evaluate for the impact of pIgR expression on overall survival.

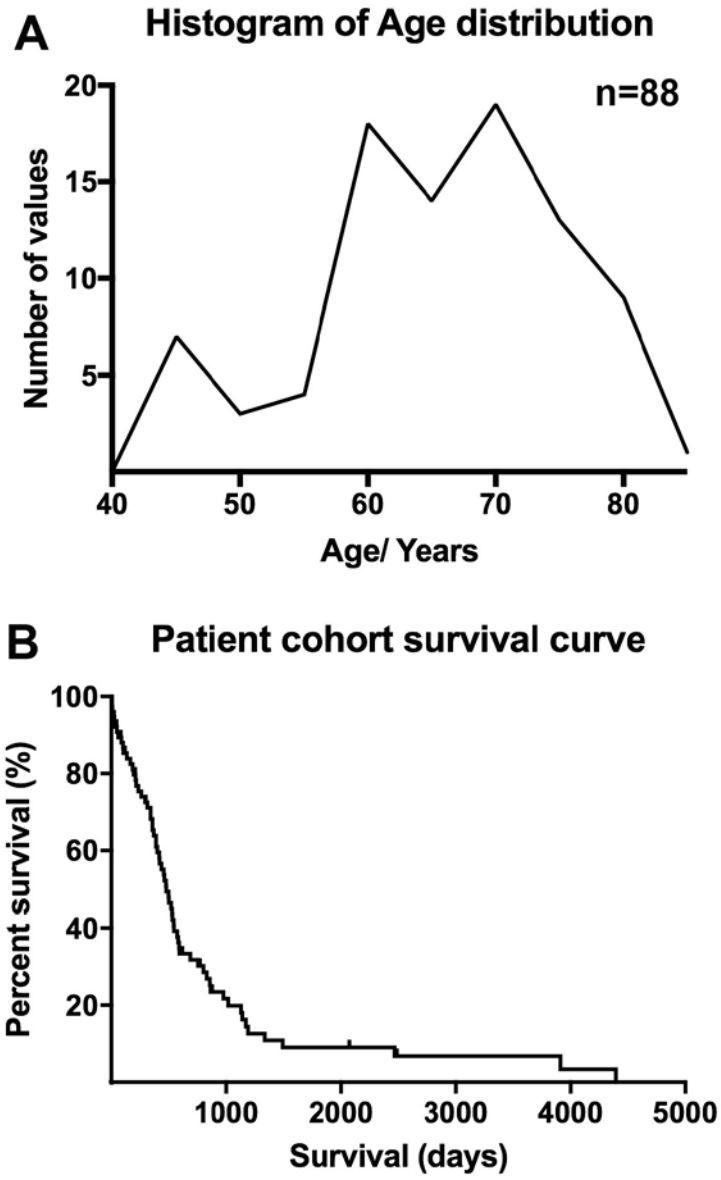

Figure 3.13: Patient characteristics.

A total of 88 patients had sufficient data for analysis. A) Age distribution amongst all PDAC patients in the cohort. Median age 67 (IQR, 60-73) years. B) Kaplan-Meier survival curve for patient cohort. Median survival 481 (IQR, 273-802) days.

Patient demographics confirm a peak age of 60-70 years and the survival

curve similar to other studies (236) (**Figure 3.11**).

		Overall	Low pIgR Score	High pIgR Score	P Value
		N = 88	N = 60	N = 28	
Age	Median	67	67	67	0.8534*
	Range	43 – 83	46 – 83	43 – 80	
Survival (days)	Median	518	486	583	0.2791**
	95% CI	535 - 905	474 - 961	444 - 1008	
Gender	Male	46	32	14	0.8950**
	Female	42	28	14	
T Stage	pT1-2	32	22	10	0.5857**
	pT3-4	56	38	18	
Nodes	pN0	36	25	11	0.8941***
	pN1	52	35	17	
Invasion	None	22	13	9	>0.9999***
	Venous	7	6	1	
	Neural	20	13	7	
	Both	39	28	11	
Resection	R0	59	40	19	0.3816***
	R1	29	20	9	

Table 11: Association of pIgR expression in PDAC with clinicopathological parameters.

Statistical tests performed are; * t-test, ** Mann-Whitney U test, * Chi-square test**

The dichotomisation process in X-Tile allocates 0 to 3.5 as a low pIgR score, whilst 3.6 to 8 is considered high as the optimal cut-off (**Figure 3.12 A**). There was no difference in survival between patients expressing high or low pIgR staining scores (**Figure 3.12 C**). No difference was found in patient or pathological features based on this separation of patients into two groups of high and low pIgR expression (**Table 11**).

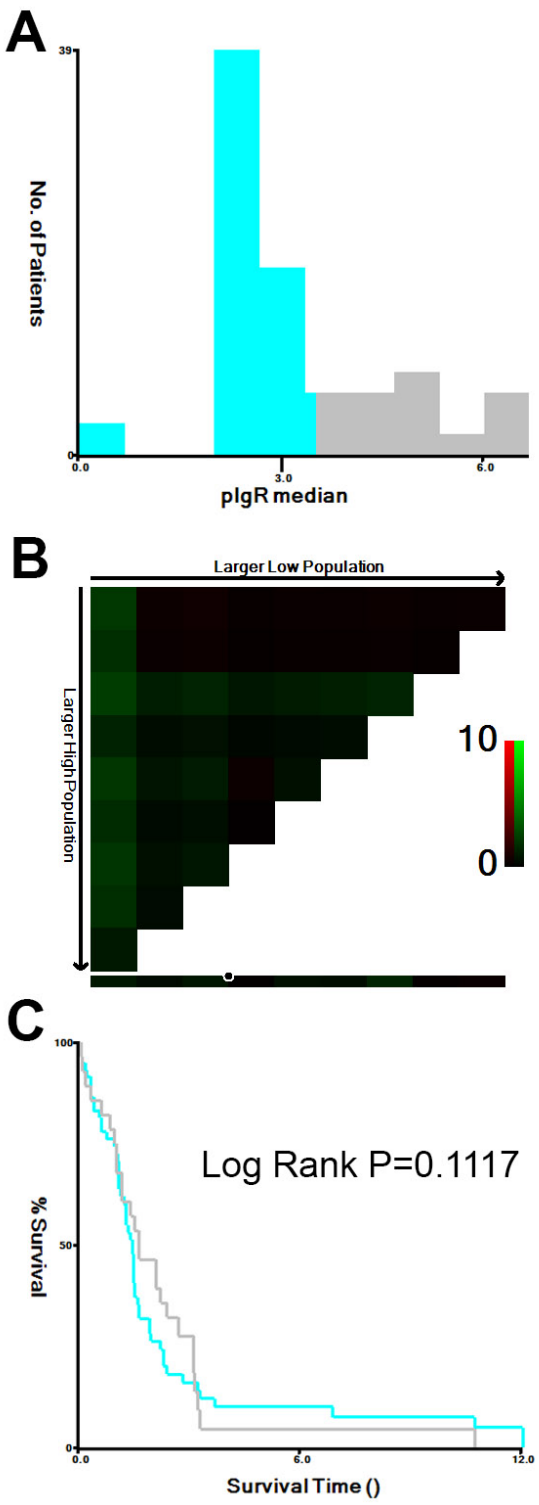

Figure 3.14: Correlation between pIgR and survival.

(A) Histogram of distribution of pIgR intensity scores for expression. (B) Pictorial representation of various population dichotomisations to determine the most optimal cut-off for differences in survival for high- and low-expressing pIgR patients. (C) Comparison of survival between high (grey line) and low (blue line) pIgR expressing patients. Log Rank, p=0.1117.

3.6 pIgR and systemic factors

Having proven that pIgR is not an independent prognostic marker in PDAC in my limited sample of patients, I investigated its association with systemic factors to evaluate the association of pIgR with patient, inflammatory and tumour invasive characteristics.

Theoretically, younger patients may be more able to cope with the insult of a larger operation and may be prone to lower rates of inflammatory complications. However, there have been no significant differences shown in 30-day survival and 90-day readmission rates according to age (237). Separating the patient cohort according to age does not show a difference in pIgR intensity staining (**Figure 3.13 A**).

Dividing the cohort according to male and female shows no difference in pIgR staining intensity (**Figure 3.13 B**).

The patient sample data was investigated for tumour characteristics, such as local invasion, differentiation of tumour and nodal involvement. Alongside this, I also collated patient data for pre-operative blood tests. With pIgR related in normal physiology to IgA and inflammatory processes, I collated data of WCC and C - reactive protein. These markers are currently used as an indicator of inflammation, thus a potential correlation between pIgR and these inflammatory markers may indicate a correlation with earlier stages of PDAC development.

Dividing tumours according to pathological differentiation showed no difference in pIgR median intensity staining scores (**Figure 3.14 A**). Invasion into neural and venous structures confers poor survival. However, there is no association between pIgR staining intensity and local invasion (**Figure 3.14 B**).

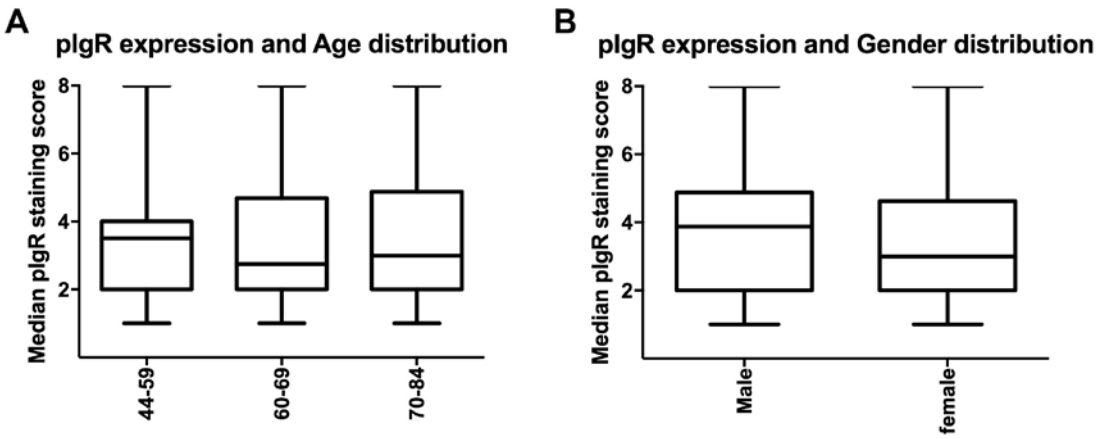

Figure 3.15: Association of pIgR expression and patient cohort.

A) Median pIgR staining intensity score according to age does not show a difference in pIgR staining. 44-59 (n=24), 60-69 (n=31), 70-84 (n=33). Kruskal-Wallis test, p=0.7344. (B) Dividing the cohort according to male and female gender shows no difference in pIgR staining intensity. male (n=46), female (n=42). Paired T test, p=0.2683.

Tumour resection margin involvement confers poor survival (238). R0 resection refers to no cancerous cells seen macroscopically and R1 means cancerous cells seen. R2 mean gross inspection demonstrates tumour at the potential resection margin. R2 resections are incomplete resections.

I have chosen to only include complete resections in R1 and R0, as R2 resection samples were not seen in our cohort. Again, there is no association between pIgR and resection margin (**Figure 3.14 C**).

Lymph node (LN) involvement is also known to be prognostic and as a result, the extent of lymphadenectomy and LN ratio has been areas of active research and debate (239). There is no clear consensus or guidelines on the minimum number of nodes that should be examined during PDAC resection, as well as the prognostic significance of number and ratio of involved nodes (240). Separating nodal metastasis negative, less than 50% nodal positive and more than 50% nodal positive also shows no difference in pIgR staining score (**Figure 3.14 D**).

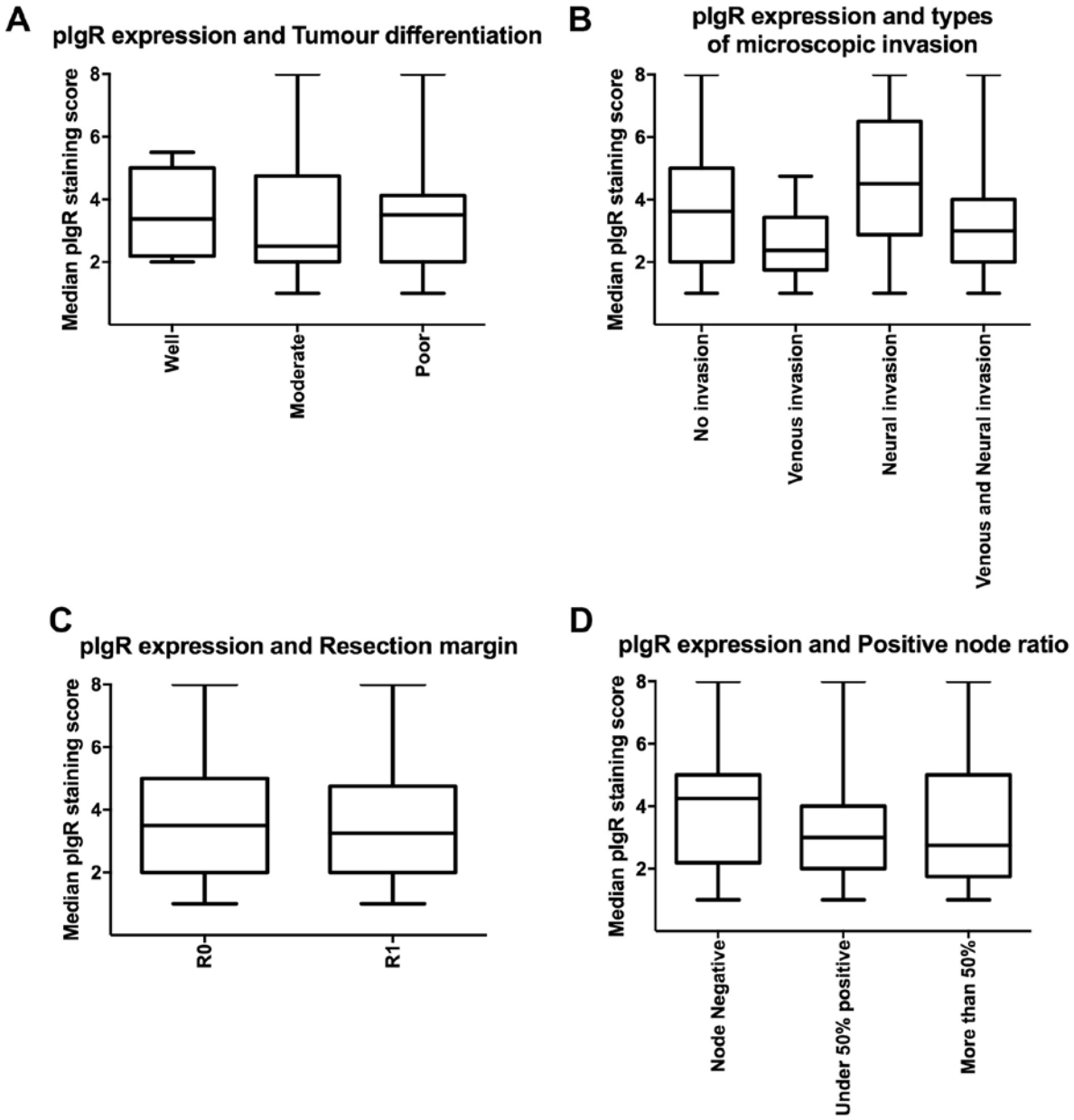

Figure 3.16: Association of pIgR expression and systemic factors.

A) Comparing pIgR staining intensity with tumour differentiation shows no significant difference across the groups. Well (n=12), Moderate (n=44), poor (n=32). Kruskal-Wallis test, p=0.9184. B) Comparing pIgR with tumour invasion into local structures shows no significant difference across the groups. No Invasion (n=22), Venous invasion (n=7), Neural invasion (n=20), venous and neural invasion (n=39). Kruskal-Wallis test, p=0.0631. C) Comparing pIgR with resection margin shows no significant difference across the groups. R0 (n=59), R1 (n=29). Mann Whitney U test, p= 0.0912. D) Comparing pIgR with positive node ratio shows no significant difference across the groups. Node negative (n=27), under 50% positive (n=45), more than 50% (n=16). Kruskal-Wallis test, p=0.5012.

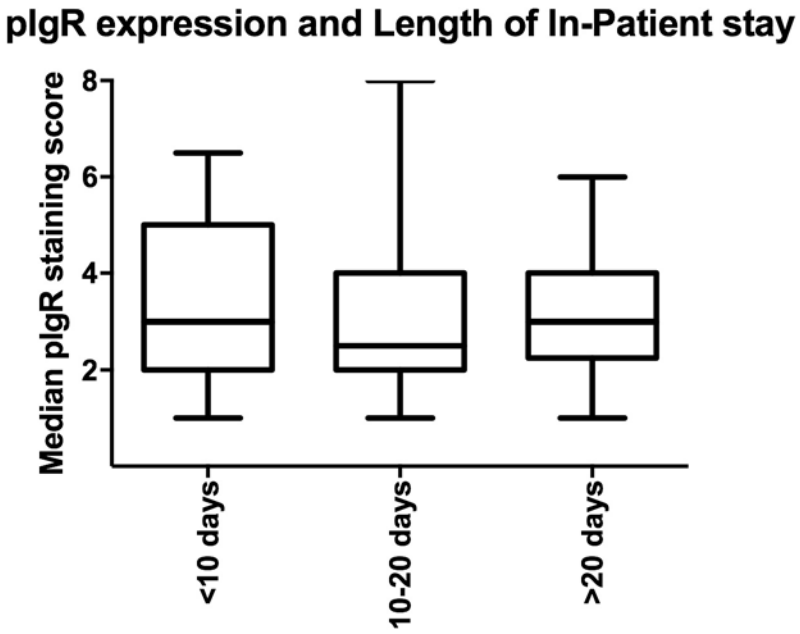

Figure 3.17: Correlation of pIgR expression with length of In-patient stay.

Comparing pIgR staining expression with length of in-patient stay shows no significant correlation. <10 days (n=11), 11-20 days (n=15), >21 days (n=13), Kruskal-Wallis test, p=0.9749. Accurate data for hospital stay was not available for 45 patients.

Length of In-patient stay is an important factor when comparing the benefits of different types of operative procedure as this maybe a surrogate marker for post-operative complications (241). I did not see any correlation between pIgR staining and length of in-patient stay (**Figure 3.15**).

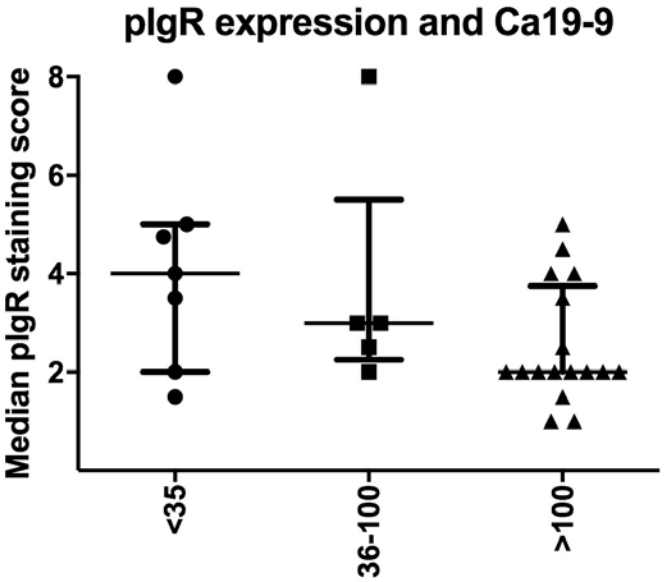

Figure 3.18: Correlation of pIgR staining intensity and pre-operative Ca19-9 result.

Comparing pIgR expression with pre-operative Ca19-9. <35 (n=7), 36-99 (n=5), >100 (n=17), Kruskal-

Wallis test, p=0.1433. Data was not available for 55 patients within 3 days pre-operatively.

Carbohydrate antigen 19-9 (Ca19-9) is currently accepted as a prognostic marker for survival after resection (242). I identified 29 patients who had a pre-operative Ca19-9 within 7 days of operation. Ca19-9 value less than 35 IU/ml is considered normal at the Royal London Hospital. Again, there is no correlation between pre-operative Ca19-9 and pIgR staining intensity (**Figure 3.16**).

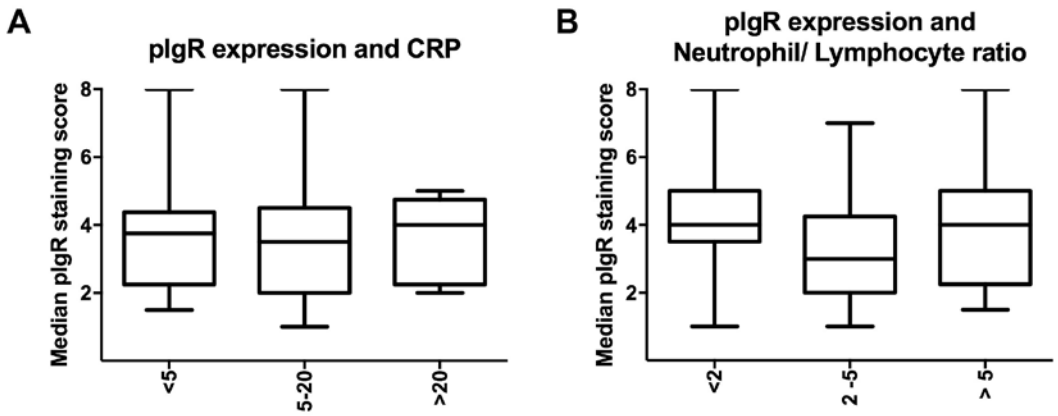

Figure 3.19: Association of pIgR staining intensity and inflammatory markers.

A) Comparing pIgR staining score with CRP. <5 (n=8), 5-20 (n=13), > 20 (n=5), Kruskal-Wallis test, p=0.8871. B) Comparing pIgR with Neutrophil/ lymphocyte ratio. <2 (n=19), 2-5 (n=37), > 5 (n=15). Kruskal-Wallis test, p=0.0449. Dunns post comparison test; <2 vs. 2-5 p=0.0659, <2 vs. >5 p>0.999, 2-5 vs.>5 p=0.2991.Data was no available for CRP for 62 patients and for blood counts for 15 patients within 3 days pre-operatively.

C-reactive protein is a pentameric protein found in blood plasma whose levels rise in response to inflammation. Although used as a sign of acute inflammatory response clinically, it is of minimal significance as a prognostic marker, especially in the post-operative period (243). However, with a correlation to potential influx of inflammatory mediators in the initial phase on tumour development (203), I sought to explore a correlation with pIgR and CRP taken within 12 hours pre-operatively. However, again no correlation was seen (**Figure 3.17 A**).

In order to exhaust the inflammatory association of pIgR with patient characteristics, I sought to investigate neutrophil and lymphocyte values. Neutrophils are generally considered the first line of defence and are the most abundant granulocyte, accounting for up to 70% of total White Cell Count. Lymphocytes account for B cell, T cells and Natural Killer cell populations amongst others (244). Again, neutrophil and lymphocyte counts were measured within 12 hours of operation and a ratio was also determined (Neutrophils/ Lymphocytes), as this may have a prognostic impact (234) (**Figure 3.17 B**).

3.7 pIgR and tissue factors

PDAC is characterised by intense desmoplastic stroma containing cancer-associated fibroblasts. These activated fibroblasts express alpha-smooth muscle (αSMA) and a large amount of extra-cellular matrix (79). The stroma in PDAC promotes tumour formation, invasion and metastasis (79). By providing a physical barrier, it can also be considered to aid in radio- and chemo-resistance (245). However, this is not universally accepted. By investigating sonic hedgehog (66) in PDAC and genetically engineered mouse models, Rhim et al demonstrated some components of the stroma can act to restrain tumour growth (65).

3.7.1 αSMA Immunofluorescence staining of paraffin sections

αSMA has been investigated previously as a potential prognostic marker for PDAC (246, 247), by attempting to identify a correlation between αSMA and patient survival. As an independent prognostic marker, no one has yet found a correlation with αSMA and survival. However, Sato et al noted palladin (247), which is an actin binding protein and has been used recently as a cancer associated fibroblast is a surrogate indicator of treatment after chemoradiation therapy.

I sought to confirm previously noted findings related to αSMA, but also if there was any correlation with αSMA staining and pIgR expression (**Figure 3.18**).

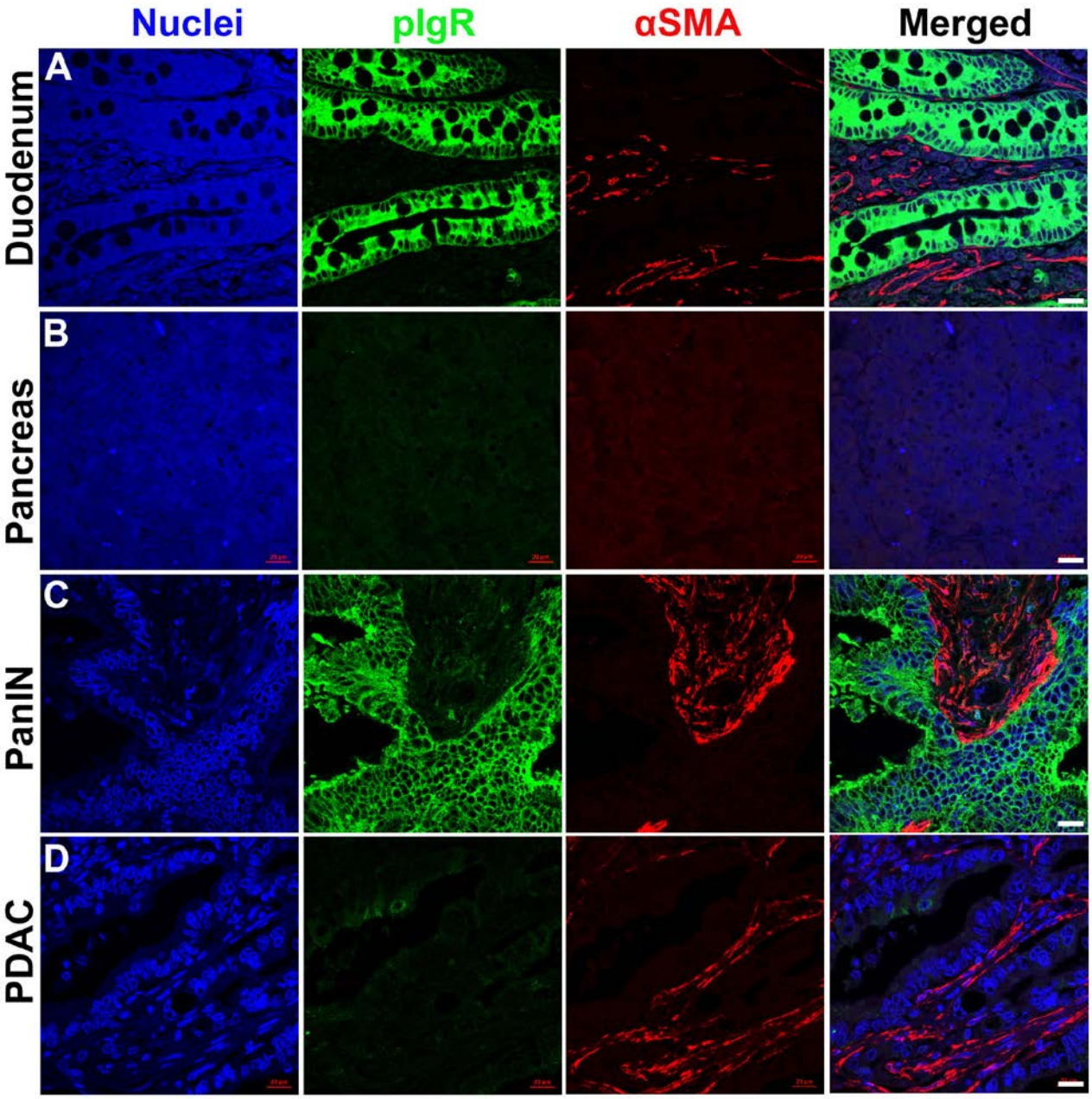

Figure 3.20: Representative images of sections from human PDAC.

Samples stained with pIgR (green) and αSMA (red), comparing progression from normal pancreatic ducts to invasive PDAC. Duodenum was used as a positive control. Scale bar 20µm.

3.7.2 Comparing survival with αSMA staining

Kadaba et al investigated the role of desmoplastic stroma in the context of 3D organotypic models, noting *in vitro* a reciprocal relationship between E-cadherin and pIgR in cancer cells was dependent on the stromal content of human pancreatic cancer. I sought to corroborate these findings *in vivo*.

Tumour specimens were collected from 88 PDAC patients during curative resections in the Royal London Hospital, Whitechapel, England, as discussed previously.

TMA stained for pIgR and αSMA were scored and collated scores were compared to patient survival as discussed previously in Materials section. Sequential sections of TMA blocks were stained for pIgR and E-cadherin then αSMA and pIgR. pIgR staining intensity was confirmed to be the same in both sets.

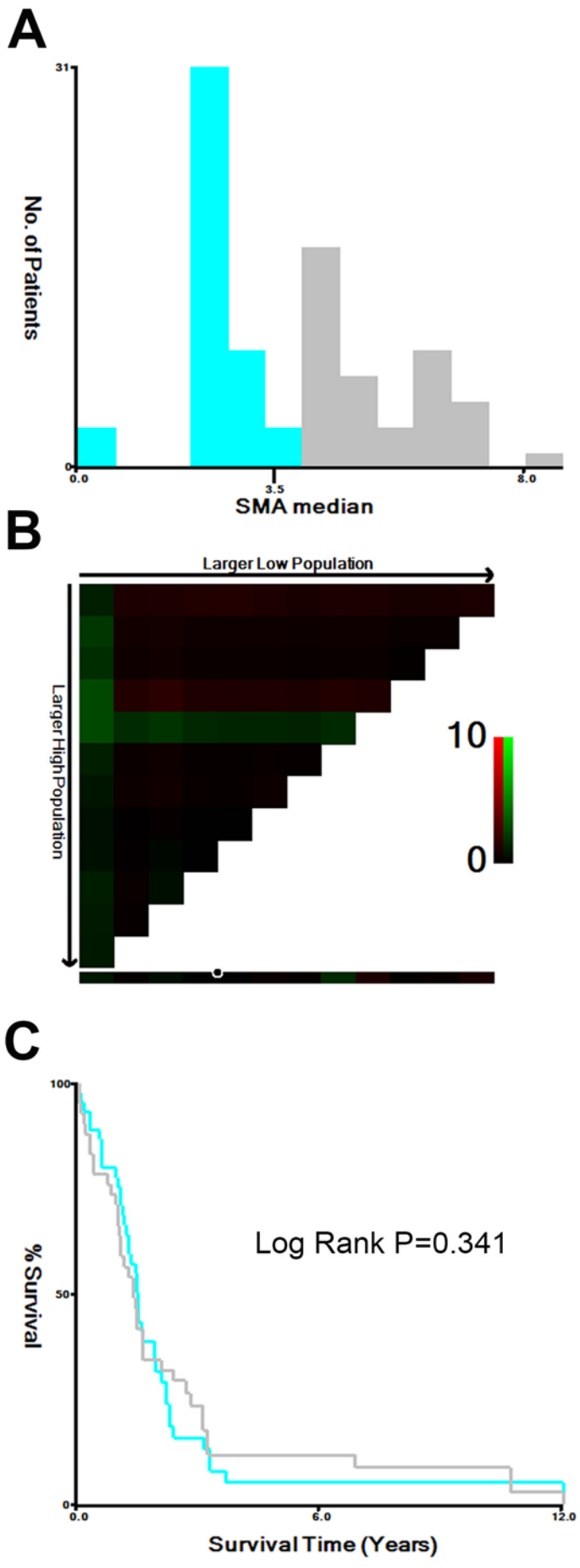
A
31
No. of Patients
0
0.0
3.5
8.0
SMA median
B
Larger Low Population
Larger High Population
10
0
C
100
50
0
% Survival
Log Rank P=0.341
0.0
6.0
12.0
Survival Time (Years)

Figure 3.21: Correlation between αSMA and survival.

(A) Histogram distribution of αSMA expression. (B) Pictorial representation of various population dichotomisations to determine the most optimal cut-off for differences in survival for high- and low-expressing αSMA patients. (C) Comparison of survival between high (grey line) and low (blue line) expressing patients. Log Rank, p=0.341, Corrected Miller Seigmund, p=1.

Using the X-tile program, as explained previously, the patients that had been scored for αSMA were dichotomised. The light blue colour represents low αSMA expression cohort whilst grey is the high expression cohort (**Figure 3.19 A**). The dichotomisation process allocates 0 to 4 as a low score, whilst 4.5 to 8 are considered high. The low scoring group had 54 patients whilst the high scoring group had 34.

Reviewing pictorial representations of the correlation between patient survival and αSMA scoring, should there be a positive correlation, we would expect to see patches of bright red or green, based on a positive or negative correlation. The lack of colour indicates a poor relationship between level of score and eventual survival (**Figure 3.19 B**)

Overall survival was assessed using the Kaplan-Meier method, where by low scores of combined αSMA (blue line) and high scores (grey line) are represented. αSMA staining intensity score alone has no impact on patient survival in this cohort (**Figure 3.19 C**).

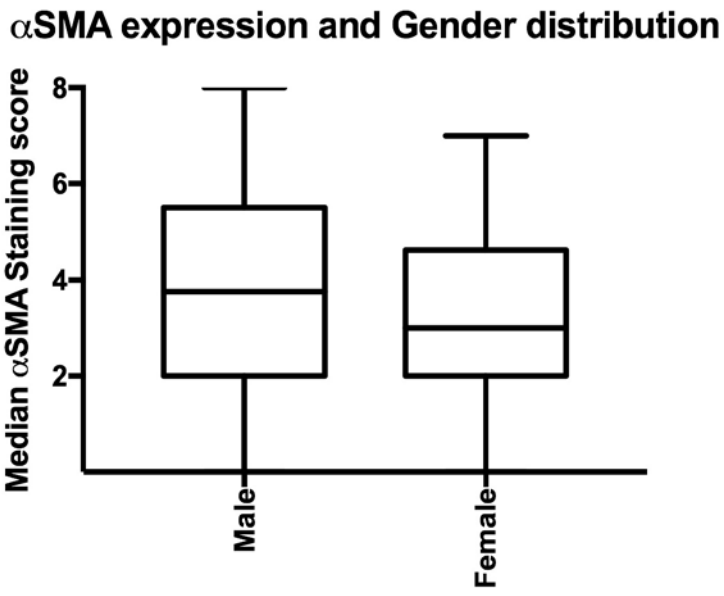

Figure 3.22: Association of αSMA and gender.

Dividing the cohort based on gender shows no difference in αSMA staining intensity. Male (n=46), Female (n=42). Paired t test, p=0.3466

Dividing the cohort according to male and female shows no difference in αSMA staining intensity (**Figure 3.20**).

Tumour necrosis and hypoxia has been considered to be a result of systemic inflammation (248). Patients with neutrophil infiltration around the tumour may have a poorer prognosis than those without infiltration, whereas patients with lymphocyte around the tumour may be associated with a better prognosis (249). Circulating neutrophil-lymphocyte ratio is a reflection of systemic inflammation and was explored in 3.5. However, αSMA is a marker for activated pancreatic stellate cells (PSCs) in PDAC. PSCs affect cancer growth, survival, metastasis, angiogenesis and immunosurveillance through the secretion of various cytokines, such as CXCL12 and secreted protein acidic and rich in cysteine (SPARC) (250). My theory was higher circulating cytokines in the presence of activated stellate cells may therefore have a correlation. Thus I only compared the total white cell count (WCC) with αSMA expression. Again, blood results were included if within 12 hours pre-operatively. There is no correlation with αSMA staining and WCC (**Figure 3.21**).

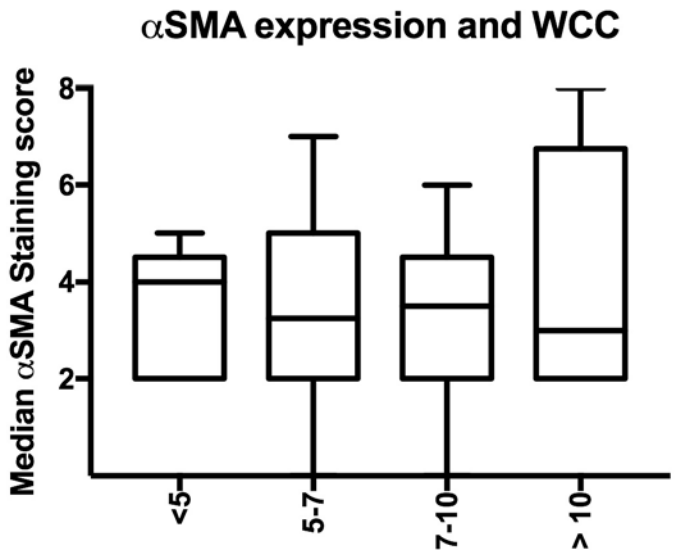

Figure 3.23: Association of αSMA and White cell count (WCC).

Comparison of pre-operative WCC, with WCC results separated according to <5 (n=5), 5-7 (n=36), 7-10 (n=33) and >10 (n=13). There is no correlation with αSMA staining and WCC. Kruskal-Wallis test, p=0.4238.

Correlating αSMA with pathological differentiation, i.e. well, moderate and poorly would attempt to demonstrate an association with increasing activated PSCs in a tumour. However, no difference in αSMA median staining score was observed (**Figure 3.22**).

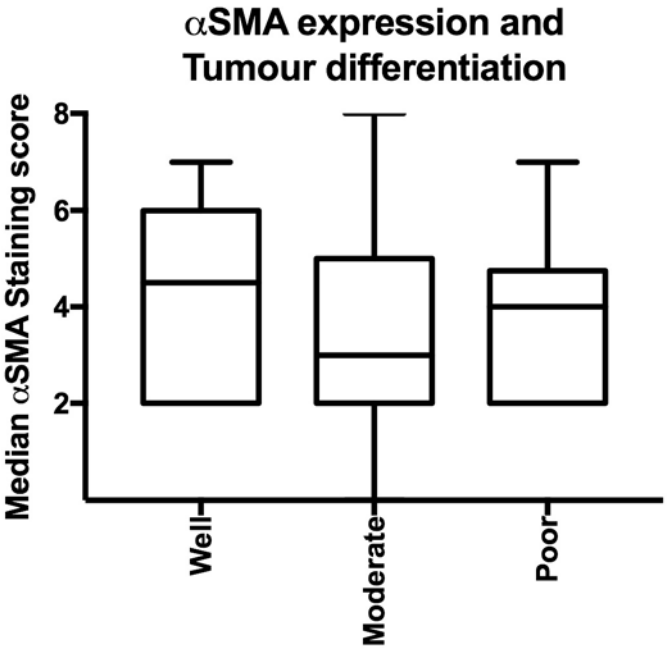

Figure 3.24: Association of αSMA and tumour differentiation.

Correlation of αSMA staining intensity with pathological tumour differentiation shows no significant difference. Well (n=11), Moderate (n=44), Poorly (n=33). Kruskal-Wallis test, p=0.5661.

3.7.3 Association of pIgR and αSMA staining

Having investigated αSMA and pIgR independently as prognostic markers in PDAC, I sought to explore a direct correlation between the two. Does increasing activated PSCs relate to increasing pIgR expression? For each core, scores were given as previously described for pIgR and αSMA staining intensity. A direct plot of the two scores was made to investigate any association (**Figure 3.23 A**).

As there are a finite number of values, each dot can represent many tens of cores (**Figure 3.23 B**). However, there is no linear progress of the dots and thus signifying no correlation between the two markers. Pearson r correlation coefficient 0.504 demonstrates no direct correlation between these two markers.

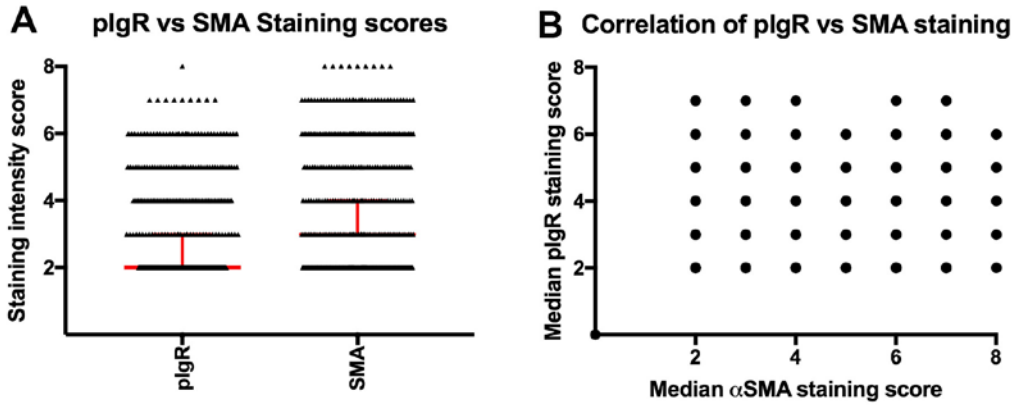

Figure 3.25: Correlation of pIgR and αSMA staining

(A) A total of 375 cores had sufficient staining to be included in the analysis. Both markers ranged from 0 to 8 for staining intensity. pIgR median score was 2; αSMA median score was 3 (B) Each core score for αSMA and pIgR were plotted against each other. Pearson's correlation coefficient, r=0.504.

3.7.4 Picrosirius Red staining of paraffin sections

PSCs have been identified as the main producers of abundant extracellular matrix (ECM) (74) associated with pancreatic desmoplastic stroma. In PDAC, several components of the ECM, including collagen-type1, have been shown to promote tumour growth, therapy resistance, and metastasis (251). Although the desmoplastic tissue in PDAC is a product of activated PSCs, the highest ECM deposition is not always found where the highest stromal activity is detected. In peri-tumoural areas, PSCs may outnumber the cancer cells without significant ECM deposition (252). In contrast, vast amounts of desmoplastic tissue may contain only a few PSCs (251).

With regard to the temporal sequence of events, αSMA expression, which reflects PSC activity, should precede collagen deposition because it is the product of the activated PSCs (234). Through their production of matrix metalloproteinases, both PSCs and cancer cells can degrade the previously deposited ECM (253). Thus, turnover of the ECM is a dynamic process, and immunohistochemical analysis of a specimen may give a static picture of disparity between different disease duration and stromal activity.

I have already investigated PDAC specimens in relation to the PSC marker αSMA. However, a relevant marker for collagen used in our lab is Picrosirius Red, whilst others have used Masson's Trichrome (246). Developed by Junqueira et al in 1979 (254), Picrosirius red has proved a useful stain to study collagen networks across various tissues. Debate remains over its usefulness to distinguish different collagen types, but it remains an accepted method of collagen analysis (255).

It has been demonstrated previously that pancreatic cancer cells activate stellate cells and that PSCs in turn promote tumour growth and chemoresistance through excessive ECM production *in vitro* (256). I sought to confirm previously noted findings, but to ideally create a biomarker panel for PDAC, including pIgR.

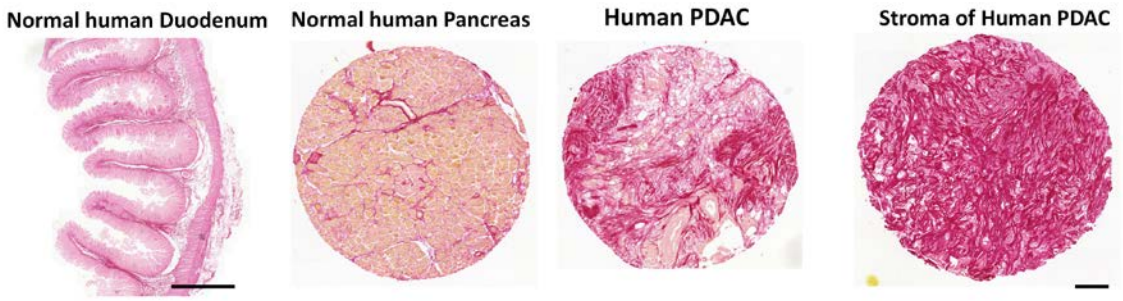

Figure 3.26: Picrosirius Red stains in tissue sections of human PDAC.

Scale bar 150µm

As previously described in with pIgR and αSMA, I attempted to identify a link between Picrosirius red and survival of PDAC patients. I performed the observation with 56 patients and I used X-tile, as described previously to dichotomise the group. With results ranging from 15 to 12566, X tile identified low expression as 15 to 313 (n=24). Whilst 320 to 12566 was the high expression (n=32) (**Figure 3.25 C**). The middle pictorial representation of correlations between patient population and Picrosirius red scoring demonstrates patches of bright red, identifying a potential correlation.

Overall survival was assessed using the Kaplan-Meier method, where by low scores of combined Picrosirius red (blue line) and high scores (grey line) are represented. There is a clear separation of the blue and grey lines, with a supposed poor prognosis with lower Picrosirius red staining.

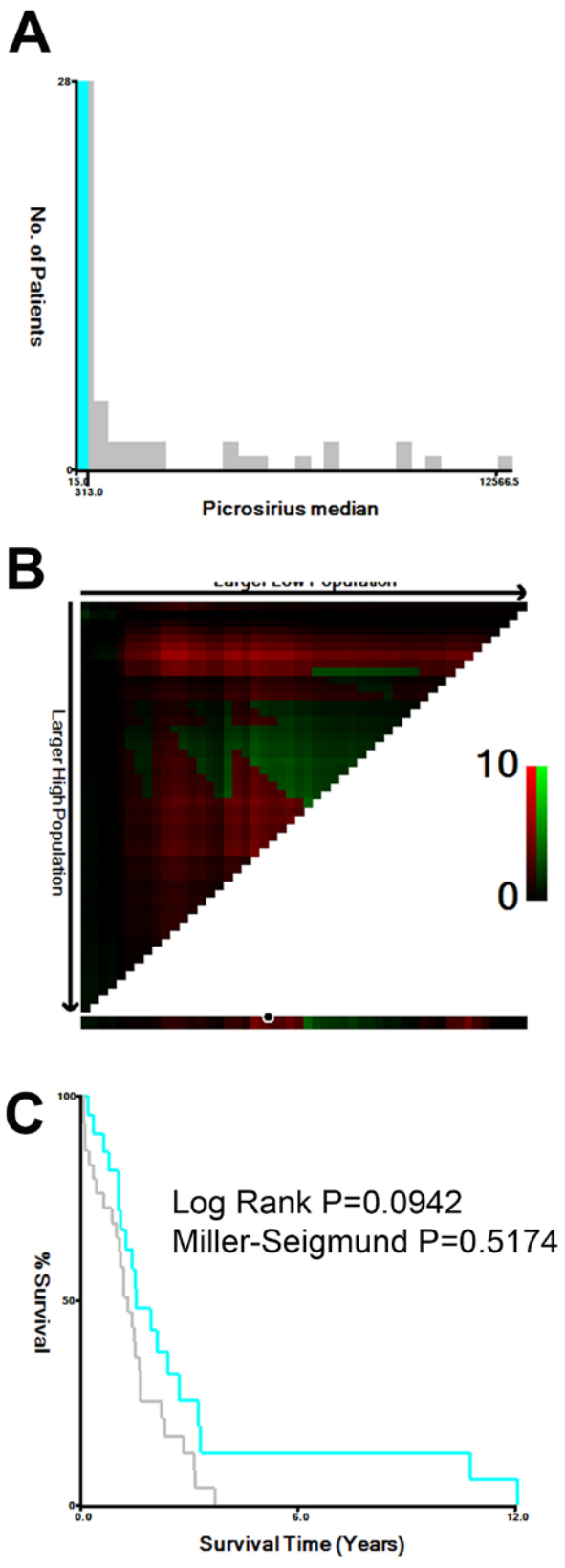

Figure 3.27: Association of Picrosirius red and survival.

(A) Histogram distribution of Picrosirius Red expression. (B) Pictorial representation of various population dichotomisations to determine the most optimal cut-off for differences in survival for high- and low-expressing Picrosirius Red patients. (C) Comparison of survival between high (grey line) and low (blue

line) expressing patients. Log Rank, p=0.0942, Corrected Miller Seigmund, p=0.517473.

My data demonstrates high collagen deposition showed a trend towards better survival which has been demonstrated previously (234). Erkan et al also noted a paradoxical correlation with αSMA and collagen (234). I could find no correlation between αSMA and collagen deposition (**Figure 3.26**).

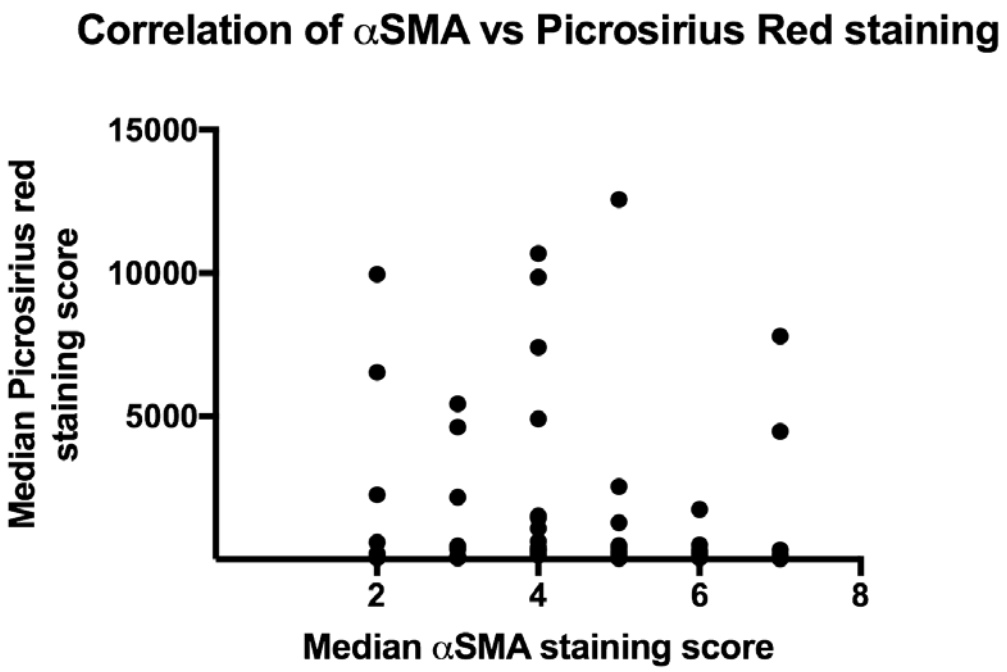

Figure 3.28: Correlation of Picrosirius Red and αSMA staining.

Correlating the two markers shows a Pearson correlation co-efficient of -0.085. n=53

3.7.4 Association of pIgR and Picrosirius Red staining

Having investigated Picrosirius red and pIgR independently as prognostic markers in PDAC, I sought to explore a direct correlation between the two. Does increasing stromal content relate to increasing pIgR expression? For each core, scores were given as previously described for pIgR and Picrosirius red staining intensity. A direct plot of the two scores did not show a correlation (**Figure 3.27 A**).

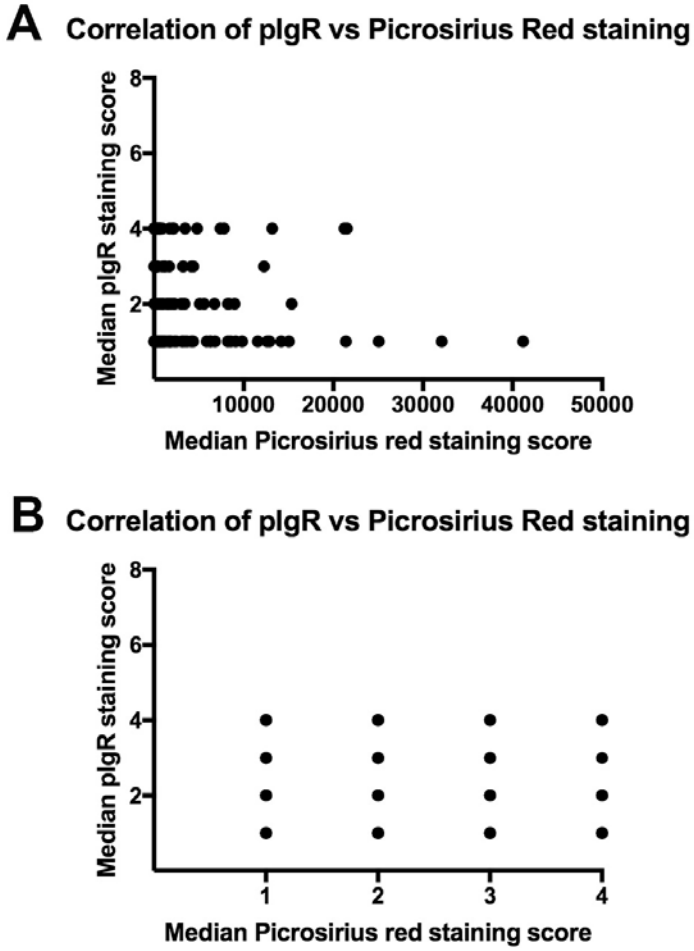

Figure 3.29: Correlation of pIgR and Picrosirius red.

(A) pIgR staining ranged from 0-8, whilst Picrosirius red ranged up to 45000. (B) Normalised Picrosirius red values compared to pIgR score. Pearson's correlation coefficient r= -0.1758.

A total of 260 cores had sufficient staining to be included in the analysis. Picrosirius Red values range up to 45000. In an attempt to normalise the Picrosirius red data, I scaled the data using X-tile. Staining intensities were rationalised as follows:

0-99:	1
100-1199:	2
1200-6999:	3
>7000:	4

The main aim for normalising the Picrosirius red data was to enable me to potentially combine the already investigated markers to form a potential panel to investigate PDAC. Picrosirius red had such a large scale of effectively infinite numbers, that it would have been difficult had I not. However, investigating correlation

with pIgR and Picrosirius red staining intensity shows no direct correlation; even with the normalised score (**Figure 3.27 B**).

3.7.5 Comparing survival of combined pIgR, αSMA and Picrosirius Red

Having independently investigated pIgR, E-cadherin, αSMA and Picrosirius red expression and their relationship to PDAC, I sought to explore the correlation of the markers and the potential for a potential prognostic marker for PDAC. Sequential sections of the TMAs were stained for pIgR, E-cadherin, αSMA and Picrosirius red and staining scores for each core were recorded, as described previously. Having normalised Picrosirius red scores, these values were used rather than raw values. Scores for each marker were combined and median scores taken to compare with survival characteristics.

Two combinations of markers were investigated:

1) pIgR, αSMA and Picrosirius red
2) pIgR, αSMA, Picrosirius red and E-cadherin

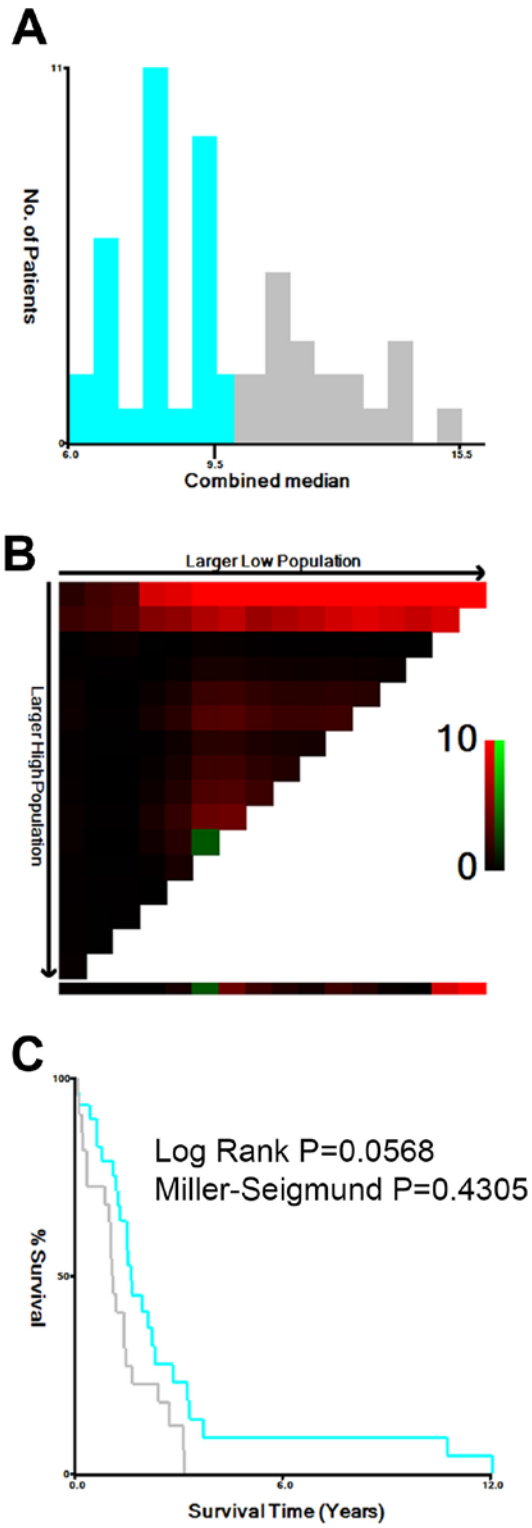

Figure 3.30: Panel 1 (pIgR, αSMA and Picrosirius Red combined score) biomarker for PDAC.

(A) Histogram distribution of Panel 1 biomarker expression. (B) Pictorial representation of various population dichotomisations to determine the most optimal cut-off for differences in survival for high- and low-expressing Panel 1 biomarker patients. (C) Comparison of survival between high (grey line) and low

(blue line) expressing patients. Log Rank, p=0.0568, Corrected Miller Seigmund, p=0.4305.

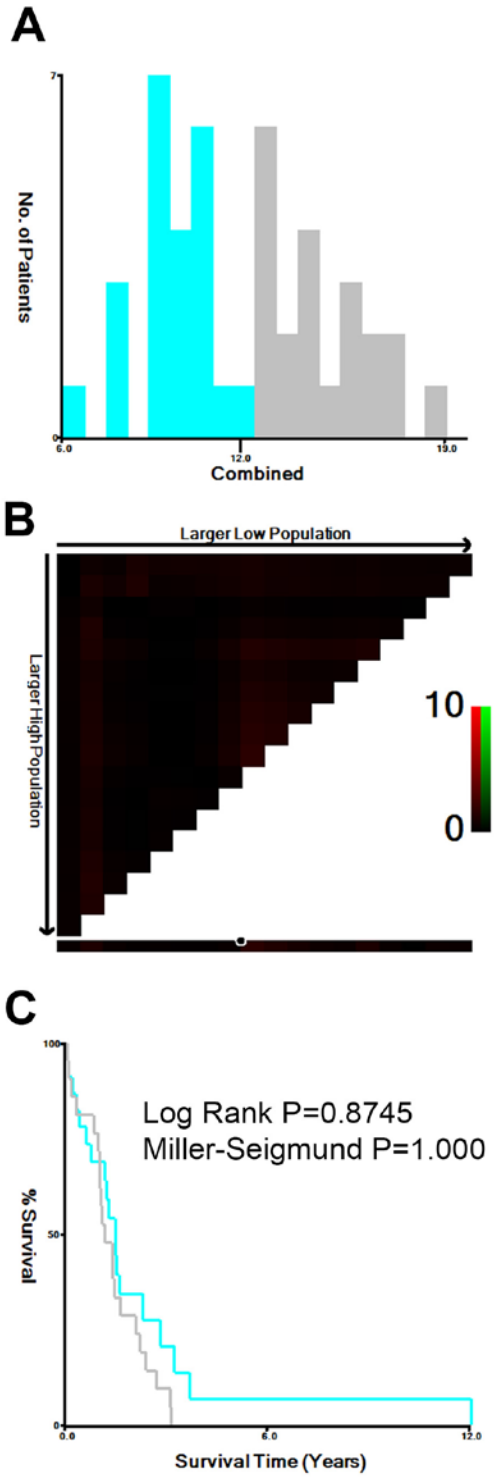

Figure 3.31: Panel 2 (pIgR, αSMA, Picrosirius Red and E-cadherin) biomarker for PDAC

(A) Histogram distribution of panel 2 expression. (B) Pictorial representation of various population dichotomisations to determine the most optimal cut-off for differences in survival for high- and low-expressing Picrosirius Red patients. (C) Comparison of survival between high (grey line) and low (blue

line) of panel 2 expressing patients. Log Rank, p=0.8745, Corrected Miller Seigmund, p=1.

For simplicity, the 3 marker variant (pIgR, αSMA and Picrosirius red) will be referred to as Panel 1, whilst the version with all four markers (pIgR, αSMA, Picrosirius red and E-cadherin) will be referred to Panel 2.

Figure 3.28 A demonstrates an X-tile based histogram showing population division. The light blue colour represents low Panel 1 expression score cohort whilst grey is the high expression cohort. The dichotomisation process allocates up to 9.5 as a low score, whilst 10 to 15.5 is considered high. The low scoring group had 30 patients whilst the high scoring group had 26.

Unlike in previous correlation, a pictorial representation of correlations between patient population and Panel 1 scoring demonstrate patches of bright red. This indicates a potential correlation (**Figure 3.28 B**).

Overall survival was assessed using the Kaplan-Meier method, where by low scores of combined Panel 1 (blue line) and high scores (grey line) are represented. High combined expression of Panel 1 is associated with a trend towards poor prognosis (**Figure 3.28 C**).

In Figure 3.29 A, the light blue colour represents low Panel 2 expression score cohort whilst grey is the high expression cohort. The dichotomisation process allocates up to 12.5 as a low score, whilst 13 to 19 is considered high. The low scoring group had 25 patients whilst the high scoring group had 25.

Unlike Panel 1, the addition of a forth marker shows no obvious bright patches and one would assume no direct correlation (**Figure 3.29 B**).

Overall survival was assessed using the Kaplan-Meier method, where by low scores of combined Panel 2 (blue line) and high scores (grey line) are represented. High combined expression is associated with poorer survival, but the data is not as significant at Panel 1 (Miller-Seigmund P=1.000) (**Figure 3.29 C**)

3.8 Discussion

3.8.1 Role of pIgR in gastrointestinal cancers

I have summarised the finding on pIgR expression in all cancers to date, suggesting a different role in various cancers studied. This may be related to baseline, physiological pIgR expression as a requirement for mucosal defences where mucosal surfaces are exposed to high antigen load. Consequently it is not surprising that the initial work regarding the role of pIgR focused around Streptococcal pneumonia, suggested a possible role in oropharyngeal cancers (182). The hypothesis that pIgR was being used by cancer cells as a mechanism to spread or metastasise could, however, not be proven (257).

Subsequently, Ocak et al (258) investigated pIgR in lung cancers, noting down-regulation of pIgR in lung cancer, suggesting that loss of pIgR expression occurs early and is associated with enhanced cancer cell proliferation and poor prognosis. Fristedt et al (171) investigated pIgR in the context of oesophageal and gastric adenocarcinoma, noting high pIgR expression independently predicted a decreased risk of recurrence and an improved survival in patients with adenocarcinoma of the upper gastrointestinal tract.

In locations where pIgR is naturally expressed within the gastrointestinal tract, loss of expression is correlated with reduced survival such as the observation made in colorectal and oesophageal cancers (168, 178). In those normal tissues where pIgR is not expressed, cancers of those tissues expressing pIgR are associated with a poor prognosis, for example hepatocellular carcinoma (176, 179).

Three studies have investigated pIgR with regards to different pancreatic lesions using unique approaches. Fristedt et at investigated the role of pIgR in all peri-ampullary and pancreatic lesions by studying human tissue samples. They identified that high pIgR expression signifies a favourable tumour phenotype and

low expression independently predicts a reduced survival in patients with pancreatic and periampullary cancers (176). However, this correlation combined survival data for all peri-ampullary lesions, which I have demonstrated are different in pIgR expression. This includes duodenal lesions (duodenum normally expresses pIgR) along with cancers from pancreatic and biliary tract (mucosa of these organs normally do not express pIgR). Moreover, data from Fristedt et al relating solely to PDAC lesions only did not demonstrate any correlation with survival, which was in keeping with my observations, that there was no impact on survival based on pIgR expression in human PDAC. Thus, it is important to ensure histologically different entities are not considered together, and a dedicated research group is involved in such studies.

Park et al identified nine candidate biomarkers, including pIgR to distinguish between mucinous pancreatic and non-mucinous cysts using mass-spectrometry (259). Accurate differential diagnosis of mucinous cysts from non-mucinous cysts is extremely important, because mucinous cysts have a malignant potential and requires surgical resection. Park et al noted pIgR was increased in mucinous cystic lesions, compared to non-mucinous lesions. However, I did not have access to study mucinous cystic lesions.

Kadaba et al (70) briefly investigated pIgR in organotypic models, but to the best of my knowledge, this is the first detailed study on the potential prognostic value of pIgR expression in human PDAC, alongside differential expression in other peri-ampullary cancers. It is important to demonstrate or refute correlation with other known prognostic features within PDAC such as differentiation or stage or resection margin or nodal involvement. With diligent data collection I was able to demonstrate that at least in my small sample size (n=88) there was no correlation between these features and pIgR expression.

3.8.2 Association of pIgR in the pre-malignant phases of PDAC

Evaluating pIgR expression in human PDAC has provided intriguing observations. Whilst there was no demonstrable correlation between pIgR expression and survival, detailed analysis into PanIN lesions demonstrated its expression appears most prominent during pre-malignant phases of PDAC. Eventually the pre-ponderance of PanIN lesions within a given histological slide for PDAC may influence the overall score for that section, as invasive cancer ducts or poorly differentiated cancers do not seem to express pIgR.

A valid criticism would be identification of PanIN lesions in immunofluorescence slides where the morphological aspects of PanIN may be lost. However, with adequate training on H&E sections, and understanding nuclear arrangement as well as nuclear atypia, and overall ductal morphology (260, 261) on DAPI stain of immunofluorescence slides, alongside verification from corresponding H&E slides, one can ascertain PanIN lesions within immunofluorescence slides as demonstrated by me.

The proof of this approach perhaps lies in the analysis of E-cadherin expression, which has been demonstrated before {Froeling, 2009 #3115}, to be lost as PanIN progress from normal duct to invasive cancer.

Loss of E-cadherin is also noted with increased stromal activity (202).

As E-cadherin expression decreases during PanIN progression, pIgR expression increases. However, expression of both pIgR and E-cadherin are reduced in invasive PDAC. Since IgA is not expressed in PDAC or normal pancreas, then enhanced expression of pIgR in PanIN could not be associated with immunoglobulin response during PanIN formation. Therefore, I investigated the association of PDAC with stromal content. Since stromal content could not be assessed at PanIN level due to proximity of varying grade of PanIN lesions, I had to resort to summary pIgR expression and composite αSMA expression per patient (median values from three

cores).

3.8.3 Effect of pIgR on stromal content

αSMA was used to investigate active PSCs and Picrosirius red to identify collagen content.

The combination of activated PSCs and collagen representing desmoplastic stroma has been suggested to be a potential prognostic marker for patients undergoing surgery in PDAC (234). The indication from the data is that independently, low collagen expression in PDAC samples is perhaps, associated with a better prognosis, whilst there is no direct correlation with αSMA, at least from the analysis of these TMA cores.

There may be a number of explanations why the data are not in agreement with the activated stromal index published by Erkan et al (234) and Fokas et al (246). The cores focused on the cancer aspect of the PDAC. Therefore, the prominent stromal index is not, perhaps, fully represented within the TMAs analysed. Furthermore the rigorous and independent nature of dichotomisation used by X-tiles may not allow for minor statistical differences. Moreover, we can speculate that the stromal activity is a dynamic process, and there may be differences in patients recruited in various institutions.

Lastly, I tried to reconcile the stromal activity and pIgR expression with PDAC progression as demonstrated in *in vitro* experiments by Kadaba et al (70). Since, the summary score of cores were used for Picrosirius Red, αSMA and pIgR or E-cadherin expression; I lost the micro-environmental cues pertinent to each PanIN lesion. It was impossible to attribute regional stromal activity to a particular PanIN in a 3D PDAC tissue. Hence, I could not confirm the relationship between stromal activity and pIgR or E-cadherin expression.

3.8.4 Role of pIgR as a biomarker in PDAC

Pancreatic cancer remains one of the most difficult cancers to treat with the poorest prognosis. The key to improving survival rates in this disease is early detection and monitoring of disseminated and residual disease. However, this is hindered due to lack reliable diagnostic, prognostic and predictive biomarkers which mean that the majority of patients succumb to their condition within a few months

The most commonly used tumour biomarker in PDAC is carbohydrate antigen 19–9 (CA 19–9), the sensitivity is around 79 % and specificity 82 %. However, CA19-9 levels increase in other non-malignant pancreatic disorders such as chronic pancreatitis and other gastrointestinal malignancies (262).

Histopathological prognostic factors include tumour size and grade, lymph node status, resection margins and vascular or neural invasion (263). Molecular tumour markers such as MUC5A, CEACAM, E-cadherin, β-catenin, Ki-67 index, oestrogen receptor, HER2 expression, have been studied as potential prognostic markers. Unlike breast and other carcinomas, no molecular markers have been established to guide treatment and decision-making in patients with PDAC (264).

Identification of biomarkers that accurately predict disease recurrence or response to chemotherapy would be of substantial aid in individual risk assessment and treatment selection, and may even lead to novel therapies by becoming targets for molecular intervention in specific subsets of patients (265). Immunohistochemical (IHC) analysis is used widely for evaluating molecular markers in clinical tissue specimens. Although several more sophisticated methods, such as cDNA microarray, fluorescence in situ hybridization and quantitative reverse transcriptase–polymerase chain reaction, are being translated into clinical practice.

A potential issue with establishing a reliable biomarker has been the genetic basic of PDAC. PDAC tumours arise through an accumulation of a large number of genetic and epigenetic aberrations (266). No two cancers may have the same profile

of genetic mutations. The dependence on an independent prognostic genetic marker then becomes difficult. However, the idea of combining multiple markers, that independently have no direct survival benefit, makes more logical sense.

In combination, my chosen four biomarkers (pIgR, αSMA, Picrosirius red and E-cadherin) did not show as good a correlation with survival as three biomarkers (pIgR, αSMA, Picrosirius red). E-cadherin is usually expressed in normal pancreas and is not well expressed in development to PDAC and is lost relatively early in PDAC progression.

However, using pIgR in combination with αSMA and Picrosirius red demonstrates that a low combined score may confer a survival benefit.

As an independent prognostic marker in PDAC, pIgR does not show any survival benefit, however I have demonstrated it is expressed during pre-malignant stages of PDAC. Due to the inherent complex nature of PDAC progression and co-existence of various stages of PanIN lesions with invasive malignancy, as well as the multiple genetic mutations involved, pIgR may however provide more use in combination with other biomarkers, such as stromal activity and content.

In order to get additional cues as to drivers of and consequences of pIgR expression in pancreatic cancer, I next explored the role of pIgR and cancer cell and stromal behaviour in *in vitro* systems.

CHAPTER IV

RESULTS:

PART II

4.1 Introduction

The epithelial–mesenchymal transition (EMT), in which epithelial cancer cells lose their polarity and become motile mesenchymal cells, has been implicated in cancer invasion and metastasis (190). Cancer cells undergoing EMT appear to exhibit properties of cancer stem cells (267), override oncogene-induced premature senescence and apoptosis (268), and contribute to immunosuppression. Ai et al identified pIgR and its role in EMT induction *in vitro* (81). Having explored pIgR expression *in vivo* in Chapter 3, I now sought to understand the function of pIgR *in vitro*.

I initially determined baseline expression of pIgR in pancreatic cell lines. I had access to a panel of PDAC cell lines, which have all been Short Tandem Repeat (STR) profiled and screened for mycoplasma (269, 270).

Alongside cancer cells, we also have an immortalised pancreatic stellate cell (PS1) created by previous members in the group (215). As described in Materials and Methods chapter, these were STR profiled and verified with stellate cell markers GFAP, Desmin, Vimentin and αSMA (73).

To further our understanding of the role of stellate cells in different tumours, we aimed to isolate stellate cells from patients with periampullary cancers (as previously documented in Chapter 2). The method of collection initially started via outgrowth and developed to tumour digestion (unpublished observations). Each patient we could obtain viable stellate cell populations were given numerical values, with the MOCRI prefix. Cells were validated with stellate cell markers GFAP, Desmin, Vimentin and αSMA (73).

4.2 pIgR expression in pancreatic cancer cells

Initial work with PDAC cell lines focused on extraction of protein from lysate, as described in Section 2.10, which identified Capan 1 as the only positive line for pIgR expression at protein level (**Figure 4.1 A**). This was despite attempts using all pancreatic cancer cell lines in our laboratory. Western blotting had previously also identified expression was at 110kDa, significantly higher than the 83kDa according to manufacturer's documentation (Sigma Aldrich, HPA012012). Treatment of Capan 1 with Tunicamycin demonstrated a specific band to be placed at 83kDa (**Figure 4.1**). This confirmed the 110kDa band to be a true representative band of pIgR, but with glycosylation. No expression of pIgR was seen in PS1 cells or in primary pancreatic stellate cells (**Figure 4.2**).

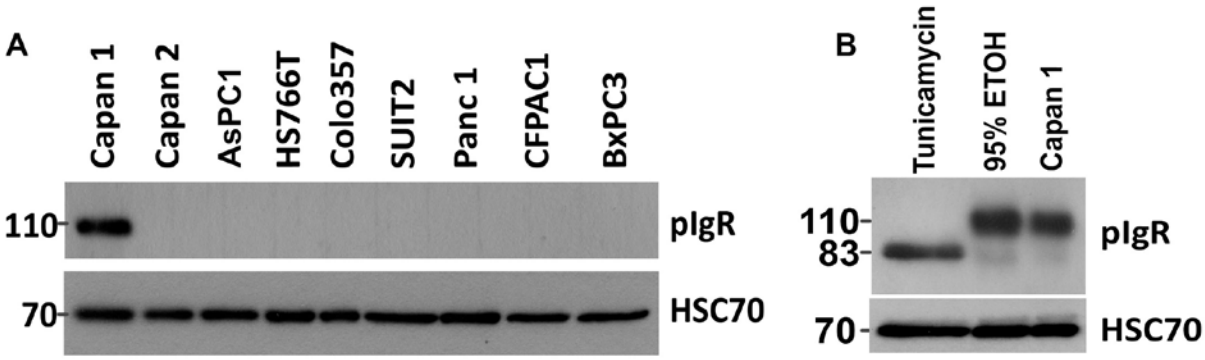

Figure 4.1: Protein expression of pIgR in PDAC cell lines.

(A) pIgR expression across all PDAC cells confirms only protein expression with Capan 1 cells. (B) Treatment with Tunicamycin confirms post-translation glycosylation of pIgR, demonstrating an effect of breaking down glycosylation bonds renders molecular weight at 83 kDa. HSC70 was used as loading control. Representative of three biological replicates.

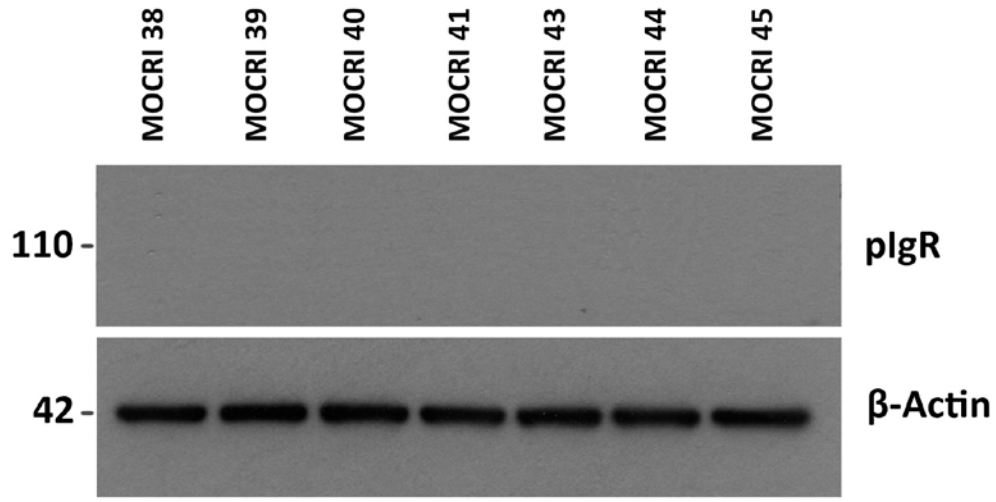

Figure 4.2: Protein expression of pIgR in primary pancreatic stellate cells.

No expression of pIgR was seen in primary pancreatic stellate cells. B-Actin was used as loading control. Representative of three biological replicates.

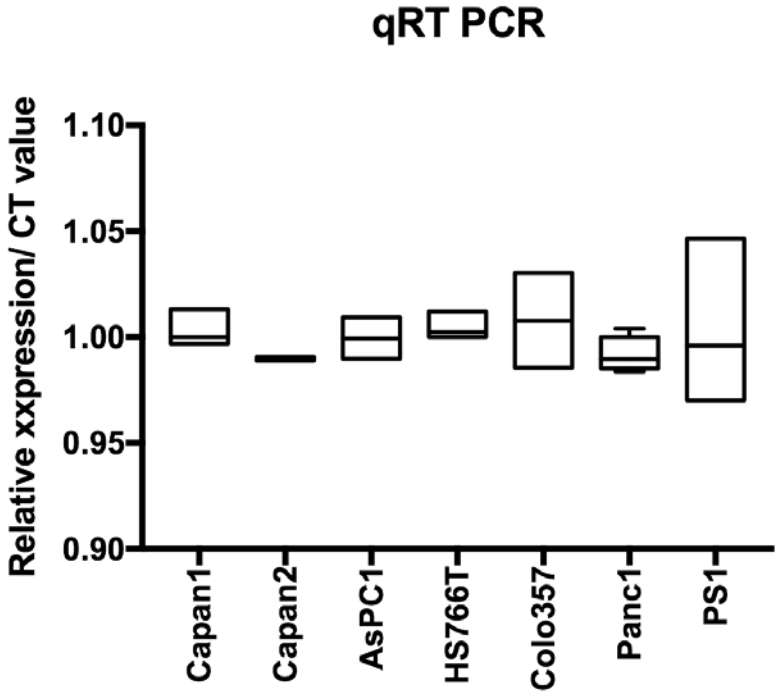

Figure 4.3: mRNA expression of pIgR in pancreatic cancer cells and PS1 cells.

qRT-PCR of pancreatic cancer cells and PS1 cells. CT values were normalised to Capan1 (positive at

protein level). Summary of three biological replicates. No significant difference in CT expression across cell types.

Immunofluorescent staining of various PDAC cancer cells on coverslips produced variable results that were not easily reproducible. Despite Capan1 being positive at protein level, a valid expression was not obtainable by immunofluorescence at 2D. This was true for all cell lines, and after numerous attempts to optimise, the technique was abandoned (results not shown). Despite Capan1 showing positive expression at protein level, there was a similar expression of pIgR at mRNA level across all pancreatic cancer and PS1 cell lines tested (**Figure 4.3**). Thus pIgR is present in pancreatic cancer cells at an mRNA level, but is not translated to protein, except in Capan1 cells.

4.3 Upstream precursors to pIgR in pancreatic cancer cells

Regulation of pIgR expression involves complex interactions among host-, microbial- and environmental-derived factors, involving transcriptional and posttranscriptional mechanisms (94). A variety of cytokines, hormones and microbes influence have been investigated (92), and previous work from Froeling et al (59) identified Interleukin 1, 4 and Tumour Necrosis Factor Alpha to be secreted by pancreatic stromal cells.

Our group has investigated the role of ATRA in modulating PSC phenotype previously. Quiescent PSCs store retinol, which is lost upon activation (59). ATRA, in combination with certain cytokines has been shown to enhance pIgR expression (271).

Previously negative cell lines for pIgR protein expression, HT29 (colorectal cancer cell line chosen because of use by other groups (272)), AsPC1 (PDAC cell line, used by Kadaba et al) and DEChTERT (normal pancreatic cell line, used as

normal control), were treated over various time courses with IL1, IL4, TNF-α and in combination with ATRA, at various concentrations in order to elicit an upregulation in pIgR protein expression.

HT29 cells have been used by others as a control for pIgR expression. As a cell line originating from a human colorectal adenocarcinoma, the expression of pIgR is likely to be varied. As such, some groups have demonstrated it expresses pIgR (81), whilst others have proved that HT29 does not express pIgR (271).

Takenouchi-Ohkubo et al demonstrated ATRA-treated HT-29 cells constitutively expressing pIgR, showed a significantly high expression of pIgR in the presence of IL-4 and/or IFN-γ, compared to ATRA-untreated cell (271).

My wild type HT29 cells did not naturally express pIgR, and this was checked with samples of other passages of HT29 from other groups within the laboratory (data not shown). These cells were also STR profiled to confirm true HT29 origin. After 48 hours of treatment with either 70% ethanol (control), 10µg of IL4 or TNFα with or without ATRA, cells demonstrated no expression or upregulation of pIgR expression (**Figure 4.4 A**).

AsPC1 cells had 48 hours of treatment with either 70% ethanol (control), 10µg of IL4 or TNFα with or without ATRA. No expression or upregulation was seen in pIgR expression (**Figure 4.4 B**). DEChTERT cells were exposed to varying concentrations of IL1, IL4 and TNFα (known upstream regulators of pIgR) for 48 hours, but no expression of pIgR was noted (**Figure 4.4 C**).

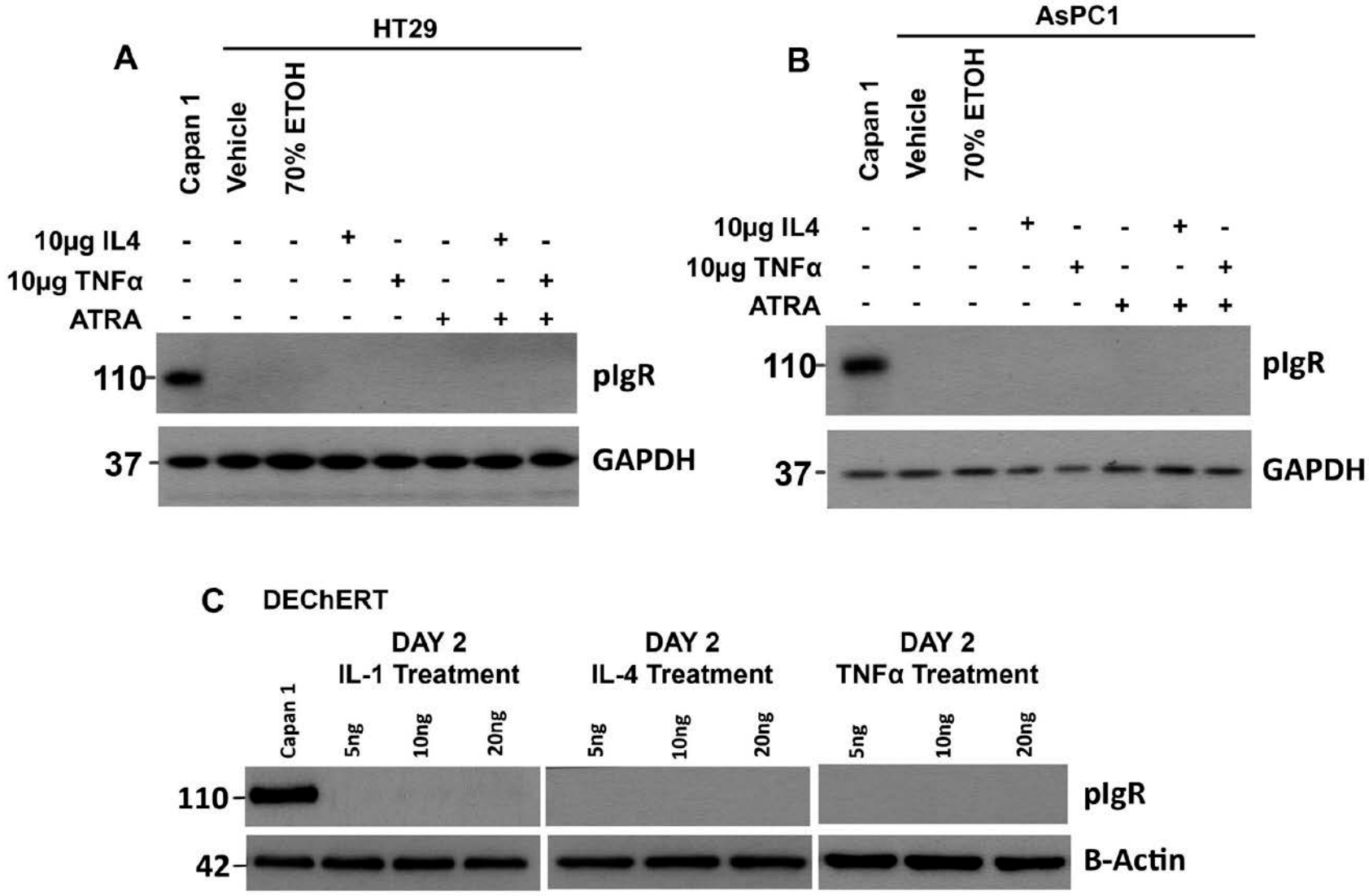
A
HT29
Capan 1
Vehicle
70% ETOH
10µg IL4
10µg TNFα
ATRA
110
pIgR
37
GAPDH
B
AsPC1
Capan 1
Vehicle
70% ETOH
10µg IL4
10µg TNFα
ATRA
110
pIgR
37
GAPDH
C
DEChERT
DAY 2
IL-1 Treatment
DAY 2
IL-4 Treatment
DAY 2
TNFα Treatment
Capan 1
5ng
10ng
20ng
5ng
10ng
20ng
5ng
10ng
20ng
110
pIgR
42
B-Actin

Figure 4.4: Effect of introduction of cytokines and ATRA to PDAC cells.

(A) HT29 cells had 48 hours of treatment with either 70% ethanol (control), 10µg of IL4 or TNFα with or without ATRA shows no upregulation of pIgR in HT29 cells (B) AsPC1 cells had 48 hours of treatment with either 70% ethanol (control), 10µg of IL4 or TNFα with or without ATRA. No up-regulation of pIgR is seen in AsPC1 cells. (C) DEChTERT cells were exposed to varying concentrations of IL1, IL4 and TNFα, with no effect on pIgR expression. Representative of three biological replicates.

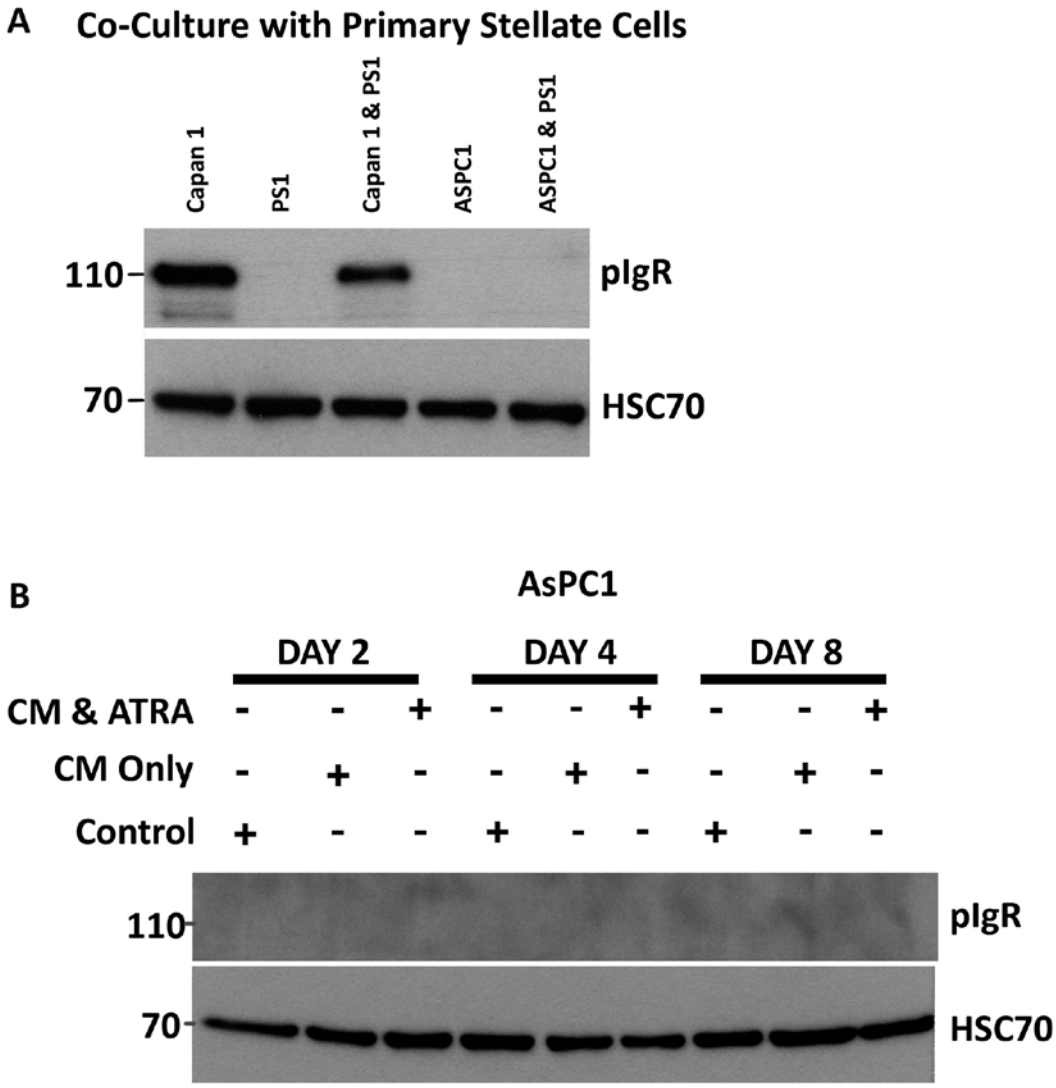

Figure 4.5: Other attempts at over-expression of pIgR.

(A) Culturing PS1 cells, at a ratio of 2:1 with AsPC1 cells in 2D causes no change in pIgR expression. (B) PS1 cells cultured for 72 hours had their media collected and the collected media (CM) was added directly to AsPC1 cells with or without ATRA. No pIgR expression is seen. Representative of three

biological replicates.

Kadaba et al noted pIgR expression in 3D organotypic models with AsPC1 and PS1 cells (70). However, culturing PS1 cells, at a ratio of 2:1 with AsPC1 cells in 2D shows no expression of pIgR (**Figure 4.5 A**).

Stellate cells are known to secrete cytokines (59), and as there is no correlation in 2D culture, but it is seen in 3D, I sought to investigate if PS1 secretions provided any upstream effect. PS1 cells cultured for 72 hours had their media collected and the collected media (CM) was added directly to AsPC1 cells with or without ATRA. Again, no pIgR expression was identified (**Figure 4.5 B**).

4.4 Effect of pIgR siRNA on Capan1 pancreatic cancer cells

Initial work with PDAC cell lines focused on extraction of protein from lysate, as described in Section 2.10, which identified Capan1 as the only positive line for pIgR expression at protein level.

Kadaba et al (70) identified pIgR to be a gene upregulated in PDAC by qRT-PCR. Their work suggested that pIgR may be involved in numerous cellular functions, such as cell signalling, inflammatory response, cell growth, death and movement. In order to investigate the effects on proliferation on Capan1 cancer cells, siRNA was used to knockdown pIgR. I could successfully down-regulate pIgR expression in Capan1 cells for up to five days (**Figure 4.6 A** & **B**).

Conditioned media from cells treated with siRNA (**Figure 4.4**) was collected with or without Tunicamycin treatment to show down regulation of pIgR secretion, but no pIgR glycosylation (**Figure 4.7**).

Cells treated with pIgR siRNA were plated in 6 well pates and cell counts were determined for up to six days. Untreated Capan1 and non-targeting siRNA acted as controls, demonstrating a reduction in cell counts after pIgR RNAi suggesting a reduction in proliferation (**Figure 4.8**).

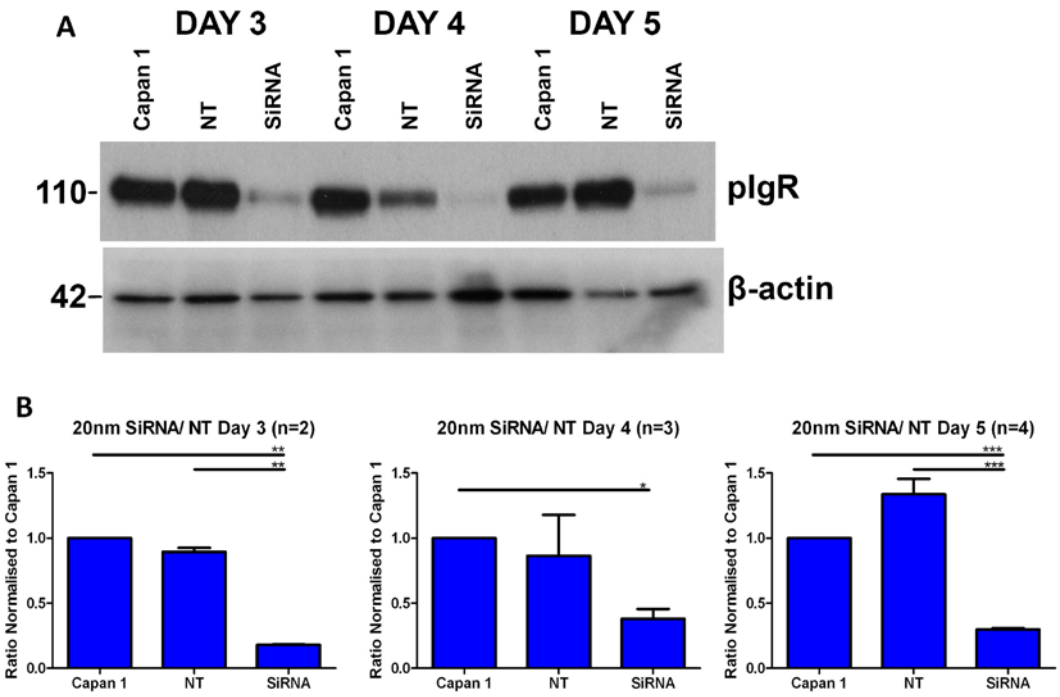

Figure 4.6: Effect of pIgR siRNA on Capan 1 pancreatic cancer cells.

Capan1 cells alone, non-targeting (NT) or pooled siRNA of pIgR represented at protein level, confirming down-regulation. (A) siRNA treatment of Capan 1 over 3, 4 and 5 days demonstrating down-regulation of pIgR at day 4. (B) Quantification of Western blot analysis over 3, 4 and 5 days at 20nm concentration of siRNA. Values are mean and SEM (n=4). Comparisons made by Kruskal-Wallis test followed by Dunn's post-hoc analysis. *** p<0.001, ** p<0.01, * p<0.05. Non-significant differences are not shown.

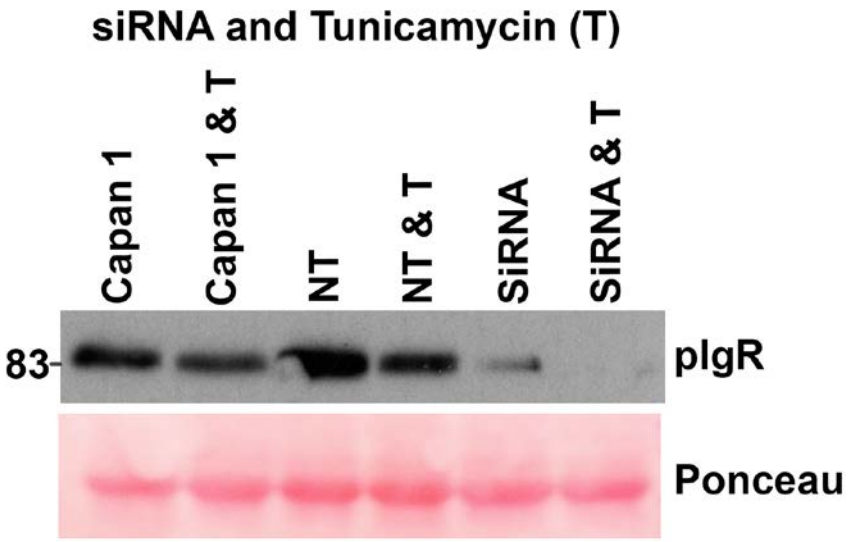

Figure 4.7: Secreted pIgR after siRNA with or without Tunicamycin treatment.

siRNA treated cells with or without Tunicamycin treatment. Collected media was concentrated and Ponceau S determined equal loading.

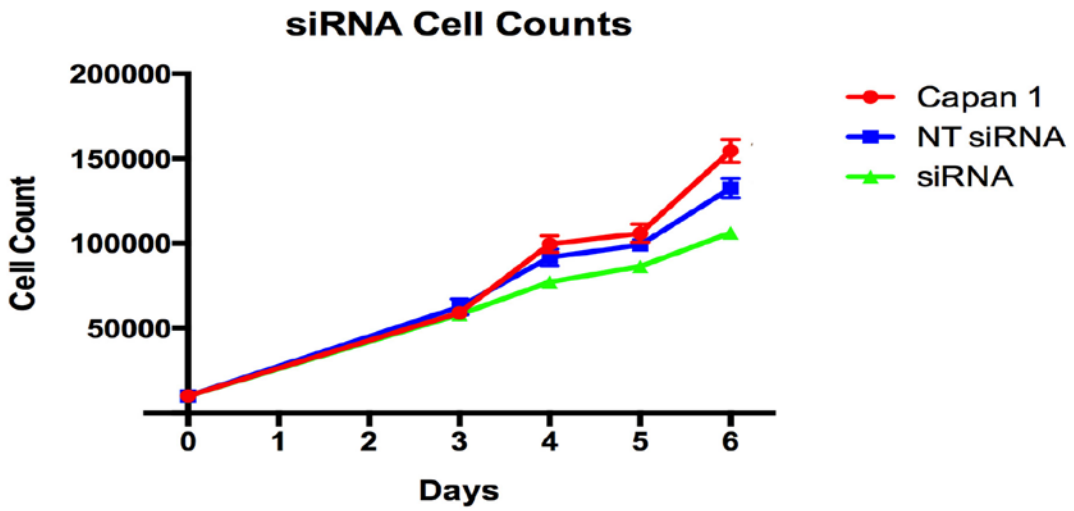

Figure 4.8: Cell proliferation after pIgR siRNA.

Cells treated with pIgR siRNA were plated in 6 well pates and cell counts were taken at 3, 4, 5 and 6 days. n=3. Comparisons made by Friedman test. Capan1 vs. NT: $p>0.9999$, Capan1 vs. siRNA: $p=0.0537$.

4.5 Effect on pIgR expression in cancer cells after RNAi and co-culture with PSC in 3D

The tumour stroma has been shown to play a definitive role in PDAC progression. 3D organotypic models also provide a more physiologically relevant system to reproduce the stroma effect on cancer cells (219). The raised air-liquid model, which was used to investigate PDAC cell invasion and the effect pIgR has, is fed from below creating a gradient that stimulates cancer cells to invade. Due to the assumed short -acting nature of the RNAi, the organotypic cultures were harvested on day 5, much shorted than previously observed (231). Once harvested, sections were immunostained for pIgR and E-cadherin.

In order to be able to distinguish between the direct effect of pIgR on cancer cells or an indirect effect via changes occurring in PSC, the results were compared with an organotypic culture of cancer cells alone.

Capan1 cells demonstrated that pIgR down-regulation after RNAi could not be maintained in 3D mono- and co-culture models (**Figure 4.9 and 4.10**). There was no difference in cancer cell number either upon RNAi and PSC co-culture (**Figure 4.11**). There was also minimal stellate cell invasion, possibly due to the short (five days only) nature of incubation, but this was not investigated further.

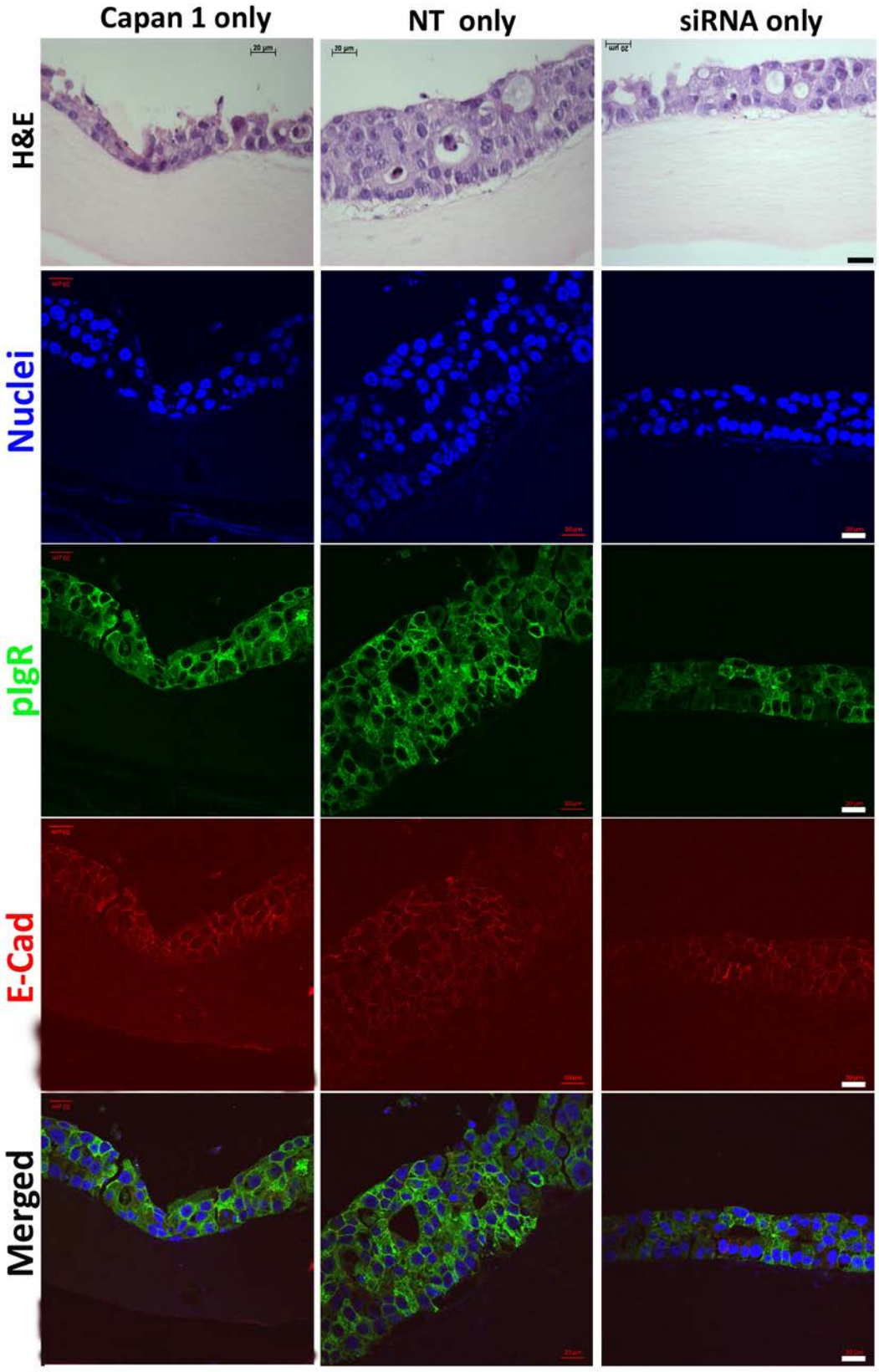

Figure 4.9: Effect of pIgR expression in cancer cells alone after RNAi in organotypics.

Representative images of organotypics with cancer cells only, compared with relevant H&E images. pIgR (green) and E-Cadherin (red). (n=3). Scale bar 20µm. Representative of two biological replicates with three technical replicates each.

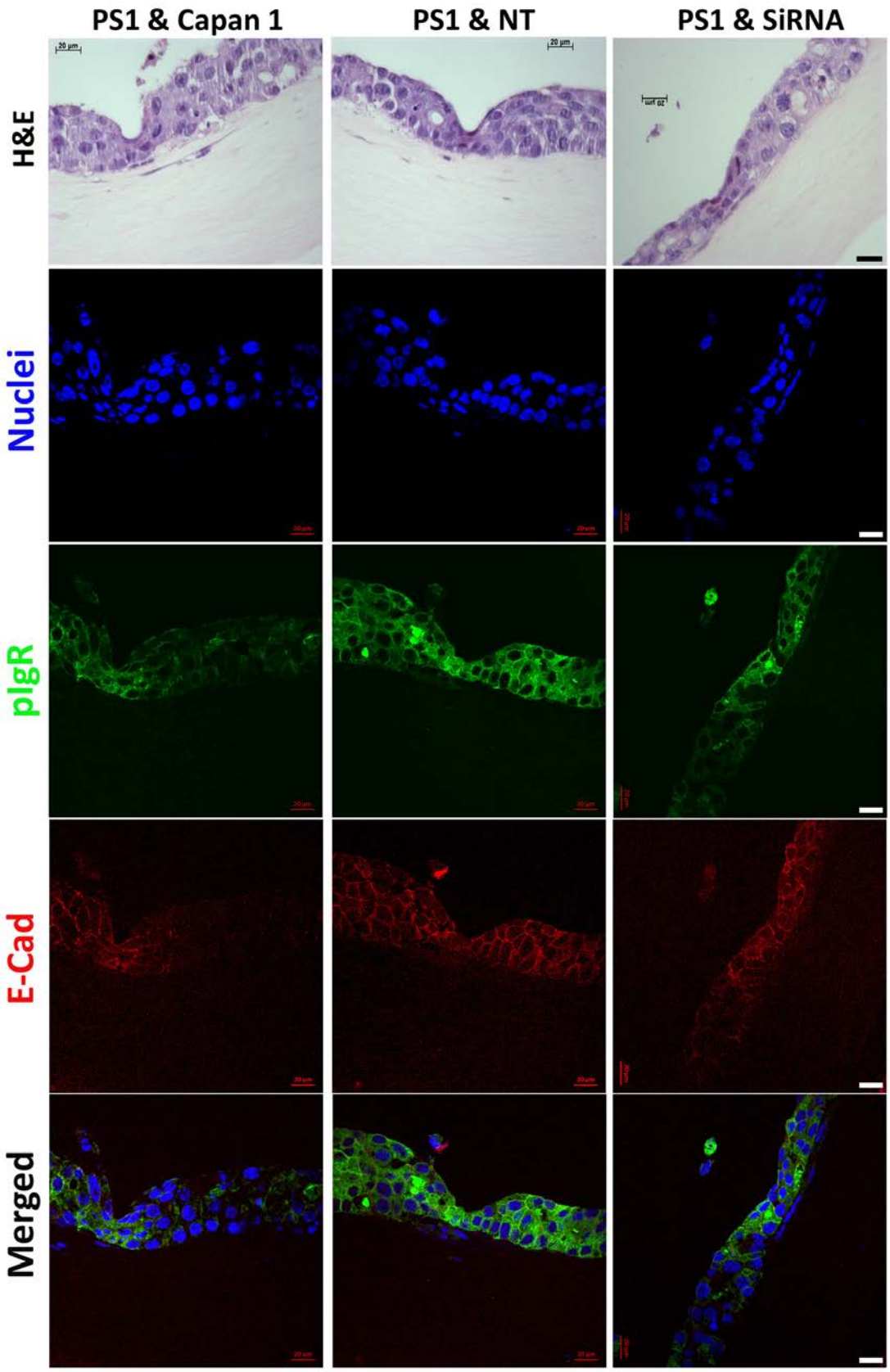

Figure 4.10: Effect of pIgR expression in cancer cell co-cultures after RNAi in organotypics.

Representative images of organotypics with stellate cells, compared with relevant H&E images. pIgR (green) and E-Cadherin (red). (n=3). Scale bar 20µm. Representative of two biological replicates

with three technical replicates each. It should be noted that the number of stellate cells is low due to delayed proliferation of stellate cells in these conditions.

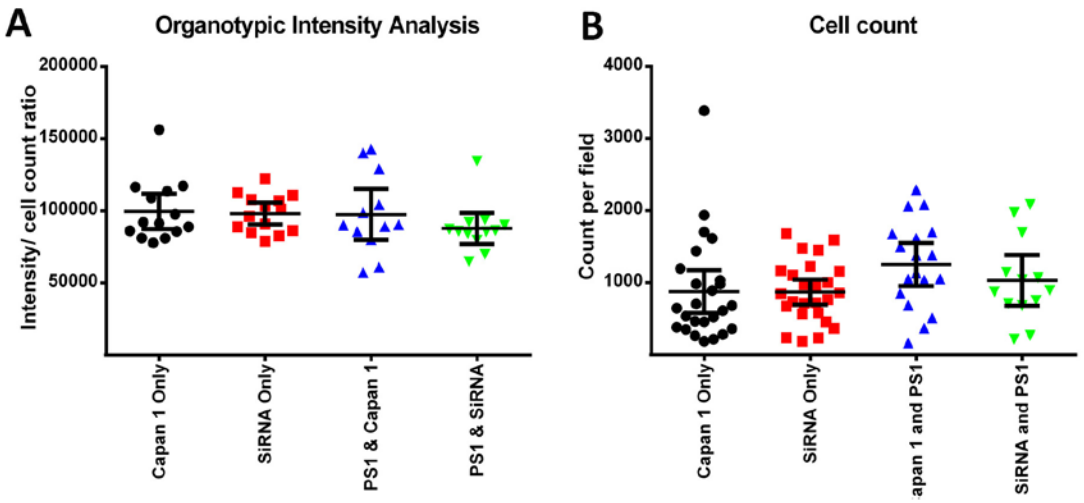

Figure 4.11: Effect of pIgR knockdown in Organotypics.

A) Comparing intensity of pIgR intensity stain. B) Comparing cell counts. Shown is median with inter quartile range. All observations were normalised to control (Capan1). Six experimental repeats were carried out resulting in 18 high power field measurements. Comparisons made by Kruskal-Wallis test followed by Dunn's post-hoc analysis. There was no significant difference.

4.6 Optimisation of pIgR shRNA

Since it was possible that the short-interfering RNA was not a valid approach in 3D co-culture models, I investigated long-term knockdown after shRNA. pIgR shRNA plasmids were kindly donated by Jing Ai, Shanghai Institute of Material Medica (179).

Puromycin dose was based on historical work in our group and the recommendation from the Ai group in order to retain the shRNA construct. However, immediate addition of Puromycin within 24 hours of shRNA transfection led to inexplicable cell death. It was assumed that the stress of manipulating RNA and immediate addition of Puromycin may have caused cell death. This shortcoming was addressed by delayed addition of Puromycin 48 hours after introduction of shRNA, which seems to rectify the situation fully.

4.7 Effect of pIgR shRNA on Capan1 pancreatic cancer cells

Capan1 cells successfully transfected with relevant shRNA were selected with RPMI media 10%FBS and 1µg/ml Puromycin, as their P-BABE vector backbone contained Puromycin resistance. Transfected cells were subsequently lysed and confirmed pIgR knockdown by Western blot (**Figure 4.12**).

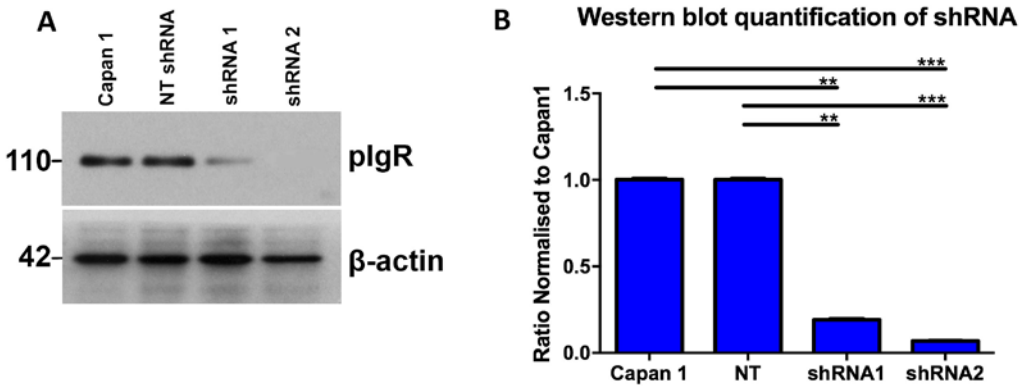

Figure 4.12: Confirmation of pIgR knockdown.

A) Western blot confirming knockout at protein level of shRNA. B) Quantification of shRNA Western blot analysis. Values are mean and SEM (n=4). Comparisons made by Kruskal-Wallis test followed by Dunn's post-hoc analysis. *** p<0.001, ** p<0.01.

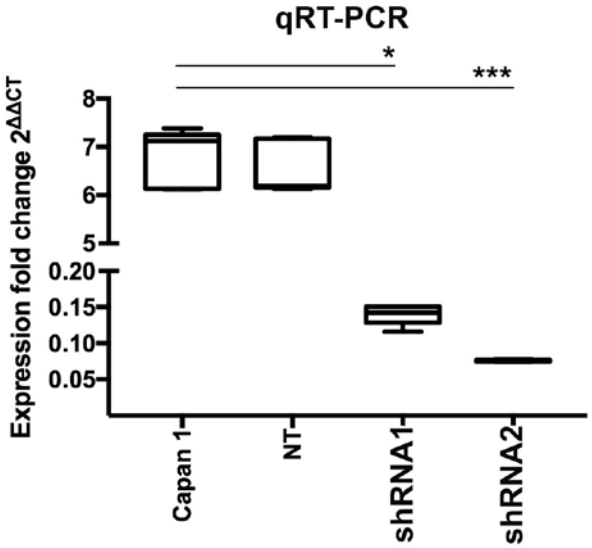

Figure 4.13: qRT-PCR of wild type and transfect shRNA.

CT values were normalised to housekeeping gene GAPDH. In order to further quantify the result, a fold change, relative to positive and negative controls provided and expression fold change. Delta CT values normalised to wild type (Capan1). Values are median and Interquartile range (n=3). Comparisons made by Kruskal-Wallis test followed by Dunn's post-hoc analysis. *** p<0.001, * p<0.05.

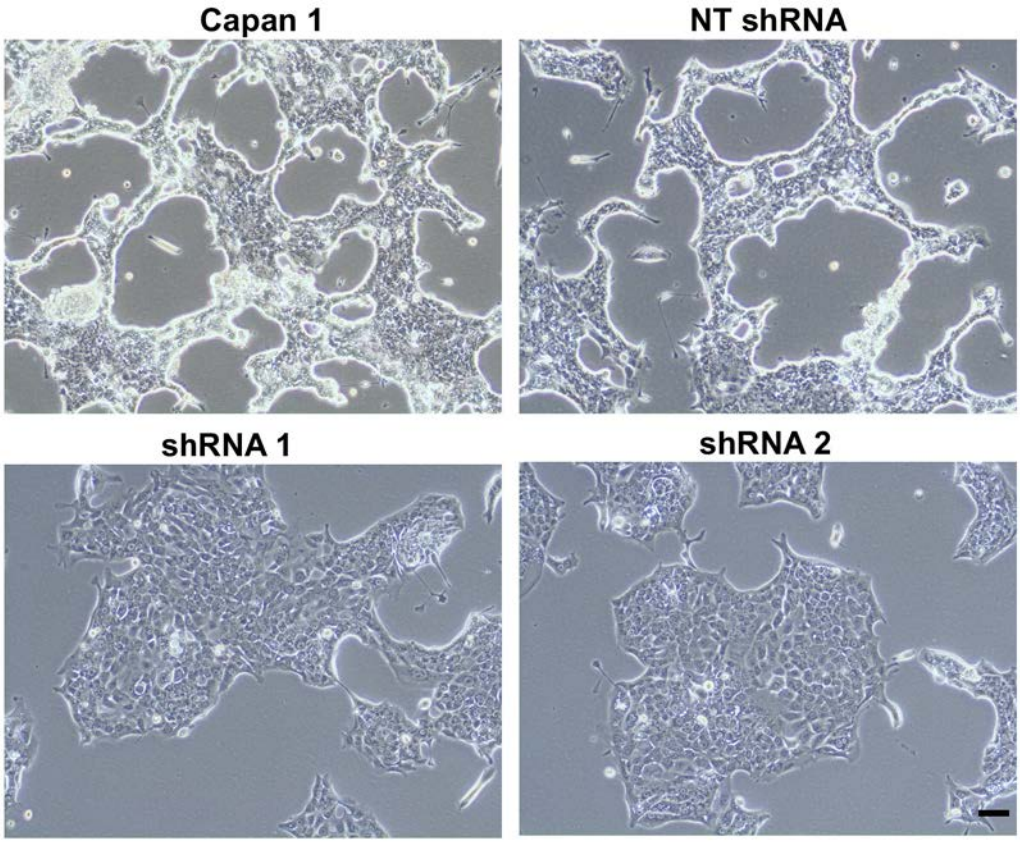

Figure 4.14: Phase contrast microscopy of pIgR shRNA cells

Phenotypic effect of pIgR shRNA on Capan 1 pancreatic cancer cells. Representative of multiple cultures and passages. Scale bar 20μm.

Western blot and quantification analysis confirms knockdown of pIgR in Capan1 cells (**Figure 4.11**). qRT-PCR further confirms knockdown of pIgR at mRNA level (**Figure 4.13**). Morphology of Capan1 cells stably expressing pIgR shRNA causes cells to lose the luminal forming ability and become colony forming (**Figure 4.14**). Capan1 cells and cells with relevant shRNA were plated in 6 well plates at a confluency of $2x10^5$, and daily cell counts were taken up to seven days (**Figure 4.15**).

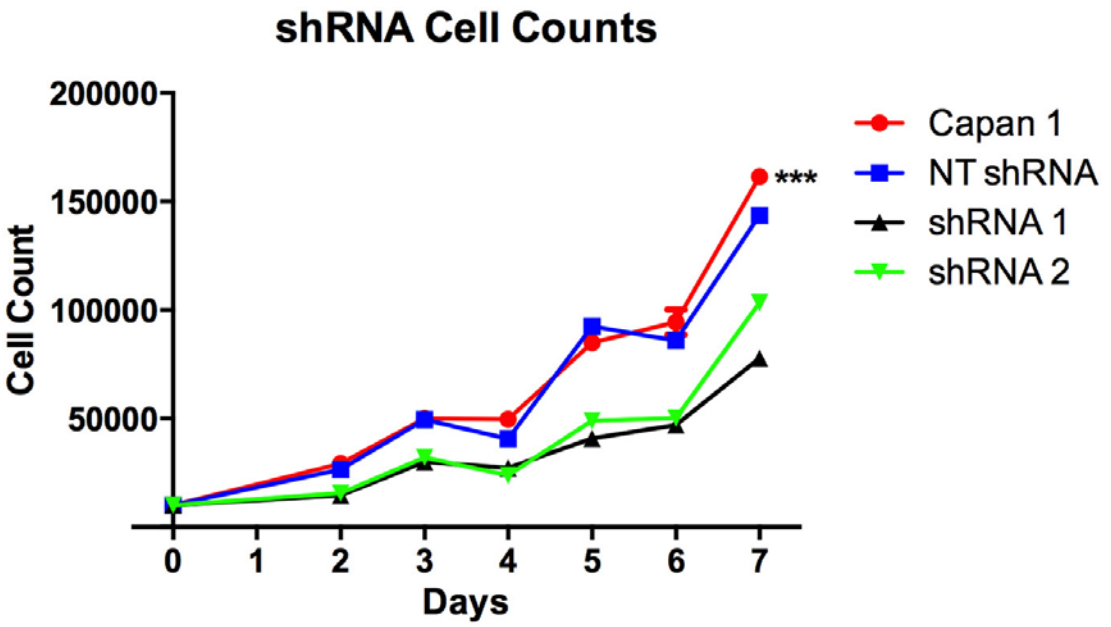

.

Figure 4.15: Cell counts after 7 days of shRNA transfection.

Cells treated with pIgR shRNA were plated in 6 well pates and cell counts were taken every days for 7 days. Values represented as mean and SEM (n=3). Capan1 vs. NT, Friedman test, p>0.9999, Capan1 vs. shRNA1, Friedman test, p=0.0021, Capan1 vs. shRNA2, Friedman test, p=0.0437.

Sequential cell counts demonstrate loss of pIgR correlate with reduced rate of cell proliferation as demonstrated after RNAi (**Figure 4.15**). Loss of pIgR however shows no association with changes in EMT markers expression, such as E-cadherin and Vimentin (**Figure 4.16**). Further functional analysis of cells depleted of pIgR demonstrates reduced migration, adhesion and viability (**Figure 4.17**). pIgR knockout in scratch assay demonstrates a delay in wound closure, and also an apparent lack of luminal formation demonstrated in wild type cells (**Figure 4.18**).

Taken together, these results demonstrated the Capan1 cells after pIgR knockdown seem to proliferate less and are less invasive, suggesting stabilisation of epithelial phenotype.

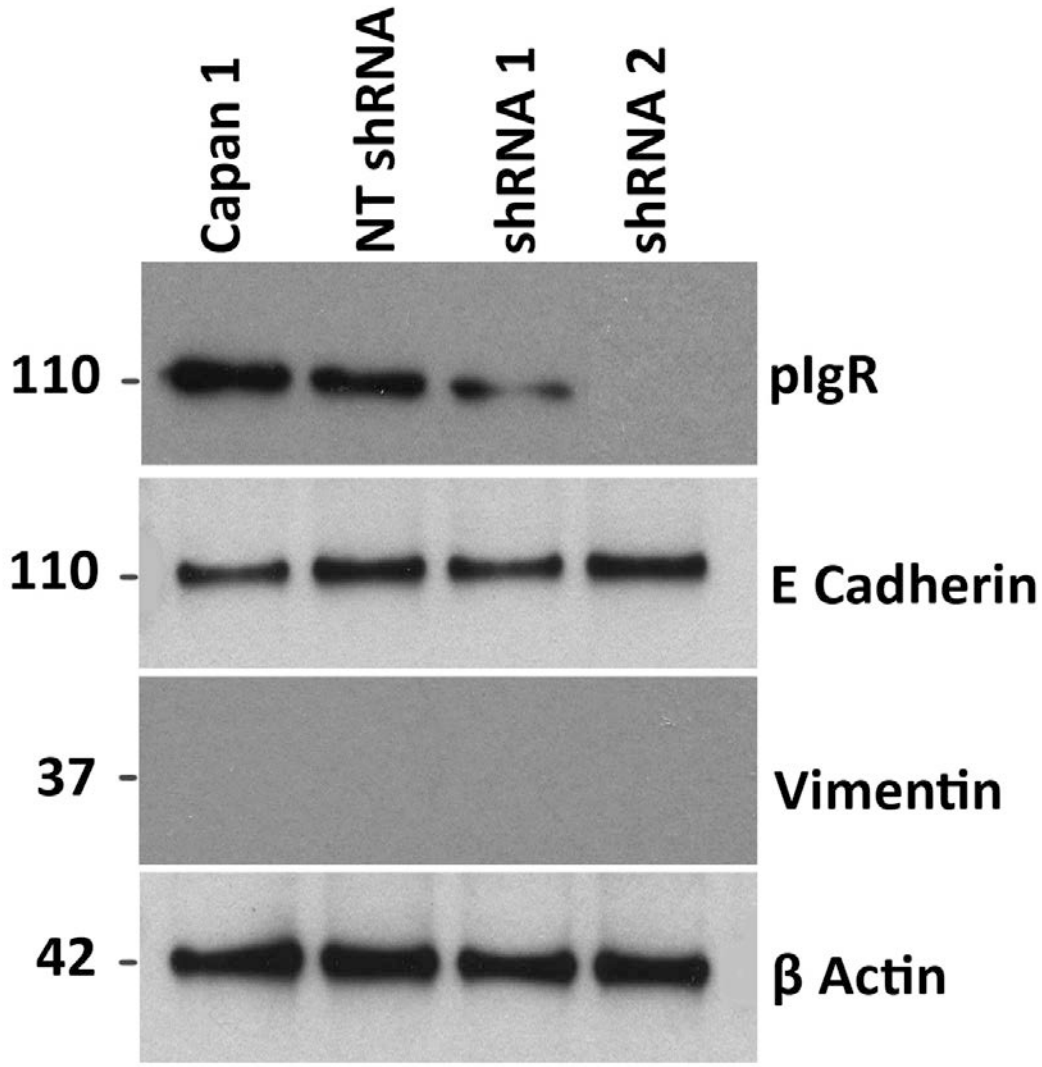

Figure 4.16: Association of pIgR knockdown and EMT.

Capan1 wild type and Capan1 cells transfected with relevant shRNA were lysed as discussed in Materials section 2.4. Probing membranes for E-cadherin and Vimentin show no change, despite pIgR knockdown. Beta Actin was used as loading control.

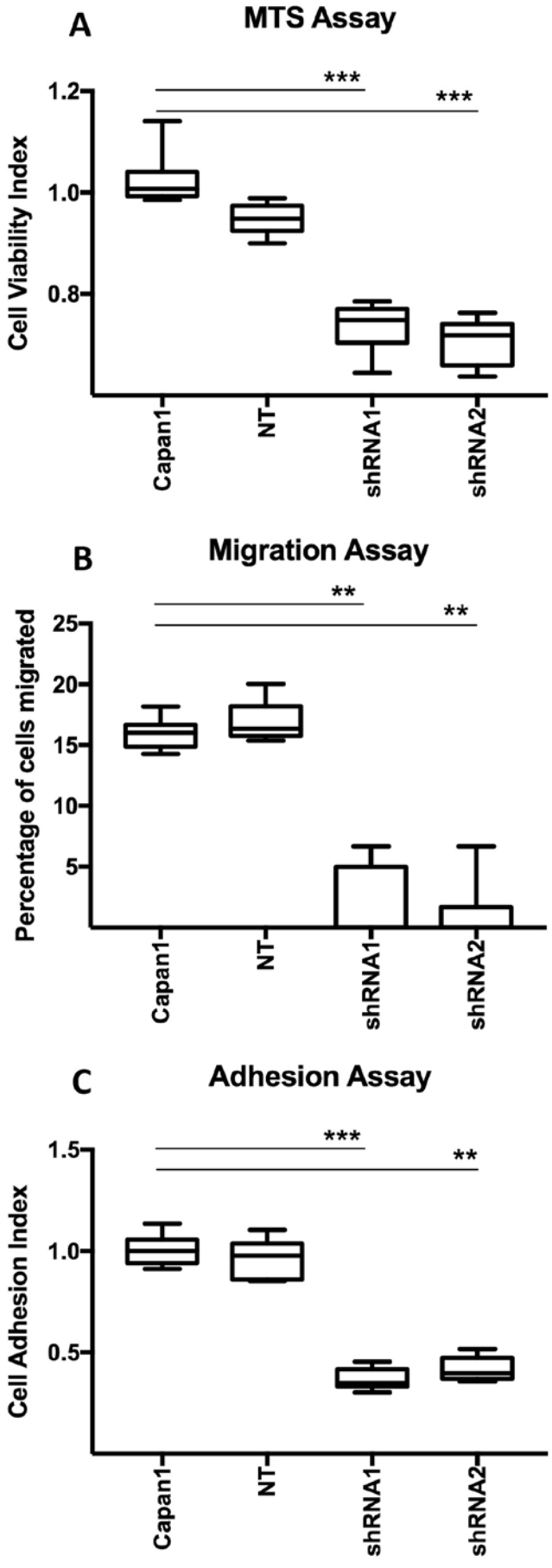
A
MTS Assay
***
***
1.2
1.0
0.8
Cell Viability Index
Capan1
NT
shRNA1
shRNA2
B
Migration Assay
**
**
25
20
15
10
5
Percentage of cells migrated
Capan1
NT
shRNA1
shRNA2
C
Adhesion Assay
***
**
1.5
1.0
0.5
Cell Adhesion Index
Capan1
NT
shRNA1
shRNA2

Figure 4.17: Functional effects of pIgR shRNA on Capan1 cells.

A) MTS assays (WST-1 reagent), carried out in triplicates, demonstrates viability, normalised to Capan1 cells. (Kruskal-Wallis P=<0.0001). Capan1 and shRNA2, 0.0003 for Capan1 and shRNA1. N=3. B) After 24 hours in transwell, a significantly lower percentage of cells that hat pIgR knockout had migrated compared to WT and NT Capan1 cells. (Kruskal-Wallis P=<0.0001) or Capan1 and shRNA2 0.0019, 0.0034 for capan1 and shRNA1. N=3. C) After 30 minutes incubation with fibronectin, remaining cells with pIgR knockout were significantly lower compared to WT and NT. (Kruskal-Wallis P=<0.0001). N=3. Comparisons made by Kruskal-Wallis test followed by Dunn's post-hoc analysis. *** $p<0.001$, ** $p<0.01$, * $p<0.05$.

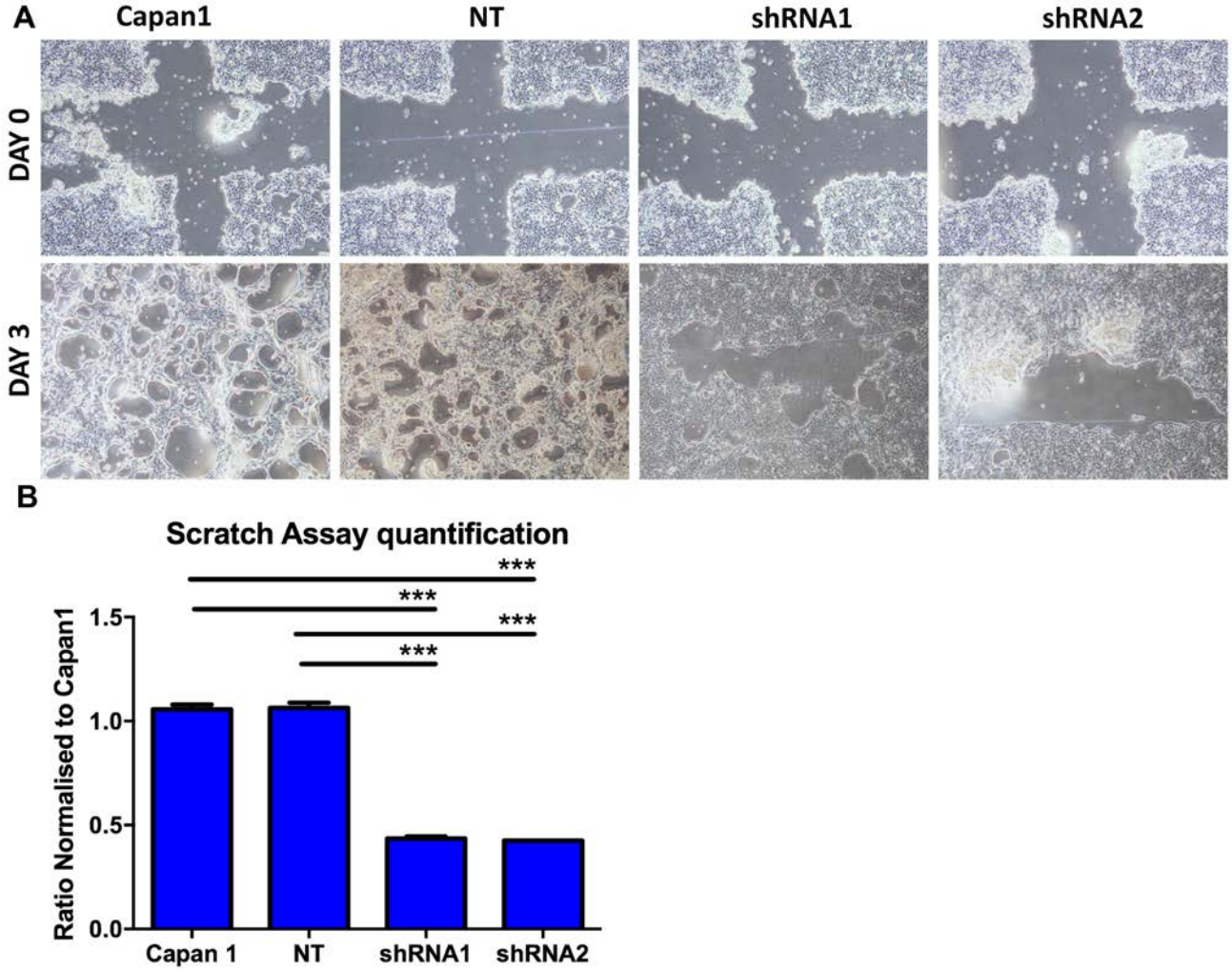

Figure 4.18: Effect of pIgR knockdown on scratch assay.

A) Comparison images taken at day 0 and 72 hours later. shRNA variants have a tendency to form islands of cells, rather than wild type and non-targeting variants. B) Statistical analysis is based on area of surface not covered by cells, normalised to Capan1 cells. Comparisons made by One-way ANOVA followed by Holm-Sidak post-hoc analysis. *** $p<0.001$, ** $p<0.01$, * $p<0.05$.

4.8 Effect of pIgR shRNA on cancer cell phenotype using organotypic model

Capan 1 cells successfully transfected with relevant shRNA were selected with RPMI media 10%FBS and 1µg/ml Puromycin, as their P-BABE vector backbone contained Puromycin resistance, whilst Capan 1 cells alone were used as a control. The treated or control Capan 1 cells were admixed with PS1 stellate cells in a 2:1 ratio (shown previously (70)) to be the optimum PS1: cancer cell ratio for invasion in this organotypic model). Gels were raised to a grid and fed with fresh medium every other day for 10 days in total. I could confirm enhanced proliferation of cancer cells upon addition of stellate cells. However, this effect was abrogated upon pIgR knockdown. In order to be able to distinguish between the direct effect of pIgR on cancer cells or and indirect effect via changes occurring by stellate cells, the results were compared with an organotypic culture of cancer cells alone.

Representative H&E stained images of sections of Capan1 and shRNA variations with and without co-culture of stellate cells are shown in **Figure 4.19** and **4.20**. Overall, organotypic gels containing stellate cells are more contracted and thicker, with a more significant cancer cell layer thickness. Wild type Capan1 and NT organotypics with stellate cells also appear to form more luminal structures compared to pIgR depleted gels. More interestingly, lack of pIgR in Capan1 cells causes less contracted gels with a reduced cancer cell layer thickness. These interactions suggest that pIgR expression may increase stellate cell activity. I therefore sought to quantify these preliminary observations.

Capan1 cells have been noted to form luminal structures in organotypic models, and this is more pronounced when cultured with PS1 cells, which has been noted previously (70). However, cancer cells with pIgR knockdown form smaller and fewer luminal structures, and this was not revoked after addition of stellate cells (**Figure 4.21**).

Organotypic gels cultured with PS1 cells are more contracted and have thicker gels than compared gels containing only cancer cells (219). Knockout of pIgR in

cancer cells co-cultured with PS1 cells had thinner and longer gels confirming activity of stellate cells was affected (**Figure 4.22**).

Cancer cell and stellate cells proliferate at various rates and knockout of pIgR caused reduction in cancer cell proliferation as confirmed by total cell area and quantitating analysis of nucleic staining. The layer of cells formed at the top of the ECM gel was also reduced on knockout of pIgR (**Figure 4.23**).

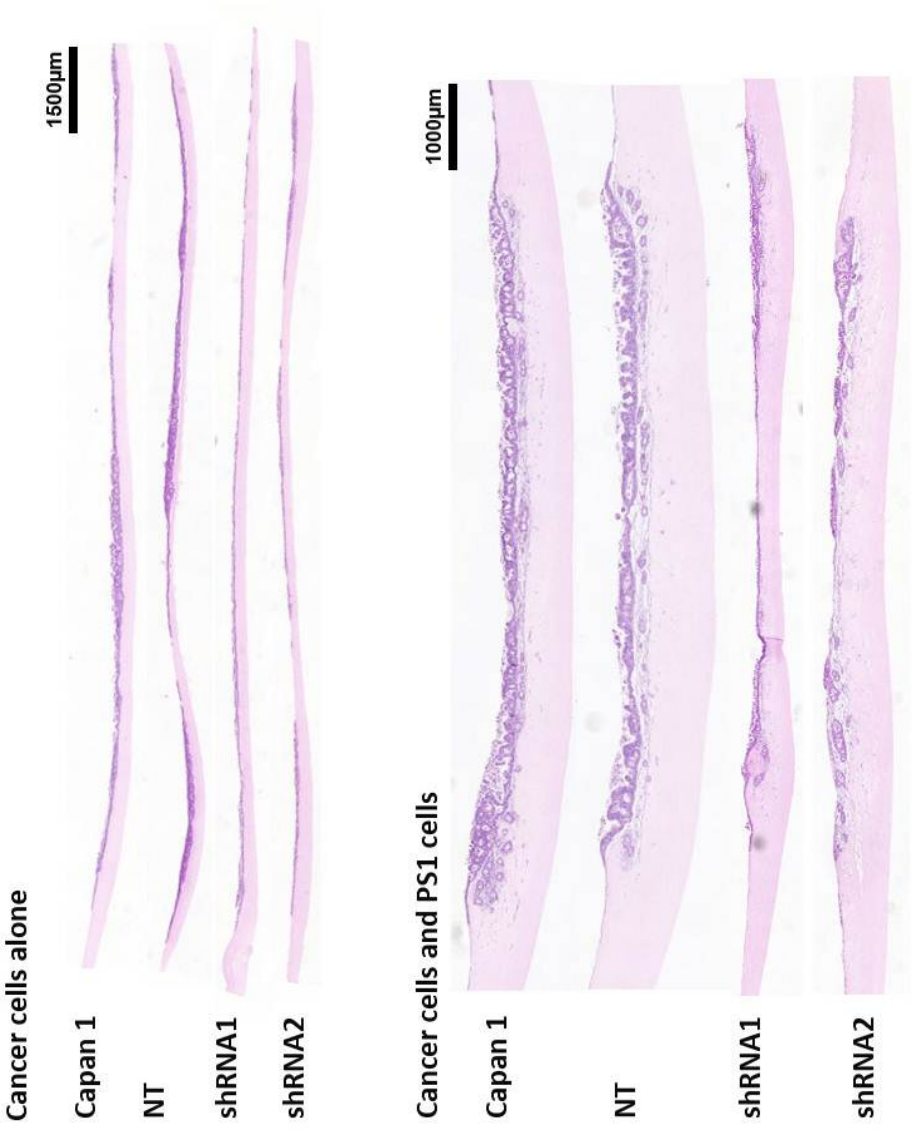

Figure 4.19: Haematoxylin and Eosin stained sections from organotypic cultures.

Representative images of H&E stained sections with organotypics of cancer cells alone or in co-culture with PS1 cells. Scale bar 1500µm for cancer cells alone, 1000µm for images with PS1 cells.

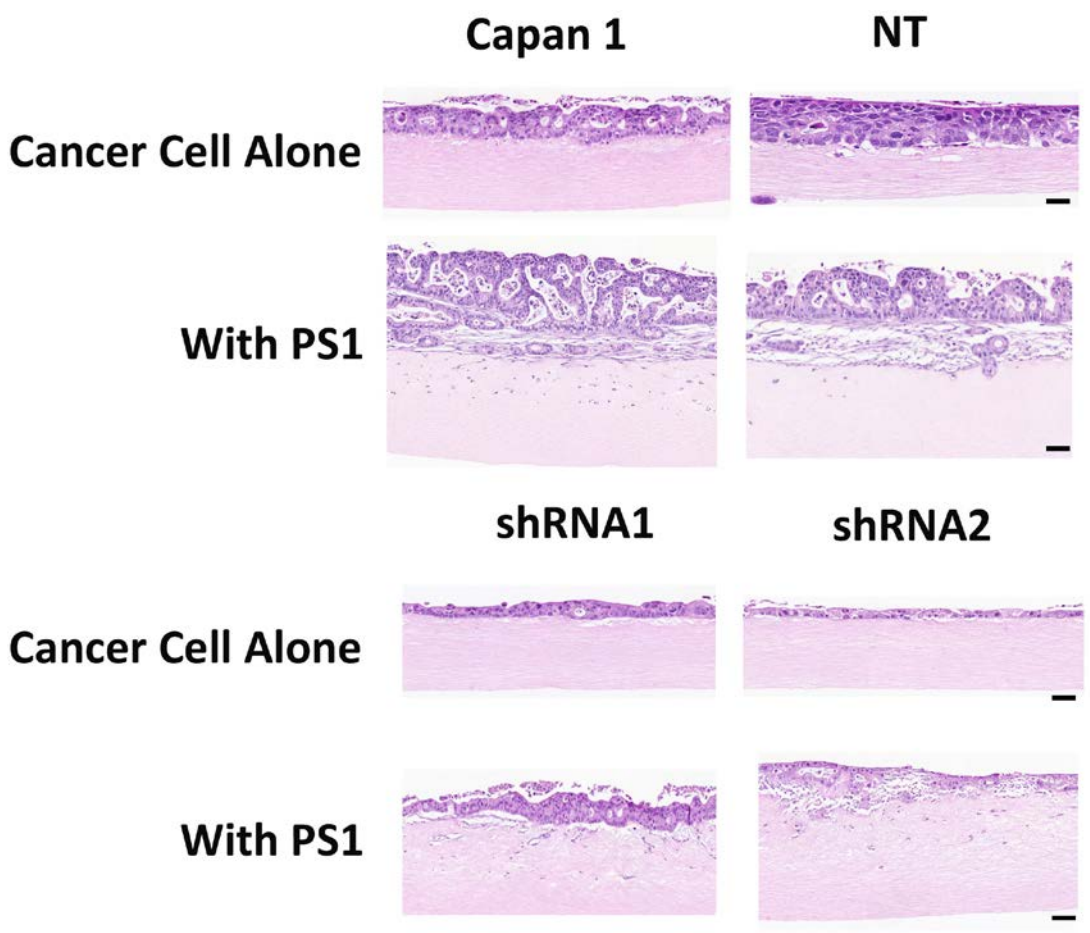

Figure 4.20: Close up cross sectional H&E stained sections from Organotypic cultures.

Magnified representative images of organotypics demonstrated in Figure 4.19. Scale bar 100µm.

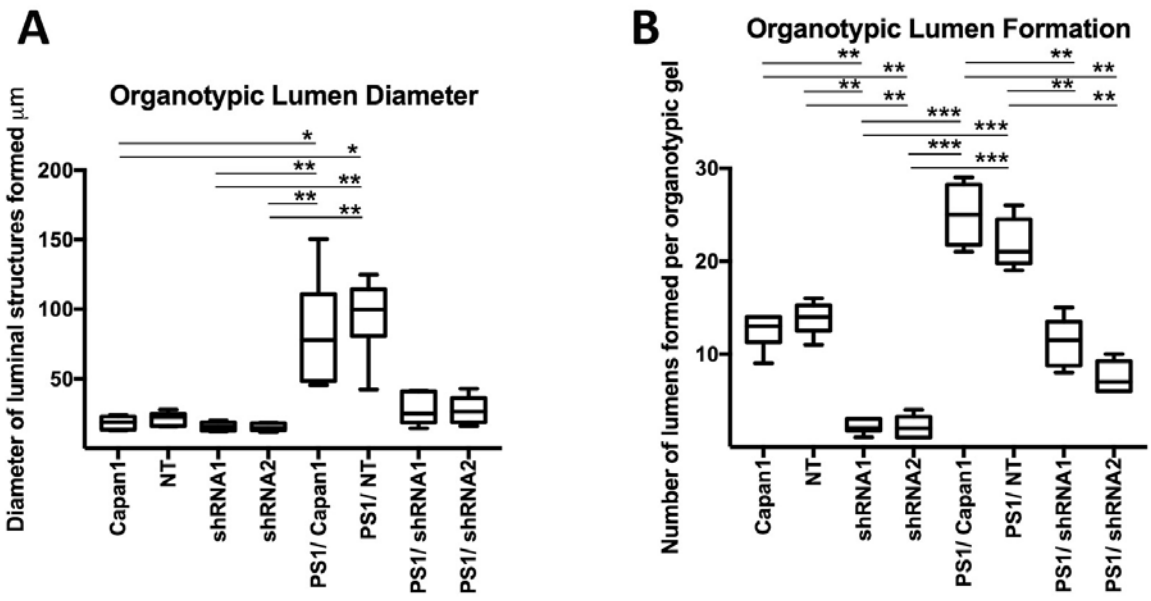

Figure 4.21: Effect of pIgR knockout in cancer cell lumen formation.

Summary data from organotypics with and without PS1 cells. Data is from three experiments, all performed in replicate, thus a total of 9 organotypics per condition. A) Box and whisker plot with median interquartile range of diameter of luminal structures formed. Luminal structures were defined as having epithelial cells circumferentially. n=9. Comparisons made by Kruskal-Wallis test followed by Dunn's post-hoc analysis. ** p<0.01.B) Box and whisker plot with median interquartile range of number of luminal structures formed. Luminal structures were defined as having epithelial cells circumferentially. N=9. Comparisons made by Kruskal-Wallis test followed by Dunn's post-hoc analysis. *** p<0.001, ** p<0.01, * p<0.05.

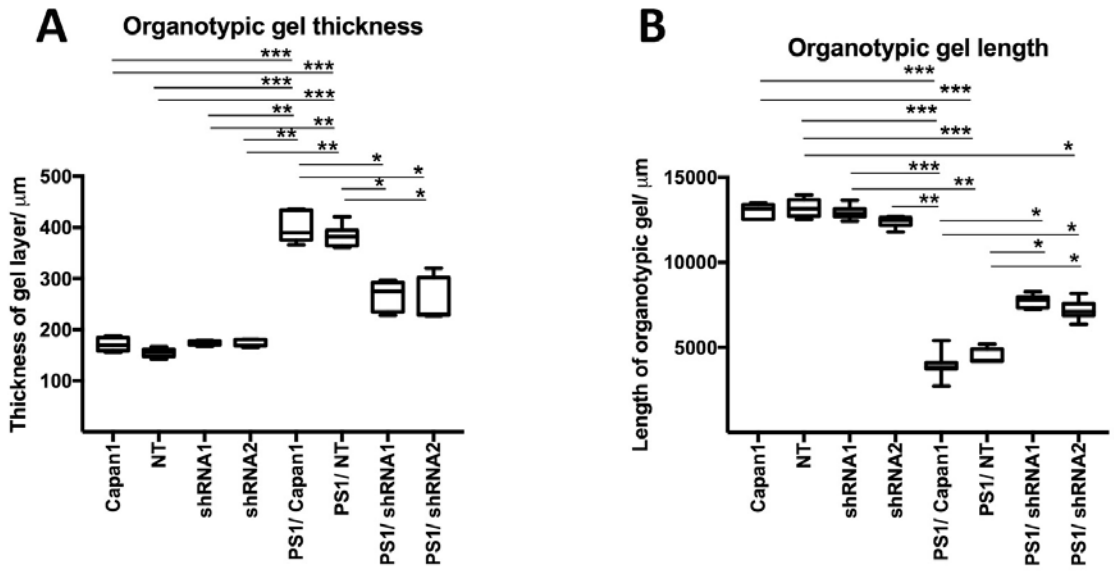

Figure 4.22: Effect of pIgR knockout in Organotypic gel structure.

Summary data from organotypics with and without PS1 cells. Data is from three experiments, all performed in replicate, thus a total of 9 organotypics per condition. A) Box and whisker plot with median interquartile range of organotypic gel thickness. N=9. Comparisons made by Kruskal-Wallis test followed by Dunn's post-hoc analysis. ** $p<0.01$. B) Box and whisker plot with median interquartile range of organotypic gel length. N=9. Comparisons made by Kruskal-Wallis test followed by Dunn's post-hoc analysis. *** $p<0.001$, ** $p<0.01$, * $p<0.05$.

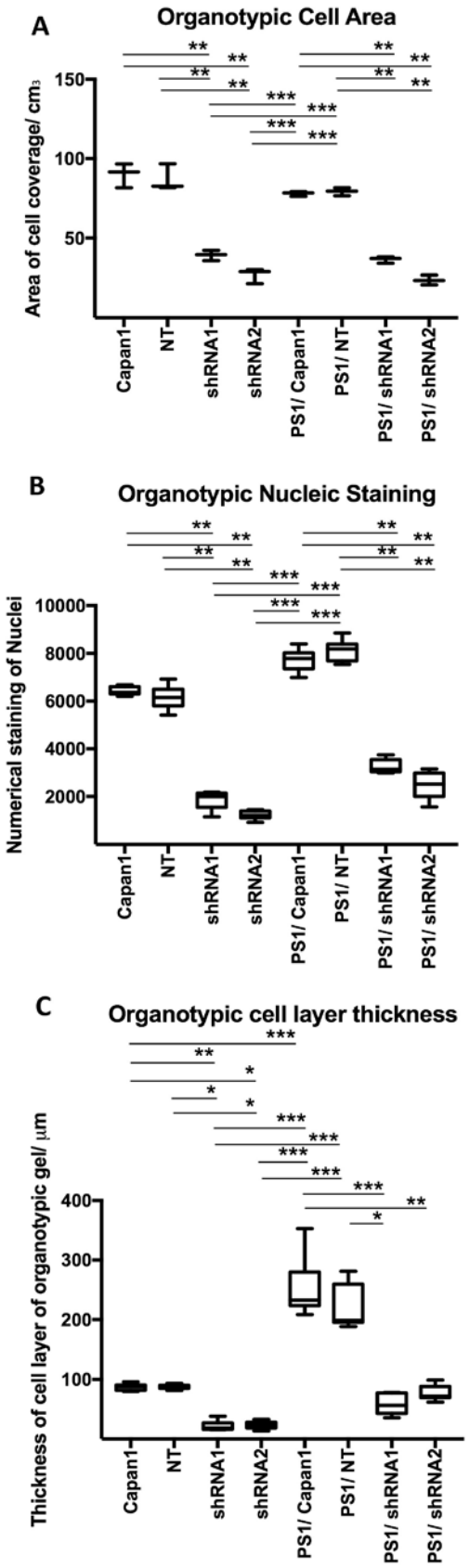
A
Organotypic Cell Area
Area of cell coverage/ cm3
150
100
50
Capan1
NT
shRNA1
shRNA2
PS1/ Capan1
PS1/ NT
PS1/ shRNA1
PS1/ shRNA2
B
Organotypic Nucleic Staining
Numerical staining of Nuclei
10000
8000
6000
4000
2000
C
Organotypic cell layer thickness
Thickness of cell layer of organotypic gel/ µm
400
300
200
100

Figure 4.23: Effect of pIgR knockdown in cancer cell layer.

Summary data from organotypics with and without PS1 cells. Data is from three experiments, all performed in replicate, thus a total of 9 organotypics per condition. A) Box and whisker plot with median interquartile range of organotypic cell area (as explained in Materials 2.9). N=9. Comparisons made by Kruskal-Wallis test followed by Dunn's post-hoc analysis. *** p<0.001, ** p<0.01, * p<0.05. B) Box and whisker plot with median interquartile range of organotypic nucleic staining. N=9. Comparisons made by Kruskal-Wallis test followed by Dunn's post-hoc analysis. *** p<0.001, ** p<0.01, * p<0.05. C) Box and whisker plot with median interquartile range of organotypic cell layer thickness. N=9. Comparisons made by Kruskal-Wallis test followed by Dunn's post-hoc analysis. *** p<0.001, ** p<0.01, * p<0.05.

4.9 Changes in epithelial and stromal activity upon pIgR knockdown

First of all, I wanted to confirm sustained knockdown of pIgR in organotypic cultures. Addition of PSC seems to enhance pIgR expression in parental and NT cancer cells, but not after pIgR knockdown in cancer cells. pIgR knockdown remains apparent in 3D models, even after addition of stellate cells, although addition of stellate cells seemed to increase the intensity of pIgR staining (**Figures 4.24 – 4.26**).

pIgR deplete and wild type Capan1 organotypics with and without stellate cells were stained with numerous markers to investigate the effect of pIgR in a 3D model of PDAC. E-cadherin had been demonstrated in Chapter 3 to have an inverse interaction with pIgR to a degree furthermore Froeling et al had demonstrate loss of E-cadherin upon addition of stellate cells (202). E-cadherin is noted to be reduced upon addition of stellate cells, but there is no change after pIgR knockdown (**Figure 4.27**).

Cytokeratins are proteins of keratin-containing filaments in epithelial cells. There numerous subtypes and loss of cytokeratin can be associated with malignant transformation (273). Addition of stellate cells bears no effect on cytokeratin expression; however, loss of pIgR is associated with an increase in cytokeratin expression (**Figures 4.28 - 4.30**). This is likely to represent that loss of pIgR has stabilised Capan1 cells to a more stable epithelial phenotype.

αSMA has been used as a marker of stellate cell activity (59). Upon pIgR knockdown in cancer cells, αSMA is significantly reduced. Therefore it is possible that pIgR expression may modulate PSC activity (**Figure 4.31**).

The ZEB family interacts with other transcriptional regulators and their activities are modulated by post-translational modifications and phosphorylation. These proteins trigger and EMT by repression of epithelial markers and activation of mesenchymal properties (273). Modulation of pIgR had no effect on Zeb1 expression, but its expression seems inversely associated with E-cadherin, and increases with stellate cell activation (**Figure 4.32 – Figure 4.34**).

Picrosirius red was also investigated in Chapter 3 and is used as a surrogate marker for ECM content. Its expression was increased in organotypics with stellate cells. Although not significant, it appears that lack of pIgR seems to reduce expression of Picrosirius red (**Figures 4.35 and 4.36**). This observation maybe in keeping with reduced αSMA activity noted in Figure 4.31.

Ezrin has been used as a marker for apico-basal polarity and for lumen formation (274), since my observations noted reduced luminal formation in organotypics lacking pIgR in cancer cells. Ezrin expression in cancer cells is markedly reduced upon pIgR knockdown (**Figures 4.37 and 4.38**).

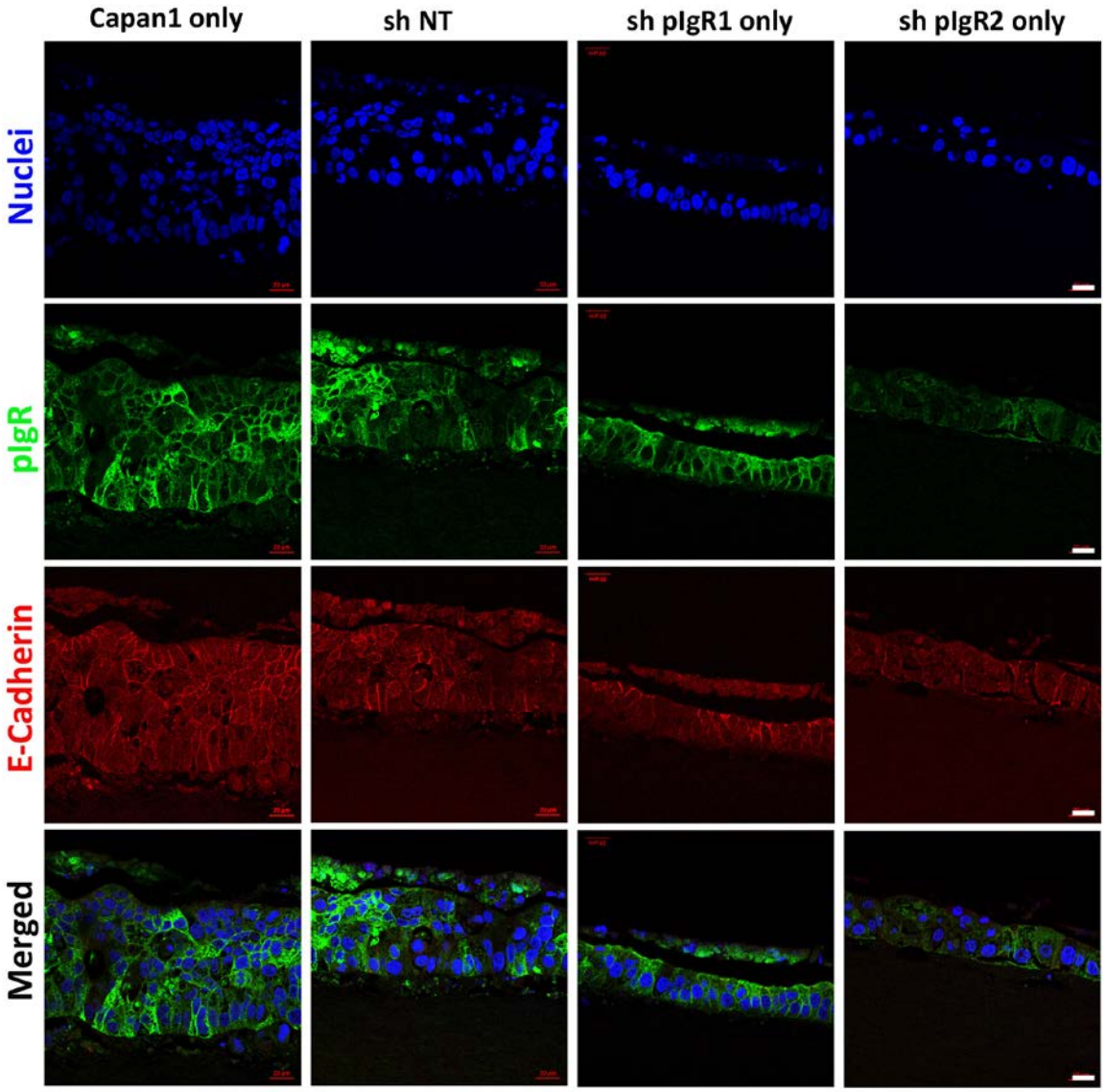

Figure 4.24: pIgR and E-cadherin interaction in pIgR knockdown 3D models.

Representative images of organotypics with pIgR shRNA. pIgR (green) and E-Cadherin (red). Scale bar 20µm.

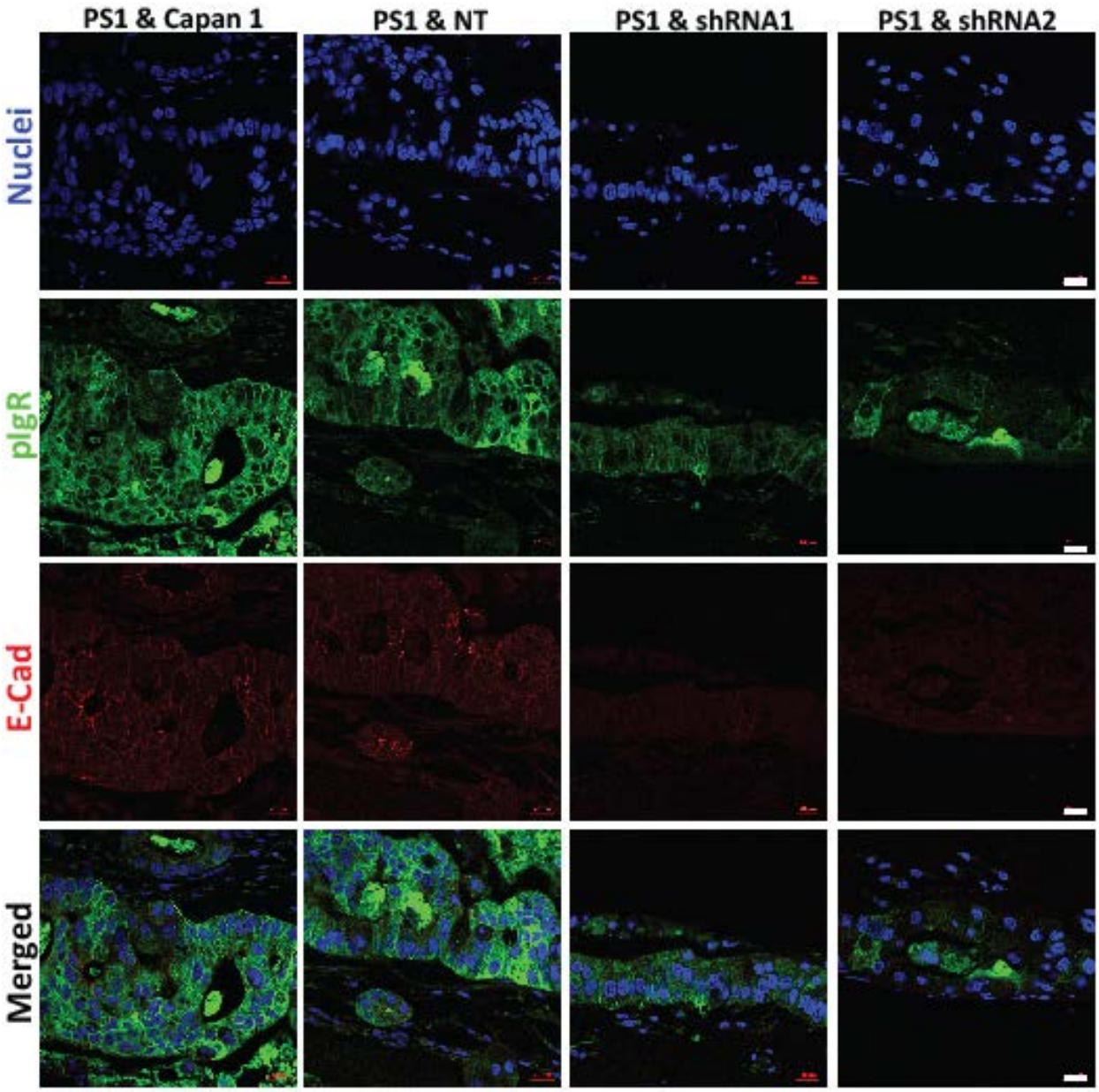

Figure 4.25: pIgR and E-cadherin interaction in pIgR knockdown 3D models.

Representative images of organotypics with pIgR shRNA. pIgR (green) and E-Cadherin (red). Scale bar 20µm.

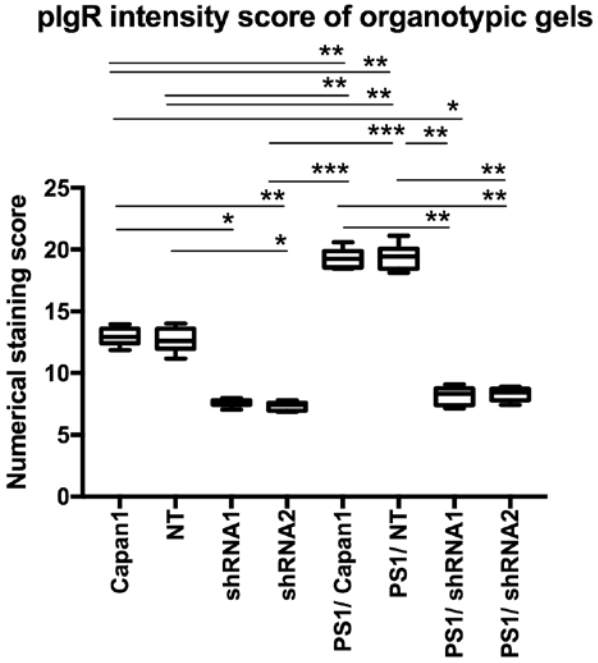

Figure 4.26: pIgR expression in organotypic models.

Box and whisker plot with median and interquartile range of pIgR staining intensity. N=9. Comparisons made by Kruskal-Wallis test followed by Dunn's post-hoc analysis. *** p<0.001, ** p<0.01, * p<0.05.

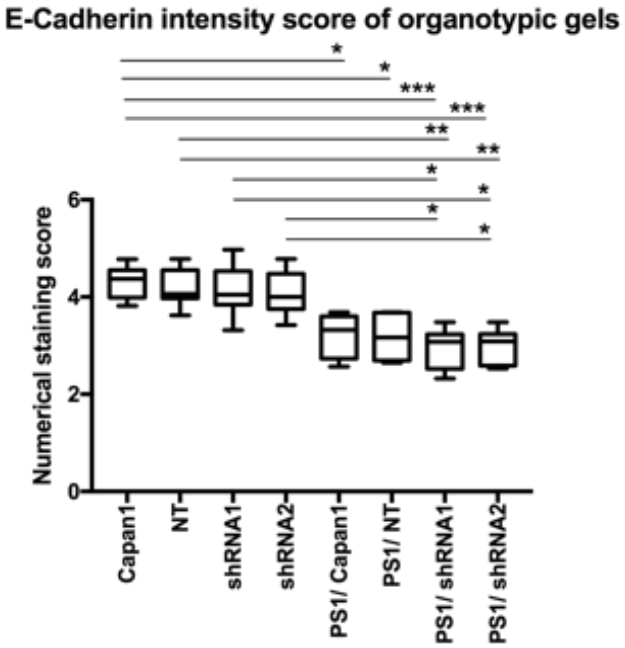

Figure 4.27: E-cadherin expression in organotypic models.

Box and whisker plot with median and interquartile range of E-cadherin staining intensity. N=9. Comparisons made by Kruskal-Wallis test followed by Dunn's post-hoc analysis. *** p<0.001, ** p<0.01, * p<0.05.

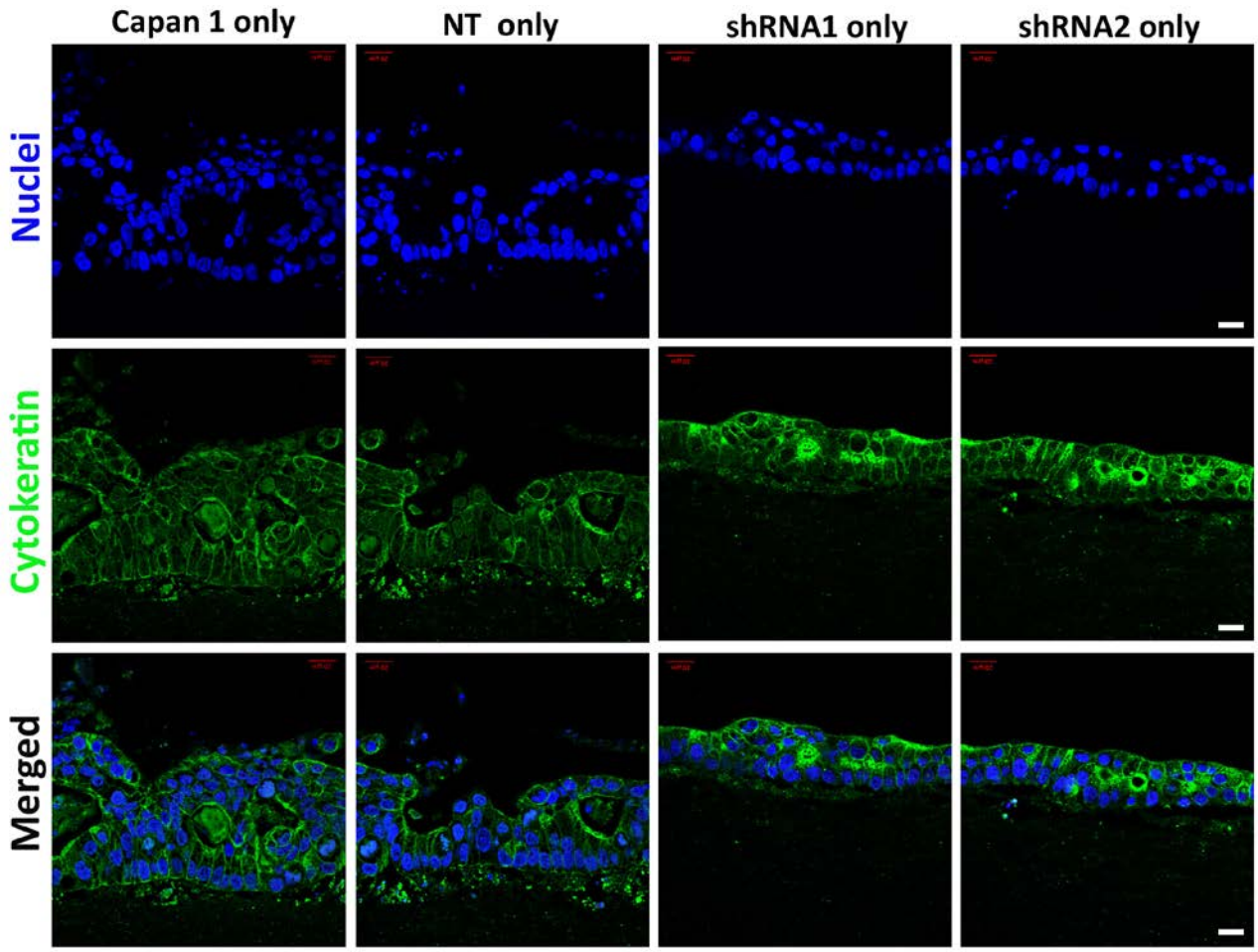

Figure 4.28: Cytokeratin interaction in pIgR knockdown 3D models.

Representative images of organotypics with pIgR shRNA. Cytokeratin (CK) (green). Scale bar 20µm.

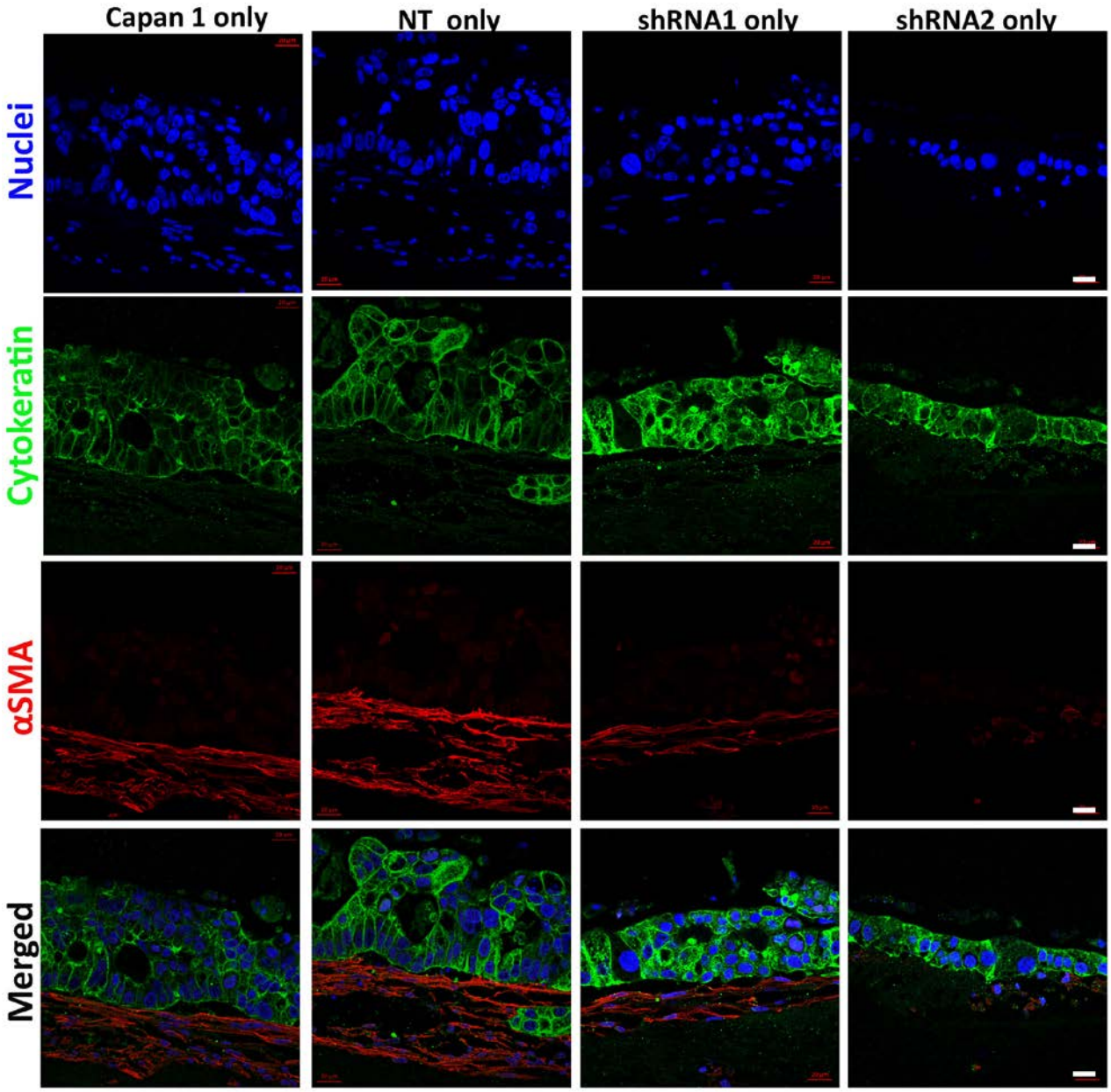

Figure 4.29: Cytokeratin and αSMA interaction in pIgR knockdown 3D models.

Representative images of organotypics with pIgR shRNA. Cytokeratin (CK) (green) and αSMA (red). Scale bar 20µm.

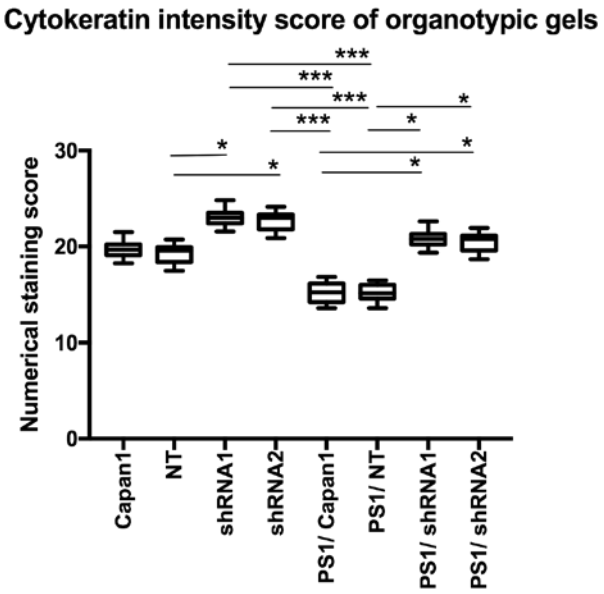

Figure 4.30: Cytokeratin expression in organotypic models.

Box and whisker plot with median and interquartile range of Cytokeratin staining intensity. N=9. Comparisons made by Kruskal-Wallis test followed by Dunn's post-hoc analysis. *** p<0.001, ** p<0.01, * p<0.05.

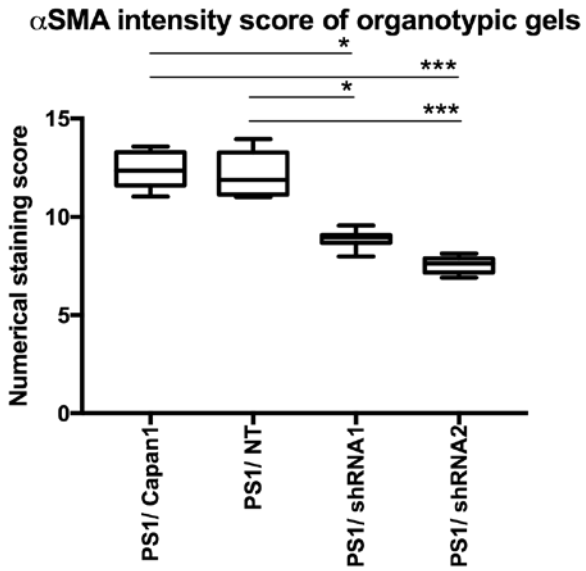

Figure 4.31: αSMA expression in organotypic models.

Box and whisker plot with median and interquartile range of αSMA staining intensity. N=9. Comparisons made by Kruskal-Wallis test followed by Dunn's post-hoc analysis. *** p<0.001, ** p<0.01, * p<0.05.

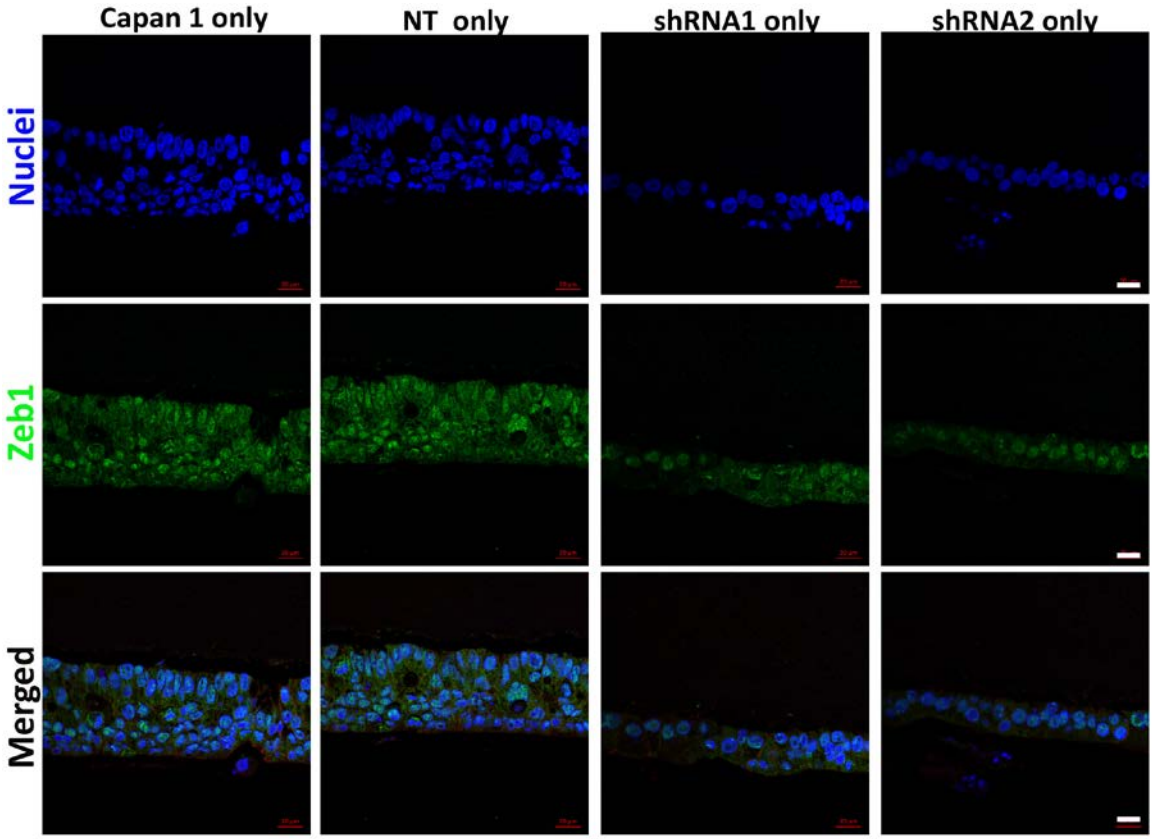

Figure 4.32: Zeb1 interaction in pIgR knockout 3D models.

Representative images of organotypics with pIgR shRNA. Zeb1 (green). Scale bar 20µm.

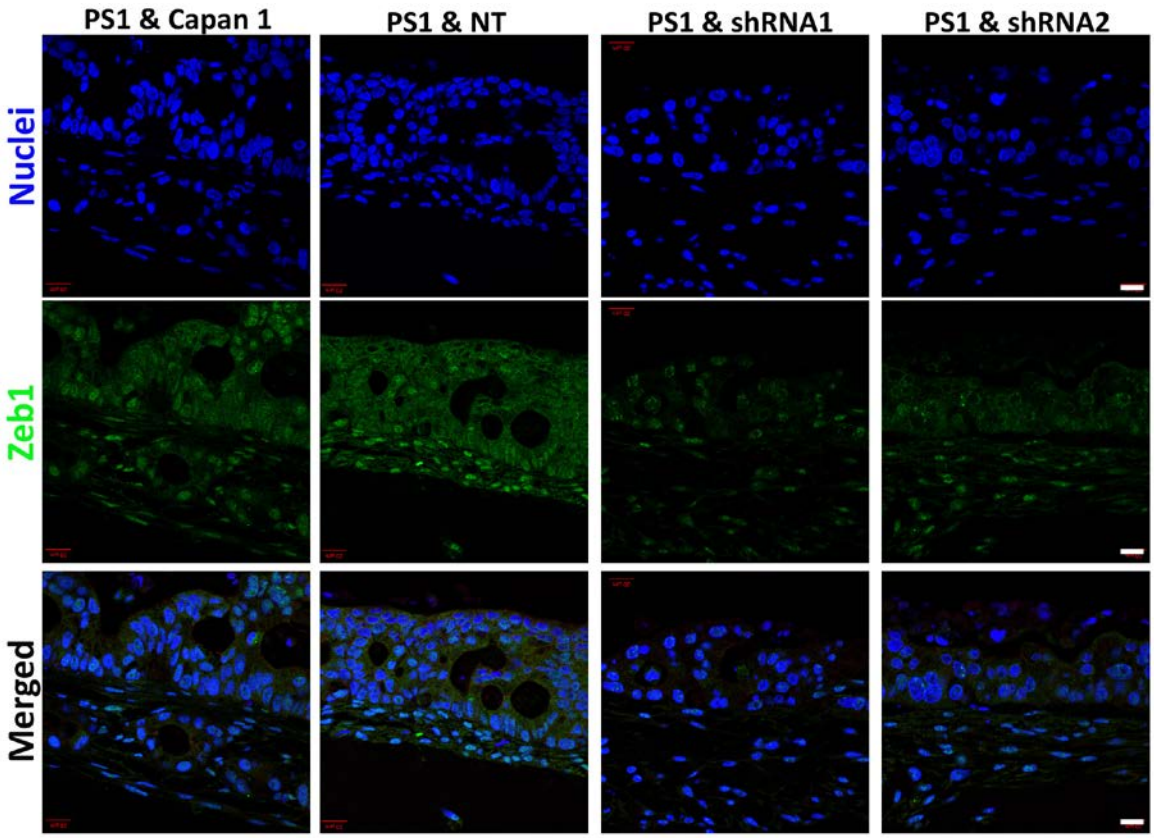

Figure 4.33: Zeb1 interaction in pIgR knockout 3D models.

Representative images of organotypics with pIgR shRNA. Zeb1 (green). Scale bar 20µm.

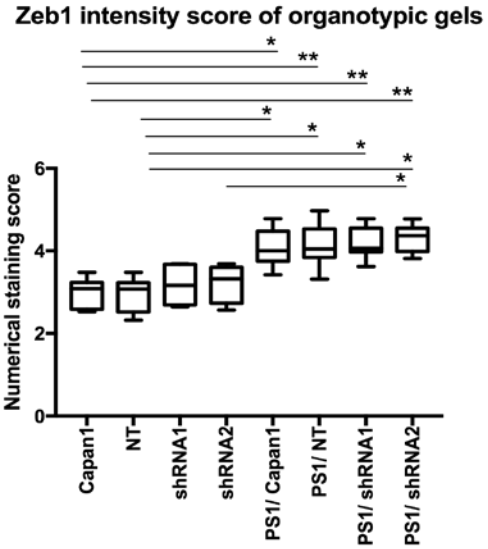

Figure 4.34: Zeb1 expression in organotypic models.

Box and whisker plot with median and interquartile range of Zeb1 staining intensity. N=9. Comparisons made by Kruskal-Wallis test followed by Dunn's post-hoc analysis. *** $p<0.001$, ** $p<0.01$, * $p<0.05$.

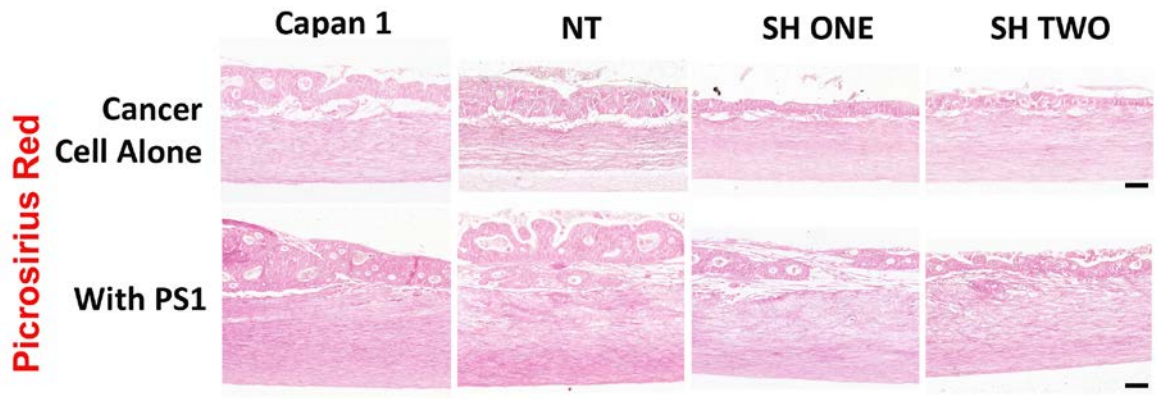

Figure 4.35: Picrosirius Red expression in pIgR knockout 3D models.

Representative images of organotypics with pIgR shRNA. Scale bar 20µm.

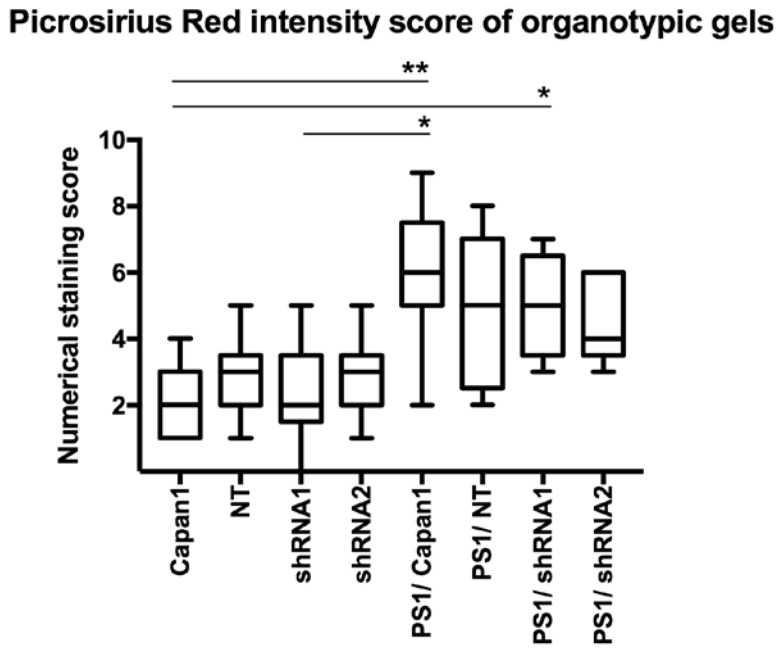

Figure 4.36: Picrosirius red expression in organotypic models.

Box and whisker plot with median and interquartile range of Picrosirius red staining intensity. N=9. Comparisons made by Kruskal-Wallis test followed by Dunn's post-hoc analysis. *** $p<0.001$, ** $p<0.01$, * $p<0.05$.

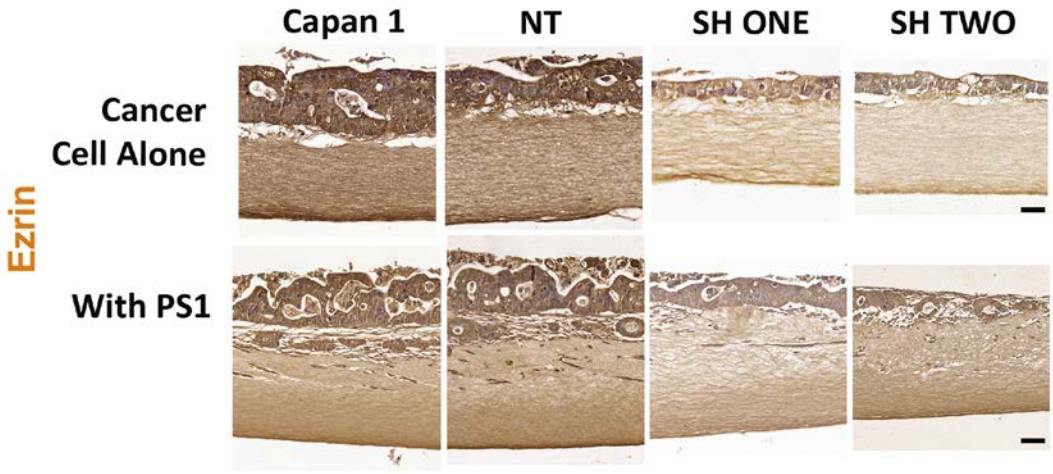

Figure 4.37: Ezrin expression in pIgR knockout 3D models.

Representative images of organotypics with pIgR shRNA. Scale bar 20µm.

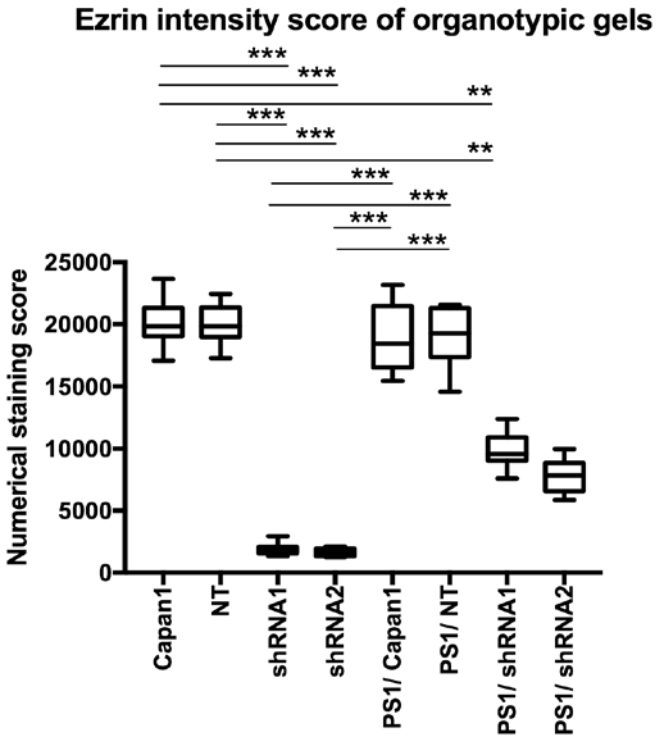

Figure 4.38: Ezrin expression in organotypic models.

Box and whisker plot with median and interquartile range of Ezrin staining intensity. N=9. Comparisons made by Kruskal-Wallis test followed by Dunn's post-hoc analysis. *** $p<0.001$, ** $p<0.01$, * $p<0.05$.

4.10 Optimisation of pIgR over-expression

Since there was only one pancreatic cancer cell line with endogenous pIgR protein expression, and there was no induction of pIgR protein expression on other pancreatic cancer cell lines, I wanted to confirm my observation of pIgR knockdown with pIgR over-expression in cancer cells not expressing pIgR. pIgR cDNA was obtained (pBS-pIgR cDNA was a gift from Pamela Bjorkman (Addgene plasmid #12109)). Stab culture overnight elicited colonies, which were picked and processed using QIAprep Spin Miniprep Kit (QIAGEN, #27104) as per manufacture's protocol, to generate enough DNA for subsequent introduction to mammalian cloning vectors.

4.10.1 Optimisation of Digestion

In order to extract the 2900 base pair sequence of pIgR, attempts were made to optimise its extraction. Initial work focused on PCR based digestion, to ligate and amplify volumes. However, multiple reading errors in the PCR process gave negligible amounts of DNA (data not shown).

Next I focused on gel digestion with ligation enzymes. Again, multiple issues arose. Initial digestion with ECOR1 alone and double digestion with Xba1 and HindIII revealed a large band around 3000 base pairs. The assumption was that this band contained both pIgR (2900 base pairs) and the vector pBluescript (3200 base pairs). To further the protocol, an additional third enzyme, Bsa1, was added, in an attempt to split the transport vector and reveal pIgR. Although simple in theory, based on each enzyme having different optimal temperature and buffers, optimizing the reaction proved troublesome in real terms. However, addition of further bovine serum albumin (NEB, #B9000) provided stable digestion conditions (**Figure 4.39**).

4.10.2 Optimisation of Cloning

Having successfully ligated the pIgR segment, the aim was to introduce it into a mammalian vector, for eventual introduction into human cells. Initial attempts with MIGR1 (a backbone provided by Dr Capasso, Barts Cancer Institute) proved

unsuccessful, with low volumes and subsequent negative transformation of bacteria. Change was made with use of PCDNA4T/0 (Invitrogen #V1020-20) as the vector. Although initially high volumes and long digestions were used, eventually success was made with low volume of pIgR and PCDNA4T/0 (**Figure 4.39**).

4.10.3 Optimisation of Transformation

The cloned sequence was introduced into pCDNA4/TO (Invitrogen) in the presence of T4 DNA ligase (NEB) and transformed into TOP10 (DH5α) *Escherichia coli (E. Coli)* cells. Transformed cells were selected on a LB plate containing 100 μg/mL ampicillin at 37°C for 16 hours. Positive transformants were inoculated into LB broth containing 100 μg/mL ampicillin for plasmid propagation. The following day, the liquid broth was centrifuged for 10minutes at 5400rpm, half of the product being retained for glycerol stock (500μl glycerol and 500μl broth media) for long-term storage. The other half was subsequently processed using QIAprep Spin Miniprep Kit (QIAGEN, 27104) as per manufacture's protocol, to generate enough DNA for subsequent introduction into cancer cells.

4.10.4 Other methods of pIgR expression

With inconclusive results, 3 further methods of pIgR expression were sought. The OSLO vector (Human pIgR cDNA-containing pcDNA3.1 (+)) was a generous gift from Dr Finn-Eirik Johansen (Rikshospitalet University Hospital, Oslo, Norway) (179). After sequencing confirmation (**Figure 4.41**), Hela, AsPC1 and Capan2 cells were exposed to OLSO vector, as described in material and methods.

TrueORF pIgR plasmid and HaloTag plasmids were introduced to Hela cells, AsPC1 and Capan2 cells, as described in Materials and methods. pIgR expression was manipulated in Hela cells only (**Figure 4.42**). No expression was seen in AsPC1 or Capan2 cells lines (data not shown). This would require further optimisation.

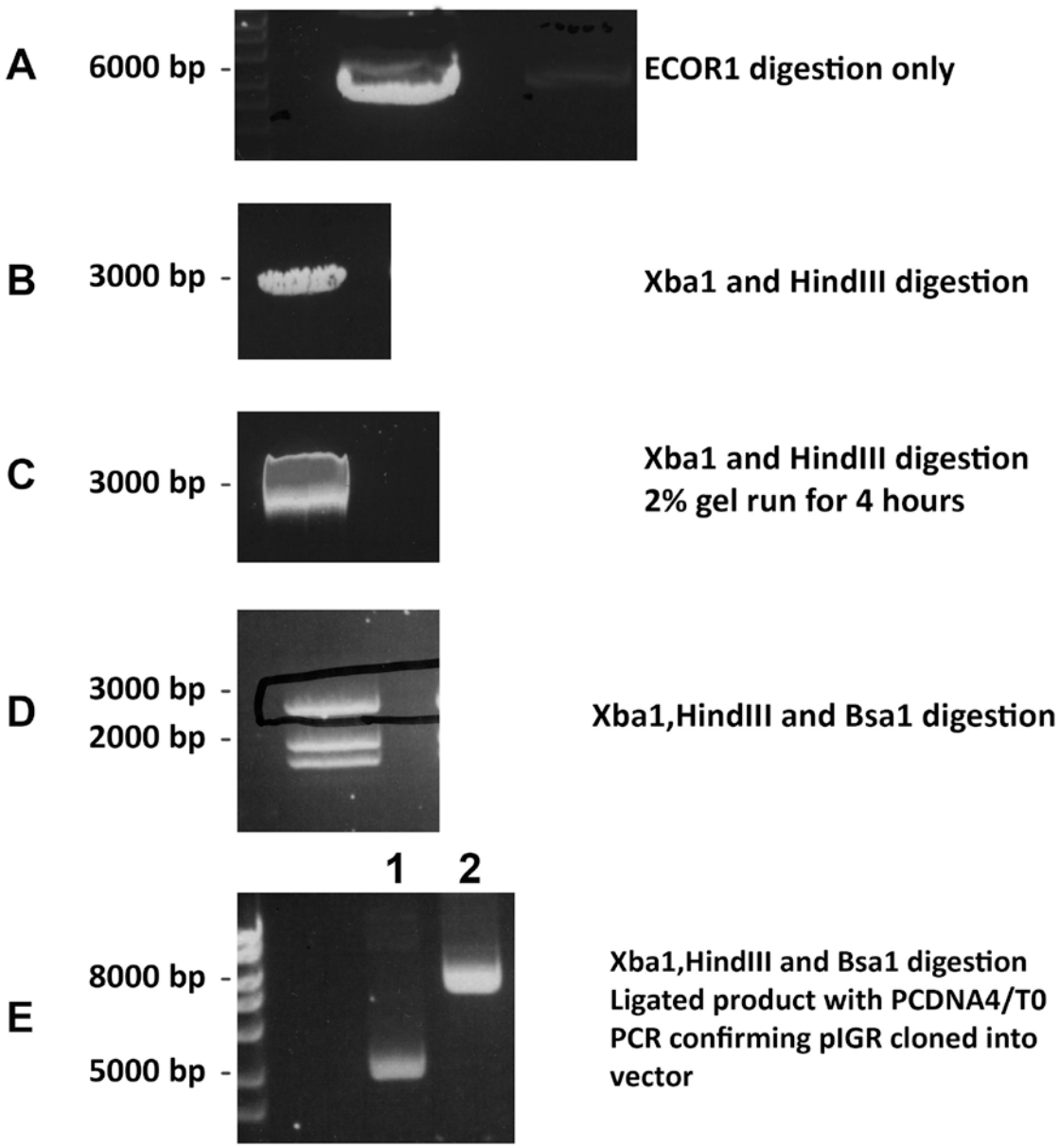

Figure 4.39: Confirmatory images of digestion of pIgR cDNA.

Attempts to optimise ligation of pBS-pIgR cDNA using multiple digestion enzymes. A) Digestion using ECOR1 only linearised the plasmid, but did not separate pIgR from the pBluescript vector, providing a band just under 6000bp. B) Digestion with Xba1 and HindIII also linearised, but did not separate pIgR from the transport vector, providing bands at 3000bp. C) Attempts to run the digestion of products shown in Figure 4.39 B for a longer time in a higher viscosity gel also failed to release pIgR from the backbone vector. D) Combination digestion using Xba1, HindIII and Bsa1 revealed pIgR (top band) and separated the pBluescript into two separate fragments. E) Confirmatory digestion of ligated products form figure D to reveal pIgR had ligated onto the mammalian cloning vector (lane 2). Lane 1 is the empty vector.

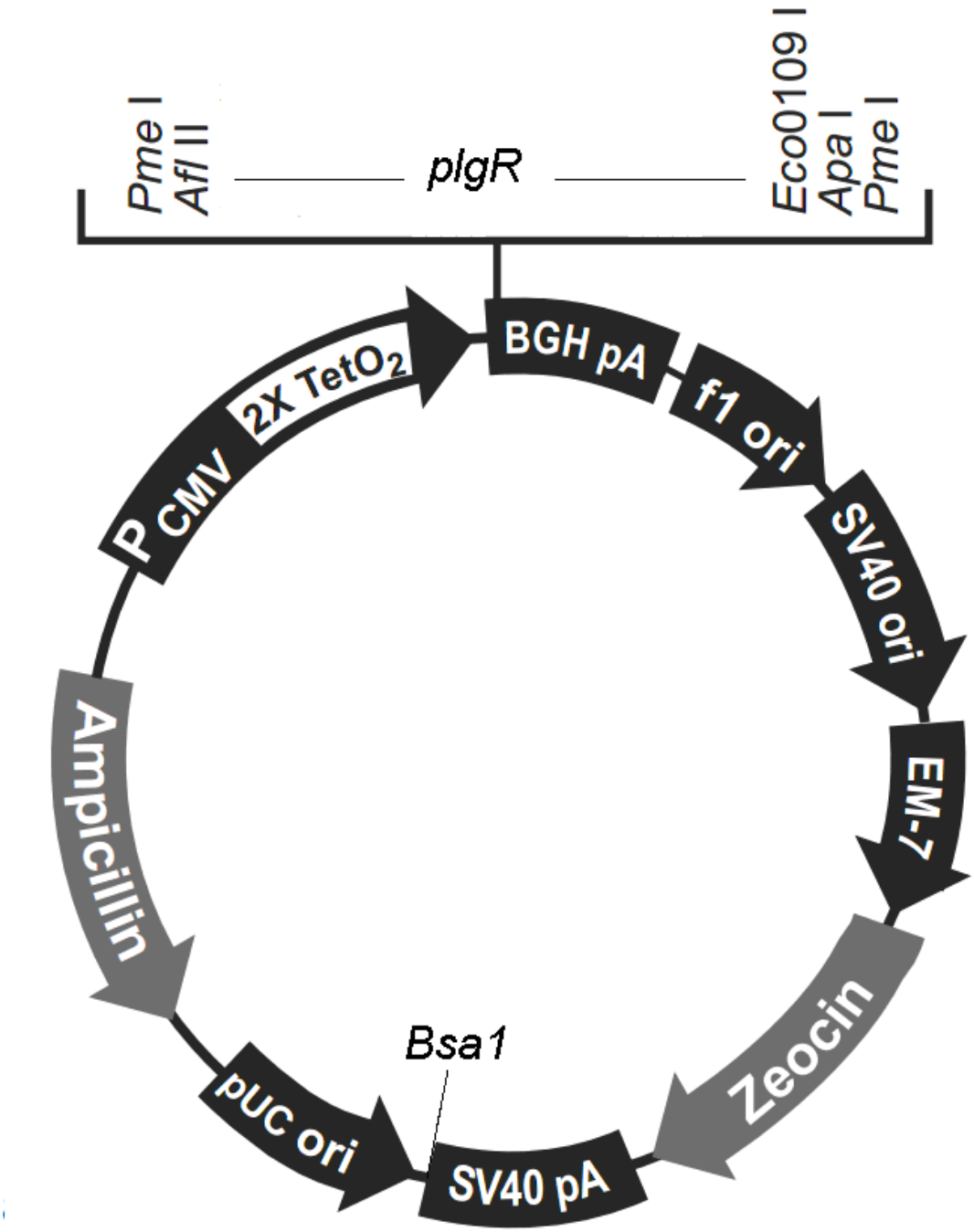

Figure 4.40: Modification of PCDNA4/T0

Restriction enzymes HindIII and Xba1 were used in order to introduce pIgR, whilst Bsa1 was used to split the backbone, enabling extraction of the pIgR segment at digestion.

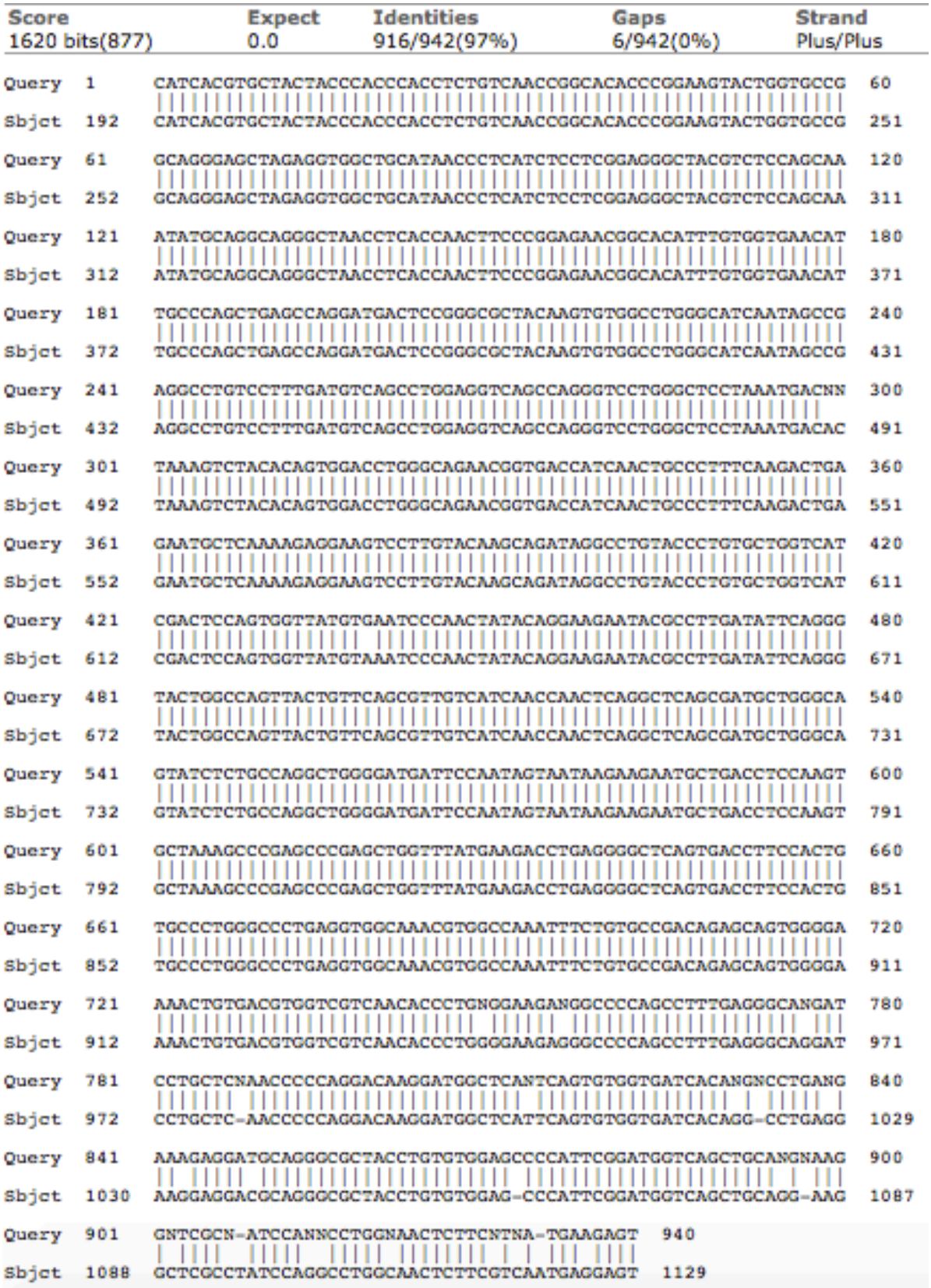

Figure 4.41: Sequencing result of pIgR OSLO clone confirming a 97% alignment.

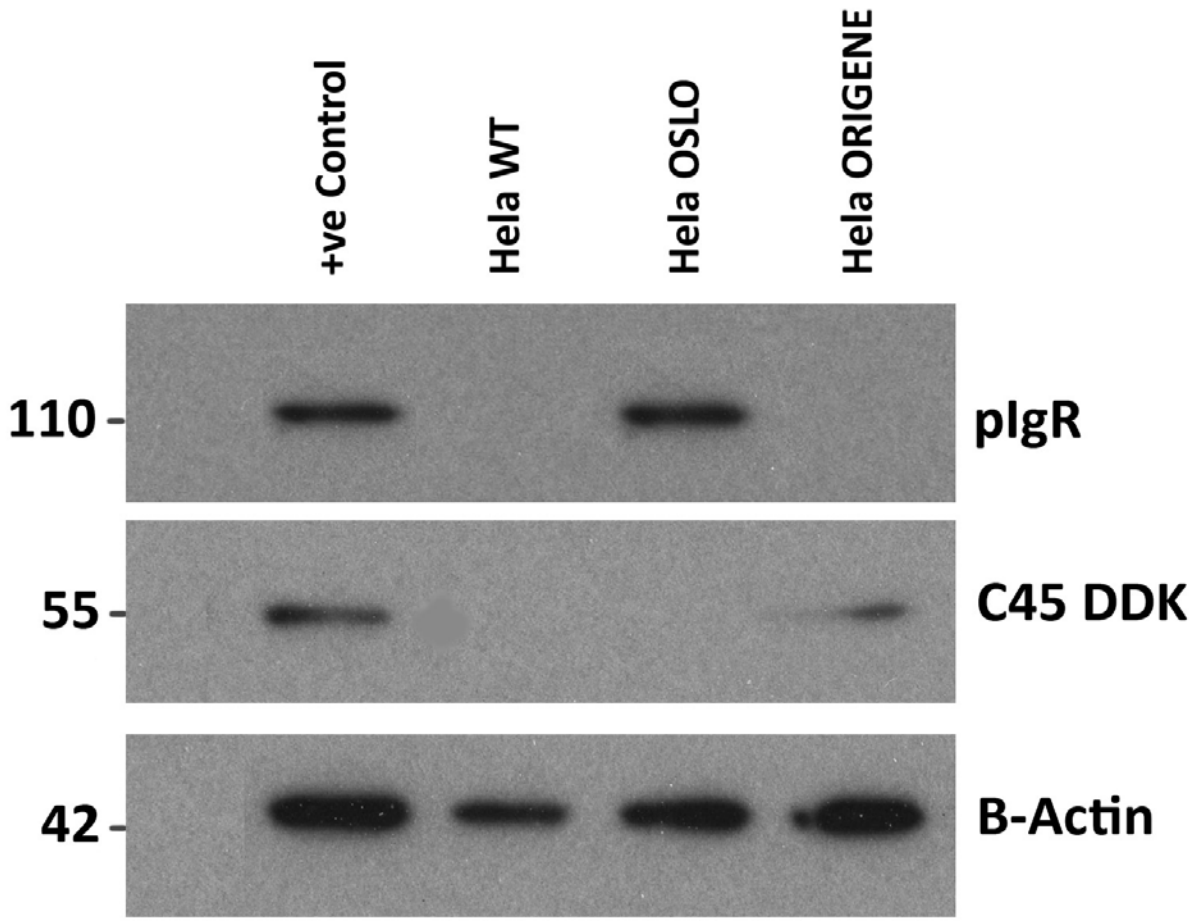

Figure 4.42: Introduction of pIgR into Hela cells

3 methods of pIgR introduction into cells were trialled. OSLO vector was successfully induced into Hela cells, which were used as an experimental control, as to a certain degree was OriGene vector (C45 DDK is the associated tag). I was unable to introduce HaloTag into Hela cells (results not shown). This procedure was repeated for AsPC1 and Capan2 cells, but no transfection was seen (results not shown).

4.11 Discussion

Technical aspects

I encountered a number of technical difficulties which I tried to overcome with guidance from senior colleagues and my supervisors. Some of these technical challenges remain insurmountable, but gave me valuable training.

The first problem was unavailability of a second pancreatic cancer cell line with endogenous pIgR protein expression. I expanded by panel from initial 5 to over 12 cancer cell lines. I confirmed mRNA expression. However protein expression could be demonstrated only in once cancer cell line. I wanted to ensure that I had correct cell lines, and they were repeat STR profiled for this project. I am pleased to report that there was no contamination from other cell lines, and the cell lines were 100% match with ATCC profiles. Next I ensured that the cancer cell lines were mycoplasma negative as this may affect protein expression.

Ideally, the experiments should be repeated with shRNA to demonstrate the role of pIgR on cell migration, adhesion and invasion using another cell line. The rate of pIgR synthesis is influenced by a number of cytokines and hormones that regulate the mucosal immune system. The HT-29 human colon carcinoma cell line has widely been used to model the regulation of pIgR expression by intestinal epithelial cells (95, 118). Expression of pIgR by HT-29 cells is up-regulated by the pro-inflammatory cytokines IFN-γ (275), TNF-α (276) and IL-1, as well as the Th2-type cytokine IL-4 (277, 278). Studies of cytokines produced by *in vitro*-stimulated human intestinal lamina propria mononuclear cells suggested that the pro-inflammatory cytokine IFN-γ was the central regulator of pIgR expression by intestinal epithelial cells (279).

At the molecular level, IFN-γ has been shown to increase pIgR mRNA levels by a mechanism dependent on de novo protein synthesis (280). IFN-γ and TNF-α cause de novo synthesis of the transcription factor IFN regulatory factor (IRF)-1 in HT-29 cells and that IRF-1 binds to a regulatory element in exon 1 of the human pIgR gene (281). IRF-1 mRNA is known to be induced by pro-inflammatory cytokines, and

this transcription factor has widely been implicated in the regulation of immune responses (282). However, addition of cytokines into PDAC cell lines proved unsuccessful.

pIgR mRNA level was similar across multiple PDAC cell lines. However, only in Capan1 was the mRNA translated to protein level expression. Attempts to treat other cells lines that were negative at protein level for pIgR with known upstream cytokine regulators ultimately proved unsuccessful. Attempts to trigger pIgR expression at 2D level with interactions with stellate cells also proved unsuccessful.

However, pIgR in 3D models is expressed, even in cells lines negative for pIgR in 2D models. PDAC cell lines are, like in PDAC itself, amassed with a multitude of genetic mutations. Although I was unable to effect a successful over expression in PDAC cell lines, it remains likely that previously investigated cytokines are unlikely upstream regulators in PDAC cells. Also, in the context of PDAC cell lines, there is likely to be a post-translational effects that are controlled by other genes, hence we are unable to see expression at protein level. Another theory maybe that pIgR expression is associated with earlier, more epithelial characteristics, which established PDAC cancer cells lines, may silence post transcriptionally. We have access to human PDAC cell lines, but no human PanIN cell lines are available to further investigate.

Initial attempts with organotypic cultures using siRNA transfected cells proved to provide no obvious difference in cell counts or pIgR expression between controls and pIgR siRNA treated cells. Numerous reasons exist, but namely the duration of the siRNA effect may well have worn off. Maximal 2D knockdown was noted up to day 7, however, by the time transfection had occurred, and loaded onto gels and extracted, time duration was 10 days. The short duration of siRNA was overcome with difficulties using shRNA to induce stable knockdown of pIgR to enable long-term organotypic cultures and demonstrate the relationship between stroma and pIgR expression, as postulated by Kadaba et al., (70).

Further issues were encountered to enable stable transduction of pIgR using a range of vector expression systems, to get success only in the HeLa cells in the time allocated for my PhD studies.

4.11.2 Downstream effect of pIgR

Inflammatory responses to tumour development are two-fold, initially serving to eliminate rogue premalignant and malignant cells (283). As tumours progress, they evade immune surveillance, but also provoke an inflammatory response (284). By recruiting a variety of immune cells types, tumours are able to secrete a diverse set of signalling molecules that promote cellular proliferation and remodel the extracellular matrix to favour epithelial mesenchymal transition (EMT) (285).

Cancer cells undergoing EMT imitate the properties of stem cells (267), can bypass processes such as apoptosis (268) and contribute to immunosuppression (286), thus providing a role of EMT in tumour recurrence. The role and actions of EMT also seem to provide a link between inflammation and cancer metastasis (284).

Rhim et al, (287) investigated the process of EMT, identifying tagged cells invading the bloodstream, prior to frank malignancy in transgenic murine model of PDAC. They implied that the epithelial cancer cells lost cellular polarity as well as cell-cell adhesion, to gain migratory and invasive properties similar to mesenchymal cells.

The ability of certain inflammatory stimuli to activate and stabilise EMT provides a link between inflammation, EMT and subsequent tumour and metastatic development. Ai et al (81) identified pIgR as one such manifestation of linkage of inflammatory stimulus. pIgR aberrant expression has previously been associated with HCC (192). Ai et al demonstrated pIgR over-expression is implicated in EMT initiated cross talk of transforming growth factor beta (TGF-ß) with inflammatory mediators (TNF-α, interferon-γ and interleukin-4). TGF-ß has been implicated in later stages of tumour progression with carcinogenesis and in promoting immune evasion and angiogenesis (193).

Ai et al also noted *in vivo*, pIgR-overexpressing cells yielded higher numbers of experimental lung metastases compared with control counter-parts, thus pIgR over-expression can promote colonisation. They also detected decreased levels of epithelial markers (E-Cadherin, cytokeratins) and increased levels of mesenchymal markers, Vimentin and phospho-Smad2/3 in pIgR-over-expressing HCC specimens (194).

Previous work in our laboratory (70) identified aberrant expression of pIgR in 3D organotypic culture models and a possible role of pIgR in cell signalling, cell growth, death and movement using *in silico* analysis.

4.11.3 Modulation of pIgR in PDAC cancer cells

Initial work in 2D cell culture, identified only Capan1, amongst nine pancreatic cancer cell lines, to have pIgR protein detectable by Western blotting. Therefore, subsequent work utilised Capan1 cells. Initial knockdown with pIgR siRNA in Capan1 cells identified a significant reduction in cell counts over a period of six days, when compared to control siRNA transfected cells. This is in keeping with reports suggesting that pIgR is linked to cell proliferation (70). There may be potential off-target effects from siRNA as noted by a slight reduction in pIgR expression with non-targeting siRNA.

In order to counter act potential off-target effects, shRNAs and its longer term knockdown was utilised. The shRNA plasmids were a kind donation from the Ai group (179), providing a non-targeting shRNA construct along with two pIgR shRNA constructs. Initial siRNA data with progressive cell counts demonstrates Capan1 cancer cells lacking pIgR proliferate at a slower rate than those with pIgR. This was also confirmed with a stable transfection.

Organotypic cultures utilising shRNA provided interesting observations, relating to the effect of lack of pIgR. Organotypic gels, when lacking pIgR had reduced cell number and were longer and thicker than wild-type and non-targeting

Capan1 cells. However, expression of pIgR and EMT markers, when normalised to cell number was not affected.

It would appear that lack of pIgR provides lack of luminal formation and reduction in rates of proliferation. However, Capan1 are considered well differentiated cell line and are more likely to be affected by minor genetic alterations. Interestingly, both at 2D and 3D model level of PDAC, pIgR has no interaction with EMT markers.

4.11.4 Modulation of pIgR and its association with EMT

E-cadherin is a marker of cell-cell junctions and adhesion. Loss of E-cadherin is associated with progression to EMT (70). The inherent inverse relationship of pIgR with E-Cadherin raises the question as to the involvement of pIgR with phases of Epithelial-to-Mesenchymal transition (EMT). Rhim et al (287) investigated the effect of EMT, identifying tagged cells invading bloodstream, prior to frank malignancy being able to be detected. Their suggestion was a process by which epithelial cells lost polarity and cell-cell adhesion, instead gaining migratory and invasive properties to become mesenchymal cells.

They noted circulating pancreatic cells maintained a mesenchymal phenotype, exhibited stem cell properties and seeded the liver. The notion of EMT and invasiveness were most abundant at inflammatory foci, and induction of pancreatitis increased the number of circulating pancreatic cells, and treatment with immunosuppressive Dexamethasone abolished dissemination. Further work has also investigated the emergence of PanIN lesions and the appearance of inflammatory stroma characterised by activated fibroblasts and myeloid-derived cells (288). Inflammation is commonly correlated with tumour initiation and progression (289), whilst accelerating pancreatic carcinogenesis in adult *Kras* mutant mice (290).

Rhim's work was the clearest confirmation that, at the earliest stages of cellular invasion *in situ*, inflammation enhances cancer progression in part by facilitating EMT and entry into circulation. His work also went on to identify markers to

distinguish between epithelial and mesenchymal cells, demonstrating E-cadherin, EpCAM and CK19 were all used as markers of epithelial cell linage, whilst Zeb1 and YFP were to be used as mesenchymal markers.

As epithelial cells undergo EMT and progressively lose their E-Cadherin content, pIgR inversely increases and Cytokeratin increases with loss of pIgR, suggesting a pro-cancerous role for pIgR in the early stages of PDAC development.

However, investigating pIgR expression in organotypics with Zeb1 and E-cadherin demonstrated no significant change due to expression of pIgR, but a change only related to stellate cell presence.

4.11.5 Modulation of pIgR and its association with stellate cells

Questions arise also about the effect of PS1 stellate cells in 3D culture and the effect they may well have on pIgR expression in cancer cell as well as cancer cell proliferation. It is likely that as cells are arranged in a luminal forming structure, with the enhancement of the apico-basal polarity, the expression of pIgR is more apparent (274). Interestingly, the organotypic models lacking pIgR had lower stellate cell activity (noted by αSMA and Picrosirius red staining), proving a role for pIgR in stellate cell activity.

Ultimately, knockdown of pIgR in Capan1 cells has a profound reduction in cell proliferation, adhesion and its effects in organotypics, primarily activation of stellate cells. However, as an independent factor in PDAC development, it is masked by a multitude of other genetic mutations and post-translation effects.

Cell culture work was perhaps slightly inhibited due to the nature of when pIgR is likely to be most significant, i.e. during the pre-malignant phases. Unlike other cancers such as breast, pre-malignant cell lines are as yet not established for PDAC. However, it may be of interest in the future to investigate its function in modulating stellate cells.

CONCLUSIONS

I have investigated pIgR expression in human PDAC. Investigating its role in other cancers demonstrates varied roles and this may be related to baseline, physiological pIgR expression as a requirement for mucosal defences where mucosal surfaces are exposed to high antigen load.

pIgR expression in human PDAC provides no demonstrable correlation between pIgR expression and survival. There is however a prominent expression of pIgR during pre-malignant phases of PDAC, whilst invasive cancer ducts and poorly differentiated cancers do not express pIgR.

As E-cadherin expression decreases during PanIN progression, pIgR expression increases. However, expression of both pIgR and E-cadherin are reduced in invasive PDAC.

Attempts to introduce pIgR into other pancreatic cells lines provided disappointing results. pIgR mRNA level was similar across multiple PDAC cell lines. However, only in Capan1 was the mRNA translated to protein level expression. This may be due to previously investigated upstream regulators of pIgR not affecting the same result in PDAC, whilst post-transcriptional effects by other genes cannot be accounted for in 2 and 3D modelling.

Modulation of pIgR in 2D investigations demonstrated Capan1 cancer cells lacking pIgR proliferate at a slower rate than those with pIgR. Organotypic gels, when lacking pIgR had reduced cell number and were longer and thicker than wild-type and non-targeting Capan1 cells. However, expression of pIgR and EMT markers, when normalised to cell number was not affected. Lack of pIgR provides lack of luminal formation, correlated with Ezrin expression and reduction in rates of proliferation.
Investigating pIgR expression in organotypics with EMT markers, Zeb1 and E-cadherin demonstrated no significant change due to expression of pIgR, but a change

only related to stellate cell presence. This may signify that pIgR provides secondary signalling pathways for stellate cells in PDAC.

The exact nature of when pIgR is most expressed and likely to be of most significance, i.e. during pre-malignant phases in PanIN lesions is yet to be addressed. Unlike other cancers, such as breast, pre-malignant cell lines are yet to be established and we would need pre-malignant cell lines to further investigate its functional role in modulating stellate cell activity.

It would also be interesting to study the role of pIgR in a model of pancreas development such as chronic pancreatitis also, which is a known risk factor for PDAC, to further investigate its interaction with inflammatory conditions such as auto-immune pancreatitis.

Its expression is early in PDAC development and ultimately, pIgR confers no survival benefit independently. However use of pIgR in combination with αSMA and Picrosirius red demonstrates that a low combined score may confer a survival benefit.

FURTHER WORK

We have reviewed the role of pIgR in PDAC and noted its expression in early stages of PDAC. It is disappointing the lack of results seen, as there is interesting *in vitro* data regarding its manipulation of organotypics. Whilst I think *in vivo* analysis of pIgR in human PDAC is complete. Independently, pIgR expression confers no survival benefit in PDAC.

It would be interesting to pursue the idea of pIgR as part of a biomarker panel. Whether pIgR, in combination with a series of other biomarkers, due to tumour heterogeneity, could provide us a panel to identify lesions such as PDAC or mucinous lesions remains to be seen.

The link with chronic pancreatitis and PDAC could be investigated further with pIgR. To understand the progression from a chronic, benign condition to a malignancy and the role of pIgR would be interesting. It may be interesting to look at more patient biopsies of chronic pancreatitis and its correlation to PDAC development.

It would be interesting to investigate pIgR *in vitro* in cell lines mimicking human PanIN stages, which are as yet unobtainable. We were unable to provide adequate answers to the regulation of pIgR expression, and this may have been answered with adequate modulation of pIgR in other cell lines.

Ultimately, within the confines of the time-limit of a PhD, these ideas and theories were not manageable.

REFERENCES:

1. Cid-Arregui A, Juarez V. Perspectives in the treatment of pancreatic adenocarcinoma. World J Gastroenterol. 2015;21(31):9297-316.
2. Kumar V, Abbas A. Robbins and Cotran Pathologic Basis of Disease. 9th ed. Kumar V, Abbas A, editors. Canada: Elsevier Saunders; 2015.
3. Rosai J. Rosai and Ackerman's Surgical Pathology. 9th ed. Rosai J, editor. London: Mosby; 2004.
4. Cancer Research UK – Pancreatic Cancer Epidemiology 2014. Available from: http://publications.cancerresearchuk.org/cancerstats/statspancreatic/keyfactspancreas.html.
5. Brune KA, Lau B, Palmisano E, Canto M, Goggins MG, Hruban RH, et al. Importance of age of onset in pancreatic cancer kindreds. J Natl Cancer Inst. 2010;102(2):119-26.
6. Singh SM, Reber HA. Surgical palliation for pancreatic cancer. Surg Clin North Am. 1989;69(3):599-611.
7. Hariharan D, Saied A, Kocher HM. Analysis of mortality rates for pancreatic cancer across the world. HPB (Oxford). 2008;10(1):58-62.
8. Kocher HM, Alrawashdeh W. Pancreatic cancer. BMJ Clin Evid. 2010;2010.
9. Chari ST, Leibson CL, Rabe KG, Ransom J, de Andrade M, Petersen GM. Probability of pancreatic cancer following diabetes: a population-based study. Gastroenterology. 2005;129(2):504-11.
10. Doll R, Peto R, Wheatley K, Gray R, Sutherland I. Mortality in relation to smoking: 40 years' observations on male British doctors. Bmj. 1994;309(6959):901-11.
11. Chari ST, Leibson CL, Rabe KG, Timmons LJ, Ransom J, de Andrade M, et al. Pancreatic cancer-associated diabetes mellitus: prevalence and temporal association with diagnosis of cancer. Gastroenterology. 2008;134(1):95-101.
12. Pannala R, Basu A, Petersen GM, Chari ST. New-onset diabetes: a potential clue to the early diagnosis of pancreatic cancer. Lancet Oncol. 2009;10(1):88-95.
13. Ghaneh P, Costello E, Neoptolemos JP. Biology and management of pancreatic cancer. Gut. 2007;56(8):1134-52.
14. Harsha HC, Kandasamy K, Ranganathan P, Rani S, Ramabadran S, Gollapudi S, et al. A compendium of potential biomarkers of pancreatic cancer. PLoS Med. 2009;6(4):e1000046.
15. Zhao WY, Luo M, Sun YW, Xu Q, Chen W, Zhao G, et al. Computed tomography in diagnosing vascular invasion in pancreatic and periampullary cancers: a systematic review and meta-analysis. Hepatobiliary Pancreat Dis Int. 2009;8(5):457-64.
16. Hidalgo M. Pancreatic cancer. N Engl J Med. 2010;362(17):1605-17.
17. Pylayeva-Gupta Y, Lee Kyoung E, Hajdu Cristina H, Miller G, Bar-Sagi D. Oncogenic Kras-Induced GM-CSF Production Promotes the Development of Pancreatic Neoplasia. Cancer Cell. 2012;21(6):836-47.
18. Giovannini M, Thomas B, Erwan B, Christian P, Fabrice C, Benjamin E, et al. Endoscopic ultrasound elastography for evaluation of lymph nodes and pancreatic masses: a multicenter study. World J Gastroenterol. 2009;15(13):1587-93.
19. Volmar KE, Vollmer RT, Jowell PS, Nelson RC, Xie HB. Pancreatic FNA in 1000 cases: a comparison of imaging modalities. Gastrointest Endosc. 2005;61(7):854-61.
20. Park HS, Lee JM, Choi HK, Hong SH, Han JK, Choi BI. Preoperative evaluation of pancreatic cancer: comparison of gadolinium-enhanced dynamic MRI with MR cholangiopancreatography versus MDCT. Journal of magnetic resonance imaging : JMRI. 2009;30(3):586-95.
21. Kauhanen SP, Komar G, Seppanen MP, Dean KI, Minn HR, Kajander SA, et al. A prospective diagnostic accuracy study of 18F-fluorodeoxyglucose positron

emission tomography/computed tomography, multidetector row computed tomography, and magnetic resonance imaging in primary diagnosis and staging of pancreatic cancer. Ann Surg. 2009;250(6):957-63.
22. Hariharan D, Constantinides V, Kocher HM, Tekkis PP. The role of laparoscopy and laparoscopic ultrasound in the preoperative staging of patients with resectable colorectal liver metastases: a meta-analysis. Am J Surg. 2012;204(1):84-92. doi: 10.1016/j.amjsurg.2011.07.018. Epub 2 Jan 14.
23. Jemal A, Clegg LX, Ward E, Ries LA, Wu X, Jamison PM, et al. Annual report to the nation on the status of cancer, 1975-2001, with a special feature regarding survival. Cancer. 2004;101(1):3-27.
24. Neoptolemos JP, Russell RC, Bramhall S, Theis B. Low mortality following resection for pancreatic and periampullary tumours in 1026 patients: UK survey of specialist pancreatic units. UK Pancreatic Cancer Group. Br J Surg. 1997;84(10):1370-6.
25. Burris HA, 3rd, Moore MJ, Andersen J, Green MR, Rothenberg ML, Modiano MR, et al. Improvements in survival and clinical benefit with gemcitabine as first-line therapy for patients with advanced pancreas cancer: a randomized trial. J Clin Oncol. 1997;15(6):2403-13.
26. Cunningham D, Chau I, Stocken DD, Valle JW, Smith D, Steward W, et al. Phase III Randomized Comparison of Gemcitabine Versus Gemcitabine Plus Capecitabine in Patients With Advanced Pancreatic Cancer. J Clin Oncol. 2009;27(33):5513-8.
27. Von Hoff DD, Ramanathan RK, Borad MJ, Laheru DA, Smith LS, Wood TE, et al. Gemcitabine plus nab-paclitaxel is an active regimen in patients with advanced pancreatic cancer: a phase I/II trial. J Clin Oncol. 2011;29(34):4548-54.
28. Conroy T, Desseigne F, Ychou M, Bouche O, Guimbaud R, Becouarn Y, et al. FOLFIRINOX versus gemcitabine for metastatic pancreatic cancer. N Engl J Med. 2011;364(19):1817-25.
29. Wang-Gillam A, Li CP, Bodoky G, Dean A, Shan YS, Jameson G, et al. Nanoliposomal irinotecan with fluorouracil and folinic acid in metastatic pancreatic cancer after previous gemcitabine-based therapy (NAPOLI-1): a global, randomised, open-label, phase 3 trial. Lancet. 2016;387(10018):545-57.
30. Mukherjee S, Hurt CN, Bridgewater J, Falk S, Cummins S, Wasan H, et al. Gemcitabine-based or capecitabine-based chemoradiotherapy for locally advanced pancreatic cancer (SCALOP): a multicentre, randomised, phase 2 trial. Lancet Oncol. 2013;14(4):317-26.
31. Neoptolemos JP, Palmer DH, Ghaneh P, Psarelli EE, Valle JW, Halloran CM, et al. Comparison of adjuvant gemcitabine and capecitabine with gemcitabine monotherapy in patients with resected pancreatic cancer (ESPAC-4): a multicentre, open-label, randomised, phase 3 trial. Lancet. 2017;389(10073):1011-24.
32. Uesaka K, Boku N, Fukutomi A, Okamura Y, Konishi M, Matsumoto I, et al. Adjuvant chemotherapy of S-1 versus gemcitabine for resected pancreatic cancer: a phase 3, open-label, randomised, non-inferiority trial (JASPAC 01). Lancet. 2016;388(10041):248-57.
33. Hruban RH, Maitra A, Goggins M. Update on pancreatic intraepithelial neoplasia. Int J Clin Exp Pathol. 2008;1(4):306-16.
34. Feldmann G, Beaty R, Hruban RH, Maitra A. Molecular genetics of pancreatic intraepithelial neoplasia. J Hepatobiliary Pancreat Surg. 2007;14(3):224-32. Epub 2007 May 29.
35. Hingorani SR, Wang L, Multani AS, Combs C, Deramaudt TB, Hruban RH, et al. Trp53R172H and KrasG12D cooperate to promote chromosomal instability and widely metastatic pancreatic ductal adenocarcinoma in mice. Cancer Cell. 2005;7(5):469-83.
36. Guerra C, Schuhmacher AJ, Canamero M, Grippo PJ, Verdaguer L, Perez-

Gallego L, et al. Chronic pancreatitis is essential for induction of pancreatic ductal adenocarcinoma by K-Ras oncogenes in adult mice. Cancer Cell. 2007;11(3):291-302.
37. Maitra A, Hruban RH. Pancreatic cancer. Annu Rev Pathol. 2008;3:157-88.
38. Hruban RH, Goggins M, Parsons J, Kern SE. Progression model for pancreatic cancer. Clin Cancer Res. 2000;6(8):2969-72.
39. Koorstra JB, Hustinx SR, Offerhaus GJ, Maitra A. Pancreatic carcinogenesis. Pancreatology. 2008;8(2):110-25. doi: 10.1159/000123838. Epub 2008 Apr 1.
40. Bailey JM, Hendley AM, Lafaro KJ, Pruski MA, Jones NC, Alsina J, et al. p53 mutations cooperate with oncogenic Kras to promote adenocarcinoma from pancreatic ductal cells. Oncogene. 2015.
41. Jones S, Zhang X, Parsons DW, Lin JC, Leary RJ, Angenendt P, et al. Core signaling pathways in human pancreatic cancers revealed by global genomic analyses. Science. 2008;321(5897):1801-6.
42. Couch FJ, Johnson MR, Rabe KG, Brune K, de Andrade M, Goggins M, et al. The prevalence of BRCA2 mutations in familial pancreatic cancer. Cancer Epidemiol Biomarkers Prev. 2007;16(2):342-6.
43. Whitcomb DC. Genetic risk factors for pancreatic disorders. Gastroenterology. 2013;144(6):1292-302.
44. Rustgi AK. Familial pancreatic cancer: genetic advances. Genes Dev. 2014;28(1):1-7.
45. Chen JM, Ferec C. Genetics and pathogenesis of chronic pancreatitis: the 2012 update. Clinics and research in hepatology and gastroenterology. 2012;36(4):334-40.
46. Campbell PJ, Yachida S, Mudie LJ, Stephens PJ, Pleasance ED, Stebbings LA, et al. The patterns and dynamics of genomic instability in metastatic pancreatic cancer. Nature. 2010;467(7319):1109-13.
47. Korsse SE, Harinck F, van Lier MG, Biermann K, Offerhaus GJ, Krak N, et al. Pancreatic cancer risk in Peutz-Jeghers syndrome patients: a large cohort study and implications for surveillance. Journal of medical genetics. 2013;50(1):59-64.
48. Cancer risks in BRCA2 mutation carriers. J Natl Cancer Inst. 1999;91(15):1310-6.
49. Roberts NJ, Klein AP. Genome-wide sequencing to identify the cause of hereditary cancer syndromes: with examples from familial pancreatic cancer. Cancer Lett. 2013;340(2):227-33.
50. Gall TM, Wasan H, Jiao LR. Pancreatic cancer: current understanding of molecular and genetic aetiologies. Postgrad Med J. 2015.
51. Hruban RH, Takaori K, Klimstra DS, Adsay NV, Albores-Saavedra J, Biankin AV, et al. An illustrated consensus on the classification of pancreatic intraepithelial neoplasia and intraductal papillary mucinous neoplasms. Am J Surg Pathol. 2004;28(8):977-87.
52. Hruban RH, Adsay NV, Albores-Saavedra J, Compton C, Garrett ES, Goodman SN, et al. Pancreatic intraepithelial neoplasia: a new nomenclature and classification system for pancreatic duct lesions. Am J Surg Pathol. 2001;25(5):579-86.
53. van Heek NT, Meeker AK, Kern SE, Yeo CJ, Lillemoe KD, Cameron JL, et al. Telomere shortening is nearly universal in pancreatic intraepithelial neoplasia. Am J Pathol. 2002;161(5):1541-7.
54. Hustinx SR, Leoni LM, Yeo CJ, Brown PN, Goggins M, Kern SE, et al. Concordant loss of MTAP and p16/CDKN2A expression in pancreatic intraepithelial neoplasia: evidence of homozygous deletion in a noninvasive precursor lesion. Mod Pathol. 2005;18(7):959-63.
55. Brugge WR, Lewandrowski K, Lee-Lewandrowski E, Centeno BA, Szydlo T, Regan S, et al. Diagnosis of pancreatic cystic neoplasms: a report of the cooperative pancreatic cyst study. Gastroenterology. 2004;126(5):1330-6.
56. Matthaei H, Schulick RD, Hruban RH, Maitra A. Cystic precursors to invasive

pancreatic cancer. Nat Rev Gastroenterol Hepatol. 2011;8(3):141-50.
57. Baker ML, Seeley ES, Pai R, Suriawinata AA, Mino-Kenudson M, Zamboni G, et al. Invasive mucinous cystic neoplasms of the pancreas. Exp Mol Pathol. 2012;93(3):345-9.
58. Mahadevan D, Von Hoff DD. Tumor-stroma interactions in pancreatic ductal adenocarcinoma. Mol Cancer Ther. 2007;6(4):1186-97.
59. Froeling FE, Feig C, Chelala C, Dobson R, Mein CE, Tuveson DA, et al. Retinoic Acid-Induced Pancreatic Stellate Cell Quiescence Reduces Paracrine Wnt-beta-Catenin Signaling to Slow Tumor Progression. Gastroenterology. 2011;141(4):1486-97.
60. Zhang W, Erkan M, Abiatari I, Giese NA, Felix K, Kayed H, et al. Expression of extracellular matrix metalloproteinase inducer (EMMPRIN/CD147) in pancreatic neoplasm and pancreatic stellate cells. Cancer Biol Ther. 2007;6(2):218-27. Epub 2007 Feb 25.
61. Masamune A, Shimosegawa T. Signal transduction in pancreatic stellate cells. J Gastroenterol. 2009;44(4):249-60.
62. Olive KP, Jacobetz MA, Davidson CJ, Gopinathan A, McIntyre D, Honess D, et al. Inhibition of Hedgehog Signaling Enhances Delivery of Chemotherapy in a Mouse Model of Pancreatic Cancer. Science. 2009;324(5933):1457-61.
63. Olive KP. Clinical Trial: IPI-926-03
For metastatic pancreatic ductal adenocarcinoma patients who have not been treated with other chemotherapy 2012. Available from: http://www.olivelab.org/ipi-926-03.html.
64. Ozdemir BC, Pentcheva-Hoang T, Carstens JL, Zheng X, Wu CC, Simpson TR, et al. Depletion of carcinoma-associated fibroblasts and fibrosis induces immunosuppression and accelerates pancreas cancer with reduced survival. Cancer Cell. 2014;25(6):719-34.
65. Rhim AD, Oberstein PE, Thomas DH, Mirek ET, Palermo CF, Sastra SA, et al. Stromal elements act to restrain, rather than support, pancreatic ductal adenocarcinoma. Cancer Cell. 2014;25(6):735-47.
66. Maliar A, Servais C, Waks T, Chmielewski M, Lavy R, Altevogt P, et al. Redirected T Cells That Target Pancreatic Adenocarcinoma Antigens Eliminate Tumors and Metastases in Mice. Gastroenterology. 2012.
67. Froeling FE, Kocher HM. Homeostatic restoration of desmoplastic stroma rather than its ablation slows pancreatic cancer progression. Gastroenterology. 2015;148(4):849-50.
68. Whatcott CJ PR, Von Hoff DD,. Desmoplasia and chemoresistance in pancreatic cancer 2012. Available from: https://www.ncbi.nlm.nih.gov/books/NBK98939/.
69. Chang Q, Jurisica I, Do T, Hedley DW. Hypoxia predicts aggressive growth and spontaneous metastasis formation from orthotopically grown primary xenografts of human pancreatic cancer. Cancer Res. 2011;71(8):3110-20.
70. Kadaba R, Birke H, Wang J, Hooper S, Andl CD, Di Maggio F, et al. Imbalance of desmoplastic stromal cell numbers drives aggressive cancer processes. J Pathol. 2013;230(1):107-17. doi: 10.1002/path.4172. Epub 2013 Mar 21.
71. Negus RP, Stamp GW, Hadley J, Balkwill FR. Quantitative assessment of the leukocyte infiltrate in ovarian cancer and its relationship to the expression of C-C chemokines. Am J Pathol. 1997;150(5):1723-34.
72. Moir JA, Mann J, White SA. The role of pancreatic stellate cells in pancreatic cancer. Surg Oncol. 2015.
73. Apte MV, Haber PS, Applegate TL, Norton ID, McCaughan GW, Korsten MA, et al. Periacinar stellate shaped cells in rat pancreas: identification, isolation, and culture. Gut. 1998;43(1):128-33.
74. Bachem MG, Schneider E, Gross H, Weidenbach H, Schmid RM, Menke A, et al. Identification, culture, and characterization of pancreatic stellate cells in rats and humans. Gastroenterology. 1998;115(2):421-32.

75. Apte MV, Yang L, Phillips PA, Xu Z, Kaplan W, Cowley M, et al. Extracellular matrix composition significantly influences pancreatic stellate cell gene expression pattern: role of transgelin in PSC function. Am J Physiol Gastrointest Liver Physiol. 2013;305(6):G408-17.
76. Riopel MM, Li J, Liu S, Leask A, Wang R. beta1 integrin-extracellular matrix interactions are essential for maintaining exocrine pancreas architecture and function. Lab Invest. 2013;93(1):31-40.
77. Phillips PA, Yang L, Shulkes A, Vonlaufen A, Poljak A, Bustamante S, et al. Pancreatic stellate cells produce acetylcholine and may play a role in pancreatic exocrine secretion. Proc Natl Acad Sci U S A. 2010;107(40):17397-402.
78. Berna MJ, Seiz O, Nast JF, Benten D, Blaker M, Koch J, et al. CCK1 and CCK2 receptors are expressed on pancreatic stellate cells and induce collagen production. J Biol Chem. 2010;285(50):38905-14.
79. Neesse A, Michl P, Frese KK, Feig C, Cook N, Jacobetz MA, et al. Stromal biology and therapy in pancreatic cancer. Gut. 2011;60(6):861-8.
80. Hanahan D, Weinberg RA. Hallmarks of cancer: the next generation. Cell. 2011;144(5):646-74.
81. Ai J, Tang Q, Wu Y, Xu Y, Feng T, Zhou R, et al. The role of polymeric immunoglobulin receptor in inflammation-induced tumor metastasis of human hepatocellular carcinoma. J Natl Cancer Inst. 2011;103(22):1696-712. doi: 10.093/jnci/djr360. Epub 2011 Oct 24.
82. Kierszenbaum A. Histology and Cell Biology: An Introduction to Pathology. St Louis: Mosby; 2002.
83. Eckmann L, Kagnoff MF. Intestinal mucosal responses to microbial infection. Springer Semin Immunopathol. 2005;27(2):181-96. Epub 2005 Jun 1.
84. Macpherson AJ, McCoy KD, Johansen FE, Brandtzaeg P. The immune geography of IgA induction and function. Mucosal Immunol. 2008;1(1):11-22. doi: 10.1038/mi.2007.6.
85. Brandtzaeg P, Johansen FE. Mucosal B cells: phenotypic characteristics, transcriptional regulation, and homing properties. Immunol Rev. 2005;206:32-63.
86. Lamm ME. Interaction of antigens and antibodies at mucosal surfaces. Annu Rev Microbiol. 1997;51:311-40.
87. Norderhaug IN, Johansen FE, Schjerven H, Brandtzaeg P. Regulation of the formation and external transport of secretory immunoglobulins. Crit Rev Immunol. 1999;19(5-6):481-508.
88. Mostov KE, Kraehenbuhl JP, Blobel G. Receptor-mediated transcellular transport of immunoglobulin: synthesis of secretory component as multiple and larger transmembrane forms. Proc Natl Acad Sci U S A. 1980;77(12):7257-61.
89. Takahashi T, Iwase T, Takenouchi N, Saito M, Kobayashi K, Moldoveanu Z, et al. The joining (J) chain is present in invertebrates that do not express immunoglobulins. Proc Natl Acad Sci U S A. 1996;93(5):1886-91.
90. Tomasi TB, Jr., Tan EM, Solomon A, Prendergast RA. Characteristics of an Immune System Common to Certain External Secretions. J Exp Med. 1965;121:101-24.
91. Mestecky J, Lam J, Strober W, Bienenstock J, McGee D, Mayer L. Mucosal Immunology: Elsevier; 2005.
92. Mostov KE. Transepithelial transport of immunoglobulins. Annu Rev Immunol. 1994;12:63-84.
93. Natvig IB, Johansen FE, Nordeng TW, Haraldsen G, Brandtzaeg P. Mechanism for enhanced external transfer of dimeric IgA over pentameric IgM: studies of diffusion, binding to the human polymeric Ig receptor, and epithelial transcytosis. J Immunol. 1997;159(9):4330-40.
94. Kaetzel CS. The polymeric immunoglobulin receptor: bridging innate and adaptive immune responses at mucosal surfaces. Immunol Rev. 2005;206:83-99.

95. Mostov K, Su T, ter Beest M. Polarized epithelial membrane traffic: conservation and plasticity. Nat Cell Biol. 2003;5(4):287-93.
96. Fallgreen-Gebauer E, Gebauer W, Bastian A, Kratzin HD, Eiffert H, Zimmermann B, et al. The covalent linkage of secretory component to IgA. Structure of sIgA. Biol Chem Hoppe Seyler. 1993;374(11):1023-8.
97. Phalipon A, Cardona A, Kraehenbuhl JP, Edelman L, Sansonetti PJ, Corthesy B. Secretory component: a new role in secretory IgA-mediated immune exclusion in vivo. Immunity. 2002;17(1):107-15.
98. Lindh E. Increased risistance of immunoglobulin A dimers to proteolytic degradation after binding of secretory component. J Immunol. 1975;114(1 Pt 2):284-6.
99. Johansen FE, Pekna M, Norderhaug IN, Haneberg B, Hietala MA, Krajci P, et al. Absence of epithelial immunoglobulin A transport, with increased mucosal leakiness, in polymeric immunoglobulin receptor/secretory component-deficient mice. J Exp Med. 1999;190(7):915-22.
100. Shimada S, Kawaguchi-Miyashita M, Kushiro A, Sato T, Nanno M, Sako T, et al. Generation of polymeric immunoglobulin receptor-deficient mouse with marked reduction of secretory IgA. J Immunol. 1999;163(10):5367-73.
101. Asano M, Komiyama K. Polymeric immunoglobulin receptor. J Oral Sci. 2011;53(2):147-56.
102. Krajci P, Grzeschik KH, Geurts van Kessel AH, Olaisen B, Brandtzaeg P. The human transmembrane secretory component (poly-Ig receptor): molecular cloning, restriction fragment length polymorphism and chromosomal sublocalization. Hum Genet. 1991;87(6):642-8.
103. Hirunsatit R, Kongruttanachok N, Shotelersuk K, Supiyaphun P, Voravud N, Sakuntabhai A, et al. Polymeric immunoglobulin receptor polymorphisms and risk of nasopharyngeal cancer. BMC Genet. 2003;4:3. Epub 2003 Jan 21.
104. Deitcher DL, Mostov KE. Alternate splicing of rabbit polymeric immunoglobulin receptor. Mol Cell Biol. 1986;6(7):2712-5.
105. Hamburger AE, West AP, Jr., Bjorkman PJ. Crystal structure of a polymeric immunoglobulin binding fragment of the human polymeric immunoglobulin receptor. Structure. 2004;12(11):1925-35.
106. Spencer J, Klavinskis LS, Fraser LD. The human intestinal IgA response; burning questions. Front Immunol. 2012;3:108.(doi):10.3389/fimmu.2012.00108. eCollection 2012.
107. Kaetzel CS. Polymeric Ig receptor: defender of the fort or Trojan horse? Curr Biol. 2001;11(1):R35-8.
108. Kaetzel CS. The polymeric immunoglobulin receptor: bridging innate and adaptive immune responses at mucosal surfaces. Immunol Rev. 2005;206:83-99.
109. Haelens A, Verrijdt G, Schoenmakers E, Alen P, Peeters B, Rombauts W, et al. The first exon of the human sc gene contains an androgen responsive unit and an interferon regulatory factor element. Mol Cell Endocrinol. 1999;153(1-2):91-102.
110. Johansen FE, Kaetzel CS. Regulation of the polymeric immunoglobulin receptor and IgA transport: new advances in environmental factors that stimulate pIgR expression and its role in mucosal immunity. Mucosal immunology. 2011;4(6):598-602.
111. Emmerson CD, van der Vlist EJ, Braam MR, Vanlandschoot P, Merchiers P, de Haard HJ, et al. Enhancement of polymeric immunoglobulin receptor transcytosis by biparatopic VHH. PLoS One. 2011;6(10):e26299. doi: 10.1371/journal.pone.0026299. Epub 2011 Oct 14.
112. Jacob R, Naim HY. Apical membrane proteins are transported in distinct vesicular carriers. Curr Biol. 2001;11(18):1444-50.
113. Nelson WJ, Yeaman C. Protein trafficking in the exocytic pathway of polarized epithelial cells. Trends Cell Biol. 2001;11(12):483-6.

114. Orzech E, Cohen S, Weiss A, Aroeti B. Interactions between the exocytic and endocytic pathways in polarized Madin-Darby canine kidney cells. J Biol Chem. 2000;275(20):15207-19.
115. Harris BZ, Lim WA. Mechanism and role of PDZ domains in signaling complex assembly. J Cell Sci. 2001;114(Pt 18):3219-31.
116. Mostov KE, Verges M, Altschuler Y. Membrane traffic in polarized epithelial cells. Curr Opin Cell Biol. 2000;12(4):483-90.
117. Lamm ME. Current concepts in mucosal immunity. IV. How epithelial transport of IgA antibodies relates to host defense. Am J Physiol. 1998;274(4 Pt 1):G614-7.
118. Mazanec MB, Nedrud JG, Kaetzel CS, Lamm ME. A three-tiered view of the role of IgA in mucosal defense. Immunol Today. 1993;14(9):430-5.
119. Connerly PL. How Do Proteins Move Through the Golgi Apparatus? Nature Education [Internet]. 2010; 3(9):[60 p.].
120. Glick BS, Malhotra V. The curious status of the Golgi apparatus. Cell. 1998;95(7):883-9.
121. Rojas R, Apodaca G. Immunoglobulin transport across polarized epithelial cells. Nat Rev Mol Cell Biol. 2002;3(12):944-55.
122. Casanova JE, Apodaca G, Mostov KE. An autonomous signal for basolateral sorting in the cytoplasmic domain of the polymeric immunoglobulin receptor. Cell. 1991;66(1):65-75.
123. Shurety W, Stewart NL, Stow JL. Fluid-phase markers in the basolateral endocytic pathway accumulate in response to the actin assembly-promoting drug Jasplakinolide. Mol Biol Cell. 1998;9(4):957-75.
124. Babbey CM, Ahktar N, Wang E, Chen CC, Grant BD, Dunn KW. Rab10 regulates membrane transport through early endosomes of polarized Madin-Darby canine kidney cells. Mol Biol Cell. 2006;17(7):3156-75. Epub 2006 Apr 26.
125. Lock JG, Stow JL. Rab11 in recycling endosomes regulates the sorting and basolateral transport of E-cadherin. Mol Biol Cell. 2005;16(4):1744-55. Epub 2005 Feb 2.
126. Orimo A, Gupta PB, Sgroi DC, Arenzana-Seisdedos F, Delaunay T, Naeem R, et al. Stromal Fibroblasts Present in Invasive Human Breast Carcinomas Promote Tumor Growth and Angiogenesis through Elevated SDF-1/CXCL12 Secretion. Cell. 2005;121(3):335-48.
127. Fialka I, Steinlein P, Ahorn H, Bock G, Burbelo PD, Haberfellner M, et al. Identification of syntenin as a protein of the apical early endocytic compartment in Madin-Darby canine kidney cells. J Biol Chem. 1999;274(37):26233-9.
128. Song W, Bomsel M, Casanova J, Vaerman JP, Mostov K. Stimulation of transcytosis of the polymeric immunoglobulin receptor by dimeric IgA. Proc Natl Acad Sci U S A. 1994;91(1):163-6.
129. Singer KL, Mostov KE. Dimerization of the polymeric immunoglobulin receptor controls its transcytotic trafficking. Mol Biol Cell. 1998;9(4):901-15.
130. Luton F, Cardone MH, Zhang M, Mostov KE. Role of tyrosine phosphorylation in ligand-induced regulation of transcytosis of the polymeric Ig receptor. Mol Biol Cell. 1998;9(7):1787-802.
131. Luton F, Mostov KE. Transduction of basolateral-to-apical signals across epithelial cells: ligand-stimulated transcytosis of the polymeric immunoglobulin receptor requires two signals. Mol Biol Cell. 1999;10(5):1409-27.
132. Zerial M, McBride H. Rab proteins as membrane organizers. Nat Rev Mol Cell Biol. 2001;2(2):107-17.
133. Snoeck V, Peters IR, Cox E. The IgA system: a comparison of structure and function in different species. Vet Res. 2006;37(3):455-67. Epub 2006 Feb 23.
134. W Strober SF, N Lycke IgA B cell development. In: JT Lam WS, J Bienenstock, DW McGee, L Mayer, editor. Mucosal immunology. 3. 3 ed2005. p. 583–616
135. CS Kaetzel KM. Immunoglobulin transport and the polymeric immunoglobulin

receptor. In: JT Lam WS, J Bienenstock, DW McGee, L Mayer, editor. Mucosal immunology. 3. 3 ed2005. p. 211-50.
136. Kaetzel CS, Robinson JK, Chintalacharuvu KR, Vaerman JP, Lamm ME. The polymeric immunoglobulin receptor (secretory component) mediates transport of immune complexes across epithelial cells: a local defense function for IgA. Proc Natl Acad Sci U S A. 1991;88(19):8796-800.
137. Eiffert H, Quentin E, Wiederhold M, Hillemeir S, Decker J, Weber M, et al. Determination of the molecular structure of the human free secretory component. Biol Chem Hoppe Seyler. 1991;372(2):119-28.
138. Ogura Y. Transient expression of polymeric immunoglobulin receptor in human adenocarcinoma cell line HT-29. J Oral Sci. 2005;47(1):15-20.
139. Breitfeld PP, Harris JM, Mostov KE. Postendocytotic sorting of the ligand for the polymeric immunoglobulin receptor in Madin-Darby canine kidney cells. J Cell Biol. 1989;109(2):475-86.
140. Rhoades R, Pflanzer R. Human Physiology. 4th ed: Thompson Learning; 2002.
141. Underdown BJ, Schiff JM. Immunoglobulin A: strategic defense initiative at the mucosal surface. Annu Rev Immunol. 1986;4:389-417.
142. Kunisawa J, Kiyono H. A marvel of mucosal T cells and secretory antibodies for the creation of first lines of defense. Cell Mol Life Sci. 2005;62(12):1308-21.
143. Fagarasan S, Honjo T. Intestinal IgA synthesis: regulation of front-line body defences. Nat Rev Immunol. 2003;3(1):63-72.
144. Kerr MA. The structure and function of human IgA. Biochem J. 1990;271(2):285-96.
145. Delacroix DL, Dive C, Rambaud JC, Vaerman JP. IgA subclasses in various secretions and in serum. Immunology. 1982;47(2):383-5.
146. Simell B, Kilpi T, Kayhty H. Subclass distribution of natural salivary IgA antibodies against pneumococcal capsular polysaccharide of type 14 and pneumococcal surface adhesin A (PsaA) in children. Clin Exp Immunol. 2006;143(3):543-9.
147. Mestecky J, Russell MW, Jackson S, Brown TA. The human IgA system: a reassessment. Clin Immunol Immunopathol. 1986;40(1):105-14.
148. Macpherson AJ, Slack E. The functional interactions of commensal bacteria with intestinal secretory IgA. Curr Opin Gastroenterol. 2007;23(6):673-8.
149. Almogren A, Senior BW, Loomes LM, Kerr MA. Structural and functional consequences of cleavage of human secretory and human serum immunoglobulin A1 by proteinases from Proteus mirabilis and Neisseria meningitidis. Infect Immun. 2003;71(6):3349-56.
150. Mestecky J, Russell MW, Elson CO. Intestinal IgA: novel views on its function in the defence of the largest mucosal surface. Gut. 1999;44(1):2-5.
151. Johansen FE, Braathen R, Brandtzaeg P. The J chain is essential for polymeric Ig receptor-mediated epithelial transport of IgA. J Immunol. 2001;167(9):5185-92.
152. Brandtzaeg P. Mucosal and glandular distribution of immunoglobulin components: differential localization of free and bound SC in secretory epithelial cells. J Immunol. 1974;112(4):1553-9.
153. Bastian A, Kratzin H, Eckart K, Hilschmann N. Intra- and interchain disulfide bridges of the human J chain in secretory immunoglobulin A. Biol Chem Hoppe Seyler. 1992;373(12):1255-63.
154. Kobayashi K, Vaerman JP, Bazin H, LeBacq-Verheyden AM, Heremans JF. Identification of J-chain in polymeric immunoglobulins from a variety of species by cross-reaction with rabbit antisera to human J-chain. J Immunol. 1973;111(5):1590-4.
155. Moldoveanu Z, Egan ML, Mestecky J. Cellular origins of human polymeric and monomeric IgA: intracellular and secreted forms of IgA. J Immunol. 1984;133(6):3156-62.
156. Halpern MS, Koshland ME. Noval subunit in secretory IgA. Nature.

1970;228(5278):1276-8.
157. Johansen FE, Braathen R, Brandtzaeg P. Role of J chain in secretory immunoglobulin formation. Scand J Immunol. 2000;52(3):240-8.
158. Garcia-Pardo A, Lamm ME, Plaut AG, Frangione B. J chain is covalently bound to both monomer subunits in human secretory IgA. J Biol Chem. 1981;256(22):11734-8.
159. Baruch EN, Berg AL, Besser MJ, Schachter J, Markel G. Adoptive T cell therapy: An overview of obstacles and opportunities. Cancer. 2017;123(S11):2154-62.
160. Kamta J, Chaar M, Ande A, Altomare DA, Ait-Oudhia S. Advancing Cancer Therapy with Present and Emerging Immuno-Oncology Approaches. Frontiers in oncology. 2017;7:64.
161. Shen M, Ren X. Highlights on immune checkpoint inhibitors in non-small cell lung cancer. Tumour Biol. 2017;39(3):1010428317695013.
162. Komatsubara KM, Carvajal RD. Immunotherapy for the Treatment of Uveal Melanoma: Current Status and Emerging Therapies. Current oncology reports. 2017;19(7):45.
163. Donato EM, Fernandez-Zarzoso M, De La Rubia J. Immunotherapy for the treatment of Hodgkin lymphoma. Expert review of hematology. 2017;10(5):417-23.
164. Thaiss CA, Zmora N, Levy M, Elinav E. The microbiome and innate immunity. Nature. 2016;535(7610):65-74.
165. Kaetzel CS. Cooperativity among secretory IgA, the polymeric immunoglobulin receptor, and the gut microbiota promotes host-microbial mutualism. Immunology letters. 2014;162(2 Pt A):10-21.
166. Brock SC, McGraw PA, Wright PF, Crowe JE, Jr. The human polymeric immunoglobulin receptor facilitates invasion of epithelial cells by Streptococcus pneumoniae in a strain-specific and cell type-specific manner. Infect Immun. 2002;70(9):5091-5.
167. Fan Q, Jia WH, Zhang RH, Yu XJ, Chen LZ, Feng QS, et al. [Correlation of polymeric immunoglobulin receptor gene polymorphisms to susceptibility of nasopharyngeal carcinoma]. Ai Zheng. 2005;24(8):915-8.
168. Agesen TH, Sveen A, Merok MA, Lind GE, Nesbakken A, Skotheim RI, et al. ColoGuideEx: a robust gene classifier specific for stage II colorectal cancer prognosis. Gut. 2012;61(11):1560-7. Epub 2012 Jan 2.
169. Traicoff JL, De Marchis L, Ginsburg BL, Zamora RE, Khattar NH, Blanch VJ, et al. Characterization of the human polymeric immunoglobulin receptor (PIGR) 3'UTR and differential expression of PIGR mRNA during colon tumorigenesis. J Biomed Sci. 2003;10(6 Pt 2):792-804.
170. Gologan A, Acquafondata M, Dhir R, Sepulveda AR. Polymeric immunoglobulin receptor-negative tumors represent a more aggressive type of adenocarcinomas of distal esophagus and gastroesophageal junction. Arch Pathol Lab Med. 2008;132(8):1295-301.
171. Fristedt R, Gaber A, Hedner C, Nodin B, Uhlen M, Eberhard J, et al. Expression and prognostic significance of the polymeric immunoglobulin receptor in esophageal and gastric adenocarcinoma. J Transl Med. 2014;12:83.
172. Khattar NH, Lele SM, Kaetzel CS. Down-regulation of the polymeric immunoglobulin receptor in non-small cell lung carcinoma: correlation with dysregulated expression of the transcription factors USF and AP2. J Biomed Sci. 2005;12(1):65-77.
173. DeSouza LV, Grigull J, Ghanny S, Dube V, Romaschin AD, Colgan TJ, et al. Endometrial carcinoma biomarker discovery and verification using differentially tagged clinical samples with multidimensional liquid chromatography and tandem mass spectrometry. Mol Cell Proteomics. 2007;6(7):1170-82.
174. Rossel M, Billerey C, Bittard H, Ksiazek P, Alber D, Revillard JP, et al. Alterations in polymeric immunoglobulin receptor expression and secretory

component levels in bladder carcinoma. Urological research. 1991;19(6):361-6.
175. Berntsson J, Lundgren S, Nodin B, Uhlen M, Gaber A, Jirstrom K. Expression and prognostic significance of the polymeric immunoglobulin receptor in epithelial ovarian cancer. Journal of ovarian research. 2014;7:26.
176. Fristedt R, Elebro J, Gaber A, Jonsson L, Heby M, Yudina Y, et al. Reduced expression of the polymeric immunoglobulin receptor in pancreatic and periampullary adenocarcinoma signifies tumour progression and poor prognosis. PLoS One. 2014;9(11):e112728.
177. Liu F, Ye P, Bi T, Teng L, Xiang C, Wang H, et al. COLORECTAL Polymeric Immunoglobulin Receptor Expression is Correlated with Hepatic Metastasis and Poor Prognosis in Colon Carcinoma Patients with Hepatic Metastasis. Hepatogastroenterology. 2014;61(131):652-9.
178. Alvi MA, Liu X, O'Donovan M, Newton R, Wernisch L, Shannon NB, et al. DNA methylation as an adjunct to histopathology to detect prevalent, inconspicuous dysplasia and early-stage neoplasia in Barrett's esophagus. Clin Cancer Res. 2013;19(4):878-88. doi: 10.1158/078-0432.CCR-12-2880. Epub 012 Dec 14.
179. Ai J, Tang Q, Wu Y, Xu Y, Feng T, Zhou R, et al. The role of polymeric immunoglobulin receptor in inflammation-induced tumor metastasis of human hepatocellular carcinoma. J Natl Cancer Inst. 2012;103(22):1696-712.
180. Su T, Chapin SJ, Bryant DM, Shewan AM, Young K, Mostov KE. Reduced immunoglobulin A transcytosis associated with immunoglobulin A nephropathy and nasopharyngeal carcinoma. J Biol Chem. 2011;286(52):44921-5.
181. Ocak S, Pedchenko TV, Chen H, Harris FT, Qian J, Polosukhin V, et al. Loss of polymeric immunoglobulin receptor expression is associated with lung tumourigenesis. Eur Respir J. 2012;39(5):1171-80. doi: 10.83/09031936.0184410. Epub 2011 Sep 29.
182. Chang Y, Lee TC, Li JC, Lai TL, Chua HH, Chen CL, et al. Differential expression of osteoblast-specific factor 2 and polymeric immunoglobulin receptor genes in nasopharyngeal carcinoma. Head Neck. 2005;27(10):873-82.
183. Jemal A, Siegel R, Xu J, Ward E. Cancer Statistics, 2010. CA: A Cancer Journal for Clinicians. 2010;60(5):277-300.
184. Block TM, Mehta AS, Fimmel CJ, Jordan R. Molecular viral oncology of hepatocellular carcinoma. Oncogene. 2003;22(33):5093-107.
185. Llovet JM, Zucman-Rossi J, Pikarsky E, Sangro B, Schwartz M, Sherman M, et al. Hepatocellular carcinoma. Nature reviews Disease primers. 2016;2:16018.
186. Yang JD, Roberts LR. Hepatocellular carcinoma: A global view. Nat Rev Gastroenterol Hepatol. 2010;7(8):448-58. doi: 10.1038/nrgastro.2010.100. Epub Jul 13.
187. Marquardt JU, Galle PR, Teufel A. Molecular diagnosis and therapy of hepatocellular carcinoma (HCC): an emerging field for advanced technologies. J Hepatol. 2012;56(1):267-75. doi: 10.1016/j.jhep.2011.07.007. Epub Jul 23.
188. Rhim AD, Mirek ET, Aiello NM, Maitra A, Bailey JM, McAllister F, et al. EMT and dissemination precede pancreatic tumor formation. Cell. 2012;148(1-2):349-61.
189. Jou J, Diehl AM. Epithelial-mesenchymal transitions and hepatocarcinogenesis. J Clin Invest. 2010;120(4):1031-4. doi: 10.172/JCI42615. Epub 2010 Mar 24.
190. Thiery JP, Acloque H, Huang RY, Nieto MA. Epithelial-mesenchymal transitions in development and disease. Cell. 2009;139(5):871-90. doi: 10.1016/j.cell.2009.11.007.
191. Singh A, Settleman J. EMT, cancer stem cells and drug resistance: an emerging axis of evil in the war on cancer. Oncogene. 2010;29(34):4741-51. doi: 10.1038/onc.2010.215. Epub Jun 7.
192. Rossel M, Seilles E, Voigt JJ, Vuitton D, Legait N, Revillard JP. Polymeric Ig receptor expression in hepatocellular carcinoma. Eur J Cancer. 1992;28A(6-7):1120-4.
193. Meulmeester E, Ten Dijke P. The dynamic roles of TGF-beta in cancer. J Pathol. 2011;223(2):205-18. doi: 10.1002/path.2785. Epub 010 Oct 18.

194. Sphyris N, Mani SA. pIgR: frenemy of inflammation, EMT, and HCC progression. J Natl Cancer Inst. 2012;103(22):1644-5.
195. Bosman FT, Carneiro, F., Hruban, R.H., Theise, N.D. WHO Classification of Tumours of the Digestive System, Fourth Edition. Lyon: Agency for Research in Cancer; 2010.
196. Pomianowska E, Grzyb K, Westgaard A, Clausen OP, Gladhaug IP. Reclassification of tumour origin in resected periampullary adenocarcinomas reveals underestimation of distal bile duct cancer. Eur J Surg Oncol. 2012;38(11):1043-50.
197. Kimura W, Futakawa N, Zhao B. Neoplastic diseases of the papilla of Vater. J Hepatobiliary Pancreat Surg. 2004;11(4):223-31.
198. Morini S, Perrone G, Borzomati D, Vincenzi B, Rabitti C, Righi D, et al. Carcinoma of the ampulla of Vater: morphological and immunophenotypical classification predicts overall survival. Pancreas. 2013;42(1):60-6.
199. Westgaard A, Tafjord S, Farstad IN, Cvancarova M, Eide TJ, Mathisen O, et al. Pancreatobiliary versus intestinal histologic type of differentiation is an independent prognostic factor in resected periampullary adenocarcinoma. BMC Cancer. 2008;8:170.
200. Khattar NH, Lele SM, Kaetzel CS. Down-regulation of the polymeric immunoglobulin receptor in non-small cell lung carcinoma: correlation with dysregulated expression of the transcription factors USF and AP2. Journal of biomedical science. 2005;12(1):65-77.
201. Erkan M, Reiser-Erkan C, Michalski CW, Deucker S, Sauliunaite D, Streit S, et al. Cancer-stellate cell interactions perpetuate the hypoxia-fibrosis cycle in pancreatic ductal adenocarcinoma. Neoplasia. 2009;11(5):497-508.
202. Froeling FE, Mirza TA, Feakins RM, Seedhar A, Elia G, Hart IR, et al. Organotypic culture model of pancreatic cancer demonstrates that stromal cells modulate E-cadherin, beta-catenin, and Ezrin expression in tumor cells. Am J Pathol. 2009;175(2):636-48.
203. Ene-Obong A, Clear AJ, Watt J, Wang J, Fatah R, Riches JC, et al. Activated pancreatic stellate cells sequester CD8+ T cells to reduce their infiltration of the juxtatumoral compartment of pancreatic ductal adenocarcinoma. Gastroenterology. 2013;145(5):1121-32.
204. Kononen J, Bubendorf L, Kallioniemi A, Barlund M, Schraml P, Leighton S, et al. Tissue microarrays for high-throughput molecular profiling of tumor specimens. Nat Med. 1998;4(7):844-7.
205. Torhorst J, Bucher C, Kononen J, Haas P, Zuber M, Kochli OR, et al. Tissue microarrays for rapid linking of molecular changes to clinical endpoints. Am J Pathol. 2001;159(6):2249-56.
206. Fogh J, Wright WC, Loveless JD. Absence of HeLa cell contamination in 169 cell lines derived from human tumors. J Natl Cancer Inst. 1977;58(2):209-14.
207. Sipos B, Moser S, Kalthoff H, Torok V, Lohr M, Kloppel G. A comprehensive characterization of pancreatic ductal carcinoma cell lines: towards the establishment of an in vitro research platform. Virchows Arch. 2003;442(5):444-52.
208. Schoumacher RA, Ram J, Iannuzzi MC, Bradbury NA, Wallace RW, Hon CT, et al. A cystic fibrosis pancreatic adenocarcinoma cell line. Proc Natl Acad Sci U S A. 1990;87(10):4012-6.
209. Dammann R, Schagdarsurengin U, Liu L, Otto N, Gimm O, Dralle H, et al. Frequent RASSF1A promoter hypermethylation and K-ras mutations in pancreatic carcinoma. Oncogene. 2003;22(24):3806-12.
210. Chen WH, Horoszewicz JS, Leong SS, Shimano T, Penetrante R, Sanders WH, et al. Human pancreatic adenocarcinoma: in vitro and in vivo morphology of a new tumor line established from ascites. In Vitro. 1982;18(1):24-34.
211. Metzgar RS, Gaillard MT, Levine SJ, Tuck FL, Bossen EH, Borowitz MJ. Antigens of human pancreatic adenocarcinoma cells defined by murine

monoclonal antibodies. Cancer Res. 1982;42(2):601-8.
212. Sipos B, Real FX, Moore P, Kalthoff H, Scarpa A, Klöppel G. Gress TM, Neoptolemos JP, Lemoine NR, Real FX. Genetic and cellular characteristics of pancreatic carcinoma cell lines. Exocrine pancreas cancer. 2005;The European Pancreatic Cancer-Research Cooperative (EPC-RC).
213. Lieber M, Mazzetta J, Nelson-Rees W, Kaplan M, Todaro G. Establishment of a continuous tumor-cell line (panc-1) from a human carcinoma of the exocrine pancreas. Int J Cancer. 1975;15(5):741-7.
214. Elsasser HP, Lehr U, Agricola B, Kern HF. Establishment and characterisation of two cell lines with different grade of differentiation derived from one primary human pancreatic adenocarcinoma. Virchows Arch B Cell Pathol Incl Mol Pathol. 1992;61(5):295-306.
215. Li NF, Kocher HM, Salako MA, Obermueller E, Sandle J, Balkwill F. A novel function of colony-stimulating factor 1 receptor in hTERT immortalization of human epithelial cells. Oncogene. 2009;28(5):773-80.
216. Furukawa T, Duguid WP, Rosenberg L, Viallet J, Galloway DA, Tsao MS. Long-term culture and immortalization of epithelial cells from normal adult human pancreatic ducts transfected by the E6E7 gene of human papilloma virus 16. Am J Pathol. 1996;148(6):1763-70.
217. Kluwe J, Wongsiriroj N, Troeger JS, Gwak GY, Dapito DH, Pradere JP, et al. Absence of hepatic stellate cell retinoid lipid droplets does not enhance hepatic fibrosis but decreases hepatic carcinogenesis. Gut.
218. Carapuca EF, Gemenetzidis E, Feig C, Bapiro TE, Williams MD, Wilson AS, et al. Anti-stromal treatment together with chemotherapy targets multiple signalling pathways in pancreatic adenocarcinoma. J Pathol. 2016.
219. Coleman SJ, Watt J, Arumugam P, Solaini L, Carapuca E, Ghallab M, et al. Pancreatic cancer organotypics: High throughput, preclinical models for pharmacological agent evaluation. World J Gastroenterol. 2014;20(26):8471-81.
220. Biosystems L. ARIOL - Product guide 2017 [cited 2017]. Aiol - Clinical IHC and FISH Capture & Analysis]. Available from: http://www.leicabiosystems.com/digital-pathology/aperio-digital-pathology-slide-scanners/products/ariol/downloads/.
221. Minot DM, Kipp BR, Root RM, Meyer RG, Reynolds CA, Nassar A, et al. Automated cellular imaging system III for assessing HER2 status in breast cancer specimens: development of a standardized scoring method that correlates with FISH. Am J Clin Pathol. 2009;132(1):133-8.
222. Ong CW, Kim LG, Kong HH, Low LY, Wang TT, Supriya S, et al. Computer-assisted pathological immunohistochemistry scoring is more time-effective than conventional scoring, but provides no analytical advantage. Histopathology. 2010;56(4):523-9.
223. Zabaglo L, Salter J, Anderson H, Quinn E, Hills M, Detre S, et al. Comparative validation of the SP6 antibody to Ki67 in breast cancer. J Clin Pathol. 2010;63(9):800-4.
224. Clear AJ, Lee AM, Calaminici M, Ramsay AG, Morris KJ, Hallam S, et al. Increased angiogenic sprouting in poor prognosis FL is associated with elevated numbers of CD163+ macrophages within the immediate sprouting microenvironment. Blood. 2010;115(24):5053-6.
225. Bolton KL, Garcia-Closas M, Pfeiffer RM, Duggan MA, Howat WJ, Hewitt SM, et al. Assessment of automated image analysis of breast cancer tissue microarrays for epidemiologic studies. Cancer Epidemiol Biomarkers Prev. 2010;19(4):992-9.
226. Kirkegaard T, Edwards J, Tovey S, McGlynn LM, Krishna SN, Mukherjee R, et al. Observer variation in immunohistochemical analysis of protein expression, time for a change? Histopathology. 2006;48(7):787-94.
227. Makohon-Moore A, Iacobuzio-Donahue CA. Pancreatic cancer biology and genetics from an evolutionary perspective. Nat Rev Cancer. 2016;16(9):553-65.

228. Brosens LA, Hackeng WM, Offerhaus GJ, Hruban RH, Wood LD. Pancreatic adenocarcinoma pathology: changing "landscape". Journal of gastrointestinal oncology. 2015;6(4):358-74.
229. Bruno ME, Rogier EW, Arsenescu RI, Flomenhoft DR, Kurkjian CJ, Ellis GI, et al. Correlation of Biomarker Expression in Colonic Mucosa with Disease Phenotype in Crohn's Disease and Ulcerative Colitis. Dig Dis Sci. 2015;60(10):2976-84.
230. Nystrom ML, Thomas GJ, Stone M, Mackenzie IC, Hart IR, Marshall JF. Development of a quantitative method to analyse tumour cell invasion in organotypic culture. J Pathol. 2005;205(4):468-75.
231. Froeling FE, Marshall JF, Kocher HM. Pancreatic cancer organotypic cultures. J Biotechnol. 2010;148(1):16-23.
232. Choudhury KR, Yagle KJ, Swanson PE, Krohn KA, Rajendran JG. A Robust Automated Measure of Average Antibody Staining in Immunohistochemistry Images. Journal of Histochemistry and Cytochemistry. 2010;58(2):95-107.
233. Bronsert P, Kohler I, Werner M, Makowiec F, Kuesters S, Hoeppner J, et al. Intestinal-type of differentiation predicts favourable overall survival: confirmatory clinicopathological analysis of 198 periampullary adenocarcinomas of pancreatic, biliary, ampullary and duodenal origin. BMC Cancer. 2013;13:428.
234. Erkan M, Michalski CW, Rieder S, Reiser-Erkan C, Abiatari I, Kolb A, et al. The activated stroma index is a novel and independent prognostic marker in pancreatic ductal adenocarcinoma. Clin Gastroenterol Hepatol. 2008;6(10):1155-61.
235. Kadaba R, Birke H, Wang J, Hooper S, Andl CD, Di Maggio F, et al. Imbalance of desmoplastic stromal cell numbers drives aggressive cancer processes. J Pathol. 2013;230(1):107-17.
236. Coupland VH, Kocher HM, Berry DP, Allum W, Linklater KM, Konfortion J, et al. Incidence and survival for hepatic, pancreatic and biliary cancers in England between 1998 and 2007. Cancer Epidemiol. 2012.
237. Kantor O, Talamonti MS, Stocker SJ, Wang CH, Winchester DJ, Bentrem DJ, et al. A Graded Evaluation of Outcomes Following Pancreaticoduodenectomy with Major Vascular Resection in Pancreatic Cancer. J Gastrointest Surg. 2016;20(2):284-92.
238. Emmadi R, Wiley EL. Evaluation of resection margins in breast conservation therapy: the pathology perspective-past, present, and future. International journal of surgical oncology. 2012;2012:180259.
239. House MG, Gonen M, Jarnagin WR, D'Angelica M, DeMatteo RP, Fong Y, et al. Prognostic significance of pathologic nodal status in patients with resected pancreatic cancer. J Gastrointest Surg. 2007;11(11):1549-55.
240. Osipov A, Naziri J, Hendifar A, Dhall D, Rutgers JK, Chopra S, et al. Impact of margin status and lymphadenectomy on clinical outcomes in resected pancreatic adenocarcinoma: implications for adjuvant radiotherapy. Journal of gastrointestinal oncology. 2016;7(2):239-47.
241. De Reuver PR, Mittal A, Neale M, Gill AJ, Samra JS. Extended pancreatoduodenectomy as defined by the International Study Group for Pancreatic Surgery is associated with worse survival but not with increased morbidity. Surgery. 2015;158(1):183-90.
242. Distler M, Pilarsky E, Kersting S, Grutzmann R. Preoperative CEA and CA 19-9 are prognostic markers for survival after curative resection for ductal adenocarcinoma of the pancreas - a retrospective tumor marker prognostic study. Int J Surg. 2013;11(10):1067-72.
243. Solaini L, Atmaja BT, Watt J, Arumugam P, Hutchins RR, Abraham AT, et al. Limited utility of inflammatory markers in the early detection of postoperative inflammatory complications after pancreatic resection: Cohort study and meta-analyses. Int J Surg. 2015;17:41-7.
244. Brandtzaeg P. Development and basic mechanisms of human gut immunity.

Nutrition reviews. 1998;56(1 Pt 2):S5-18.
245. Provenzano PP, Cuevas C, Chang AE, Goel VK, Von Hoff DD, Hingorani SR. Enzymatic targeting of the stroma ablates physical barriers to treatment of pancreatic ductal adenocarcinoma. Cancer Cell. 2012;21(3):418-29.
246. Wang LM, Silva MA, D'Costa Z, Bockelmann R, Soonawalla Z, Liu S, et al. The prognostic role of desmoplastic stroma in pancreatic ductal adenocarcinoma. Oncotarget. 2016;7(4):4183-94.
247. Sato D, Tsuchikawa T, Mitsuhashi T, Hatanaka Y, Marukawa K, Morooka A, et al. Stromal Palladin Expression Is an Independent Prognostic Factor in Pancreatic Ductal Adenocarcinoma. PLoS One. 2016;11(3):e0152523.
248. Guthrie GJ, Roxburgh CS, Horgan PG, McMillan DC. Does interleukin-6 link explain the link between tumour necrosis, local and systemic inflammatory responses and outcome in patients with colorectal cancer? Cancer treatment reviews. 2013;39(1):89-96.
249. Clark EJ, Connor S, Taylor MA, Madhavan KK, Garden OJ, Parks RW. Preoperative lymphocyte count as a prognostic factor in resected pancreatic ductal adenocarcinoma. HPB (Oxford). 2007;9(6):456-60.
250. Pan B, Liao Q, Niu Z, Zhou L, Zhao Y. Cancer-associated fibroblasts in pancreatic adenocarcinoma. Future oncology (London, England). 2015;11(18):2603-10.
251. Erkan M, Kleeff J, Gorbachevski A, Reiser C, Mitkus T, Esposito I, et al. Periostin creates a tumor-supportive microenvironment in the pancreas by sustaining fibrogenic stellate cell activity. Gastroenterology. 2007;132(4):1447-64.
252. Yen TW, Aardal NP, Bronner MP, Thorning DR, Savard CE, Lee SP, et al. Myofibroblasts are responsible for the desmoplastic reaction surrounding human pancreatic carcinomas. Surgery. 2002;131(2):129-34.
253. Bissell MJ, Radisky D. Putting tumours in context. Nat Rev Cancer. 2001;1(1):46-54.
254. Junqueira LC, Bignolas G, Brentani RR. Picrosirius staining plus polarization microscopy, a specific method for collagen detection in tissue sections. The Histochemical journal. 1979;11(4):447-55.
255. Lattouf R, Younes R, Lutomski D, Naaman N, Godeau G, Senni K, et al. Picrosirius red staining: a useful tool to appraise collagen networks in normal and pathological tissues. J Histochem Cytochem. 2014;62(10):751-8.
256. Bachem MG, Schunemann M, Ramadani M, Siech M, Beger H, Buck A, et al. Pancreatic carcinoma cells induce fibrosis by stimulating proliferation and matrix synthesis of stellate cells. Gastroenterology. 2005;128(4):907-21.
257. Su T, Chapin SJ, Bryant DM, Shewan AM, Young K, Mostov KE. Reduced immunoglobulin A transcytosis associated with immunoglobulin A nephropathy and nasopharyngeal carcinoma. J Biol Chem. 2011;286(52):44921-5. doi: 10.1074/jbc.M111.296731. Epub 2011 Nov 15.
258. Ocak S, Pedchenko TV, Chen H, Harris FT, Qian J, Polosukhin V, et al. Loss of polymeric immunoglobulin receptor expression is associated with lung tumourigenesis. The European respiratory journal. 2012;39(5):1171-80.
259. Park J, Yun HS, Lee KH, Lee KT, Lee JK, Lee SY. Discovery and Validation of Biomarkers That Distinguish Mucinous and Nonmucinous Pancreatic Cysts. Cancer Res. 2015;75(16):3227-35.
260. Hruban RH, Wilentz RE, Goggins M, Offerhaus GJ, Yeo CJ, Kern SE. Pathology of incipient pancreatic cancer. Ann Oncol. 1999;10 Suppl 4:9-11.
261. Hruban RH, Goggins M, Parsons J, Kern SE. Progression model for pancreatic cancer. Clin Cancer Res. 2000;6(8):2969-72.
262. Buxbaum JL, Eloubeidi MA. Molecular and clinical markers of pancreas cancer. Jop. 2010;11(6):536-44.
263. Garcea G, Dennison AR, Pattenden CJ, Neal CP, Sutton CD, Berry DP. Survival following curative resection for pancreatic ductal adenocarcinoma. A systematic

review of the literature. Jop. 2008;9(2):99-132.
264. Tuveson DA, Neoptolemos JP. Understanding metastasis in pancreatic cancer: a call for new clinical approaches. Cell. 2012;148(1-2):21-3.
265. Ansari D, Rosendahl A, Elebro J, Andersson R. Systematic review of immunohistochemical biomarkers to identify prognostic subgroups of patients with pancreatic cancer. Br J Surg. 2011;98(8):1041-55.
266. Nones K, Waddell N, Song S, Patch AM, Miller D, Johns A, et al. Genome-wide DNA methylation patterns in pancreatic ductal adenocarcinoma reveal epigenetic deregulation of SLIT-ROBO, ITGA2 and MET signaling. Int J Cancer. 2014;135(5):1110-8.
267. Mani SA, Guo W, Liao MJ, Eaton EN, Ayyanan A, Zhou AY, et al. The epithelial-mesenchymal transition generates cells with properties of stem cells. Cell. 2008;133(4):704-15. doi: 10.1016/j.cell.2008.03.027.
268. Ansieau S, Bastid J, Doreau A, Morel AP, Bouchet BP, Thomas C, et al. Induction of EMT by twist proteins as a collateral effect of tumor-promoting inactivation of premature senescence. Cancer Cell. 2008;14(1):79-89. doi: 10.1016/j.ccr.2008.06.005.
269. Li NF, Gemenetzidis E, Marshall FJ, Davies D, Yu Y, Frese K, et al. RhoC interacts with integrin alpha5beta1 and enhances its trafficking in migrating pancreatic carcinoma cells. PLoS One. 2013;8(12):e81575.
270. Coleman SJ, Chioni AM, Ghallab M, Anderson RK, Lemoine NR, Kocher HM, et al. Nuclear translocation of FGFR1 and FGF2 in pancreatic stellate cells facilitates pancreatic cancer cell invasion. EMBO Mol Med. 2014;6(4):467-81.
271. Takenouchi-Ohkubo N, Asano M, Chihaya H, Chung-Hsuing WU, Ishikasa K, Moro I. Retinoic acid enhances the gene expression of human polymeric immunoglobulin receptor (pIgR) by TNF-alpha. Clinical and experimental immunology. 2004;135(3):448-54.
272. Bruno ME, Kaetzel CS. Long-term exposure of the HT-29 human intestinal epithelial cell line to TNF causes sustained up-regulation of the polymeric Ig receptor and proinflammatory genes through transcriptional and posttranscriptional mechanisms. J Immunol. 2005;174(11):7278-84.
273. Garg M. Epithelial-mesenchymal transition - activating transcription factors - multifunctional regulators in cancer. World journal of stem cells. 2013;5(4):188-95.
274. Kocher HM, Sandle J, Mirza TA, Li NF, Hart IR. Ezrin interacts with Cortactin to form podosomal rosettes in pancreatic cancer cells. Gut. 2009;58(2):271-84.
275. Piskurich JF, France JA, Tamer CM, Willmer CA, Kaetzel CS, Kaetzel DM. Interferon-gamma induces polymeric immunoglobulin receptor mRNA in human intestinal epithelial cells by a protein synthesis dependent mechanism. Molecular immunology. 1993;30(4):413-21.
276. Kvale D, Brandtzaeg P, Lovhaug D. Up-regulation of the expression of secretory component and HLA molecules in a human colonic cell line by tumour necrosis factor-alpha and gamma interferon. Scandinavian journal of immunology. 1988;28(3):351-7.
277. Carol M, Lambrechts A, Van Gossum A, Libin M, Goldman M, Mascart-Lemone F. Spontaneous secretion of interferon gamma and interleukin 4 by human intraepithelial and lamina propria gut lymphocytes. Gut. 1998;42(5):643-9.
278. Denning GM. IL-4 and IFN-gamma synergistically increase total polymeric IgA receptor levels in human intestinal epithelial cells. Role of protein tyrosine kinases. J Immunol. 1996;156(12):4807-14.
279. Youngman KR, Fiocchi C, Kaetzel CS. Inhibition of IFN-gamma activity in supernatants from stimulated human intestinal mononuclear cells prevents up-regulation of the polymeric Ig receptor in an intestinal epithelial cell line. J Immunol. 1994;153(2):675-81.
280. Krajci P, Tasken K, Kvale D, Brandtzaeg P. Interferon-gamma stimulation of messenger RNA for human secretory component (poly-Ig receptor) depends on

continuous intermediate protein synthesis. Scandinavian journal of immunology. 1993;37(2):251-6.
281. Piskurich JF, Youngman KR, Phillips KM, Hempen PM, Blanchard MH, France JA, et al. Transcriptional regulation of the human polymeric immunoglobulin receptor gene by interferon-gamma. Molecular immunology. 1997;34(1):75-91.
282. Taniguchi T, Lamphier MS, Tanaka N. IRF-1: the transcription factor linking the interferon response and oncogenesis. Biochim Biophys Acta. 1997;1333(1):M9-17.
283. Borghesi L, Milcarek C. From B cell to plasma cell: regulation of V(D)J recombination and antibody secretion. Immunol Res. 2006;36(1-3):27-32.
284. Lopez-Novoa JM, Nieto MA. Inflammation and EMT: an alliance towards organ fibrosis and cancer progression. EMBO Mol Med. 2009;1(6-7):303-14. doi: 10.1002/emmm.200900043.
285. Wu Y, Deng J, Rychahou PG, Qiu S, Evers BM, Zhou BP. Stabilization of snail by NF-kappaB is required for inflammation-induced cell migration and invasion. Cancer Cell. 2009;15(5):416-28. doi: 10.1016/j.ccr.2009.03.016.
286. Kudo-Saito C, Shirako H, Takeuchi T, Kawakami Y. Cancer metastasis is accelerated through immunosuppression during Snail-induced EMT of cancer cells. Cancer Cell. 2009;15(3):195-206. doi: 10.1016/j.ccr.2009.01.023.
287. Rhim AD, Mirek ET, Aiello NM, Maitra A, Bailey JM, McAllister F, et al. EMT and dissemination precede pancreatic tumor formation. Cell. 2012;148(1-2):349-61. doi: 10.1016/j.cell.2011.11.025.
288. Aguirre AJ, Bardeesy N, Sinha M, Lopez L, Tuveson DA, Horner J, et al. Activated Kras and Ink4a/Arf deficiency cooperate to produce metastatic pancreatic ductal adenocarcinoma. Genes Dev. 2003;17(24):3112-26.
289. Grivennikov SI, Greten FR, Karin M. Immunity, inflammation, and cancer. Cell. 2010;140(6):883-99.
290. Guerra C, Collado M, Navas C, Schuhmacher AJ, Hernandez-Porras I, Canamero M, et al. Pancreatitis-induced inflammation contributes to pancreatic cancer by inhibiting oncogene-induced senescence. Cancer Cell. 2011;19(6):728-39.

APPENDIX

ABC TMA Cores

TMA	Slide	Age	Survival	Diagnosis	dead	sex	WCC	neutro	lymphocy	CRP	ca 19-9	differentiation	T (of TNM)	other	N (of TNM)	Nodes	Total nodes	Resection (R0/1/2
					0 is dea	1 is male, 2 is female						1 is well, 2 is moderate, 3is poo		0 is nil, 1 is venous, 2 i		positive	total	
A	1	59	4647	Neuroendocrine	0	2												
A	2																	
A	3																	
A	4	57	5295	Ampullary Cancer	2	1												
A	5																	
A	6																	
A	7	47	713	Ampullary Cancer	0	2												
A	8																	
A	9																	
A	10	62	41	Duodenal adenoma	0	1												
A	11																	
A	12																	
A	13	78	35	AMP adenoma	0	2												
A	14																	
A	15																	
A	16	67	169	AMP adenoma	0	1												
A	17																	
A	18																	
A	19	43	1099	AMP adenoma	2	2												
A	20																	
A	21																	
A	22	53	964	cholangio	0	2						2	3	2	0	0	13	0
A	23																	
A	24																	
A	25	75	1910	cholangio	2	2						2	2	0	0	0	6	0
A	26																	
A	27																	
A	28	53	261	cholangio	0	1	17.9	16.6	0.5			3	3	1	1	1	4	1
A	29																	
A	30																	
A	31	58	3785	endocrine	2	1										0	6	0
A	32																	
A	33																	
A	34	68	3297	ipmn	2	2	9.5	5	3.6							0	10	0
A	35																	
A	36																	
A	37	67	299	pdac	2	1	6.5	5	0.9			3	2	1	1			1
A	38																	
A	39																	
A	40	68	1129	pdac	0	1						2	3	3	1	4	16	0
A	41																	
A	42																	
A	43	66	2838	cp	2	2												
A	44																	
A	45																	

A	46	55	#VALUE!	cp														
A	47																	
A	48																	
A	49	60	356	PDAC	0	2	4.9	3.1	1.4			3		0				0
A	50																	
A	51																	
A	52	58	8	Cholangiocarcinoma	0	1	4.7	3.8	0.8	<5		2		0				0
A	53																	
A	54																	
A	55	67	299	pdac	2	1	6.5	5	0.9			3	2	1	1			1
A	56																	
A	57																	
A	58	46	261	pdac	0	1	9.2	5.3	3			3	2	0	1	1	7	1
A	59																	
A	60																	
A	61	60	499	pdac	0	1	6.9	4.4	1.7			1	2	0	1	2	6	1
A	62																	
A	63																	
B	1	69	798	pdac	0	2	11.4	8.7	2.1		4	2		1				0
B	2																	
B	3																	
B	4	67	860	pdac	0	2	6.9	3.7	2.6			3	3	0	0	2	3	0
B	5																	
B	6																	
B	7	64	579	pdac	0	2	10.3	7.7	1.9			1	3	0	0	0	12	0
B	8																	
B	9																	
B	10	67	827	pdac	0	2	3.8	2.3	1.2		71	2	3	1	1	1	8	0
B	11																	
B	12																	
B	13	63	4393	pdac	0	1	9.4	5.3	3.3			1	2	0	0	0	2	0
B	14																	
B	15																	
B	16	58	528	pdac	0	1	6.5	3.8	2.1	9		3	2	3	1	2	5	0
B	17																	
B	18																	
B	19	58	3912	pdac	0	1	9.9	6.9	2.1	6		3	3	2	0	0	7	1
B	20																	
B	21																	
B	22	75	750	pdac	0	2	10.2	7.8	1.8	36	115	1	2	3	1	3	14	0
B	23																	
B	24																	
B	25	72	587	pdac	0	1	9.5	7.2	1.8	209	1283	2	1	0	0	0	7	0
B	26																	
B	27																	
B	28	47	105	pdac	0	1	9.9	9.1	0.3	32	185	3	3	3	1	2	11	0
B	29																	

B	30																	
B	31	79	1171	pdac	0	2	5.9	3.5	1.9		<1	1	2	0	0	0	3	0
B	32																	
B	33																	
B	34	77	134	pdac	0	2	4.8	3.3	1	12	1281	2	2	3	0	0	13	0
B	35																	
B	36																	
B	37	47	48	pdac	0	1	7.1	3.4	3	8	722	2	3	0	1	8	12	1
B	38																	
B	39																	
B	40	66	539	pdac	0	2	6.1	4	1.5	<5	35	3	2	3	0	0	7	1
B	41																	
B	42																	
B	43	60	879	pdac	2	1	6	5	0.6	11		2	3	0	1	5	7	0
B	44																	
B	45																	
B	46	80	211	pdac	0	2	7.1	4.2	2.3		85	2	1	2	0	0	6	0
B	47																	
B	48																	
B	49	54	1190	pdac	0	1	6.9	1.7	4.7			2	2	2	1	7	33	0
B	50																	
B	51																	
B	52	69	685	pdac	0	1	13.5	11.9	0.9	<5	29	3	3	3	1	1	8	0
B	53																	
B	54																	
B	55	68	1129	pdac	0	1						2	3	3	1	4	16	0
B	56																	
B	57																	
B	58	64	2506	Ampullary Cancer	0	1	10.5	6.3	1.7	16		2	3	0	1	3	3	0
B	59																	
B	60																	
B	61	69	526	pdac	0	2	6.3	3.8	1.5	10	549	2	3	3	1	8	19	0
B	62																	
B	63																	
B	64	71	101	pdac	0	2	9.4	6.8	1.5			2	3	3	1	2	8	0
B	65																	
B	66																	
B	67	77	357	pdac	0	2	8	3.5	3.6			2	3	2	0	0	7	1
B	68																	
B	69																	
B	70	57	387	pdac	0	1	8.1	5.5	1.4	<5	65.4	2	2	2	1	3	12	0
B	71																	
B	72																	
B	73	49	454	pdac	0	1	7.9	6	1.3	<5		2	3	2	1	2	15	0
B	74																	
B	75																	
B	76	62	461	pdac	0	2	8	4.3	2.8	<5		2	3	0	0	0	3	1

B	77																	
B	78																	
B	79	64	543	pdac	0	1	7.7	6.7	0.7			2	1	2	0	0	15	1
B	80																	
B	81																	
B	82	62	341	pdac	0	1	5.3	2.8	1.3		8.3	2	3	0	0	0	6	0
B	83																	
B	84																	
C	1	74	599	pdac	2	2	10.6	9.1	0.8			2	3	3	1	1	6	0
C	2																	
C	3																	
C	4	80	119	pdac	2	2	5.6	4.6	0.7			2	3	2	1	2	2	1
C	5																	
C	6																	
C	7	61	34	pdac	2	1	7.7	5.2	1.2	36	523	1	2	3	1	2	8	1
C	8																	
C	9																	
C	10	66	399	pdac	0	2	6.8	2.9	3.2		177.5	3	3	3	1	1	7	0
C	11																	
C	12																	

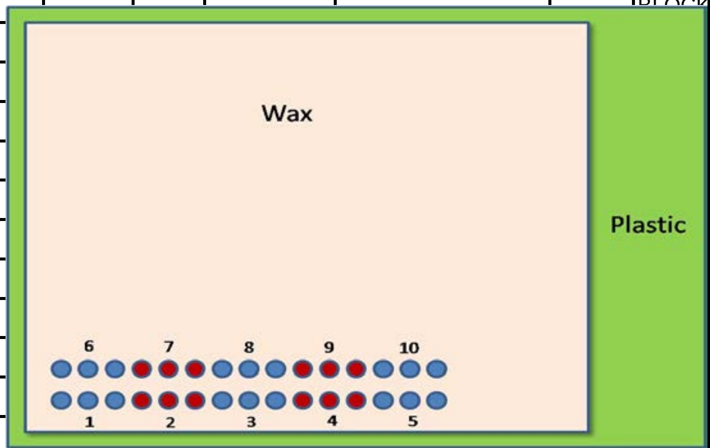

BLOCK	PDAC	PDAC	PDAC	PDAC	PDAC	PDAC	PDAC	PDAC	PDAC			
	PDAC	PDAC	PDAC	PDAC	PDAC	PDAC	CP	CP	CP			
	N	N	N	N	N	N	CP	CP	CP			
	N	N	N	N	N	N	N	N	N			
	N	N	N	N	N	N	N	N	N			
	N	N	N	N	N	N	N	N	N			
	N	N	N	N	N	N	N	N	N			
	PDAC	PDAC	PDAC	PDAC	PDAC	PDAC	PDAC	PDAC	PDAC	PDAC	PDAC	PDAC
	PDAC	PDAC	PDAC	PDAC	PDAC	PDAC	PDAC	PDAC	PDAC	PDAC	PDAC	PDAC
	PDAC	PDAC	PDAC	PDAC	PDAC	PDAC	PDAC	PDAC	PDAC	PDAC	PDAC	PDAC
	PDAC	PDAC	PDAC	PDAC	PDAC	PDAC	PDAC	PDAC	PDAC	PDAC	PDAC	PDAC
	PDAC	PDAC	PDAC	PDAC	PDAC	PDAC	PDAC	PDAC	PDAC	PDAC	PDAC	PDAC
	PDAC	PDAC	PDAC	PDAC	PDAC	PDAC	PDAC	PDAC	PDAC	PDAC	PDAC	PDAC
	PDAC	PDAC	PDAC	PDAC	PDAC	PDAC	PDAC	PDAC	PDAC	PDAC	PDAC	PDAC
BLOCK	PDAC	PDAC	PDAC									
C	PDAC	PDAC	PDAC	PDAC	PDAC	PDAC	PDAC	PDAC	PDAC			

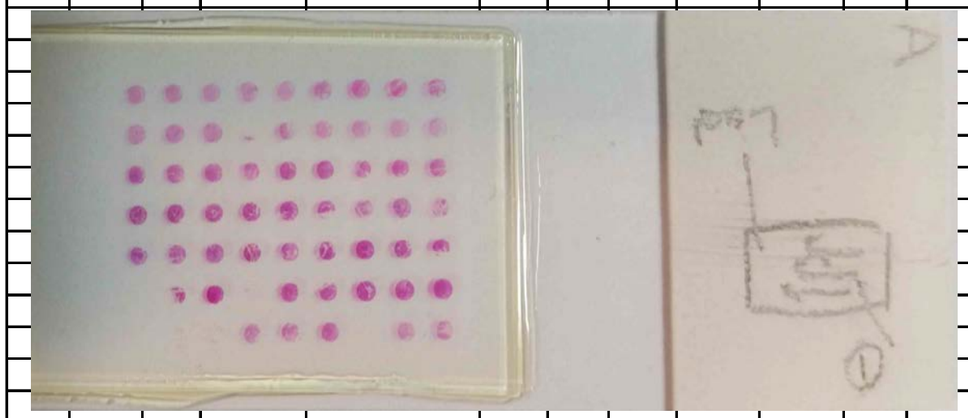

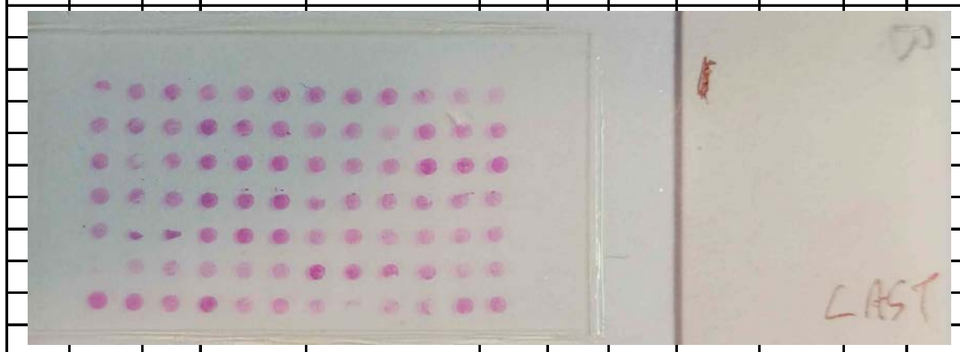
LAST

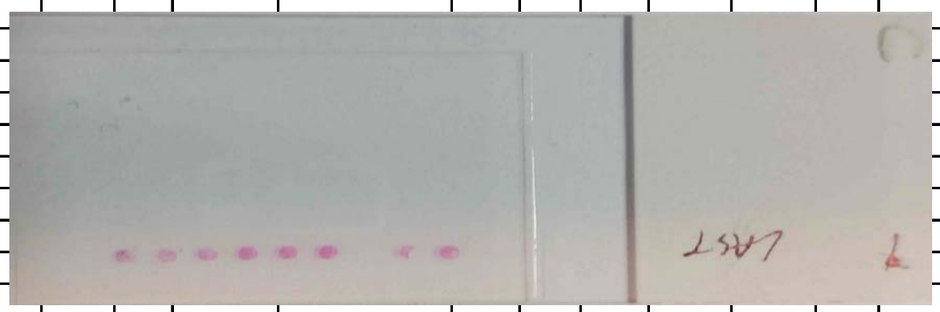

AW1

TMA Pos	Age	Survival	Diagnosis	dead	sex	WCC	neutro	lymphoc	CRP	ca 19-9	differentiation	T (of TNM)	other	N (of TNM)	Nodes	Total nodes	Resection
				0 is de	1 is male, 2 is female						1 is well, 2 is moderate, 3is		0 is nil, 1 is venous,		positive	total	(R0/1/2)
A1	70	7	PDAC	0	1	8.4	6.4	2	5	190							
A2																	
A3																	
A4																	
A5																	
A6																	
A7	70	419	PDAC	0	2	6.6	3	3			2	3	2	1	4	18	0
A8																	
A9																	
A10																	
A11																	
A12																	
A13	76	207	PDAC	2	1	6.2	4	1.8		197	2	3	3	1	2	7	0
A14																	
A15																	
A16																	
B1																	
B2																	
B3	78	36	Benign Pancreas	2	2												
B4																	
B5																	
B6																	
B7																	
B8																	
B9	45	296	PDAC	0	1	10	5.3	3.8		158	2	3	3	1	3	19	1
B10																	
B11																	
B12																	
B13																	
B14																	
B15	60	769	PDAC	2	2	8.2	7.1	0.8			2	2	3	1	2	19	1
B16																	
C1																	
C2																	
C3																	
C4																	
C5	49	2723	Endocrine	1	2						2		0	0	0	9	1
C6																	
C7																	
C8																	
C9																	
C10																	
C11	44	976	PDAC	0	1	10.9	9.2	1.2	9		2	3	2	1	4	12	1
C12																	
C13																	
C14																	
C15																	
C16																	
D1	75	215	PDAC	0	1	10	6.5	2.5	18	1190	2	2	3	1	7	11	0
D2																	
D3																	
D4																	
D5																	
D6																	
D7	79	64	Lymphoma	2	1												
D8																	
D9																	
D10																	
D11																	
D12																	
D13	80	24	PDAC	0	1	9.4	5.4	3.2	<5		3	3	3	1	2	9	1
D14																	
D15																	
D16																	
E1																	
E2																	
E3	78	10	PDAC	0	1	17.8	13.2	1.9	101		2	3	2	0	0	20	0
E4																	
E5																	
E6																	
E7																	
E8																	
E9-E14	56	74	PDAC	2	1	4.4	2.3	1.5									
E15	57	260	Duodenal Ca	0	1						3	4	3	1	4	11	0
E16																	
F1																	
F2																	
F3																	
F4																	
F6	61	508	PDAC	0	1	7	3.9	2.3	14								
F7																	
F8																	
F9																	
F10																	
F11																	
F12	71	341	PDAC	0	2	8.2	5.1	2.4			3	2	3	1	5	22	1
F13																	
F14																	
F15																	
F16																	
G1	67	1489	PDAC	0	1						3	3	1	1	1	4	0

G2																	
G3																	
G4																	
G5																	
G6																	
G7	57	336	Cholangiocarcinom	0	2	7.4	3.2	3.6	95		2	4	2	X			0
G8																	
G9																	
G10																	
G11																	
G12																	
G13	74	1017	PDAC	0	2	7.3	5.1	1.4	46		3	3	3	0	0	6	0
G14																	
G15																	
G16																	
H1																	
H2																	
H3	67	1334	PDAC	0	2	8.7	5.3	2.3	<5		2	3	3	1	2	13	0
H4																	
H5																	
H6																	
H7																	
H8																	
H9	70	571	PDAC	0	2	6.7	4.9	1.3		83.9	2	3	3	1	3	11	1
H10																	
H11																	
H12																	
H13																	
H14																	
H15	73	6	PDAC	0	2	8.1	5	2.5	<5		2	3	3	1	6	8	1
H16																	
I1																	
I2																	
I3																	
I4																	
I5	67	589	PDAC	0	2	9.4	6.4	1.6	85	435.8	2	2	3	1	2	14	1
I6																	
I7																	
I8																	
I9																	
I10																	
I11	78	83	PDAC	2	2	7.2	4.2	1.9	<5	55.6	1	2	2	0	0	3	1
I12																	
I13																	
I14																	
I15																	
I16																	

a1	a2	a3	a4	a5	a6	a7	a8	a9	a10	a11	a12	a13	a14	a15	a16
b1	b2	b3	b4	b5	b6	b7	b8	b9	b10	b11	b12	b13	b14	b15	b16
c1	c2	c3	c4	c5	c6	c7	c8	c9	c10	c11	c12	c13	c14	c15	c16
d1	d2	d3	d4	d5	d6	d7	d8	d9	d10	d11	d12	d13	d14	d15	d16
e1	e2	e3	e4	e5	e6	e7	e8	e9	e10	e11	e12	e13	e14	e15	e16
f1	f2	f3	f4	f5	f6	f7	f8	f9	f10	f11	f12	f13	f14	f15	f16
g1	g2	g3	g4	g5	g6	g7	g8	g9	g10	g11	g12	g13	g14	g15	g16
h1	h2	h3	h4	h5	h6	h7	h8	h9	h10	h11	h12	h13	h14	h15	h16
i1	i2	i3	i4	i5	i6	i7	i8	i9	i10	i11	i12	i13	i14	i15	i16

AW2

TMA Pos	Tissue	Age	Survival	Diagnosis	dead	sex	WCC	neutro	lymphoc	CRP	ca 19-9	differentiation	T (of TNM)	other	N (of TNM)	Nodes	Total nodes	Resection
					0 is de	1 is male, 2 is female						1 is well, 2 is moderate, 3is		0 is nil, 1 is venous, 2		positive	total	(R0/1/2)
A1	Tumour	65	946	cholangiocarci	0	1						3	4	0	1	1	13	0
A2	Tumour																	
A3	Tumour																	
A4	Pan stroma																	
A5	Pan stroma																	
A6	Pan stroma																	
A7	Tumour	62	518	PDAC	0	2	8.4	7.2	0.9	5	334.3	3	3	3	1	3	9	0
A8	Tumour																	
A9	Tumour																	
A10	Pan stroma																	
A11	Pan stroma																	
A12	Pan stroma																	
A13	Tumour	84	367	PDAC	0	1						3	4	3	1	1	8	0
a14	Tumour																	
B1	Tumour																	
B2	Pan stroma																	
B3	Pan stroma																	
B4	Pan stroma																	
B5	normal control	59	253	mucinous cyst	2	2						2	2		0	0	3	0
B6	normal control																	
B7	normal control																	
B8	normal control																	
B9	normal control																	
B10	normal control																	
B11	Tumour	65	2440	chronic pancre	2	1												
B12	Tumour																	
B13	Tumour																	
B14	Pan stroma																	
C1	Pan stroma																	
C2	Pan stroma																	
D1	T	68	1129	PDAC	0	1						2	3	3	1	4	16	0
D2	T																	
D3	T																	
D4	S																	
D5	S																	
D6	S																	
D7	T	69	526	pdac	0	2	6.3	3.8	1.5	10	549	2	3	3	1	8	19	0
D8	T																	
D9	T																	
D10	S																	
D11	S																	
D12	S																	
D13	T	71	101	pdac	0	2						2	3	3	1	2	8	0
D14	T																	
E1	T																	
E2	S																	
E3	S																	
E4	S																	
E5	T	77	357	pdac	0	2						2	3	2	0	0	7	1
E6	T																	
E7	T																	
E8	S																	
E9	S																	
E10	S																	
E11	T	57	387	pdac	0	1						2	2	2	1	3	12	0
E12	T																	
E13	T																	
E14	S																	
F1	S																	
F2	S																	

F3	T	62	461	pdac	0	2						2	3	0	0	0	3	1
F4	T																	
F5	T																	
F6	S																	
F7	S																	
F8	S																	
F9	T	64	543	pdac	0	1						2	1	2	0	0	15	1
F10	T																	
F11	T																	
F12	S																	
F13	S																	
F14	S																	
G1	T	62	341	pdac	0	1						2	3	0	0	0	6	0
G2	T																	
G3	T																	
G4	S																	
G5	S																	
G6	S																	
G7	T	80	119	pdac	2	2						2		2				1
G8	T																	
G9	T																	
G10	S																	
G11	S																	
G12	S																	
G13	T	61	34	pdac	2	1						1	2	3	1	2	8	1
G14	T																	
H1	T																	
H2	S																	
H3	S																	
H4	S																	

Plastic	a1	a2	a3	a4	a5	a6	a7	a8	a9	a10	a11	a12	a13	a14
	b1	b2	b3	b4	b5	b6	b7	b8	b9	b10	b11	b12	b13	b14
	c1	c2	c3	c4	c5	c6	c7	c8	c9	c10	c11	c12	c13	c14
	d1	d2	d3	d4	d5	d6	d7	d8	d9	d10	d11	d12	d13	d14
	e1	e2	e3	e4	e5	e6	e7	e8	e9	e10	e11	e12	e13	e14
	f1	f2	f3	f4	f5	f6	f7	f8	f9	f10	f11	f12	f13	f14
	g1	g2	g3	g4	g5	g6	g7	g8	g9	g10	g11	g12	g13	g14
	h1	h2	h3	h4										

AW3

TMA Pos	Age	Survival	Diagnosis	dead	sex	WCC	neutro	lymphoc	CRP	ca 19-9	differentiation	T (of TNM)	other	N (of TNM)	Nodes	Total nodes	Resection (R0/1/2)
				0 is de	1 is male, 2 is female						1 is well, 2 is moderate, 3is		0 is nil, 1 is venous		positive	total	
A1	79	387	PDAC	0	2	6.6	4.9	1.2		30	3	3	2	1	2	10	0
A2																	
A3																	
A4																	
A5																	
A6																	
A7	71	435	pdac	0	1	8.3	4.4	3	11		3	3	3	1	1	16	0
A8																	
A9																	
A10																	
A11																	
A12																	
A13	76	109	cholangiocarc	2	2						3	4	3	1	3	9	0
A14																	
B1																	
B2																	
B3																	
B4																	
B5	79	797	cholangiocarc	0	1						3	3	2	0	0	8	0
B6																	
B7																	
B8																	
B9																	
B10																	
B11	45	905	cholangiocarc	0	1						2	3	2	1	1	3	0
B12																	
B13																	
B14																	
C1																	
C2																	
C3	61	484	cholangiocarc	2	2						2	3	1	1	3	11	0
C4																	
C5																	
C6																	
C7																	
C8																	
C9	81	157	IPMN	2	1						3	1	0	0	0	10	0
C10																	
C11																	
C12																	
C13																	
C14																	
D1	70	19	cholangiocarc	0	1						2	3	3	1	1	10	0
D2																	
D3																	
D4																	
D5																	
D6																	
D7	58	26	pdac biopsy	0	1	7.4	4.6	1.8	15		3		3				
D8																	
D9																	
D10																	
D11																	
D12																	
D13	77	170	pdac biopsy	0	1	9.2	7.3	1.2	103		2						
D14																	
E1																	
E2																	
E3																	
E4																	
E5	51	497	pdac	0	1	5.1	3.3	1.4			3	1	3	0	0	10	0
E6																	
E7																	
E8																	
E9																	
E10																	
E11	60	1139	pdac	0	1	8.6	4	3.6	<5		3	2	3	1	3	10	0
E12																	
E13																	
E14																	
F1																	
F2																	
F3	75	855	cholangiocarc	2	1	11	9.5	0.8	52	133		3	3	0	0	9	0
F4																	
F5																	
F6																	
F7																	
F8																	
F9	72	414	pdac	0	2	6.7	4.1	1.9	<5		3	2	3	0	0	16	0
F10																	
F11																	
F12																	
F13																	
F14																	
G1	73	46	pdac	2	1	8.4	4.6	2.9	7		3	1	2	0	0	21	0
G2																	
G3																	
G4																	
G5																	
G6																	
G7	69	60	pdac	0	2	7.1	4.7	1.4	18		3	1	1	1	9	26	1

G8																	
G9																	
G10																	
G11																	
G12																	
G13	53	4	cholangiocarc	0	2						1	4	3	1	4	12	1
G14																	
H1																	
H2																	
H3																	
H4																	
H5																	
H6																	
H7																	
H8																	
H9																	
H10																	
H11																	
H12																	
H13																	
I1																	

Plasti	a1	a2	a3	a4	a5	a6	a7	a8	a9	a10	a11	a12	a13	a14
	b1	b2	b3	b4	b5	b6	b7	b8	b9	b10	b11	b12	b13	b14
	c1	c2	c3	c4	c5	c6	c7	c8	c9	c10	c11	c12	c13	c14
	d1	d2	d3	d4	d5	d6	d7	d8	d9	d10	d11	d12	d13	d14
	e1	e2	e3	e4	e5	e6	e7	e8	e9	e10	e11	e12	e13	e14
	f1	f2	f3	f4	f5	f6	f7	f8	f9	f10	f11	f12	f13	f14
	g1	g2	g3	g4	g5	g6	g7	g8	g9	g10	g11	g12	g13	g14
	h1	h2	h3	h4	h5	h6	h7	h8	h9	h10	h11	h12	h13	h14
	i1													

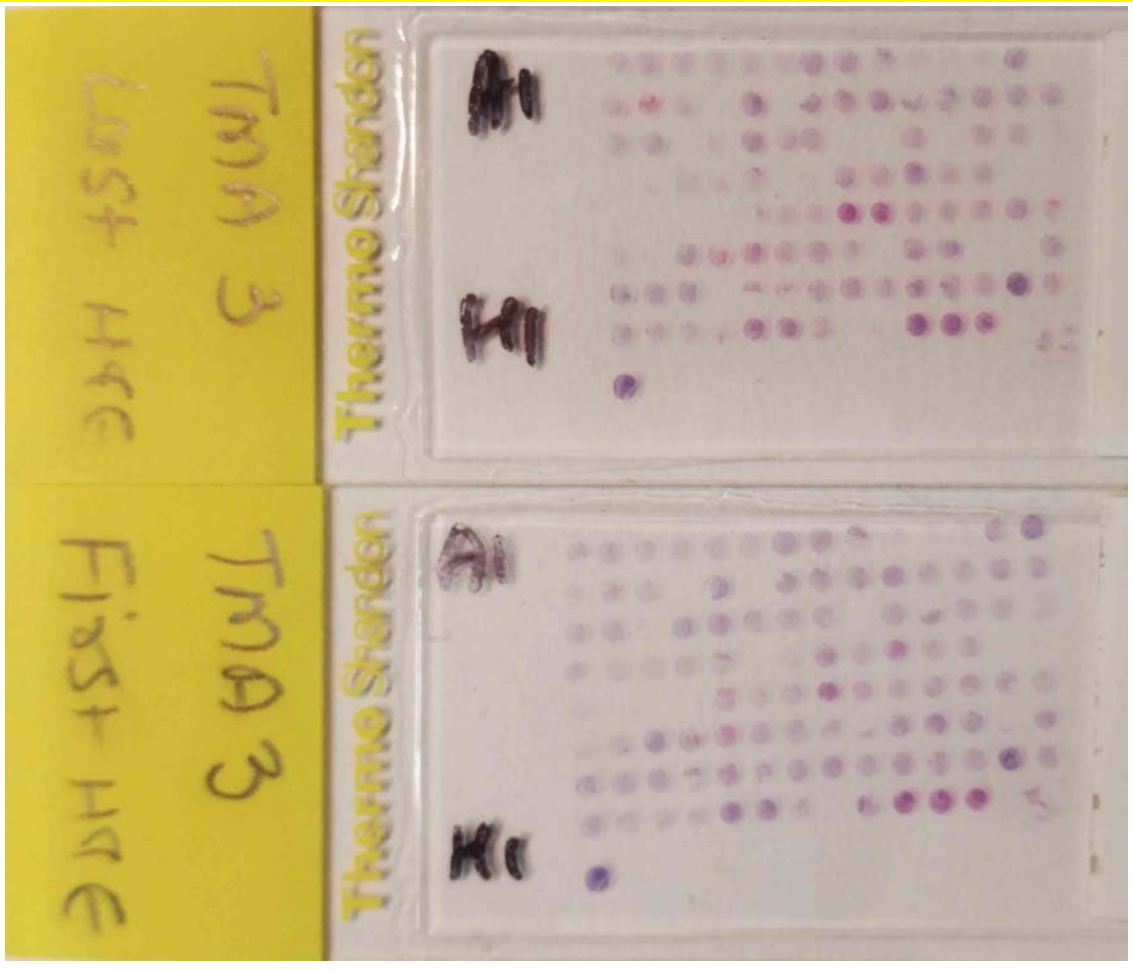

AW4

TMA Pos	Age	Survival	Diagnosis	dead	sex	WCC	neutro	lymphoc	CRP	ca 19-9	differentiation	T (of TNM)	other	N (of TNM)	Nodes	Total nodes	Resection (R0/1/2)
				0 is de	1 is male, 2 is female						1 is well, 2 is moderate, 3is p		0 is nil, 1 is venous		positive	total	
A1	60	356	pdac	0	2	4.9	3.1	1.4			3		0				0
A2																	
A3																	
A4																	
A5																	
A6																	
A7	58	8	pdac	0	1						2		0				0
A8																	
A9																	
A10																	
A11																	
A12																	
A13	67	299	pdac	2	1	6.5	5	0.9			3	2	1	1			1
A14																	
B1																	
B2																	
B3																	
B4																	
B5	46	261	pdac	0	1	9.2	5.3	3			3	2	0	1	1	7	1
B6																	
B7																	
B8																	
B9																	
B10																	
B11	60	499	pdac	0	1	6.9	4.4	1.7			1	2	0	1	2	6	1
B12																	
B13																	
B14																	
C1																	
C2																	
C3	69	798	pdac	0	2	11.4	8.7	2.1		4	2		1				0
C4																	
C5																	
C6																	
C7																	
C8																	
C9	67	860	pdac	0	2	6.9	3.7	2.6			3	3	0	0	2	3	0
C10																	
C11																	
C12																	
C13																	
C14																	
D1	64	579	pdac	0	2	10.3	7.7	1.9			1	3	0	0	0	12	0
D2																	
D3																	
D4																	
D5																	
D6																	
D7	67	827	pdac	0	2	3.8	2.3	1.2		71	2	3	1	1	1	8	0
D8																	
D9																	
D10																	
D11																	
D12																	
D13	63	4393	pdac	0	1	9.4	5.3	3.3			1	2	0	0	0	2	0
D14																	
E1																	
E2																	
E3																	
E4																	
E5	58	528	pdac	0	1	6.5	3.8	2.1	9		3	2	3	1	2	5	0
E6																	
E7																	
E8																	
E9																	
E10																	
E11	58	3912	pdac	0	1	9.9	6.9	2.1	6		3	3	2	0	0	7	1
E12																	
E13																	
E14																	
F1																	
F2																	
F3	75	750	pdac	0	2	10.2	7.8	1.8	36	115	1	2	3	1	3	14	0
F4																	
F5																	
F6																	
F7																	
F8																	
F9	72	587	pdac	0	1	9.5	7.2	1.8	209	1283	2	1	0	0	0	7	0
F10																	
F11																	
F12																	
F13																	
F14																	
G1	47	105	pdac	0	1	9.9	9.1	0.3	32	185	3	3	3	1	2	11	0
G2																	
G3																	
G4																	
G5																	
G6																	
G7	79	1171	pdac	0	2	5.9	3.5	1.9		<1	1	2	0	0	0	3	0

G8																		
G9																		
G10																		
G11																		
G12																		
G13	77	134	pdac	0	2	4.8	3.3	1	12	1281	2	2	3	0	0	13	0
G14																		
H1																		
H2																		
H3																		
H4																		
H5	47	48	pdac	0	1	7.1	3.4	3	8	722	2	3	0	1	8	12	1
H6																		
H7																		
H8																		
H9																		
H10																		
H11	66	539	pdac	0	2	6.1	4	1.5	<5	35	3	2	3	0	0	7	1
H12																		
H13																		
H14																		
I1																		
I2																		
I3	60	879	pdac	2	1	6	5	0.6	11		2	3	0	1	5	7	0
I4																		
I5																		
I6																		
I7																		
I8																		
I9	80	211	pdac	0	2	7.1	4.2	2.3		85	2		2				0
I10																		
I11																		
I12																		
I13																		
I14																		
J1	54	1190	pdac	0	1	6.9	1.7	4.7			2	2	2	1	7	33	0
J2																		
J3																		
J4																		
J5																		
J6																		
J7	69	685	pdac	0	1	13.5	11.9	0.9	<5	29	3	3	3	1	1	8	0
J8																		
J9																		
J10																		
J11																		
J12																		
J13																		
J14																		

Block 4

slide map

Plasti	a1	a2	a3	a4	a5	a6	a7	a8	a9	a10	a11	a12	a13	a14
	b1	b2	b3	b4	b5	b6	b7	b8	b9	b10	b11	b12	b13	b14
	c1	c2	c3	c4	c5	c6	c7	c8	c9	c10	c11	c12	c13	c14
	d1	d2	d3	d4	d5	d6	d7	d8	d9	d10	d11	d12	d13	d14
	e1	e2	e3	e4	e5	e6	e7	e8	e9	e10	e11	e12	e13	e14
	f1	f2	f3	f4	f5	f6	f7	f8	f9	f10	f11	f12	f13	f14
	g1	g2	g3	g4	g5	g6	g7	g8	g9	g10	g11	g12	g13	g14
	h1	h2	h3	h4	h5	h6	h7	h8	h9	h10	h11	h12	h13	h14
	i1	i2	i3	i4	i5	i6	i7	i8	i9	i10	i11	i12	i13	i14
	j1	j2	j3	j4	j5	j6	j7	j8	j9	j10	j11	j12	j13	j14

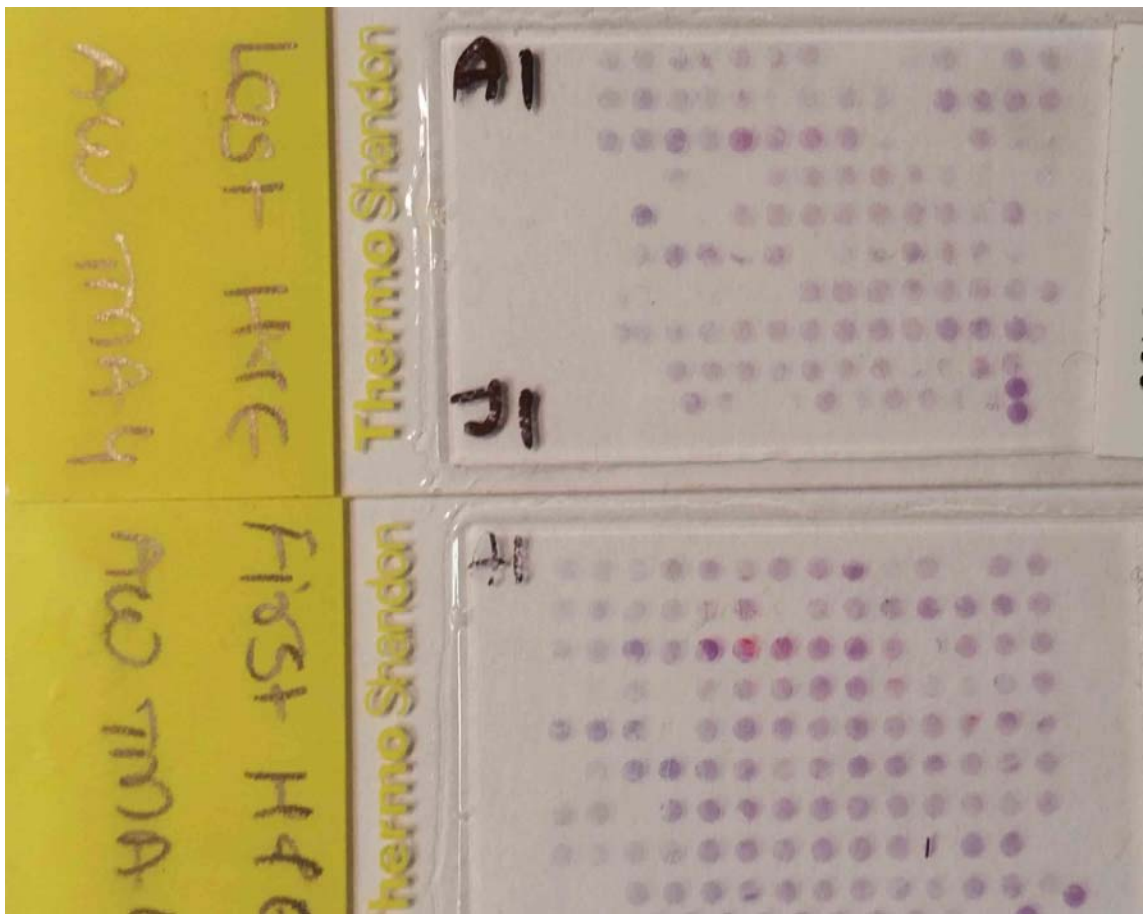

OPTMA1

TMA Pos	Age	Survival	Diagnosis	dead	sex	WCC	neutro	lymphoc	CRP	ca 19-9	differentiation	T (of TNM)	other	N (of TNM)	Nodes	Total nodes	Resection (R0/1/2)
				0 is de	1 is male, 2 is female						1 is well, 2 is moderate, 3		0 is nil, 1 is venous		positive	total	
A1																	
A2																	
A3																	
A4																	
A5	55	29	NET	0	2												
A6																	
A7																	
A8																	
A9																	
A10																	
A11	40	349	Insulinoma	2	1												
A12																	
A13																	
A14																	
A15																	
B1																	
B2	70	1915	ampullary adeı	0	2												
B3																	
B4																	
B5																	
B6																	
B7																	
B8	80	41	Duodenal Canc	0	2						3	4	1	0	0	8	
B9																	
B10																	
B11																	
B12																	
B13																	
B14	65	379	Ampullary canc	2	2						2	4	3	1	2	12	
B15																	
C1																	
C2																	
C3																	
C4																	
C5	64	2494	Cholangiocarci	1	2						3	4	2	1	1	13	
C6																	
C7																	
C8																	
C9																	
C10																	
C11																	
C12																	
C13																	
C14	52	1840	Duodenal Canc	2	1						3	3	0	1	21	24	
C15																	
D1																	
D2																	
D3																	
D4																	
D5	64	25	Duodenal Canc	0	1	9	7.7	0.6			3	4	0	0	0	24	
D6																	
D7																	
D8																	
D9																	
D10																	
D11	75	1253	Duodenal aden	0	2						2	4	1	0	0	14	
D12																	
D13																	
D14																	
D15																	
E1																	
E2																	
E3																	
E4																	
E5	78	16	Ampullary ade	2	2							Tis	0	0	0	8	
E6																	
E7																	
E8																	
E9																	
E10																	
E11	65	72	Duodenal canc	0	1						2	4	1	1	4	12	
E12																	
E13																	
E14																	
E15																	
F1																	
F2																	
F3																	
F4																	
F5	78	1168	Duodenal Canc	0	2						2	3	1	1	1	4	
F6																	
F7																	
F8																	
F9																	
F10																	
F11	77	616	PDAC	2	2	7.4	5.4	1.3	<5	150	2	1	0	1	node positive, but no number on CRS		
F12																	
F13																	
F14																	
F15																	
G1																	
G2																	
G3																	
G4																	
G5	56	118	Insulinoma	2	1												
G6																	
G7																	
G8	44	1189	Insulinoma	2	2						1						
G9																	
G10																	
G11																	
G12																	
G13																	
G14	46	1862	Duodenal Canc	2	2						2		3		0	15	
G15																	
H1																	
H2																	
H3																	
H4																	
H5																	
H6																	
H7																	
H8	73	2074	PDAC	1	1	9.7	8.4	0.6	19		3	3	3	1	3	23	
H9																	
H10																	
H11																	
H12																	
H13																	
H14																	
H15																	
I1																	

OPTMA1															I1
	H15	H14	H13	H12	H11	H10	H9	H8	H7	H6	H5	H4	H3	H2	H1
	G15	G14	G13	G12	G11	G10	G9	G8	G7	G6	G5	G4	G3	G2	G1
	F15	F14	F13	F12	F11	F10	F9	F8	F7	F6	F5	F4	F3	F2	F1
	E15	E14	E13	E12	E11	E10	E9	E8	E7	E6	E5	E4	E3	E2	E1
	D15	D14	D13	D12	D11	D10	D9	D8	D7	D6	D5	D4	D3	D2	D1
	C15	C14	C13	C12	C11	C10	C9	C8	C7	C6	C5	C4	C3	C2	C1
	B15	B14	B13	B12	B11	B10	B9	B8	B7	B6	B5	B4	B3	B2	B1
	A15	A14	A13	A12	A11	A10	A9	A8	A7	A6	A5	A4	A3	A2	A1

OPTMA2

TMA Pos	Age	Survival	Diagnosis	dead	sex	WCC	neutro	lymphocy	CRP	ca 19-9	differentiation	T (of TNM)	other	N (of TNM)	Nodes	Total nodes	Resection (R0/1/2)
				0 is de	1 is male, 2 is female						1 is well, 2 is moderate, 3i		0 is nil, 1 is venous		positive	total	(R0/1/2)
A1																	
A2	57	623	Cholangiocarcinoma	0	1						2	4	3	1	3	6	
A3																	
A4																	
A5																	
A6																	
A7																	
A8																	
A9																	
A10																	
A11	73	1376	ampullary adenoma	0							3						
A12																	
A13																	
A14																	
A15																	
B1																	
B2																	
B3																	
B4																	
B5	70	1513	mucinous cystadenon	2	2						3	2	1	0	0	11	
B6																	
B7																	
B8																	
B9																	
B10																	
B11	66	1268	Ampullary cancer	2	2						1	2	0	0	0	15	
B12																	
B13																	
B14																	
B15																	
C1																	
C2																	
C3																	
C4																	
C5	32	2479	pseudopapillary panc	2	2							2		x			
C6																	
C7																	
C8																	
C9																	
C10																	
C11																	
C12																	
C13																	
C14	40	48	NET	2	2						1						
C15																	
D1																	
D2	60	2677	GIST	2	2												
D3																	
D4																	
D5																	
D6																	
D7																	
D8	70	294	PDAC	0	2	8.7	4.5	3.3	<5	605	2						
D9																	
D10																	
D11	70	1513	mucinous cystadenon	2	2						3	2	1	0	0	11	
D12																	
D13																	
D14																	
D15																	
E1																	

OPTMA2															E1
	D15	D14	D13	D12	D11	D10	D9	D8	D7	D6	D5	D4	D3	D2	D1
	C15	C14	C13	C12	C11	C10	C9	C8	C7	C6	C5	C4	C3	C2	C1
	B15	B14	B13	B12	B11	B10	B9	B8	B7	B6	B5	B4	B3	B2	B1
	A15	A14	A13	A12	A11	A10	A9	A8	A7	A6	A5	A4	A3	A2	A1

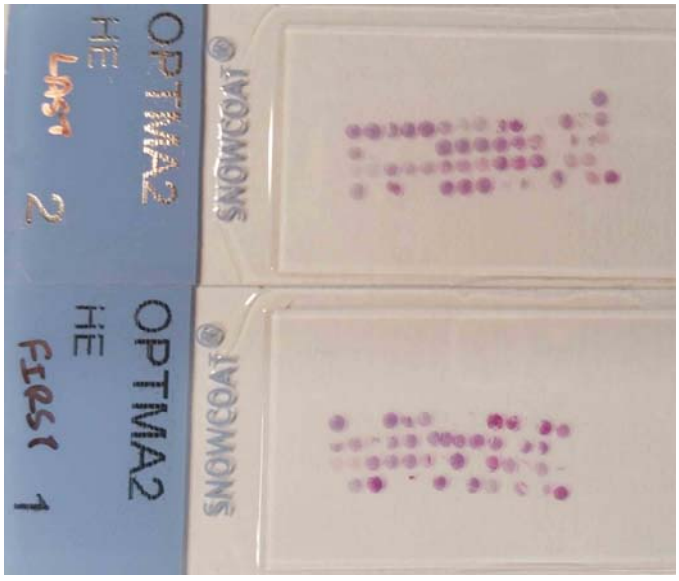

P2TMA3

TMA Pos	Age	Survival	Diagnosis	dead	sex	WCC	neutro	lymphoc	CRP	ca 19-9	differentiati	T (of TNM)	other	N (of TNM)	Nodes	Total nodes	Resection (R0/1/2)
				0 is de	1 is male, 2 is female						1 is well, 2 is moderate,		0 is nil, 1 is venous,		positive	total	
A1																	
A2	61	472	Cholangiocarcinoma	0	1						3	4	1	1	4	15	
A3																	
A4																	
A5																	
A6																	
A7																	
A8																	
A9																	
A10																	
A11	43	1680	Benign pancreas	0	1						1		0				
A12																	
A13																	
A14																	
A15																	
B1																	
B2	64	2494	Cholangiocarcinoma	1	2						3	4	2	1	1	13	
B3																	
B4																	
B5																	
B6																	
B7																	
B8																	
B9																	
B10																	
B11	52	1840	Duodenal Cancer	2	1						3	3	0	1	21	24	
B12																	
B13																	
B14																	
B15																	
C1																	
C2	64	25	Duodenal Cancer	0	1	9	7.7	0.6			3	4	0	0	0	24	
C3																	
C4																	
C5																	
C6																	
C7																	
C8	75	1253	Duodenal adenocarci	0	2						2	4	1	0	0	14	
C9																	
C10																	
C11																	
C12																	
C13																	
C14																	
C15																	
D1																	
D2	78	16	Ampullary adenoma	2	2							Tis	0	0	0	8	
D3																	
D4																	
D5																	
D6																	
D7																	
D8	65	72	Duodenal cancer	0	1						2	4	1	1	4	12	
D9																	
D10																	
D11																	
D12																	
D13																	
D14																	
D15																	
E1																	
E2	78	1168	Duodenal Cancer	0	2						2	3	1	1	1	4	
E3																	
E4																	
E5																	
E6																	
E7																	
E8	41	511	Benign pancreas	2	1								0				
E9																	
E10																	
E11																	
E12																	
E13																	
E14	77	616	PDAC	2	2	7.4	5.4	1.3	<5	150	2	1	0	1	node positive, but no number on CRS		
E15																	
F1																	
F2																	
F3																	
F4																	
F5																	
F6																	
F7																	
F8	41	1652	Benign pancreas	2	1												
F9																	
F10																	
F11																	
F12																	
F13																	
F14	46	1862	Duodenal Cancer	2	2						2		3		0	15	
F15																	
G1																	
G2																	
G3																	
G4																	
G5																	
G6																	
G7																	
G8	73	2074	PDAC	1	1	9.7	8.4	0.6	19		3	3	3	1	3	23	
G9																	
G10																	
G11																	
G12																	
G13																	
G14																	
G15																	
H1																	
H2	30	250	pancreatitis (benign)	2	1												
H3																	
H4																	
H5																	
H6																	
H7																	
H8	57	623	Cholangiocarcinoma	0	1						2	4	3	1	3	8	
H9																	
H10																	
H11																	
H12																	
H13																	
H14																	
H15																	
I1																	
I2	73	1376	ampullary adenoma	0							3						
I3																	
I4																	

P2TMA3												I4	I3	I2	I1
	H15	H14		H13	H12	H11	H10	H9	H8	H7	H6	H5	H4	H3	H2	H1
	G15	G14		G13	G12	G11	G10	G9	G8	G7	G6	G5	G4	G3	G2	G1
	F15	F14		F13	F12	F11	F10	F9	F8	F7	F6	F5	F4	F3	F2	F1
	E15	E14		E13	E12	E11	E10	E9	E8	E7	E6	E5	E4	E3	E2	E1
	D15	D14		D13	D12	D11	D10	D9	D8	D7	D6	D5	D4	D3	D2	D1
	C15	C14		C13	C12	C11	C10	C9	C8	C7	C6	C5	C4	C3	C2	C1
	B15	B14		B13	B12	B11	B10	B9	B8	B7	B6	B5	B4	B3	B2	B1
	A15	A14		A13	A12	A11	A10	A9	A8	A7	A6	A5	A4	A3	A2	A1

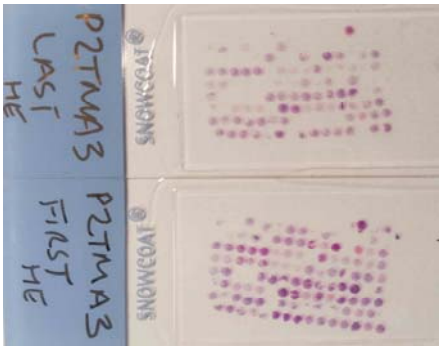

P3TMA1

TMA Pos	Age	Survival	Diagnosis	dead	sex	WCC	neutro	lymphoc	CRP	ca 19-9	differentiation	T (of TNM)	other	N (of TNM)	Nodes	Total nodes	Resection (R0/1/2)
				0 is de	1 is male, 2 is female						1 is well, 2 is moderate, 3is		0 is nil, 1 is venous,		positive	total	
A1																	
A2	58	293	PDAC	0	2												
A3																	
A4																	
A5																	
A6																	
A7																	
A8	65	70	PDAC biops	0	2	8.8	7.1	1.1			3						
A9																	
A10																	
A11																	
A12																	
A13																	
A14	49	165	PDAC	0	1	7.9	7.2	0.4	<5		3						
A15																	
B1																	
B2																	
B3																	
B4																	
B5	69	185	PDAC	0	1						2						
B6																	
B7																	
B8																	
B9																	
B10																	
B11	58	168	PDAC	0	2						2						
B12																	
B13																	
B14																	
B15																	
C1																	
C2																	
C3																	
C4																	
C5	58	635	PDAC	0	2	9	4.7	3.2	22		3						
C6																	
C7																	
C8																	
C9																	
C10																	
C11																	
C12																	
C13																	
C14	62	260	PDAC	0	2	7.4	4.1	2.4			2						
C15																	
D1																	
D2																	
D3																	
D4																	
D5	74	295	PDAC	0	1	10.9	7.7	2.4		886.3							
D6																	
D7																	
D8																	
D9																	
D10																	
D11	58	431	PDAC	0	2	6.1	3.5	2									
D12																	
D13																	
D14																	
D15																	
E1																	
E2	61	105	PDAC	0	1	5.1	3.7	0.9	27	5215	2						
E3																	
E4																	
E5																	
E6																	
E7																	
E8																	
E9																	
E10																	
E11	56	65	PDAC	0	1	4.9	2.3	2	92	0.6	3		1				
E12																	
E13																	
E14																	
E15																	
F1																	
F2																	
F3																	
F4																	
F5	58	716	Benign panc	0	2												
F6																	
F7																	
F8																	
F9																	
F10																	
F11	48	120	PDAC	0	1	5.7	3.7	1.2	<5		3						
F12																	
F13																	
F14																	
F15																	
G1																	
G2	59	255	PDAC	0	1	8.8	5.5	2.2	47		3						
G3																	
G4																	
G5																	
G6																	
G7																	
G8																	
G9																	
G10																	
G11	76	477	PDAC	0	1	6.3	4.5	1.3	144		3		2				
G12																	
G13																	
G14																	
G15																	
H1																	
H2	76	33	cholangioca	0	1	12.2	9.4	1.8	61		3						
H3																	
H4																	
H5																	
H6																	
H7																	
H8																	
H9																	
H10																	
H11																	
H12																	
H13																	
H14	70	1513	mucinous cy	2	2						3	2	1	0	0	11	
H15																	
I1																	
I2																	
I3																	
I4																	

P3 TMA1																
	H15	H14	H13	H12	H11	H10	H9	H8	H7	H6	H5	I4	I3	I2	I1
	G15	G14	G13	G12	G11	G10	G9	G8	G7	G6	G5	G4	G3	G2	G1
	F15	F14	F13	F12	F11	F10	F9	F8	F7	F6	F5	F4	F3	F2	F1
	E15	E14	E13	E12	E11	E10	E9	E8	E7	E6	E5	E4	E3	E2	E1
	D15	D14	D13	D12	D11	D10	D9	D8	D7	D6	D5	D4	D3	D2	D1
	C15	C14	C13	C12	C11	C10	C9	C8	C7	C6	C5	C4	C3	C2	C1
	B15	B14	B13	B12	B11	B10	B9	B8	B7	B6	B5	B4	B3	B2	B1
	A15	A14	A13	A12	A11	A10	A9	A8	A7	A6	A5	A4	A3	A2	A1

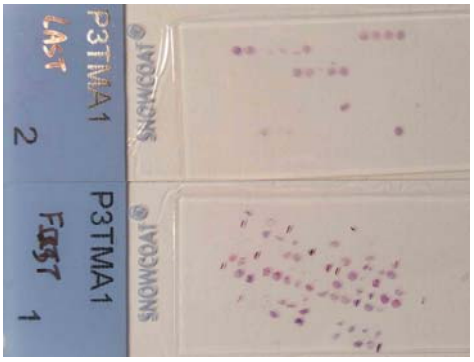

P3TMA2

TMA Pos	Age	Survival	Diagnosis	dead	sex	WCC	neutro	lymphoc	CRP	ca 19-9	differentiation	T (of TNM)	other	N (of TNM)	Nodes	Total nodes	Resection (R0/1/2)
				0 is de	1 is male, 2 is female						1 is well, 2 is moderate, 3i		0 is nil, 1 is venous		positive	total	
A1																	
A2	66	1268	Ampullary cancer	2	2						1	2	0	0	0	15	
A3																	
A4																	
A5																	
A6																	
A7																	
A8																	
A9																	
A10																	
A11	32	2479	pseudopapillary pa	2	2							2		x			
A12																	
A13																	
A14	59	2285	NET	2	2						1		0		5	16	
A15																	
B1																	
B2																	
B3																	
B4																	
B5	40	48	NET	2	2						1						
B6																	
B7																	
B8	60	2677	GIST	2	2												
B9																	
B10																	
B11																	
B12																	
B13																	
B14	72	313	PDAC	0	2	5.5	2.6	2.5	<5	5642	2						
B15																	
C1																	
C2																	
C3																	
C4																	
C5	74	236	PDAC	0	2	13.8	11.1	2.1	25	12							
C6																	
C7																	
C8																	
C9																	
C10																	
C11	51	473	PDAC	0	2	5.7	3.8	1.3		229	1						
C12																	
C13																	
C14	56	#VALUE!	PDAC	0	2	7.1	5.1	1.5	66								
C15																	
D1																	
D2	70	294	PDAC	0	2	8.7	4.5	3.3	<5	605	2						
D3																	
D4																	
D5	70	1513	mucinous cystader	2	2						3	2	1	0	0	11	
D6																	
D7																	
D8																	
D9																	
D10																	
D11	59	2465	PDAC	0	1	11.9	8.6	2	20	157.2	3	2	3	1	2	30	
D12																	
D13																	
D14																	
D15																	
E1																	
E2	32	2479	pseudopapillary pa	2	2							2		x			
E3																	
E4																	
E5	77	87	Duodenal Cancer	0	2	11.6	5.2	1.4			2						
E6																	
E7																	
E8																	
E9																	
E10																	
E11	51	664	Insulinoma	2	2												
E12																	
E13																	
E14																	
E15																	
F1																	
F2	31	820	Insulinoma	2	2												
F3																	
F4																	
F5																	
F6																	
F7																	
F8	65	36	Insulinoma	0	2												
F9																	
F10																	
F11																	
F12																	
F13																	
F14	53	2016	insulinoma pancrea	2	1						1		0				
F15																	
G1																	
G2																	
G3																	
G4																	
G5	70	1915	ampullary adenom	0	2												
G6																	
G7																	
G8																	
G9																	
G10																	
G11	80	41	Duodenal Cancer	0	2						3	4	1	0	0	8	
G12																	
G13																	
G14																	
G15																	
H1																	
H2	65	379	Ampullary cancer	2	2						2	4	3	1	2	12	
H3																	
H4																	
H5																	
H6																	
H7																	
H8	61	472	Cholangiocarcinon	0	1						3	4	1	1	4	15	
H9																	
H10																	
H11																	
H12																	
H13																	
H14																	
H15																	
I1																	

P3 TMA2																				i1
	H15	H14		H13	H12	H11	H10	H9	H8	H7	H6		H5	H4	H3	H2	H1
	G15	G14		G13	G12	G11	G10	G9	G8	G7	G6		G5	G4	G3	G2	G1
	F15	F14		F13	F12	F11	F10	F9	F8	F7	F6		F5	F4	F3	F2	F1
	E15	E14		E13	E12	E11	E10	E9	E8	E7	E6		E5	E4	E3	E2	E1
	D15	D14		D13	D12	D11	D10	D9	D8	D7	D6		D5	D4	D3	D2	D1
	C15	C14		C13	C12	C11	C10	C9	C8	C7	C6		C5	C4	C3	C2	C1
	B15	B14		B13	B12	B11	B10	B9	B8	B7	B6		B5	B4	B3	B2	B1
	A15	A14		A13	A12	A11	A10	A9	A8	A7	A6		A5	A4	A3	A2	A1

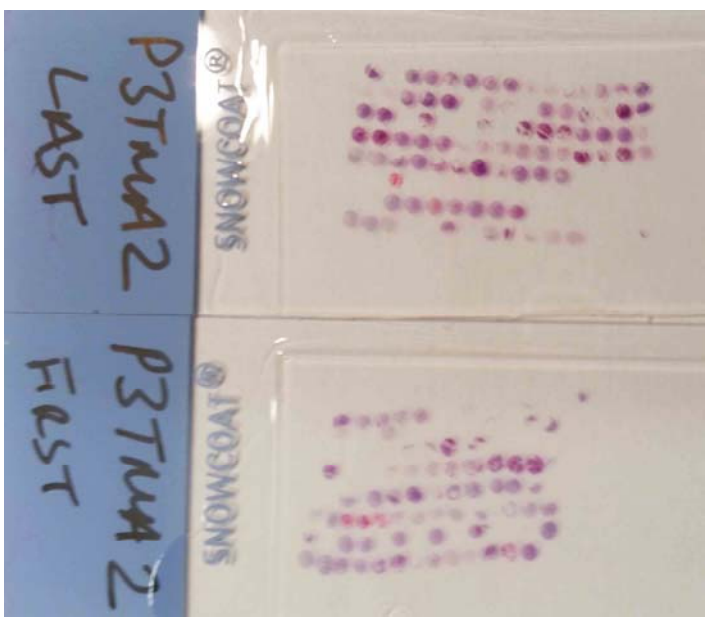

P3TMA3

TMA Pos	Age	Survival	Diagnosis	dead	sex	WCC	neutro	lymphoc	CRP	ca 19-9	differentiation	T (of TNM)	other	N (of TNM)	Nodes	Total nodes	Resection (R0/1/2)
				0 is dea	1 is male, 2 is female						1 is well, 2 is moderate, 3		0 is nil, 1 is venous		positive	total	
A1																	
A2	43	1680	Benign pancreas	0	1						1		0				
A3																	
A4																	
A5																	
A6																	
A7																	
A8	64	2494	Cholangiocarcinoma	1	2						3	4	2	1	1	13	
A9																	
A10																	
A11																	
A12																	
A13																	
A14																	
A15																	
B1																	
B2	52	1840	Duodenal Cancer	2	1						3	3	0	1	21	24	
B3																	
B4																	
B5																	
B6																	
B7																	
B8	64	25	Duodenal Cancer	0	1	9	7.7	0.6			3	4	0	0	0	24	
B9																	
B10																	
B11																	
B12																	
B13																	
B14	75	1253	Duodenal adenocarci	0	2						2	4	1	0	0	14	
B15																	
C1																	
C2																	
C3																	
C4																	
C5																	
C6																	
C7																	
C8	78	16	Ampullary adenoma	2	2							Tis	0	0	0	8	
C9																	
C10																	
C11																	
C12																	
C13																	
C14	65	72	Duodenal cancer	0	1						2	4	1	1	4	12	
C15																	
D1																	
D2																	
D3																	
D4																	
D5																	
D6																	
D7																	
D8	78	1168	Duodenal Cancer	0	2						2	3	1	1	1	4	
D9																	
D10																	
D11																	
D12																	
D13																	
D14	41	511	Benign pancreas	2	1								0				
D15																	
E1																	
E2																	
E3																	
E4																	
E5	77	616	PDAC	2	2	7.4	5.4	1.3	<5	150	2	1	0	1	node positive		
E6																	
E7																	
E8																	
E9																	
E10																	
E11																	
E12																	
E13																	
E14	41	1652	Benign pancreas	2	1												
E15																	
F1																	
F2																	
F3																	
F4																	
F5	46	1862	Duodenal Cancer	2	2						2		3		0	15	
F6																	
F7																	
F8																	
F9																	
F10																	
F11																	
F12																	
F13																	
F14	73	2074	PDAC	1	1	9.7	8.4	0.6	19		3	3	3	1	3	23	
F15																	
G1																	
G2																	
G3																	
G4																	
G5																	
G6																	
G7																	
G8	30	250	pancreatitis (benign)	2	1												
G9																	
G10																	
G11																	
G12																	
G13																	
G14	57	623	Cholangiocarcinoma	0	1						2	4	3	1	3	6	
G15																	
H1																	
H2																	
H3																	
H4																	
H5																	
H6																	
H7																	
H8	73	1376	ampullary adenoma	0							3						
H9																	
H10																	

P3 TMA3							H10	H9	H8	H7	H6	H5	H4	H3	H2	H1
	G15	G14	G13	G12	G11	G10	G9	G8	G7	G6	G5	G4	G3	G2	G1	
	F15	F14	F13	F12	F11	F10	F9	F8	F7	F6	F5	F4	F3	F2	F1	
	E15	E14	E13	E12	E11	E10	E9	E8	E7	E6	E5	E4	E3	E2	E1	
	D15	D14	D13	D12	D11	D10	D9	D8	D7	D6	D5	D4	D3	D2	D1	
	C15	C14	C13	C12	C11	C10	C9	C8	C7	C6	C5	C4	C3	C2	C1	
	B15	B14	B13	B12	B11	B10	B9	B8	B7	B6	B5	B4	B3	B2	B1	
	A15	A14	A13	A12	A11	A10	A9	A8	A7	A6	A5	A4	A3	A2	A1	

PTMA1

TMA Pos	Age	Survival	Diagnosis	dead	sex	WCC	neutro	lymphoc	CRP	ca 19-9	differentiation	T (of TNM)	other	N (of TNM)	Nodes	Total nodes	Resection (R0/1/2)
				0 is de	1 is male, 2 is female						1 is well, 2 is moderate, 3is		0 is nil, 1 is venous,		positive	total	
A1																	
A2	50	194	PDAC	0	2	4.5	2.8	1.3			1						
A3																	
A4																	
A5																	
A6																	
A7																	
A8	62	518	PDAC	0	2						3	3		1			
A9																	
A10																	
A11																	
A12																	
A13																	
A14																	
A15																	
B1																	
B2	79	387	PDAC	0	2						3	3	2	1	2	10	0
B3																	
B4																	
B5																	
B6																	
B7																	
B8	75	398	PDAC	0	1	7.3	5.6	1.1			1	3	1	1	2	12	
B9																	
B10																	
B11																	
B12																	
B13																	
B14																	
B15																	
C1																	
C2	62	2486	PDAC	1	1	6.2	3.5	2	10		3	1	2	0	0	12	
C3																	
C4																	
C5																	
C6																	
C7																	
C8																	
C9																	
C10																	
C11	74	705	PDAC	0	1	6.6	4.9	1.2	19	54	2	3	3	1	4	12	
C12																	
C13																	
C14																	
C15																	
D1																	
D2																	
D3																	
D4																	
D5	81	475	PDAC	0	2	7.1	4.3	2	8		3	3	3	1	5	16	
D6																	
D7																	
D8																	
D9																	
D10																	
D11	47	1777	Cholangioca	2	2						2	3	2	1	1	24	
D12																	
D13																	
D14																	
D15																	
E1																	
E2																	
E3																	
E4																	
E5	60	854	PDAC	0	2	8.7	5.6	2.5	<5		3	3	3	1	5	13	
E6																	
E7																	
E8																	
E9																	
E10																	
E11																	
E12																	
E13																	
E14																	
E15																	
F1																	
F2																	
F3																	
F4																	
F5	70	1513	mucinous cy	2	2							3	2	1	0	0	11
F6																	
F7																	
F8																	
F9																	
F10																	
F11	66	1268	Ampullary ca	2	2							1	2	0	0	0	15
F12																	
F13																	
F14																	
F15																	
G1																	
G2																	
G3																	
G4																	
G5	32	2479	pseudopapill	2	2								2		x		
G6																	
G7																	
G8	59	2285	NET	2	2							1		0		5	16
G9																	
G10																	
G11																	
G12																	
G13																	
G14	40	48	NET	2	2							1					
G15																	
H1																	
H2	54	42	Cholangioca	2	2							2	4	3	1	2	15
H3																	
H4																	
H5																	
H6																	
H7																	
H8																	
H9																	
H10																	
H11	69	131	Cholangioca	0	1							2	3	3	1	11	12
H12																	
H13																	
H14																	
H15																	
I1																	
I2																	
I3																	
I4																	

PTMA1															
	H15	H14	H13	H12	H11	H10	H9	H8	H7	H6	H5	I4	I3	I2	I1
	G15	G14	G13	G12	G11	G10	G9	G8	G7	G6	G5	G4	G3	G2	G1
	F15	F14	F13	F12	F11	F10	F9	F8	F7	F6	F5	F4	F3	F2	F1
	E15	E14	E13	E12	E11	E10	E9	E8	E7	E6	E5	E4	E3	E2	E1
	D15	D14	D13	D12	D11	D10	D9	D8	D7	D6	D5	D4	D3	D2	D1
	C15	C14	C13	C12	C11	C10	C9	C8	C7	C6	C5	C4	C3	C2	C1
	B15	B14	B13	B12	B11	B10	B9	B8	B7	B6	B5	B4	B3	B2	B1
	A15	A14	A13	A12	A11	A10	A9	A8	A7	A6	A5	A4	A3	A2	A1

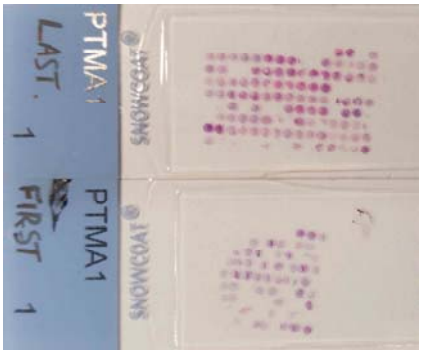

PTMA2

TMA Pos	Age	Survival	Diagnosis	dead	sex	WCC	neutro	lymphoc	CRP	ca 19-9	differentiation	T (of TNM)	other	N (of TNM)	Nodes	Total nodes	Resection (R0/1/2)
				0 is de	1 is male, 2 is female						1 is well, 2 is moderate, 3is		0 is nil, 1 is venous,		positive	total	
A1																	
A2	77	137	Cholangiocarcinoma	2	2						3	4	3	1	3	6	
A3																	
A4																	
A5																	
A6																	
A7																	
A8																	
A9																	
A10																	
A11	58	997	Cholangiocarcinoma	2	1	8.7	6.4	1.3	<5		2	3	2	1	0	18	
A12																	
A13																	
A14																	
A15																	
B1																	
B2																	
B3																	
B4																	
B5	74	551	Cholangiocarcinoma	0	2						2	3	3	1	6	13	
B6																	
B7																	
B8																	
B9																	
B10																	
B11	72	442	Cholangiocarcinoma	0	1		4.4	1.5	<5		3	4	3	1	4	20	
B12																	
B13																	
B14																	
B15																	
C1																	
C2	61	257	Cholangiocarcinoma	0	1						3	4	3	1	6	10	
C3																	
C4																	
C5																	
C6																	
C7																	
C8																	
C9																	
C10																	
C11	60	2677	GIST	2	2												
C12																	
C13																	
C14																	
C15																	
D1																	
D2	56	234	Cholangiocarcinoma	0	1						2	3		0	0	4	
D3																	
D4																	
D5																	
D6																	
D7																	
D8																	
D9																	
D10																	
D11	70	1513	mucinous cystadenom	2	2						3	2	1	0	0	11	
D12																	
D13																	
D14																	
D15																	
E1																	
E2	32	2479	pseudopapillary panc	2	2							2		x			
E3																	
E4																	
E5	65	346	Cholangiocarcinoma	0	1						3	4	3	1	6	18	
E6																	
E7																	
E8																	
E9																	
E10																	
E11																	
E12																	
E13																	
E14	53	27	PDAC	0	2	7.3	5.3	1.3	6	958	2	2	3	1	7	13	
E15																	
F1																	
F2																	
F3																	
F4																	
F5																	
F6																	
F7																	
F8	51	664	Insulinoma	2	2												
F9																	
F10																	
F11																	
F12																	
F13																	
F14	31	820	Insulinoma	2	2												
F15																	
G1																	
G2																	
G3																	
G4																	
G5	65	36	Insulinoma	0	2												
G6																	
G7																	
G8																	
G9																	
G10																	
G11	53	2016	insulinoma pancreas	2	1						1		0				
G12																	
G13																	
G14																	
G15																	
H1																	
H2	70	1915	ampullary adenoma	0	2												
H3																	
H4																	
H5																	
H6																	
H7																	
H8	80	41	Duodenal Cancer	0	2						3	4	1	0	0	8	
H9																	
H10																	
H11																	
H12																	
H13																	
H14	65	379	Ampullary cancer	2	2						2	4	3	1	2	12	
H15																	
I1																	
I2																	
I3																	
I4																	

PTMA2															
													I4	I3	I2	I1
	H15	H14		H13	H12	H11	H10	H9	H8	H7	H6	H5	H4	H3	H2	H1
	G15	G14		G13	G12	G11	G10	G9	G8	G7	G6	G5	G4	G3	G2	G1
	F15	F14		F13	F12	F11	F10	F9	F8	F7	F6	F5	F4	F3	F2	F1
	E15	E14		E13	E12	E11	E10	E9	E8	E7	E6	E5	E4	E3	E2	E1
	D15	D14		D13	D12	D11	D10	D9	D8	D7	D6	D5	D4	D3	D2	D1
	C15	C14		C13	C12	C11	C10	C9	C8	C7	C6	C5	C4	C3	C2	C1
	B15	B14		B13	B12	B11	B10	B9	B8	B7	B6	B5	B4	B3	B2	B1
	A15	A14		A13	A12	A11	A10	A9	A8	A7	A6	A5	A4	A3	A2	A1